School of Pharmacy & Bioengineering
Faculty of Medicine & Health Sciences
Keele University

Use of nanoparticles to improve the therapeutic index of navitoclax

Khaled Jamal Jad Allah Alrosan

Thesis submitted to Keele University for the degree of Doctor of Philosophy in Pharmacology

March 2022

Abstract

Ovarian cancer is considered a major health problem in women. The chemotherapeutic drugs that are used often are inadequate due to the development of drug resistance. This is related to many causes, and one of them is an evasion of apoptosis. One of the major causes that stand behind this apoptosis escaping is overexpression of anti-apoptotic BCL-2 family members. Thus, this encouraged the researchers to think about new solutions for the treatment of ovarian cancer. One of these solutions was the development of BH3 mimetics, which are small molecules inhibitors of anti-apoptotic BCL-2 family members and have the capability to cause an apoptosis in the ovarian cancer cells. Furthermore, they increase the ovarian cancer cells sensitivity to chemotherapeutic agents. Navitoclax (ABT-263) belongs to this family and has the advantage of inhibition of BCL-X_L, as well as BCL-2. Studies showed that inhibition of BCL-X_L leads to ovarian cancer regression in xenografts in mice. However, clinical investigations have been restricted because of a major side effect that navitoclax causes, which is thrombocytopenia. Thus, this led to think about new strategies to broaden its therapeutic window and formulation of navitoclax as nanoparticles is one of these strategies. This novel formulation is composed of navitoclax in addition to comb-shaped polymer (poly(allylamine) (PAA) derivatives). This polymeric backbone was modified with cholesteryl moieties (PAA-ch_5), which showed improvement in the solubilisation of several hydrophobic drugs. The specific phenomenon of nanoparticles is that they can accumulate preferentially in tumours by enhanced permeability and retention effect (EPR). Accordingly, this can lead to target navitoclax passively toward ovarian cancer cells and avoid platelets accumulation. Furthermore, this targeting can be more enhanced by attaching nanoparticles with

folate moiety because folate receptors are known to be over-expressed on ovarian cancer cells as well as other cancers.

Contents

Abstract I
List of figures VIII
List of tables XI
Abbreviations XII
Acknowledgment XVI

Chapter 1. Introduction 1
1.1. Introduction to ovarian cancer 2
1.1.1. Epidemiology 2
1.1.2. Symptoms 4
1.1.3. Risk Factors 6
1.1.4. Aetiology 7
1.1.5. Types 7
1.1.6. Staging of ovarian cancer 11
1.1.7. Diagnosis 15
1.2. Treatment 17
1.2.1. Surgery 17
1.2.2. Chemotherapy 19
1.2.3. Resistance 26
1.3. BCL-2 Family 30
1.3.1. Antiapoptotic proteins 32
1.3.2. Proapoptotic proteins 32
1.4. Navitoclax (ABT-263) 34
1.5. Cancer nanomedicine 35
1.5.1. Amphiphilic polymers 35
1.5.2. Targeting of nanoparticles 46
1.5.3. Application of nanoparticles in ovarian cancer 49

Aims and objectives 52
Aims 53

Chapter 2. Materials and methods 55
2.1. Materials 56
2.1.1. Ovarian Cancer Cell Lines 58
2.2. Methods 59

2.2.1. Drug Loading 59
2.2.2. Detection of navitoclax, poly (allylamine)- ch5 (PAA-ch_5), poly (allylamine)- ch_5-folic acid (PAA- ch_5-FA) water solubility 60
2.2.3. Quantification of encapsulated navitoclax 61
2.2.4. Release method 62
2.2.5. Photon correlation spectroscopy 62
2.2.6. Freeze drying (lyophilization) 63
2.2.7. Physical stability assay 63
2.2.8. Cells used and growth, Navitoclax stock preparation 64
2.2.9. Seeding and harvesting 64
2.2.10. Cryopreservation of adherent cell lines 65
2.2.11. Thawing cells 65
2.2.12. Proliferation assay (Sulforhodamine B (SRB) assay) 66
2.2.13. Caspase 3/7 activity assay 67
2.2.14. Trypan blue assay 69
2.2.15. Bliss independence criterion 70
2.2.16. Western blot assay 70
2.2.17. Cellular uptake 73
2.2.18. Measurement of annexin V/PI labelling 74
2.2.19. Effect of folic acid competition on cellular toxicity 75
2.2.20. Statistical analysis 77

Chapter 3. Formulation and analysis of navitoclax polymer complexes 78
3.1. Introduction 79
3.2. Factors affect nanoaggregates 82
3.3. Nano-aggregate formation 85
3.4. Nano-aggregate characterisation 87
3.5. Quantification of Drug Loading 89
3.6. Aims 91
3.7. Results 92
3.7.1. Detection of navitoclax, PAA-ch_5 using HPLC 92
3.7.2. Standard calibration curve construction 93
3.7.3. Navitoclax quantification 95
3.7.4. Effect of changing the drug: polymer ratio on loading capacity 96
3.7.5. Effect of changing polymer concentration on the loading capacity 98
3.7.6. Nano-aggregate characterisation 100
3.7.7. Drug release 101

3.7.8. Formulation Stability 102
3.8. Discussion 103
3.9. Conclusion 112

Chapter 4. The cytotoxicity of the navitoclax-PAA-ch$_5$ and its combination with Carboplatin 113
4.1. Introduction 114
4.2. The road to invention BH3 mimetics 115
4.3. BH3 mimetic drugs 116
4.3.1. ABT-737 116
4.3.2. Navitoclax (ABT-263) 117
4.4. Thrombocytopenia 120
4.5 New BH3 drugs era 121
4.5.1. Venetolcax 121
4.5.2. WEHI-539 122
4.6. BH3 profiling 127
4.7. Combination of BH3 mimetics with chemotherapy 128
4.8 Aims and goals 133
4.9 Results 134
4.9.1. Evaluation of the PAA-ch$_5$ toxicity 134
4.9.2. Cytotoxicity of the Navitoclax-PAA-ch5 versus navitoclax 138
4.9.3. Drug uptake 142
4.9.4. Combination assays 144
4.10. Discussion 153
4.11. Conclusion 161

Chapter 5. Folate targeting of PAA-ch5 nanoparticles loaded with navitoclax 162
5.1. Introduction 163
.5.2 Nanoparticles active targeting 164
5.3. Ligands 165
5.4. Folic acid 166
5.5. Folate receptors 168
5.5.1. Folate receptor alpha 170
5.6. FRA in ovarian cancer 171
5.7. Drugs targeting FRA 171
5.8. Aims 173
5.9. Results 174

5.9.1. Detection of PAA-ch$_5$-FA using HPLC 174
5.9.2. Navitoclax quantification 175
5.9.3. Effect of changing the drug: polymer ratio on loading capacity 176
5.9.4. Effect of changing polymer concentration on the loading capacity 178
5.9.5. Nano-aggregate characterization 180
5.9.6. Drug release 181
5.9.7. Formulation Stability 182
5.9.8. Detection of the PAA-ch5-FA toxicity 183
5.9.9. Cytotoxicity of the Navitoclax-PAA-Ch5-FA versus navitoclax 185
5.9.10. Caspase 3/7 assay 188
5.9.11. Drug uptake 189
5.9.12. Combination assays 191
5.9.13. Competition assay 201
5.10. Discussion 203
5.11. Conclusion 211

Chapter 6. Conclusion and future work 212
6.1. Conclusion 213
6.2. Future work 217

References 219

Appendices 219
Appendix A 219
Appendix B 219

List of figures

Figure 1.1: Ovarian cancer incidence worldwide. 4
Figure 1.2: Different Types of Ovarian Cancers according to their Origin 8
Figure 1.3: Epithelial ovarian cancer types 10
Figure 1.4: 5-year survival rate for epithelial ovarian cancer related to FIGO stage, US, 2004-2010. 12
Figure 1.5: Mechanism of action of carboplatin 21
Figure 1.6: Mechanism of action of paclitaxel 25
Figure 1.7: Palmar-plantar erythrodysesthesia syndrome 26
Figure 1.8: Mechanisms of drug resistance 28
Figure 1.9: The BCL-2 family of proteins 31
Figure 1.10: Regulation of apoptosis by the Bcl-2 family. 34
Figure 1.11: Schematic representation of block copolymers with different architectures. 39
Figure 1.12: PCL-PEEP star-shaped copolymer. 41
Figure 1.13: Basic structure of dendrimer 42
Figure 1.14: Schematic presentation of comb shaped polymer 44
Figure 1.15: EPR effect and how NPs migrate to cancerous cells 47
Figure 2.1: Ovarian cancer cell lines that were applied. (A): OVCAR-8. (B): OVSAHO 59
Figure 2.2: The self-assembly of PAA-ch$_5$ with the hydrophobic drug 60
Figure 2.3: Schematic presentation of the freeze dryer machine 67
Figure 2.4: The mechanism of action of SRB dye assay 67
Figure 2.5: (A) Caspase-3/7 cleavage of the luminogenic substrate containing the DEVD sequence. (B) Caspase-3/7 assay procedure. 68
Figure 2.6: Mechanism of action of BCA assay 72
Figure 2.7: mechanism of action for annexin V/PI staining. 75
Figure 2.8: Schematic representation for the 12-well plate that was applied to conduct folic acid competition assay 76
Figure 3.1: Critical micelle and concentration and surface concentration 85
Figure 3.2: Schematic figure of the sonication machine 87
Figure 3.3: (A) Zetasizer machine. (B) Schematic diagram of how PCS machine works. 89
Figure 3.4: (A) schematic diagram of HPLC (Czaplicki, 2013). (B) RP-HPLC machine 91
Figure 3.5: Navitoclax and PAA-ch$_5$ water solubility detection by HPLC 93
Figure 3.6: Navitoclax standard curve construction 94
Figure 3.7: Quantification of encapsulated navitoclax inside the PAA-ch$_5$ core 96
Figure 3.8: Effect of drug ratio on navitoclax encapsulation 97
Figure 3.9: Effect of changing PAA-ch$_5$ concentration on navitoclax encapsulation 99
Figure 3.10: The physical characteristics for both the polymer alone and the navitoclax-PAA-ch$_5$. 100
Figure 3.11: Navitoclax release from PAA-ch5 core 101
Figure 3.12: Physical stability for navitoclax nanoparticles with PAA-ch$_5$ polymer 103

Figure 3.13: Schematic presentation of the navitoclax encapsulation in the core of the PAA-ch$_5$ core to form a polymeric micelle 105
Figure 3.14: Schematic presentation of both (A) PAA-ch$_5$ alone (B) Navitoclax-PAA-ch$_5$ 106
Figure 4.1: Some BH3 mimetic drugs chemical structures. 123
Figure 4.2: Mitochondrial priming model 130
Figure 4.3: Morphological appearance of OVCAR-8 cells treated with PAA-ch$_5$ 135
Figure 4.4: Morphological appearance of OVSAHO cells treated with PAA-ch$_5$ 135
Figure 4.5: SRB assay for PAA-ch$_5$ on OVCAR-8 and OVSAHO 136
Figure 4.6: SRB assay for PAA-ch$_5$ on media 136
Figure 4.7: PAA-ch$_5$ cytotoxicity using trypan blue assay 137
Figure 4.8: Morphological appearance of both OVCAR-8 and OVSAHO after being treated with NP(N) and free navitoclax 139
Figure 4.9: Cytotoxicity of Navitoclax on OVCAR-8 and OVSAHO using SRB assay 139
Figure 4.10: Cytotoxicity of NP(N) and Navitoclax on OVCAR-8 and OVSAHO using trypan blue assay 140
Figure 4.11: Cytotoxicity of NP(N), Navitoclax, and PAA-ch$_5$ on OVCAR-8 and OVSAHO using caspase 3/7 assay 142
Figure 4.12: Navitoclax uptake for OVCAR-8 and OVSAHO after NP(N) and navitoclax administration in different time frames 143
Figure 4.13: Cytotoxicity of carboplatin on OVCAR-8 and OVSAHO using SRB assay 144
Figure 4.14: Morphological appearance of OVCAR-8 cells treated with several drugs combinations 145
Figure 4.15: Morphological appearance of OVSAHO cells treated with several drug combinations 145
Figure 4.16: The effect of Navitoclax-PAA and navitoclax alone when given in combination with carboplatin on OVCAR-8 using trypan blue assay 146
Figure 4.17: The effect of Navitoclax-PAA and navitoclax alone when given in combination with carboplatin on OVSAHO using trypan blue assay 147
Figure 4.18: The effect of Navitoclax-PAA and navitoclax alone when given in combination with carboplatin on (A) OVCAR-8 and (B) OVSAHO using caspase 3/7 assay 148
Figure 4.19: Effect of several drug combinations with carboplatin on PARP cleavage using western blot assay 150
Figure 4.20: Flow-cytometry images for different drug combinations 152
Figure 4.21: Relative Annexin V/PI activity for OVCAR-8 using several drug combinations 152
Figure 4.22: Cellular apoptosis for OVCAR-8 using several drug combinations using annexin V/PI assay 153
Figure 4.23: Interference between SRB dye and the high PAA-ch$_5$ concentrations 156
Figure 5.1: Active targeting using different moieties and molecules 166
Figure 5.2: Receptor mediated endocytosis mechanism 167
Figure 5.3: Normal and cancer apical surfaces distribution of folic acid receptors .. 169
Figure 5.4: PAA-ch$_5$-FA water solubility detection by HPLC 174

Figure 5.5: Quantification of encapsulated navitoclax inside the PAA-ch$_5$-FA core. 176
Figure 5.6: Effect of increasing (drug: polymer) ratio on navitoclax encapsulation.. 177
Figure 5.7: Effect of changing PAA-ch$_5$-FA concentration on navitoclax encapsulation 179
Figure 5.8: The physical characteristics for both the polymer alone and the navitoclax-PAA-ch$_5$-FA 180
Figure 5.9: Navitoclax release from PAA-ch5-FA core. 181
Figure 5.10: Physical stability for navitoclax nanoparticles with PAA-ch$_5$-FA polymer 183
Figure 5.11: Morphological appearance of OVCAR-8 cells treated with PAA-ch$_5$-FA 184
Figure 5.12: Morphological appearance of OVSAHO cells treated with PAA-ch$_5$-FA 184
Figure 5.13: PAA-ch$_5$-FA cytotoxicity using trypan blue assay 185
Figure 5.14: Morphological appearance of both OVCAR-8 and OVSAHO after being treated with NPF(N) and Navitoclax 186
Figure 5.15: Cytotoxicity of NPF(N) and Navitoclax on OVCAR-8 and OVSAHO using trypan blue assay 187
Figure 5.16: Cytotoxicity of NPF(N), Navitoclax, and PAA-ch$_5$-FA on OVCAR-8 and OVSAHO using caspase 3/7 assay 189
Figure 5.17: Navitoclax uptake for OVCAR-8 and OVSAHO after NPF(N) and navitoclax administration in different time frames 190
Figure 5.18: Morphological appearance of OVCAR-8 cells treated with several drugs combination 191
Figure 5.19: Morphological appearance of OVSAHO cells treated with several drugs combination 192
Figure 5.20: The effect of Navitoclax-PAA-ch5-FA and navitoclax alone when given in combination with carboplatin on OVCAR-8 using trypan blue assay 193
Figure 5.21: The effect of Navitoclax-PAA-ch5-FA and navitoclax alone when given in combination with carboplatin on OVSAHO using trypan blue assay 194
Figure 5.22: The effect of Navitoclax-PAA and navitoclax alone when given in combination with carboplatin on OVCAR-8 using caspase 3/7 assay 195
Figure 5.23: The effect of Navitoclax-PAA and navitoclax alone when given in combination with carboplatin on OVSAHO using caspase 3/7 assay 196
Figure 5.24: Effect of several drug combinations with carboplatin on PARP cleavage using western blot assay 198
Figure 5.25: Flow-cytometry images for different drug combinations 200
Figure 5.26: Relative Annexin V/PI activity for OVCAR-8 using several drug combinations 200
Figure 5.27: Cellular apoptosis for OVCAR-8 using several drug combinations using annexin V/PI assay 201
Figure 5.28: Cytotoxicity of Folic acid on OVSAHO using SRB assay 202
Figure 5.29: *The* effect of folic acid addition when given in combination with several drugs on OVSAHO using Trypan blue assay 203

List of tables

Table 1–1: Main symptoms reported in ovarian cancer women presenting to the primary care units.....6
Table 1–2: FIGO staging and prognosis of ovarian cancer.....13
Table 2–1: The list of materials that were used in all experiments and the supplier's names.....56
Table 2–2: Ovarian cancer cell lines used in our project and their origin.....58
Table 2–3: Drugs with their final concentrations that were used in caspase 3/7 assay.....68
Table 3–1: The effect changing navitoclax ratios on navitoclax loading capacity and encapsulation efficacy.....97
Table 3–2: The effect changing PAA-ch_5 concentration on navitoclax loading capacity and encapsulation efficacy.....99
Table 4–1: Small molecules that inhibit the BCL-2 family (BH3 mimetics) and their targets.....124
Table 5–1: The effect changing navitoclax ratios on navitoclax loading capacity and encapsulation efficacy.....177
Table 5–2: The effect changing PAA-ch_5-FA concentration on navitoclax loading capacity and encapsulation efficacy.....179

Abbreviations

ADCC	Antibody-dependent cellular cytotoxicity
AML	Acute myelocytic leukemia
AUC	Area under the curve
BAD	BCL-2 associated death promoter
BAK	BCL-2 antagonist killer 1
BAX	BCL-2 associated X protein
BCA	Bicinchoninic acid Protein assay
BCL-2	B-cell lymphoma protein 2
BCL-X_L	BCL-2 related protein, long isoform
BH3 mimetics	B-cells homology 3 mimetics
BID	BH-3 interacting domain death agonist
BIM	BCL-2 interacting protein
BMF	BCL-2-modifying factor
BNIPDaoct	Bisnaphthalimidopropyldiaaminooctane
BRCA	Breast cancer gene
BSA	Bovine serum albumin
BSO	Bilateral salpingo-oophorectomy
CA-125	Cancer antigen 125
CAC	Critical aggregation concentration
Caspase	Cysteinyl aspartic acid-protease
CBC	Complete blood count
CDC	Complement-dependent cytotoxicity
Ch_5	Cholesteryl group with 5% molar grafting
CLL	Chronic lymphocytic leukaemia
CsA	Cyclosporine A
Dansyl	Dimethylamino- 1-naphthalenesulfonyl
DAVLBH	Desacetyl vinblastine monohydrazide
DIT	Drug-induced thrombocytopenia
DLS	Dynamic light scattering
DMSO	Dimethyl sulfoxide

DOX	Doxorubicin
DSB	Double-strand break
EE	Encapsulation efficiency
EOC	Epithelial ovarian cancer
EPR	Enhanced permeability and retention
FA	Folic acid
FBS	Fetal bovine serum
FDA	Food and drug administration
FIGO	International Federation of Gynecology and Obstetrics
FL	Follicular lymphoma
fmoc	9-fluorenylmethoxy
FR	Folate receptor
FRA	Folate receptor alpha
GAPDH	Glyceraldehyde-3-phosphate dehydrogenase
GIT	Gastro-intestinal tract
GPI	Glycosylphosphatidyl-inositol
HA	Hyaluronic acid
HE-4	Human Epididymis Protein 4
HGSOC	High-grade serous ovarian carcinoma
HNPs	Hybrid nanoparticles
HR	Homologous recombination
G.C.	Gas chromatography
GOG	Gynaecologic Oncology Group
HPLC	High-performance liquid chromatography
IAPs	Inhibitor of apoptotic proteins
IBS	Irritable bowel syndrome
IC_{50}	Half maximal inhibitory concentration
IEC	Ion exchange chromatography
IL-6	Interleukin-6
IL-8	Interleukin-8
LC	Loading capacity

L.C.	Liquid chromatography
LPA	Lysophosphatidic acid
M-CSF	Macrophage colony-stimulating factor
MAP-1	Modulator of apoptosis 1
MDR	Multidrug resistance
µM	Micromolar
MOMP	Mitochondrial outer membrane permeabilization
MTT	3-(4,5-dimethylthiazol-2-yl)-2,5-diphenyltetrazolium bromide
mV	Millivolt
Naphth	Naphthalene
NAV	Navitoclax (ABT-263)
NIR-PIT	Near- infrared photoimmunotherapy
NP	Nanoparticles
NP(E)	Nanoparticles of PAA-ch_5 with no navitoclax inside
NP(N)	Nanoparticles of PAA-ch_5 with navitoclax inside
NPF(E)	Nanoparticles of PAA-ch_5-FA with no navitoclax inside
NPF(N)	Nanoparticles of PAA-ch_5-FA with navitoclax inside
NSCLC	Non-small cell lung carcinoma
OSE	Ovarian surface epithelium
PAA	Poly (allylamine)
PAMAM	Poly(amidoamine)
PARP-1	Poly (ADP-ribose) polymerase-1
PBS	Phosphate buffer saline
PCL	Poly(ε-caprolactone)
PCS	Photon correlation spectroscopy
PDI	Polydispersion index
PEEP	Poly (ethylethylene phosphate)
PEI	Polyethyeneimine

PFI	Platinum free interval
PGP	Poly-glycoproteins
PI	Propidium iodide
PLL	Poly (L-lysine)
PMSF	Phenylmethanesulfonyl fluoride
PPC	Primary peritoneal carcinoma
PPE	Palmar-plantar erythrodysesthesia
PTX	Paclitaxel
PVDF	Poly (vinylidene difluoride)
RIPA	Radioimmunoprecipitation assay
RPMI-1640	Roswell park memorial institute 1640 medium
RT	Room temperature
SCLC	Small cell lung carcinoma
Sct	Salmon calcitonin
sFRA	Serum folate receptor alpha
SMDC	Small molecule–drug conjugates
SRB	Sulforhodamine B
SURP	Super-enhanced permeability and retention
TAH	Total abdominal hysterectomy
TCA	Trichloroacetic acid
TLC	Thin-layer chromatography
TVUS	Transvaginal ultrasonography
UK	United Kingdom

Acknowledgment

In the beginning I would first thank God for being with me in my life and during my PhD. To start thanking people who have the main role to let me reach this point, I have to express my gratefulness to my lead supervisor Dr. Alan Richardson for everything during my Ph.D. study and it was really an honor to be of your students. You have been an incredible supervisor for me. I want to thank you for your support all over my 4-years PhD and for your help especially during the COVID-19 time. I really appreciate your patience, your support, and the great knowledge you served me with. Your comments, advices, and positive feedback reflected on me to let me grow as new scientist, and these comments helped me and will help in all my life as these four years are not more than a beginning in a new journey in my life. The special thanks to my second supervisor, Dr. Clare Hoskins who was more than a supervisor. I want to thank you for your help, support, and for everything and even after you left the university you kept in touch with me and supported me so words can't express how much am grateful for you. Special thanks to my sponsor, Hashemite university, Jordan for your support during my PhD journey and your cooperation. I would also thank Dr. Anthony Curtis for your help, your advices and you support. The lab technicians who were very supportive and were very kind and cooperative, Katey Cressey, John Misra, and Mark Arrowsmith. My special greetings to Dr. Ali Alsuraifi, Dr. Mohammed Jawad, Dr. Suad Ibraheem, Dr. Mohammed Abu Donia, Dr. Hamzeh Abu Owida, Dr. Hazmeh hmaidi, and Dr. Aseel Aburub, I want to thank you all for your support, your help during my PhD. I want to express my gratitude to my colleagues Dr.Idouw Fadayomi, Fatma Dogan, Tasmin Nahar, Vibin Alageswaran, Trisha Vikranth, and Gehad Iraqy. Most of all, I would like to express my very profound thanks to my mother, Wafaa, My Dad, Jamal and my lovely wife Ohood. I want to thank you all for your patience, your infinite support, your

encouraging, and your help during these years. I want to thank my wife who chose to stay with me during the COVID-19 pandemic and being away from our families. My angel, Naya, when you grow up, I hope you will have a time to read this as I sacrificed to spend enough time with you and play with you as I were busy in the lab or writing but what I want to say am so sorry and I really love you. Special thanks to my sister, Nadine, my brother, Mohammed, and my little sister, Rama, my brother-in-law, Musa, my little niece, Kady, my mother-in-law and my father-in-law, my aunts, and uncles, my friends and everyone who prayed for me and wished for me good luck. The PhD is not an easy journey, it was full of details and emotions, sadness and happiness, crying and laughs, frustrations and accomplishment so I want to thank God for being with me all over these times.

Khaled Alrosan

Chapter 1. Introduction

1.1. Introduction to ovarian cancer

Ovarian cancer is like other cancers, in which there is an abnormal and uncontrolled cellular growth on and nearby ovarian tissue. Dr Martin Swerdlow was the first who described ovarian cancer in 1959, as the mass he found was around the left fallopian tube, and it was believed that the origin of that mass was from a tissue that had a similar origin to the ovaries. Accordingly, by that time, it was named Müllerian adenocarcinomas as the exact origin was not known, but to make it simpler, it was named ovarian cancer (Mills and Fuh, 2017). Ovarian cancer is one of the four main gynaecological cancers, but unfortunately, this type of cancer has a high mortality compared with the other three types. The reason behind that is that most of the patients are diagnosed in late stages, which makes its management and treatment very complex (Toss *et al.*, 2013). Although there is a noticeable advancement in understanding ovarian cancer pathology, the survival rate remains low. Furthermore, drug resistance is also one of the leading causes responsible for low survival (Chien *et al.*, 2013). Hence, there is a need to increase awareness about this disease for both health care providers and female patients as the early diagnosis can improve the overall survival rate (Rooth, 2013) and also trying to understand the resistance mechanisms and develop new medications and treatment plans to overcome this aggressive type of cancer.

1.1.1. Epidemiology

Ovarian cancer is the seventh most common cancer in women (Brett M. *et al.*, 2017) and the third most common gynaecological cancer, coming after cervical and uterine cancer (Momenimovahed *et al.*, 2019). Unfortunately, ovarian cancer is the first most

lethal among other gynaecological tumours (Guarneri *et al.*, 2010) and the fifth cause of female cancer death (Mills and Fuh, 2017). In 2018, it affected 295,414 women with 184,799 death worldwide (Momenimovahed *et al.*, 2019). In the UK alone, it represents 4% of all cancers in women and affects 7443 new cases with 4182 deaths annually (*Ovarian cancer statistics* | *Cancer Research UK*, 2015). The median age of diagnosis is around 63 years, and 88% of patients are diagnosed at the age above 45 (Henderson *et al.*, 2018).

Although the 5-year survival has been improved from 30% to 46% for the past 40 years, unfortunately, it still has a very low 5-year survival which is due to the late diagnosis, which let the patients to reach late stages (stage III and IV). This is revealed by the percentage of the cases who are diagnosed in the late stages which exceeds 80% of cases (Mills and Fuh, 2017). Accordingly, in the late stages, the 5-year survival in stage IV has not exceeded 17% (Brett M. *et al.*, 2017; Mills and Fuh, 2017; Bhatla and Jones., 2018), and the median overall survival period is only 15-23 months (Diniz *et al.*, 2011).

Ovarian cancer is also characterised by a geographical variation with the highest prevalence of more than (8:100,000) cases in North America, Central, and East Europe, while the lowest prevalence is in Asia and Africa with less than (3:100,000) cases (Brett M. *et al.*, 2017), (Figure 1.1). Although there are similar risk factors between these countries, this variability happens due to various methods used in classification, staging and treatment regimens (Jessmon *et al.*, 2017). Of note, the race also has an important impact on ovarian cancer prevalence and mortality incidence (Brett M. *et al.*, 2017). The highest incidence is in non-Hispanic white women with

around (12 per 100,000) cases, and the lowest is in Asian and black women with around (9.3 per 100,000) cases (Peres *et al.*, 2018).

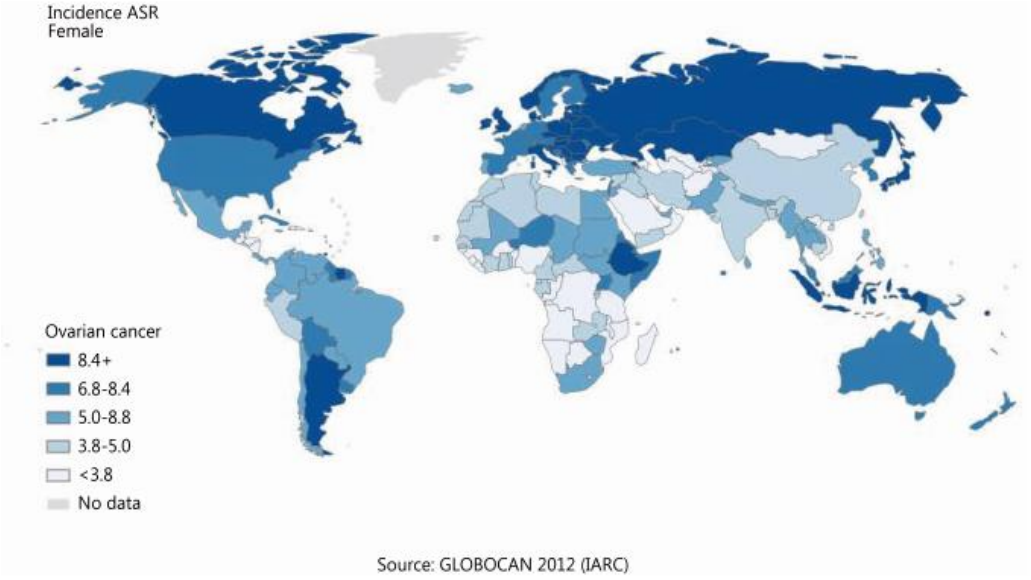

Figure 1-1: Ovarian cancer incidence worldwide *(*Brett M. *et al., 2017).*

1.1.2. Symptoms

Since ovarian cancer is characterised by delayed onset of symptoms, asymptomatic growth of the tumour, and the absence of adequate screening methods, all of these put ovarian cancer as a cause of high mortality rate (Momenimovahed *et al.*, 2019). As such, it is called a “silent killer” disease (Goff *et al.*, 2006; Gajjar *et al.*, 2012; Goff, 2012; Fathalla, 2013; Fotopoulou *et al.*, 2014; Fan *et al.*, 2016; Momenimovahed *et al.*, 2019). Although ovarian cancer screening is not recommended for all women (Goff *et al.*, 2006), there are common symptoms that must be taken into consideration, and these include pelvic and abdominal pain, urinary urgency and frequency, increase in abdominal size, bloating, difficulty eating and feeling full (Olson *et al.*, 2001; Goff *et al.*,

2006; GOFF, 2012; Al-naggar *et al.*, 2013; Fotopoulou *et al.*, 2014), (Table 1-1). Importantly, recent guidelines in the UK pointed out that, if these symptoms appear, in addition to abnormal vaginal bleeding or pelvic mass, and persistent of recent onset, there is a need to make investigations of ovarian cancer (Hamilton and Menon, 2010).

Herein, both physicians and patients must carefully notice if these symptoms happen more than 12 times per month in the year before (Goff *et al.*, 2006; Goff, 2012). This is an important indicator because it was found that 95% of patients had one symptom in the previous year of diagnosis, and 72% had recurring symptoms (Goff *et al.*, 2004). The obstacle of misdiagnosis depends not only on physicians but also on patients (Gajjar *et al.*, 2012; Goff, 2012). Physicians, in general, misdiagnose these symptoms and confuse them with irritable bowel syndrome (IBS) (Bankhead *et al.*, 2008; Goff, 2012), stress, and gastritis (Goff, 2012). Furthermore, ovarian cancer is rare, which explains why general practitioners meet on average only one case every five years (Gajjar *et al.*, 2012). On the other hand, patients do not think that these symptoms are severe (Goff, 2012). Moreover, they may believe that they are wasting the physician's time with apparently minor symptoms, and they do not realise the potential severity of the situation, especially if added to other risk factors, such as age. Unluckily, these patients, who have these thoughts, represent one-third of the people in the UK (Bhatla and Jones., 2018).

Table 1-1: Main symptoms reported in ovarian cancer women presenting to the primary care units (Goff *et al.*, 2004).

Symptoms	Frequency
Back pain	45%
Fatigue	34%
Bloating	27%
Constipation	24%
Abdominal pain	22%
Urinary symptoms	16%

1.1.3. Risk Factors

The term “Risk factor” refers to anything that increases the chance of developing a disease. Nevertheless, even if patients have many risk factors, this does not necessarily mean that they will get the disease (American Cancer Society, 2016). Ovarian cancer is a heterogeneous disease, and its heterogeneity is represented by differences in somatic and germline mutations, chemotherapy responsiveness, gene expression, and risk factors (Lu *et al.*, 2015). Ovarian cancer, like other diseases, has common risk factors and several theories link ovarian cancer with certain conditions. These conditions are continuous ovulation, an increment in gonadotropin, and an imbalance of estrogen and progesterone (Rooth, 2013). The common risk factors that have a high linkage with ovarian cancer incidence are a family history of ovarian cancer and germline mutations, hormone replacement therapy (HRT), reproductive-history related factors, age (Sundar *et al.*, 2015), in addition to obesity, and smoking

(McLemore *et al.*, 2009; Doubeni *et al*., 2016; Brett M. *et al.*, 2017; Momenimovahed *et al.*, 2019). Although statistical analysis showed that ovarian cancer could be reduced by 33-40% by decreasing risk factors, unfortunately, it is predicted that incidence and mortality rates will increase dramatically after fifteen to twenty years (Bhatla and Jones., 2018; Momenimovahed *et al.*, 2019).

1.1.4. Aetiology

The aetiology of ovarian cancer is still poorly understood. Various hypotheses have been suggested to explain ovarian cancer aetiology. These are the incessant ovulation hypothesis, the inflammation hypothesis, the androgen/progesterone hypothesis, and the gonadotropin hypothesis (Choi *et al.*, 2007), in addition to the tubal origin hypothesis, which is the most recent hypothesis (Kurman, 2018). Yet, there is no scientific consensus.

1.1.5. Types

As ovarian tissue is composed of three main types of cells: surface epithelial cells, germ cells, and stromal cells. As such, the ovarian cancer can present in various forms that depend on the type of cell it originates from (American cancer society, 2018). In addition, ovarian cancer can originate from different origin such as the fallopian tube, as discussed before. Although there are more than thirty types of ovarian cancer, ovarian cancer is classified into three main categories based on their anatomical structural origin: surface epithelial-stromal tumours, sex cord-stromal tumours, and germ cell tumours (Types & Stages - National Ovarian Cancer Coalition, 2020), (Figure

1.2). This classification is critical because each type has its own characteristics of how it spreads, diagnosed and treated (American cancer society, 2018).

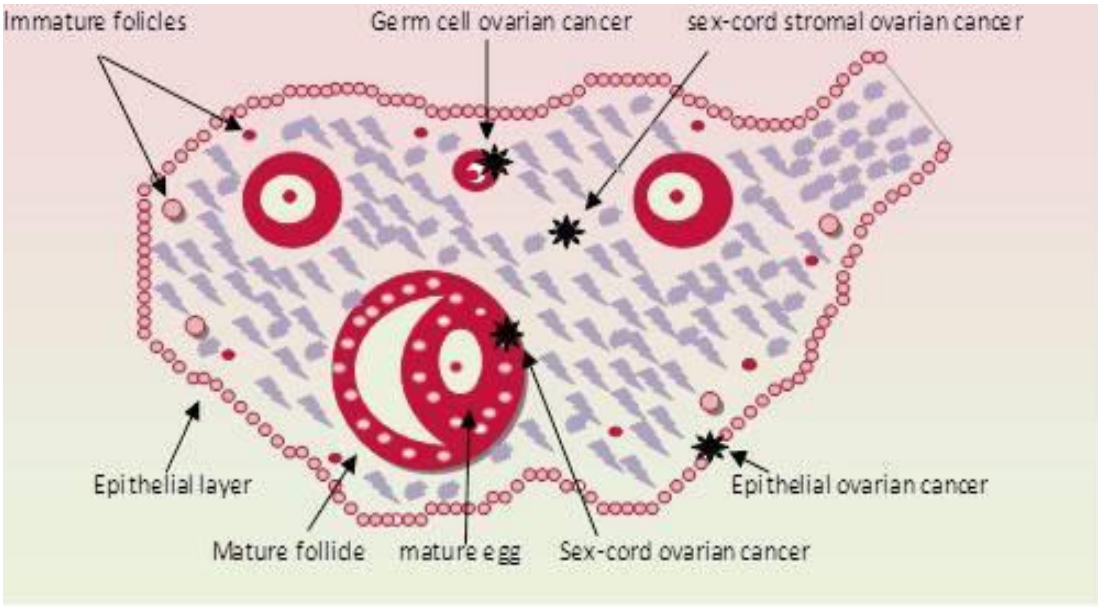

Figure 1-2: Different Types of Ovarian Cancers according to their Origin (Janbaz *et al.*, 2013).

1.1.5.1. Surface Epithelial-Stromal Tumours

The epithelium layer that covers ovaries is similar histologically to the one that covers the abdominal and pelvic cavities. It has been suggested that surface epithelial-ovarian cancers (EOC) originate from the ovarian surface epithelium (OSE). These cancers are classified based on their invasiveness as benign, borderline, and malignant. They account for 60% of all ovarian cancer types and 90% of malignant ovarian cancer (Chen et al., 2003; Modepalli and Venugopal, 2016).

A dualistic model divides epithelial ovarian cancer into two main groups, type I, and type II tumours, depending on molecular and morphological studies. Type I include

low-grade types, which are confined to one ovary, and genetically stable. They are associated with different mutations such as *KRAS, PTEN, BRAF*, which all result in morphological changes as they start as benign tumours which are non-invasive and finally become low-grade carcinoma. On the other side, type II tumours, including the high-grade types, are aggressive types and present in late stages (Kurman, 2018; Gadducci *et al.*, 2019). Furthermore, type II tumours are genetically unstable compared with type I (Kurman, 2018). Also, type II tumours have *TP53* gene mutation, while type I have other mutations, as mentioned before (Diniz *et al.*, 2011; Gadducci *et al.*, 2019), (Figure 1.3). Unfortunately, the aggressiveness of type II is reflected in the 5-year survival, which is achieved by only 30% of patients, while in type I, it reaches 55% of patients (Henderson *et al.*, 2018).

The surface epithelial-stromal group is divided into five major subtypes: mucinous (5–20%), clear cell (3–10%), serous (30–70%), endometrioid (10–20%), and undifferentiated (1%) (Rosen *et al.*, 2009). The most common histological type of epithelial Ovarian cancer is the high-grade serous ovarian carcinoma (HGSOC), representing 75% of all types (Labidi-galy *et al*., 2017), and responsible for 70-80% of ovarian cancer death (Bowtell *et al.*, 2015). Although HGSOC was originally thought to be of ovarian epithelial origin, there is an emerging theory that it originates in the fallopian tube, particularly the dysplastic lesions of the fallopian tube's distal part (Diniz *et al.*, 2011; Erickson *et al*. 2013). Importantly, it was reported that whereas the *TP53* mutations, which happens in the early stage, is prevalent in almost all cases of HGSOC, the Breast cancer gene (*BRCA*) mutation is also responsible for about 20% of cases (Tone *et al*., 2012; Fuh and Mills, 2017; Hirst *et al*., 2018).

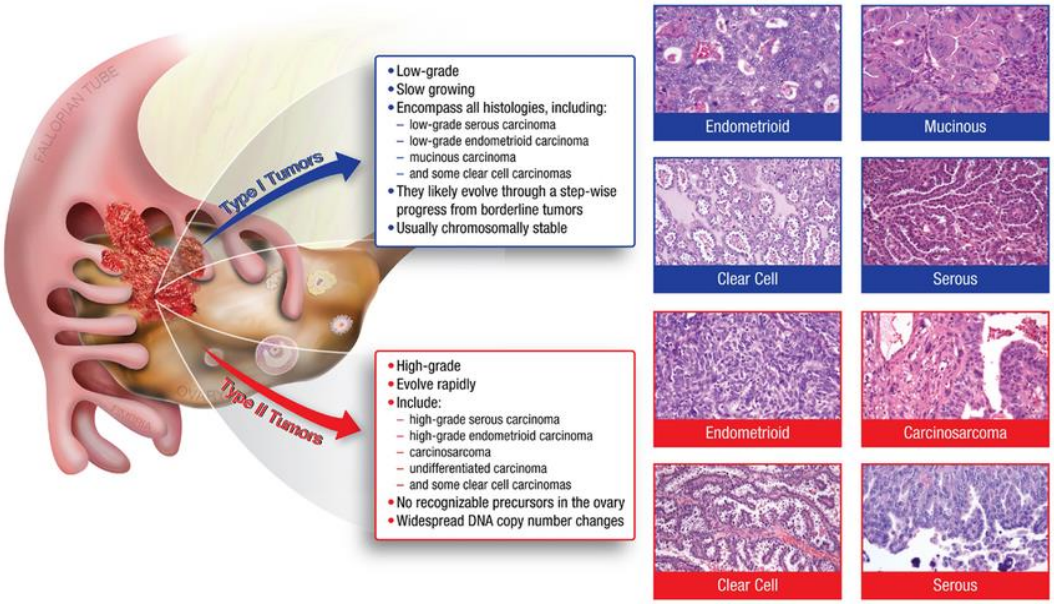

Figure 1-3: Epithelial ovarian cancer types (Jones and Drapkin, 2013).

1.1.5.2. Sex Cord-Stromal Tumours

Sex cord-stromal tumours include tumours of mesenchymal and mesonephric origin. These cancers, which possess a fibrous appearance, are rare types, affect young adults, and it was believed that they originate from the primitive sex cords or stromal cells (Horta and Cunha, 2015). Since these cells are involved in the steroid hormones production (estrogens, corticoids, and androgens), the most common symptom of this tumour is vaginal bleeding, body and facial hair grow as this type of tumour can produce male hormones (American cancer society, 2018). This type accounts for 8% of all ovarian cancer cells and 7% of malignant ovarian cancer (Horta and Cunha, 2015). The most common subtypes are Sertoli-Leydig cell tumours and granulosa-theca tumours (Types & Stages - National Ovarian Cancer Coalition, 2020).

1.1.5.3. Germ Cell Tumours

Germ cell tumours are believed to originate from primordial germ cells, which are the reproductive ovary cells. As in sex cord-tumour cancers, they mainly affect young adults and children. The symptoms of this type appear as a palpable mass with abdominal pain (Low *et al*., 2012). These tumours represent 25% of all ovarian tumours and 3–7% of malignant ovarian cancer (Chen *et al*., 2003). They have several subtypes, such as choriocarcinomas, endodermal sinus tumours, dysgerminomas, and teratoma (Goyal *et al.*, 2019). Fortunately, this type is associated with a good prognosis and can be cured (American cancer society, 2018). Notably, this type differs from epithelial-stromal tumours as they affect a large proportion of patients in Asia and Africa where the prevalence is low for epithelial-stromal tumours (Chen *et al.*, 2003).

There is another uncommon type of tumour related to ovarian cancer named primary peritoneal carcinoma (PPC). Although PPC possesses similar histological and clinical characteristics to epithelial ovarian cancer, there is an epidemiological and molecular difference between them. Despite several criteria that have been determined by the gynaecologic oncology group (GOG) in defining PPC, the treatment plan is the same as performed in EOC with surgery and platinum-based chemotherapy (Hattori *et al*., 2016; American cancer society, 2018).

1.1.6. Staging of ovarian cancer

As the detection of ovarian cancer mostly happens at an advanced stage and unfortunately, the percentage of patients who are diagnosed in the early stage represents only 15% of all patients (Mills and Fuh, 2017), and hence, this may lead to

the development of an extra-ovarian disease (Taylor and Gercel-Taylor, 2008). Furthermore, the overall 5-year survival rate does not exceed 40% worldwide and this rate did not improve significantly in the last 15 years (Brett M. *et al.*, 2017). Altogether, and since there is a close relationship between stage at presentation and survival (Rauh-hain *et al.*, 2011), early diagnosis is very important for improving overall survival (Brett M. *et al.*, 2017), (Figure 1.4).

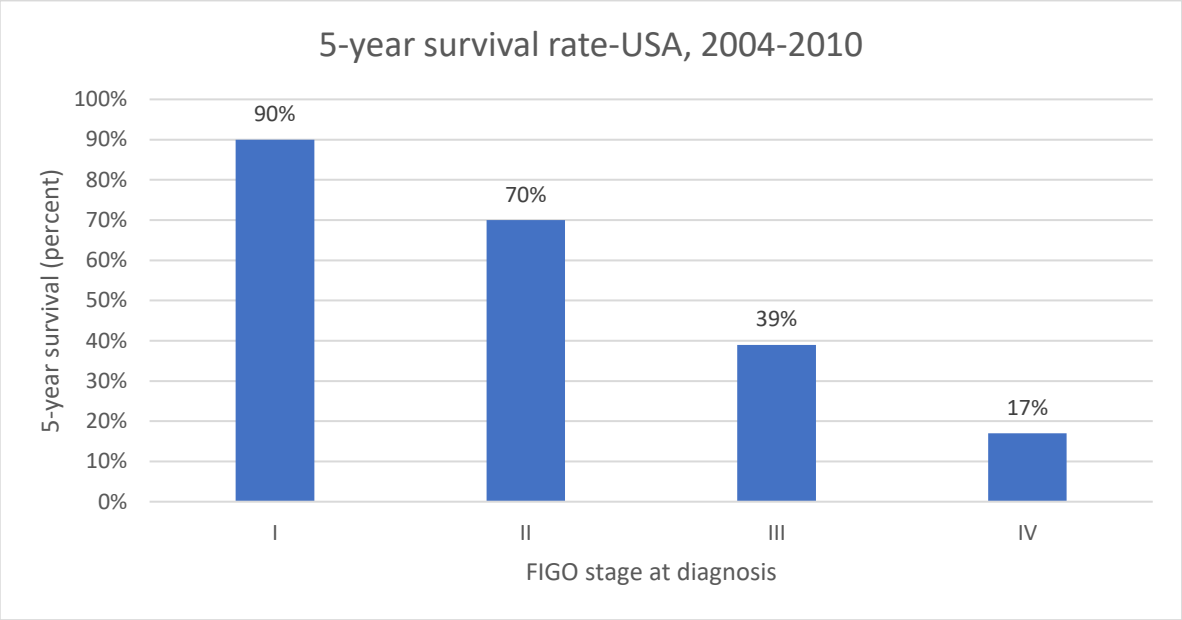

Figure 1-4: 5-year survival rate for epithelial ovarian cancer related to FIGO stage, US, 2004-2010 (Bhatla and Jones., 2018).

The international federation of gynecology and obstetrics (FIGO) is the first association that developed a staging system of gynaecologic cancer. Since 1958, it has been responsible for publishing the annual report for any changes and updates in staging and classifications for all gynaecological cancers (Kim and Song, 2009). The FIGO staging system that is used nowadays comprises ovarian cancer and combines it with

peritoneal and fallopian tube cancers (Zeppernick and Meinhold-heerlein, 2014). Table (1-2) represents the FIGO staging classification for cancer of the ovary, peritoneum, and fallopian tube.

Since most ovarian tumours are not cancerous, it is necessary for a definitive diagnosis, which determines what type of surgery to be performed (laparotomy or laparoscopy). In addition, accurate staging is very crucial in prognosis as well as in the determination of the treatment of choice (Berek *et al*., 2018).

Table 1-2: FIGO staging and prognosis of ovarian cancer *(*Berek *et al.*, 2018*).*

STAGE	CHARACTERISTICS
I	Tumour confined to ovaries or fallopian tube(s)
IA	Tumour limited to one ovary (capsule intact) or fallopian tube; no tumour on ovarian or fallopian tube surface; no malignant cells in the ascites or peritoneal washings
IB	Tumour limited to both ovaries (capsules intact) or fallopian tubes; no tumour on ovarian or fallopian tube surface; no malignant cells in the ascites or peritoneal washings
IC	Tumour limited to one or both ovaries or fallopian tubes, with any of the following:
IC1	Surgical spill

IC2	Capsule ruptured before surgery or tumour on the ovarian or fallopian tube surface
IC3	Malignant cells in the ascites or peritoneal washings
II	A tumour involves one or both ovaries or fallopian tubes with pelvic extension or peritoneal cancer
IIA	Extension and/or implants on the uterus and/or fallopian tubes and/or ovaries
IIB	Extension to other pelvic intraperitoneal tissues
III	Tumour involves one or both ovaries or fallopian tubes, or peritoneal cancer, with cytologically or histologically confirmed spread to the peritoneum outside the pelvis and/or metastasis to the retroperitoneal lymph nodes
IIIA1	Positive retroperitoneal lymph nodes only (cytologically or histologically proven):
IIIA1(i)	Metastasis up to 10 mm in greatest dimension
IIIA1(ii)	Metastasis more than 10 mm in greatest dimension
IIIA2	Microscopic extra-pelvic (above the pelvic brim) peritoneal involvement with or without positive retroperitoneal lymph nodes
IIIB	Macroscopic peritoneal metastasis beyond the pelvis up to 2 cm in greatest dimension, with or without metastasis to the retroperitoneal lymph nodes

IIIC	Macroscopic peritoneal metastasis beyond the pelvis more than 2 cm in greatest dimension, with or without metastasis to the retroperitoneal lymph nodes (includes an extension of tumour to the capsule of liver and spleen without parenchymal involvement of either organ)
IV	Distant metastasis excluding peritoneal metastases
Stage IVA	Pleural effusion with positive cytology
Stage IVB	Parenchymal metastases and metastases to extra-abdominal organs (including inguinal lymph nodes and lymph nodes outside of the abdominal cavity

1.1.7. Diagnosis

Since it has been reported that most of cases are diagnosed in late stages, it has been demonstrated that 60% of patients have metastatic disease (Sundar *et al.,* 2015; Doubeni *et al.*, 2016). Additionally, some patients may present with paraneoplastic syndrome (Doubeni *et al.*, 2016). This emphasises the need for a precise and early diagnosis. Initially, a detailed medical history must be taken from the patients and a knowledge of the family history of ovarian cancer and other cancers (Doubeni *et al.*, 2016; Berek *et al.*, 2018). Patients who have symptoms should undergo a physical examination, transvaginal ultrasonography (TVUS), and measurement of cancer antigen 125 (CA-125) (Sundar *et al.*,2015). Furthermore, there must also be a

measurement of complete blood count (CBC), blood chemistry, liver function, and calcium level to detect the paraneoplastic syndrome (Doubeni *et al.*, 2016; Smith, 2017).

.

Unfortunately, application of CA-125 is not considered the perfect choice for ovarian cancer diagnosis because of the several drawbacks this antigen possesses such as low sensitivity of CA-125 alone as it does not exceed 80% (Jelovac and Armstrong, 2011; Doubeni *et al*., 2016; Khiewvan *et al.*, 2017). Furthermore, it has poor selectivity, because it can increase in several, mostly benign, conditions such as endometriosis and menstruation (Sundar *et al*., 2015; Doubeni *et al*., 2016; Khiewvan *et al.*, 2017), pregnancy, and pelvic inflammation (Smith, 2017), which can give false-positive results. In addition to these disadvantages, this marker only increases by 50% in the early stages of the disease, making it unreliable for early detection purposes. Therefore, there was a need to find additional markers and use a panel of biomarkers to detect ovarian cancer, which can help achieve a higher sensitivity (Das and Bast Jr, 2008). There are new biomarkers have been developed, such as Human Epididymis Protein 4 (HE-4), which is more sensitive and not elevated in benign conditions (Sundar *et al*., 2015; Doubeni *et al*., 2016). Other biomarkers include Mesothelin (SMRP), Kallikriens (KLKs), Osteopontin, Lysophosphatidic acid (LPA), OVX1 in combination with macrophage colony-stimulating factor (M-CSF), interleukin-6 (IL-6) and interleukin-8 (IL-8) (Das and Bast Jr, 2008), and serum folate receptor alpha (sFRA) (Kurosaki *et al.*, 2016).

1.2. Treatment

Although there is an advancement in science and treatments, the mortality rate of ovarian cancer is still high worldwide. The standard treatment for women with ovarian cancer consists of histopathological diagnosis and staging (Hiss, 2012), followed by cytoreductive surgery and chemotherapy cycles of platinum and taxanes (Hiss, 2012; Sato and Itamochi, 2014; Van de Laar *et al.*, 2014). Herein, the choice relies on several factors such as stage, grade, type, and general health (Tapia and Diaz-padilla, 2013). Notably, the goal of ovarian cancer treatment can change in some cases, as if recurrence happens, the goal will be shifted from curative to palliative and to control symptoms in parallel with the improvement in the quality of life (Ozols, 2005). For patients diagnosed in the late stages of the disease, the primary goal of therapy is also shifted to extend the progression-free survival and overall survival (Foster *et al.*, 2009).

1.2.1. Surgery

Surgery plays a pivotal role in diagnosis, staging, and treatment (Hoskins, 1993; Vinotha *et al.*, 2016; Gadducci *et al.*, 2019). Despite the improvement in chemotherapy and biological treatment (Ramirez *et al.*, 2011), surgery is still considered one of the best choices for ovarian cancer patients and it achieves better curative results, especially in the early stages (Trimbos *et al.*, 2010). Several types of surgeries are applied in ovarian cancer management such as total abdominal hysterectomy (TAH) (removal of the uterus) and bilateral salpingo-oophorectomy (BSO) (removal of both ovaries) (Gubbels *et al.*, 2010; *Types of surgery* | *Ovarian cancer* | *Cancer Research UK*, 2016). During surgery, it is necessary to wash the peritoneal cavity using saline to get rid of cancer cells, take biopsies to determine the stage, spread of cancer, and a

need for chemotherapy (Rodriguez *et al.*, 2013). Of note, when surgery has to be performed, childbearing women need to be considered, as if there is a chance to preserve the unaffected ovary and uterus for future pregnancies. This can be carried out by doing conservative surgery such as unilateral salpingo-oophorectomy (Low *et al.*, 2012; Ledermann *et al.*, 2014).

In the early stage, surgery can often remove most of the tumour, while in the late stages, the goal of surgery is removal as much as the surgeon can (Martín-Cameán *et al.*, 2016). Moreover, surgery in the advanced stages has to be combined with chemotherapy which can be given before (neoadjuvant) or after surgery (adjuvant), where better results can be achieved (Hartnett *et al*., 2016). This type of surgery is called debulking or cytoreduction (Martín-Cameán *et al.*, 2016). Optimal cytoreduction was defined as a residue of less than one centimetre after completion of the surgery (Gómez-hidalgo *et al.*, 2015). The optimal debulking term has changed over the years and the definite complete debulking nowadays means not keeping any visible residual tumour, even less than one centimetre, as it is related to poor prognosis and survival rates. Optimal debulking has many advantages, as it was found that wholly debulked patients achieved 45.2 months overall survival, while in incomplete resection, they achieved 19.7 months in overall survival (Cortez *et al.*, 2018). In addition, Kampan *et al.* (2015) stated that for every 10% increment in optimal cytoreduction, there would be an increment in overall survival by 5.5% (Kampan *et al.*, 2015). Also, optimal debulking achieved a 28% decrease in risk for relapse and a 33% decrement in death compared with suboptimal resection (Zivanovic *et al.*, 2010).

In case of metastasis, surgery may also remove parts of the colon, bladder, and stomach (*Types of surgery | Ovarian cancer | Cancer Research UK*, 2016). For the surgery option, although it is apparently curative in 70% of cases (Gadducci *et al.*, 2019), most of the patients relapse within 24 months even after optimal cytoreductive surgery and chemotherapy (Giornelli, 2016).

1.2.2. Chemotherapy

The past thirty years have shown developments in the treatment regimen for advanced ovarian cancer (Jain and Meyer-Hermann, 2011; Luvero *et al.,*2014). The strategy to treat ovarian cancer consists of several chemotherapeutic agents and different combinations that have been used to improve overall survival, clinical response and to decrease their side effects (Pokhriyal *et al.*, 2019). Successful clinical trials have led to the dual regimen of platinum and taxanes, specifically paclitaxel and carboplatin (Bauerschlag *et al.*, 2007; Mikuła-Pietrasik *et al.*, 2018). This regimen became the standard treatment of ovarian cancer, “golden standard”, which is usually preceded by surgical cytoreduction to give better results (Mikuła-Pietrasik *et al.*, 2018). This regimen must be confined to the late stages, not early ones, as the early stages have a good prognosis, and chemotherapy in these stages has no advantage in improving overall survival as discussed before (Dinkelspiel *et al.*, 2015). Although the response rate to this regimen is relatively high (60-80%) (Jensen *et al.*, 2013) and although this regimen achieves improvements in both overall survival and progression-free survival (Piccart, 2000; Pinato *et al.*, 2013; Oliver and McGuire, 2014), it has been found that 75% of patients relapse due to the development of chemotherapy resistance (Dasari and Tchounwou, 2014). Resistance is one of the most common causes of treatment failure,

and as some patients develop resistance, others have tumours that are intrinsically resistant to chemotherapy (Jain and Meyer-Hermann, 2011; Pinato *et al.*, 2013; Luvero *et al.,* 2014).

1.2.2.1. Platinum compounds

Cisplatin (Platinex®), Carboplatin (Carboplat®), and oxaliplatin (Eloxatin®) belong to a platinum family of chemotherapeutic agents. New platinum-based agents have been approved recently in single markets, such as lobaplatin in China, nedaplatin and miriplatin in Japan, and heptaplatin in Korea (Oun *et al*., 2018). Platinum anticancer drugs are approved for the treatment of various types of tumours (Amptoulach and Tsavaris, 2011; Eckstein, 2011; Jensen *et al.*, 2013; Bruno *et al.*, 2017), such as ovarian cancer, non-small lung cancer, testicular cancer, bladder, head and neck, and cervical cancer (Cimino *et al.,* 2013). The mechanism of action of platinum-based chemotherapy involves several steps, starting with activation and aquation, followed by reacting with N7 positions in purine bases of DNA strands, which makes intra- and inter-strand crosslink in DNA. This prevents DNA from being replicated and inhibits gene expression. Consequently, cell cycle arrest happens, leading to apoptosis if DNA is not repaired (McWhinney *et al.*,2009; Dasari and Bernard Tchounwou, 2014; Johnstone *et al.,* 2014), (Figure 1.5).

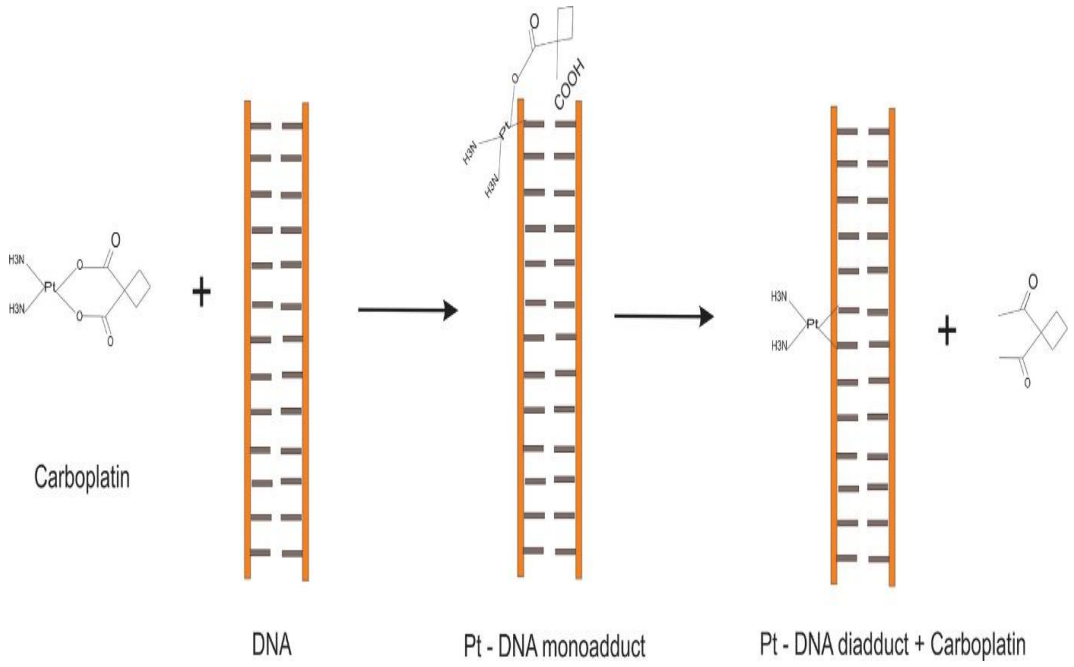

Figure 1-5: Mechanism of action of carboplatin (De Sousa *et al*., 2014).

Platinum compounds are considered as an effective and widely used family of chemotherapeutic agents. Nevertheless, there are some challenges in using them, such as developing resistance and forming secondary tumours (Cruet-Hennequart *et al.*, 2008). The problem of resistance that face platinum compounds is related to various causes, such as increment in drug destruction and deactivation before it reaches DNA, reducing drug uptake inside the tumour, and improvement in DNA repair after forming the adducts (Galluzzi *et al.*, 2012; Oun *et al*., 2018). Unfortunately, the platinum compounds are also accompanied by serious side effects resulting from the unselective attack on the rapidly developing cells. These side effects include nausea, vomiting, diarrhea, ototoxicity, nephrotoxicity, hepatotoxicity, neurotoxicity, and myelosuppression (Galluzzi *et al.*, 2012; Oun *et al*., 2018).

Cisplatin, one of the platinum chemotherapeutic agents, shares with other platinum agents the same mechanism of action. However, it was found that cisplatin can induce cancer cell death and DNA destruction by inducing oxidative stress (Mikuła-Pietrasik *et al.*, 2018). Cisplatin is used to treat several cancers like head and neck, bladder, ovarian, testicular, and lung cancer. Although cisplatin was first synthesised in 1844 by M.Peyronein, it did not take a therapeutic role until 1978 when it was approved by the food and drug administration (FDA) as the first platinum compound for the treatment of cancer (Dasari and Bernard Tchounwou, 2014; Johnstone *et al.,* 2014). Cisplatin has numerous side effects, including severe kidney injury, allergic reactions, gastrointestinal tract (GIT) problems, ototoxicity, and neurotoxicity (McWhinney *et al.,* 2009; Eckstein, 2011; Dasari and Bernard Tchounwou, 2014). Since neurotoxicity is very common with platinum agents in general, it is common with cisplatin, less so with oxaliplatin, and markedly less so with carboplatin (McWhinney *et al*.,2009). Yet, there is no effective solution if neurotoxicity happens after administering platinum compounds (Amptoulach and Tsavaris, 2011).

Despite the invention of more than 3000 platinum compounds, only thirteen compounds entered clinical trials; from all these thirteen compounds, only carboplatin was proved to have a clinical advantage over cisplatin (Mikuła-Pietrasik *et al.*, 2018). Carboplatin, a second-generation platinum compound, is more stable and with similar efficacy to cisplatin (Amptoulach and Tsavaris, 2011). It is very convenient to be administered, relatively well-tolerated and achieves a high response rate (Luvero *et al*., 2014). FDA approved carboplatin in 1989 (Kelland, 2007), and it has been approved to be used in ovarian cancer treatment as a dual regimen in combination with taxanes (Jain and Meyer-Hermann, 2011; Luvero *et al.,* 2014). Although

carboplatin has a different chemical structure compared to cisplatin and fewer side effects, it has the same anti-tumour effect. Moreover, it has lower GIT problems and less neurotoxicity and nephrotoxicity, but it has some side effects, including myelosuppression, thrombocytopenia, and anemia (Eckstein, 2011). Significantly, it has the advantage of having slower pharmacokinetics, a lower excretion rate, which means that carboplatin is kept on the body for a long time (high bioavailability), and hence, its effects will be longer as well (Dasari and Bernard Tchounwou, 2014).

Oxaliplatin, a third-generation platinum compound, was originally described late in the 1970s but its approval was postponed 30 years until being approved by FDA (Kelland, 2007). Other platinum compounds belong to the third generation include picoplatin and satraplatin (Mantia-Smaldone *et al.*, 2011). In 2002, oxaliplatin was approved to be used in the treatment of colon cancer. Its side-effects are presented by sensory neuropathy and frequent neutropenia (McWhinney *et al.*, 2009).

Platinum free interval (PFI) is the most widely used and accepted clinical surrogate to predict the chemotherapeutic agents' response and predict prognosis. It is defined as the interval between the date of the last platinum dose and the date of relapse detection. According to this definition, patients are grouped into four main classes according to PFI length (1 m, 1-6 m, 6-12 m, 12 m), and this corresponds to the clinical categorisation of patients with recurrent ovarian cancer as refractory, resistant, potentially sensitive and fully sensitive, respectively *(*Pujade-lauraine *et al*., 2019).

1.2.2.2. Taxanes

The taxanes family of drugs includes paclitaxel (Taxol®) and docetaxel (Taxotere®) (Donati and Castro, 2011, Mikuła-Pietrasik *et al.*, 2018). Oncologists have used this family since the late 1990s (Cazzaniga *et al.*, 2007). This family has been used mainly in the treatment of breast cancer (Donati and Castro, 2011), lung cancer (Donati and Castro, 2011), prostate cancer (Mang *et al.*, 2017), in addition to ovarian cancer and bladder cancer (Ojima *et al.*, 2016). They act by binding to tubulin in microtubules and these microtubules are made of α and β-tubulin (Kellogg *et al.*, 2017). These tubulin units are crucial in several cellular functions, such as mitochondrial metabolism, cell shape regulation, transport of vesicles, and chromosomes separation during mitosis (Mikuła-Pietrasik *et al.*, 2018). Taxanes act by inducing tubulin polymerisation, and this makes these microtubules non-functional because they depend on being able to dynamically polymerize or depolymerize. Taxanes bind to β-tubulin, which leads to stabilisation and prevention of depolymerisation. In the end, this leads to mitotic arrest because of chronic activation of spindle assembly checkpoint and subsequently apoptosis (Cimino *et al.*,2013; Fukada *et al.*, 2016), (Figure 1.6). Taxanes have additional mechanisms of action, including immunomodulatory effect against cancer, angiogenic inhibitory effect (Kampan *et al.*, 2015), and *in vitro* studies showed that they could induce apoptosis by BCL-2 Phosphorylation (Oshiro *et al.*, 2009; Kampan *et al.*, 2015).

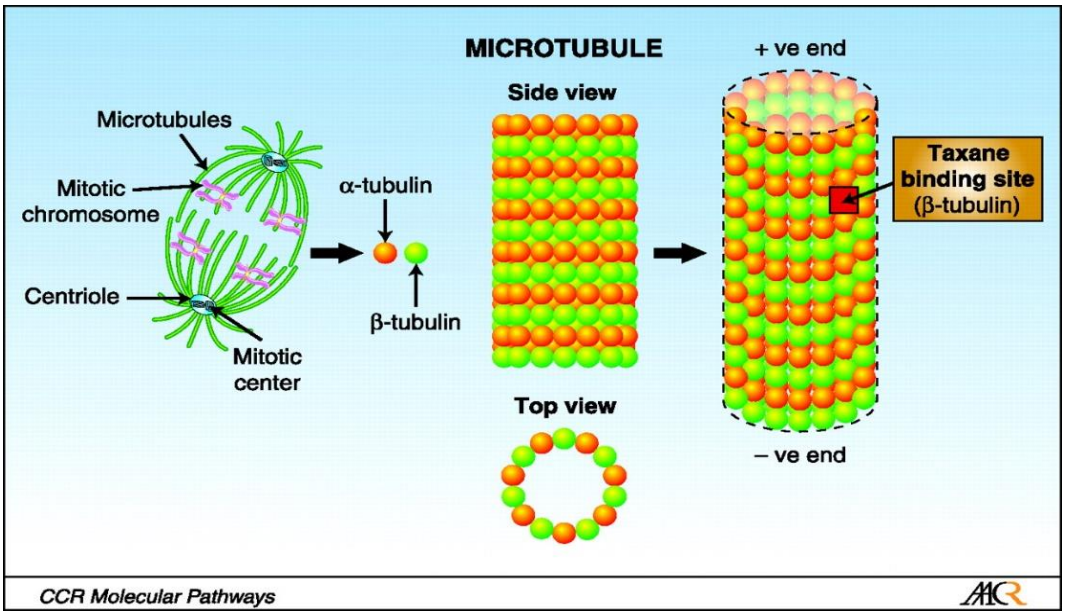

Figure 1-6: Mechanism of action of paclitaxel (Morris and Fornier, 2008).

Paclitaxel was the first taxane developed and tested. It was firstly used in the clinical application in the early 1990s (Weaver, 2014). It was extracted naturally from the bark of the *Taxus brevifolia* tree in 1962 (McGrogan *et al.*, 2008; Donati and Castro, 2011, Kampan *et al.*, 2015). The FDA approved the use of paclitaxel for ovarian and breast cancer in 1992 and 1994, respectively (Zhang *et al.*, 2014, Kampan *et al.*, 2015). Docetaxel, another taxane drug, is a semi-synthetic compound that was introduced after paclitaxel. It was extracted from *Taxus baccata* leaves (Donati and Castro, 2011). In 1996 and 1999, It was approved by the FDA to be used in breast cancer and non-small lung carcinoma, respectively (Ojima *et al*., 2016).

Significantly, Paclitaxel and Docetaxel have special pharmacokinetics (PK), having a large volume of distribution, rapid elimination, and short half-life (Minisini *et al.*, 2003). Despite the sharing in the mechanism of action between paclitaxel and Docetaxel, they

have different uses and side effects (Donati and Castro, 2011). Taxanes major side effects are nausea, vomiting, bone marrow suppression, diarrhea, hypotension, and bradycardia (Sarafraz and Ahmadi, 2008). They are also associated with neurotoxicity, myalgias, arthritis, and skin changes (McGrogan *et al.*, 2008). Although Docetaxel is less neurotoxic than paclitaxel, it has more myelosuppression when compared with paclitaxel (Berek *et al.*, 2018). Furthermore, taxanes, mainly docetaxel, are associated with a unique side effect represented by acral or palmar-plantar erythrodysesthesia (PPE) (McGrogan *et al.*, 2008; Donati and Castro, 2011), (Figure 1.7).

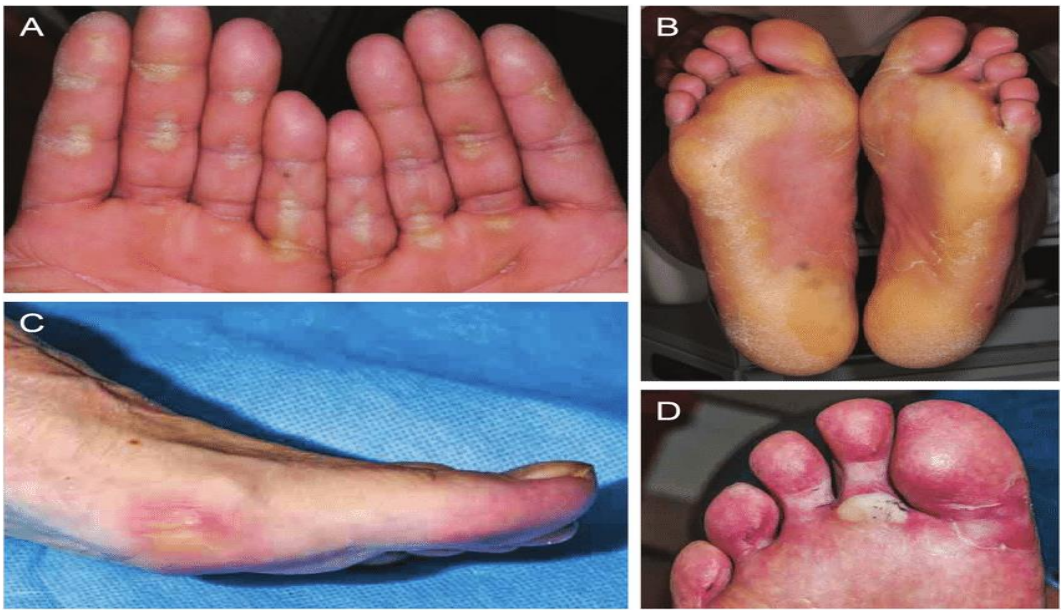

Figure 1-7: Palmar-plantar erythrodysesthesia syndrome (Gerendash and Creel, 2017).

1.2.3. Resistance

Although there have been several improvements in anticancer regimens in the previous years, resistance remains a significant obstacle for any chemotherapy success (Broxterman *et al.,* 2009; Cohen *et al.*, 2014; Christie and Bowtell, 2017) and

it accounts for 90% of chemotherapy failure (Mansoori *et al.*, 2017), which explains why it has a negative effect on the patient's overall survival (Broxterman *et al.,* 2009). In ovarian cancer, the scenario is the same, and around 75% of patients develop relapse and resistance to the chemotherapy regimen (Dasari and Tchounwou, 2014). The resistance can occur at different cellular levels and can be intrinsic or acquired. Accordingly, there must be a better understanding of the resistance mechanisms, leading to finding new solutions to fix this problem (Luqmani, 2005; Christie and Bowtell, 2017; Mansoori *et al.*, 2017; Pokhriyal *et al.*, 2019). Intrinsic resistance refers to the cancer cells that are naturally resistant to chemotherapy therapies even before being administered and after treatment, these cells predominate. In contrast, acquired chemoresistance refers to the development of resistance to chemotherapy drugs after being administered. The intrinsic resistance is due to several biological modifications that cancer cells have, such as an increase in drug efflux, decrease in drug uptake, increase in drug detoxification, (Pokhriyal *et al.*, 2019), and evasion of apoptosis (Indran *et al.*, 2011; Pokhriyal *et al.*, 2019). Furthermore, tumour heterogeneity and tumour microenvironment also represent intrinsic resistance factors (Mansoori *et al.*, 2017). In contrast, the acquired resistance results from genetic and epigenetic alterations that can help cancer cells accommodate to the chemotherapy effects. This means that chemoresistance is a multifactorial phenomenon (Pokhriyal *et al.*, 2019). Mechanisms of drug resistance are presented in (Figure 1.8).

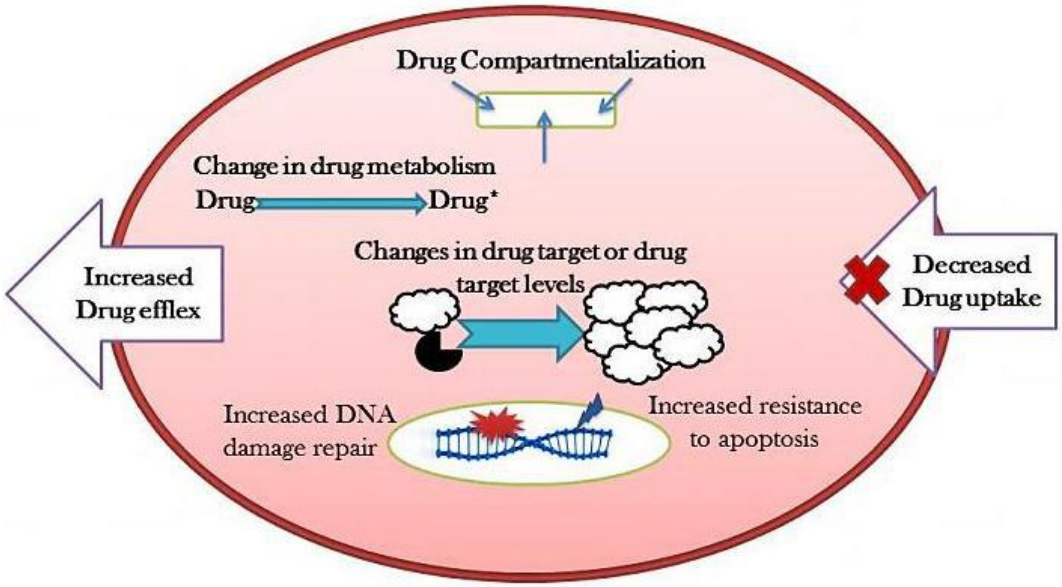

Figure 1-8: Mechanisms of drug resistance (Mansoori *et al*., 2017).

In ovarian cancer, some patients have germline mutations in breast cancer antigen-1 (*BRCA*1) and/or breast cancer antigen-2 (*BRCA*2). *BRCA1* and *BRCA2* are considered essential components in the homologous recombination (HR) mechanism responsible for repairing the DNA double-strand break (DSB). Thus, *BRCA* mutations leads to impairment in the ability to repair DNA damage by HR. Accordingly, this can explain the increased sensitivity of this cancer to platinum-based drugs (Basourakos *et al.*, 2016). In contrast, P53 protein, which plays a pivotal role in in regulating the cell cycle, is sensitive to DNA damage that happens during replication, which induces G_1 arrest and/or apoptosis. This will inhibit the defective cells production (Luqmani, 2005). The gene responsible for P53 expression is mutated in human cancers, which leads to P53 function loss. This dysfunction will permit the cells to keep replicated and will be resistant to DNA-damage induced agents. Therefore, a new method to overcome the problem of chemotherapy resistance is by reactivation of mutant P53 (Bykov *et al.*, 2017).

As not all patients have chemotherapeutic drugs resistance, at the same time, some tumours could be highly resistant to most chemotherapeutic agents, while others are sensitive. Hence, this means that there is a need to have some tests to predict the resistance. These tests will preserve patients from ineffective medications and give better results. As a result, a cell culture drug resistance assay was invented, and it depends on ^{3}H-thymidine uptake in cultured tumour cells. The specimens for this test are taken from fresh biopsies in the presence of various therapies, then these data are analysed to predict the patient's response to several therapies. Interestingly, this method has shown high accuracy (Luqmani, 2005). In addition, mRNA detection has been widely used in the study of chemotherapy resistance, which is named as transcriptomics. The transcriptomics is the study of mRNA transcripts, which are made by tissue or an organism under definite conditions and at a specific time. The profile of expressed proteins, termed proteomics, may also be used to study chemotherapy resistance. Nevertheless, its use in ovarian cancer has not yet been successful in identifying differences between chemo-sensitive and chemoresistance patient tissue samples which improve patient outcome (Pokhriyal *et al.*, 2019).

The problem of resistance deserves attention, and many solutions to solve this problem have been considered. These solutions include using new targets, such as using metabolic modifiers or chemosensitisers and targeting genetic mutations (Luqmani, 2005; Riganti and Contino, 2019). Furthermore, using a combination of different drug classes with minimal overlapping toxicities to achieve a synergistic effect is helpful (Luqmani, 2005; Mansoori *et al.*, 2017; Riganti and Contino, 2019). Using maximal dosing with a narrow cycle interval is also an option, as De souza *et al*. (2011) reported that there is a positive relationship between the chemotherapy resistance and

the length of free intervals. As such, decreasing these intervals results in a potential anticancer effect (De Souza *et al.*, 2011). Moreover, using P-glycoprotein (PGP) inhibitors is a new experimental approach, but this solution has a safety problem as it was found to cause undesirable side effects (Luqmani, 2005). Another method uses metronomic dosing, which targets associated endothelial cells that support tumour cell growth using anti-angiogenic agents (bevacizumab) in addition to a frequently regimen of chemotherapy agents (Luqmani, 2005). Also, using sequential therapy by giving single-agent therapy with non-platinum agents is one of the best solutions to solve resistance (Hansen *et al.* , 2017) .

Using non-platinum agents could be a solution to overcome resistance and these drugs showed promising results in ovarian cancer. These include anticancer drugs such as gemcitabine, pegylated liposomal doxorubicin, topotecan, and paclitaxel. However, the choice depends on the prior use history, toxicity, cost and availability (Pujade-lauraine *et al*., 2019). In addition, PARP inhibitors could be a promising choice and although there are several drugs belong to this family of medications, olaparib was the first PAPR inhibitor approved in the clinical use, and it was approved by FDA in 2014 to be used in ovarian cancer patients who have suspected *BRCA* mutation and who have been treated before with three or more of chemotherapeutic agents (Mills and Fuh, 2017; Cortez *et al.*, 2018; Gadducci *et al.*, 2019).

1.3. BCL-2 Family

The B cell lymphoma 2 (BCL-2) gene family encodes more than 20 proteins. These proteins are responsible for intrinsic apoptosis regulation (gatekeepers) through controlling mitochondrial membrane permeability and hence, they are crucial for

balancing cell survival and death (Ashkenazi *et al.*, 2017). Furthermore, some BCL-2 family proteins participate in non-apoptotic processes, such as autophagy (Lindqvist *et al.*, 2014), calcium influx, cellular senescence, redox homeostasis, inflammation and bioenergetic metabolism (Chong *et al.*, 2020). BCL-2 was first identified by chromosomal mapping as its gene is involved in a translocation in t [12;18] in the majority of cases of follicular lymphoma. BCL-2 family is classified into two major groups: pro-apoptotic (anti-survival) and anti-apoptotic (pro-survival) families (Campbell and Tait, 2018), (Figure 1.9).

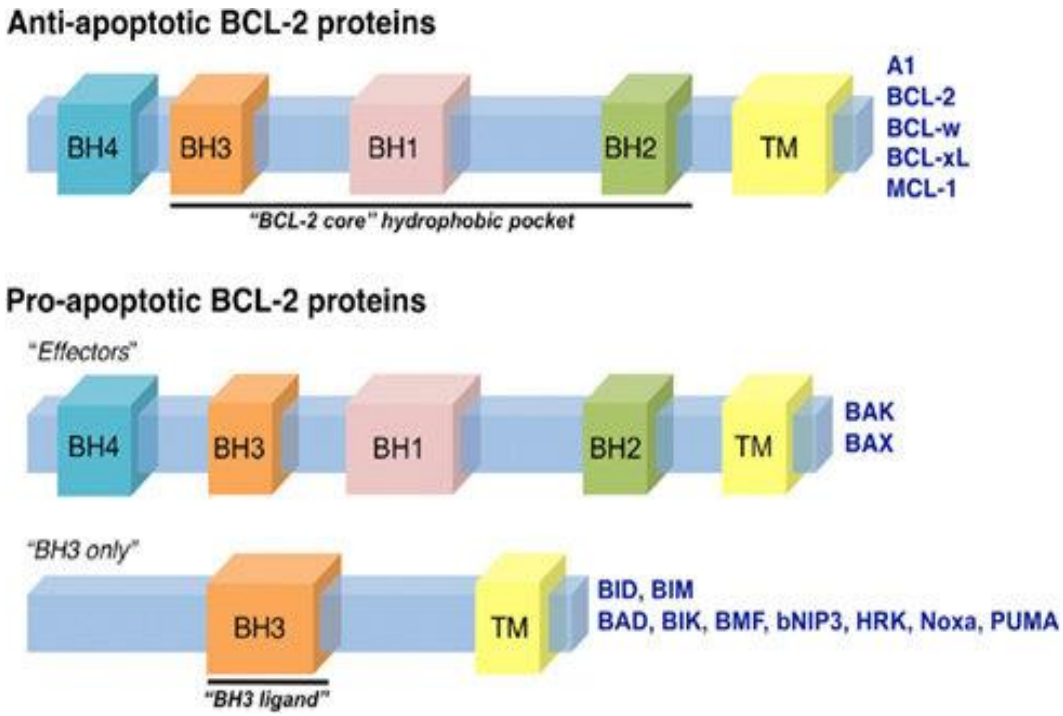

Figure 1-9: The BCL-2 family of proteins (Anvekar *et al.*, 2011).

1.3.1. Antiapoptotic proteins

Antiapoptotic BCL-2 proteins (pro-survival) have an important role in cell survival as they block the mitochondrial permeability and inhibit apoptosis (Tahir *et al.*, 2017). These proteins possess four BCL-2 homology domains (BH 1-4) in addition to the transmembrane motif (TM), and these proteins are mainly localized at the outer mitochondrial membrane (Greenberg *et al.*, 2014). There are six family members, including BCL-2, BCL-W, BFL-1, A1, BCL-X_L, and MCL-1 (Tahir *et al.*, 2017), (Figure 1.9). In ovarian cancer, the genomic atlas showed a unique expression of specific anti-apoptotic proteins. The highest expression was for BCL-X_L and MCL-1 (14%), then BCL-W (12%), while only less than 3% for BCL-2 (Abed *et al.*, 2016).

1.3.2. Proapoptotic proteins

Proapoptotic BCL-2 members are divided into effector proteins and BH3-only proteins. Their role is to induce apoptosis and terminate cell life. The effector proteins such as BOK, BAX, and BAK also have the four domains of BCL-2 homology domains (BH 1-4) in addition to the TM (Liu *et al.*, 2016; Chong *et al.*, 2020), (Figure 1.9). BAK is located on mitochondrial outer membranes, while BAX is located either in the cytosol or on the mitochondrial outer membrane (Kale *et al*., 2017). During activation, BAX moves to the outer mitochondrial membrane and, with BAK, induce permeabilization. This allows the release of several proteins, notably cytochrome C which is a key signal to trigger apoptosis, by activating caspase 9. In the case BOK, although it has a similarity with both BAX/BAK, it has an unknown function when compared with BAX and BAK (Liu *et al.*, 2016).

The BH3-only proteins (Bim, Bid (BH-3 interacting-domain death agonist), Puma, Bad (Bcl-2/Bcl-x-associated death promoter), Hrk (Harakiri), Noxa and Bmf (Bcl-2-modifying factor)), they contain the third BH domain and they bind to BCL-2 family members (Anilkumar and Prehn, 2014). However, they lack other BCL2 homology domains (BH1, BH2 and BH4), (Figure 1.9). BH3-only proteins work as stress sentinels that relay the various spectrum of apoptotic signals towards mitochondria and mitochondrial outer membrane permeabilization (MOMP) through activation of effector pro-apoptotic proteins (BAX and/or BAK) (Lopez and Tait, 2015). They are divided into sensitizers, such as BAD, NOXA, Hrk, Bmf and BIK, or activators, such as BID, BIM, and PUMA (Liu *et al.*, 2016; Tessoulin *et al.*, 2019). The difference between sensitizers and activators is that sensitizer BH3-only proteins bind to anti-apoptotic proteins, sequester them and indirectly activate BAK and BAX by preventing the apoptosis inhibitors from suppressing BAK and BAX by sequestration. In contrast, activator BH3-only proteins bind directly to BAK and BAX and activate them (Certo *et al.*, 2006; Westphal *et al*., 2014). They induce apoptosis either by direct activation of BAK or BAX or by preventing pro-survival BCL-2 family proteins from sequestering BAK or BAX (Marquez and Xu, 2012), (Figure (1.10)). Of note, it has been reported that there is another BH3-only pro-apoptotic protein that plays a role in cellular death but it belongs to Ras association domain family 1A (RASSF1A) and this protein is called Modulator of apoptosis 1 (MOAP-1) protein (Law *et al*., 2012).

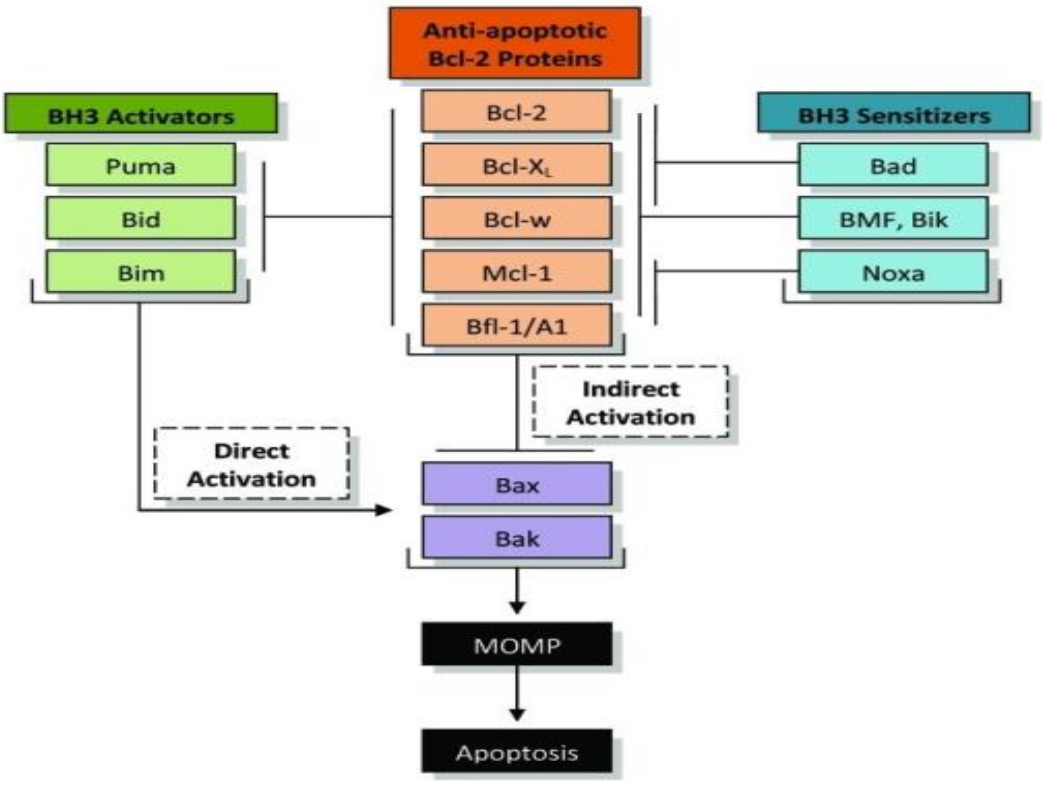

Figure 1-10: Regulation of apoptosis by the Bcl-2 family (Liu and Wang, 2012).

1.4. Navitoclax (ABT-263)

Navitoclax is the first novel BH3 mimetic that entered clinical trials (Adams and Cory, 2018). It was developed as an oral analogue for its parent drug, ABT-737. This drug has been found to have high affinity to BCL-2 and BCL-X_L (Timucin *et al.,* 2018). Furthermore, this drug showed promising results in preclinical and clinical trials (Vivo-Llorca *et al.*, 2020). Moreover, it showed a higher potency in fibrotic diseases (Mohamad Anuar *et al.*, 2020) and as a senolytic agent (He *et al.*, 2020). However, this drug is associated with low solubility, low bioavailability (Choo *et al.*, 2014). In addition, navitoclax was found to induce temporary decreases in platelet counts (Thrombocytopenia) which prevented its involvement in clinical trials (Ashkenazi *et al.*, 2017; Adams and Cory, 2018).

1.5. Cancer nanomedicine

Cancer nanomedicine is a booming area of interest with huge potential to revolutionise modern medicine. Nanotechnology offers various solutions faced by pharmaceutical industries particularly around improving poor drug physicochemical properties. These could be related to solubility, toxicity or permeability. It is estimated that around 60% of all new drug compounds are completely insoluble and this poses a major problem for their effective administration (Ganesan and Barakat, 2017). Various range of cancer nanomedicines have been applied as drug delivery systems and one class of nanotechnology making a huge difference to this arena is the use of amphiphilic polymers (Hoskins, 2020).

1.5.1. Amphiphilic polymers

Copolymers are large molecules consisting of two or more building blocks bound to each other. Amphiphilic polymers are comprised of hydrophilic and hydrophobic parts. Application of amphiphilic polymers within medical science has been given a high level of research engagement in recent years (Thompson *et al.*, 2008; Hoskins *et al*., 2012; Barnett *et al.*, 2013). The first reports of amphiphilic polymers were introduced in 1984, when they were shown to form spontaneous nanoaggregates once inserted in aqueous media (Hoskins *et al*., 2012). The self-assemblies formed in a core-shell structure where the hydrophobic segment forms an inner core to shield itself from the aqueous media (Thompson *et al.*, 2008; Hoskins *et al.*, 2010; Al Ameri *et al.*, 2020). Amphiphiles, in general, can be used for different applications such as wetting agents, surfactants, and detergents (Salager, 2002). Furthermore, they are applied in biochemical and biomedical fields to form supramolecular structures once put in the

aqueous media (Thompson *et al.*, 2008; Hoskins *et al*., 2012; Barnett *et al.*, 2013). Some polymeric nanoaggregates have been reported to be excellent universal drug solubilising agents, especially for anticancer drugs which are often highly lipophilic and problematic to administer. Several hydrophobic model drugs have been examined to study the encapsulation efficacy, and these include paclitaxel, cyclosporine A (CsA), doxorubicin (DOX). In addition, genes, proteins, and peptides have also been examined (Hoskins *et al*., 2012).

These polymer aggregates possess the ability to encapsulate lipophilic compounds and control the rate at which they become released. They can be used to improve compound solubility, stability, and permeability (Al Ameri *et al.*, 2020). Importantly, amphiphilic polymers have been reported to protect their cargo from P-glycoprotein (PGP) pumps and protect them from enzymatic degradation and mucoadhesive properties (Hoskins *et al.*, 2011). Moreover, they are considered an excellent alternative to surfactants for hydrophobic drug solubilisation (Barnett *et al.*, 2013; Alsuraifi *et al.*, 2018; Al Ameri *et al.*, 2020). The reasons behind that could be due to the unique characteristics that amphiphilic polymers have, such as the lower excipient to drug ratios needed for solubilisation and the various architectures and structures of amphiphilic polymers have. In addition, they possess higher stability that is due to having a lower critical aggregation concentration (CAC) (Alsuraifi *et al.*, 2018; Al Ameri *et al.*, 2020).

The shape and size of the self-assemblies formed from amphiphilic polymers depend on several parameters such as the ionic strength, concentration of the amphiphilic

polymer, pH, and temperature (Lombardo *et al.*, 2015). Although several interactions are responsible for forming self-assemblies, including hydrogen bonding, exchange repulsive, van der Waals, and hydrophobic interactions; the major driving factor for the self-assembly of amphiphilic polymers is the hydrophobic-hydrophobic interaction (Hoskins *et al.*, 2010; Yusa, 2012). Since the self-assemblies are formed from various architectures, they can also form various supramolecular structures in the aqueous media (Zhou *et al.*, 2009). These include nanoparticles, rod-shaped, disk-like structures, vesicles, and polymeric micelles (Hoskins *et al.*, 2011).

There are several advantages that the self-assemblies can serve, which are represented by enhancement of drug water solubility, decrease in drug resistance, a decline in the undesired adverse effects, increase in therapeutic efficacy, increment in drug-tissue exposure, and the enhancement in drug targeting. The latter is due to having a tiny size, which can help in enhancement in drug delivery either passively because of the enhancement permeability and retention effect (EPR) or actively as they can be conjugated with several moieties (Hoskins *et al.*, 2010). However, there is some debate within the nanomedicine community surrounding the plausibility of the EPR effect.

Block copolymers, star-shaped polymers, dendrimers, and graft copolymers are the major types of polymeric amphiphiles (Alsuraifi *et al.*, 2018). However, the main amphiphilic polymers responsible for self-assemblies formation are mainly two types; either amphiphilic block copolymers (most common) or amphiphilic graft copolymers (Thompson *et al.*, 2008; Hoskins *et al.*, 2011).

1.5.1.1. Block copolymers

Amphiphilic block copolymers, (Figure 1.11), are considered the most commonly studied self-assembling polymers (Hoskins *et al*., 2010). These polymers consist mainly of two parts; a hydrophilic part attached to a hydrophobic part in a linear architecture. They could be comprised of three or four segments that can polymerise together to form what is known as tri-block copolymer and tetra-block copolymers, respectively. The di-block copolymers have superior characteristics compared with tri-block characteristics by being more thermodynamically stable, having lower critical aggregation concentration (CAC), and loading high drug cargo in its core (Hussein and Youssry, 2018). These block copolymers, once put in aqueous media and at specific concentrations, the hydrophobic interactions will force the amphiphilic copolymer to form nanoaggregates (Hussein and Youssry, 2018). These type of polymers can form several architectures in liquid media such as rods, lamellar structures, and spheres (Yusa, 2012; Gao *et al.*, 2013). However, the most widely reported architecture is the spherical micelles (polymeric micelles) (Hussein and Youssry, 2018).

The self-assemblies formed from this type of polymers can encapsulate hydrophobic drugs in its inner core through hydrophobic-hydrophobic interactions. This encapsulation shields the lipophilic molecules from the aqueous environment and protects the payload from enzymatic degradation (Hoskins *et al.*, 2011). The examples of the hydrophilic segments which are employed in these types of polymers include poly (ethylene oxide) (PEO), methoxy poly (ethylene glycol) (MPEG), and poly (acrylic acid), while poly (diethyl aminoethyl methacrylate) (PDEA), poly (L-lactic acid) (PLLA), poly(styrene) (PS), and poly (propylene oxide) (PPO) are examples of hydrophobic polymer moieties that have also been reported in the literature. These monomers can

bind together to form block copolymers, and examples of amphiphilic copolymers that have been investigated are poly(ethylene glycol)-poly(γ-benzyl L-glutamate) PEG-PBLG, poly(ethylene glycol)-poly(L-lactic acid) PEG-PLLA, and poly(ethylene glycol)-poly(β-benzyl L-aspartate) PEG-PBLA (Hussein and Youssry, 2018).

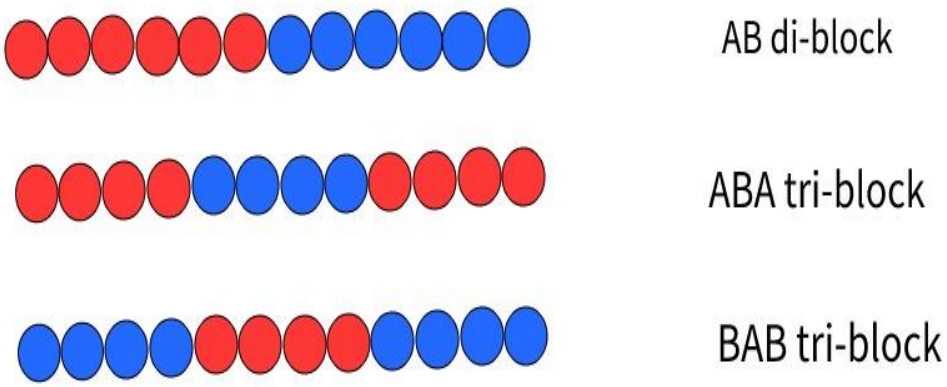

Figure 1-11: Schematic representation of block copolymers with different architectures.

Poloxamers (Pluronics®) are examples of the tri-block copolymers. These polymers are comprised of poly (ethylene oxide)-block-poly (propylene oxide)-block-poly (ethylene oxide) PEO-PPO-PEO. They are characterised by being highly biocompatible and resilient to protein adsorption and cellular adhesion because of their amphiphilic nature (Zheng and Wyman, 2016). Pluronics are types of amphiphilic polymers that are used for enhancing hydrophobic drug solubility. Examples of these drugs solubilized with this type of polymers are valproic acid, digoxin, and loperamide. Also, various anticancer agents have been used with pluronics such as doxorubicin and etoposide which were fabricated with Pluronic- P85. This Pluronic- P85 was approved to inhibit PGP, in addition to its role in drug delivery (Patel and Patel, 2017).

Moreover, Pluronic- CRL-1605 is another example that was reported to increase oral uptake of amikacin and tobramycin antimicrobials (Kabanov *et al.*, 2002).

1.5.1.2. Star shape polymer

Star shape polymers are another type of amphiphilic polymer (Hoskins *et al.*, 2012; Alsuraifi *et al.*, 2018). They are composed of a central polymer core surrounded by three or more branched polymers with different lengths (Ooya *et al.,*2003). The star-shaped polymers have been used as drug delivery carriers because of their unique characteristics. These characteristics include possessing solid structure, having high water solubility, and having modified thermal characteristics. In addition, they have shown efficacy in increasing the solubility of many hydrophobic drugs (Ooya *et al.,*2003). An example of these polymers was a star-shaped poly(ε-caprolactone) (PCL) which was attached with poly (ethylethylene phosphate) (PEEP) as a terminal block to form a PCL-PEEP star-shaped copolymer (Fonseca *et al.*, 2015). Figure (1.12), presents PCL-PEEP copolymer that Cuong and his colleagues synthesised which showed a potential ability to form nanoaggregates in aqueous solutions and was applied to encapsulate doxorubicin (DOX) (Cuong et al., 2011).

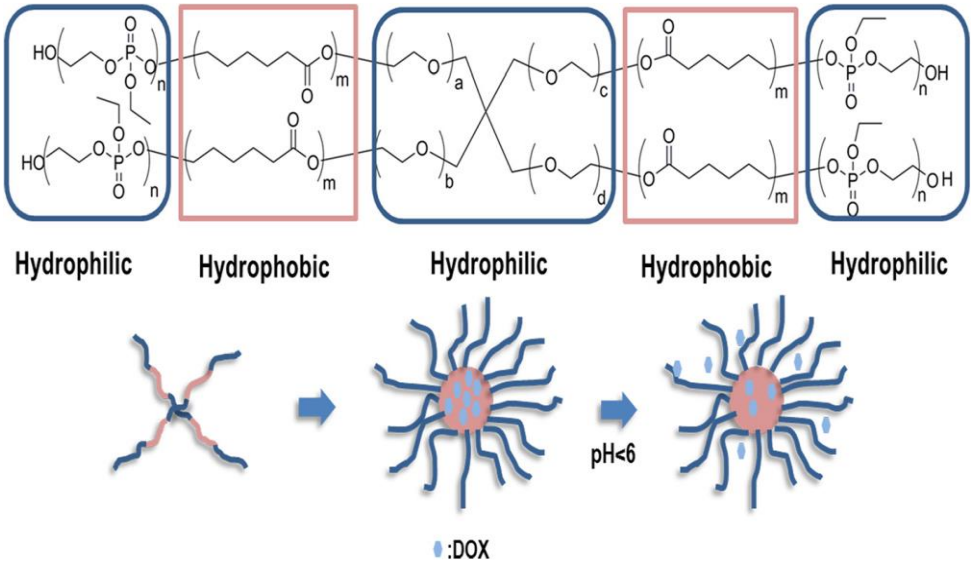

Figure 1-12: PCL-PEEP star-shaped copolymer (Fonseca *et al*., 2015).

1.5.1.3. Dendrimers

Dendrimers, (Figure 1.13), are tree-shaped, highly branch macromolecules with an average diameter of 1.5 nm -14.5 nm (Gao *et al.*, 2013). They have a unique shape with 3-dimensional characteristics (Gao *et al.*, 2013; Itani and Faraj, 2019). Dendrimers are composed of a central core attached to many branches, and its surface has many terminal groups where drugs and targeting moieties are attached (Fay and Scott, 2011; Aslan *et al.*, 2013; Mohanty, 2017). Dendrimers have different layers, and each layer is called a generation (Abbasi *et al.*, 2014). Two methods can be used to synthesize dendrimers; the divergent method (from inside toward outside) or the convergent method (from outside toward inside) (Abbasi *et al.*, 2014). This amphiphilic polymer forms a unimolecular micelle in an aqueous solution the same as star shape polymer, and they possess remarkable properties such as high stability in the water at low concentration and uniform size compared to block copolymer (Qiu and Bae, 2006). Furthermore, they can be used as an effective vehicle for hydrophobic cargo (Fay and

Scott, 2011), and the drugs that are loaded could be either loaded in the inner core or on the outer surface (Itani and Faraj, 2019). Notably, dendrimers showed higher efficacy in delivering several drugs, including anticancer drugs such as platinum compounds and doxorubicin, making it a promising method in treating cancer cells (Markman *et al.*, 2013). Dendrimers could be applied as an intelligent delivery system as it was reported that the outer functional groups have the advantage of controlling the drug release from the dendrimer core when it faces specific environments such as certain pH or facing specific enzymes (Markman *et al.*, 2013). The most dendrimer family that has been studied for drug delivery is poly(amidoamine) (PAMAM) dendrimers (Gao *et al.*, 2013; Abbasi *et al.*, 2014). This family has different characteristics, such as being water-soluble, biocompatible, non-immunogenic, and capable of delivering various molecules together (Gao *et al.*, 2013; Itani and Faraj, 2019).

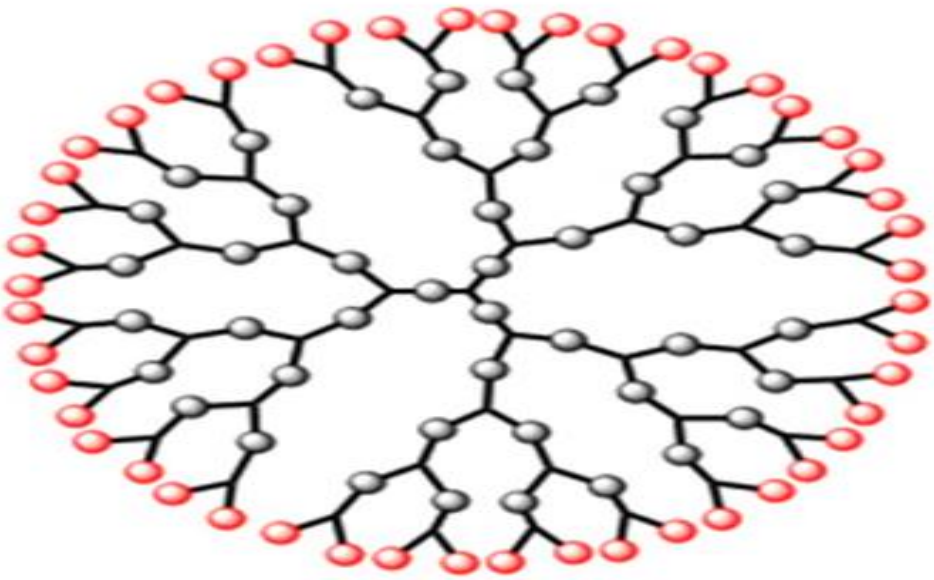

Figure 1-13: Basic structure of dendrimer (Anees et al., 2016).

1.5.1.4. Comb-shaped copolymers

Comb-shaped polymers, (Figure 1.14), gained interest in the mid-1990s (Hoskins *et al*., 2012). This is due to the remarkable properties they possess as they are sensitive to various physical and chemical stimuli such as pH, temperature, solvent composition, ionic strength, electric field, and light (Zhang *et al.*, 2007). Hence, they are considered an intelligent delivery system that can be applied to deliver not only hydrophobic drugs but also proteins and DNA (Thompson *et al.*, 2008). Furthermore, it was reported that the nanoaggregates that are formed from the comb-shaped polymers may be able to accumulate in the tumour tissue because of the EPR effect (Al Ameri *et al.*, 2020).

Graft polymers are comprised of hydrophobic (water-hating, non-polar) groups grafted on a hydrophilic (water-loving, polar) homopolymer backbone to form a comb-shaped like structure (Al Ameri *et al.*, 2020). The grafted pendant groups could be comprised of homopolymers, copolymers, and low molecular weight hydrophobic structures. The alkyl chains, acyl groups, and cholesterol groups are examples of the hydrophobic groups applied as pendant groups on the polymeric backbones (Hoskins *et al.*, 2012). Several types of hydrophilic polymer backbones were investigated, including natural and synthetic backbones (Hoskins *et al.*, 2012). The well-known natural polymers that are hydrophilic and have different chemical structures include dextran, chitosan, and hydroxypropylmethylcellulose (Thompson *et al.*, 2008; Hoskins *et al.*, 2012). For the synthetic polymers, they include poly(allylamine) (PAA) (Thompson *et al.*, 2008; Hoskins *et al.*, 2011; Hoskins *et al.*, 2012), poly(L-lysine) (PLL) (Hoskins *et al.*, 2012), and polyethyleneimine (Virgen-Ortíz *et al.*, 2017) and these backbones showed stability in physiological pH and aqueous environment (Hoskins *et al.*, 2012). The amphiphilic comb-shaped polymer can form several supramolecular structures in the

aqueous media, and these include vesicles, nanoparticles, and polymeric micelles (Thompson *et al.*, 2008).

The graft polymer showed superiority in anticancer drugs' encapsulation compared with the block copolymer counterpart and the anticancer drugs alone (Hoskins *et al.*, 2012). This is consistent with what have been demonstrated by Qui and Yan who used a graft polymer of poly(phosphazene) with ethyl tryptophan as a hydrophobic pendant group, and they reported a successful encapsulation of DOX and inducing a higher toxicity in HeLa cells (Qiu and Yan, 2009). As such, this led to the conclusion that the encapsulation of a cytotoxic drug in a non-toxic vehicle such as the one formed from the amphiphilic polymer showed a synergistic effect and a higher potency (Hoskins *et al.*, 2012).

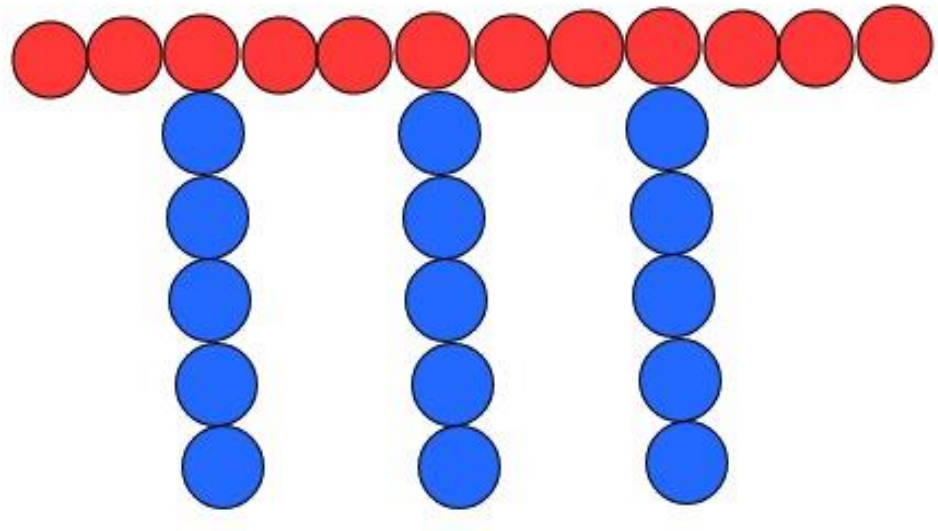

Figure 1-14: Schematic presentation of comb shaped polymer.

In spite of the broad application of the polymeric self-assemblies for intravenous administration, its oral application is much less developed. The reasons behind the slower development of oral delivery are the complexity of the gastrointestinal (G.I.) system and the barriers that the polymer with its encapsulated cargo can face when administered orally. These barriers include a variation of the pH alongside the G.I. since it is highly acidic in the stomach with pH 1.2, to small intestines with pH of 5-7 and down to the colon with a basic pH of 6-7 (Hoskins *et al.*, 2012). In addition, the food, proteolytic enzymes, the bile salts, the enterocytes, and the mucus that covers the intestines all can have a negative impact on the oral delivery of the nanocarriers and their absorption through the small intestines. Furthermore, the stability of the polymeric assemblies and being resistant to the high dilution ("sink condition") to avoid premature release is also mandatory to achieve an optimal oral drug delivery (Hoskins *et al.*, 2012). Thus, few research groups have tried to encapsulate hydrophobic drugs within the amphiphilic polymers for oral administration. The results showed an improvement in various properties include enhancement in drug solubilisation, improvement in drug uptake, protection from enzymatic degradation, and inhibition of the P-glycoprotein pump. Several amphiphilic polymers architectures have been applied in oral delivery, but the most common one was the block copolymers. Nevertheless, the dendrimers and graft polymers have also been investigated (Hoskins *et al.*, 2011; Hoskins *et al.*, 2012). The oral hydrophobic drugs that have been examined with these graft polymers include camptothecin, cyclosporine, and griseofulvin (Hoskins *et al.*, 2012).

Amphiphilic graft polymers have also been used as protein-complexation agents, with their efficacy in improving oral delivery of proteins such as salmon calcitonin (sCT) that

has been applied to the treatment of osteoporosis and Paget disease. Calcitonin was added to quaternized palmitoyl grafted poly(allylamine) (QPa), and this complex of QPa and sCT has high stability at room temperature. Furthermore, insulin also was examined, and it was added to the PAA polymer. This polymer was reported to form a complex with insulin by hydrophobic interactions, thus saving it from enzymatic degradation (Hoskins *et al.*, 2012).

1.5.2. Targeting of nanoparticles

Nanoparticles are relatively non-toxic by themselves, and they do not have any cytotoxic activity, although they can deliver cytotoxic particles to their specific site through passive or/and active targeting (Gmeiner and Ghosh, 2014). There are two kinds of targeting: passive targeting, which is represented by the enhanced permeability and retention (EPR) effect and active targeting, depending on attaching ligands for receptors on tumour tissues. Although the active and the passive targeting can happen independently and also in combination (Sebastian, 2017), the EPRE must happen first as an initial step to let the drug accumulate first and then active targeting can be achieved, which means that if active targeting follows EPRE, this will be more effective drug targeting (Yin *et al.*, 2014).

1.5.2.1. Passive targeting and EPR effect

Enhanced Permeability and retention effect (EPR, Figure (1.15)) is a special phenomenon in which macromolecular drugs distribute to a solid tumour selectively and remain there. The EPR was discovered by Maeda and his colleagues in the 1980s and it reflects the gold standard for targeting (Maeda and Matsumura, 1986). They

found that there was a selective accumulation of polymers and proteins in tumour tissue and not in normal tissue. This depends on the fact that there are differences in anatomical and pathophysiological characteristics between normal tissues and solid tumours (Yoo *et al.*, 2019; Behera and Padhi, 2020). These differences are represented by higher vascular density and angiogenesis, and defects in tumour blood vessels in cancer tissues (Garcia-Bennett *et al.,* 2011; Blanco *et al.*, 2012; Yin *et al*., 2014; Nakamura *et al.*, 2016). Importantly, It has been demonstrated that in normal tissue, there is a uniform, ordered vasculature with diameter of 8–10 μm; the opposite in tumour blood vessels, which are abnormal, leaky, have distended capillaries, and have a large diameter with 20-100 μm (Krystofiak *et al.*, 2012; Clemons *et al.*, 2018; Behera and Padhi, 2020). Furthermore, the tumour blood vessels have wide fenestrations of 200 nm to 1.2 μm and thus permit the nanoparticles to permeate through and reside in the tumour tissue (Attia *et al.*, 2019; Behera and Padhi, 2020).

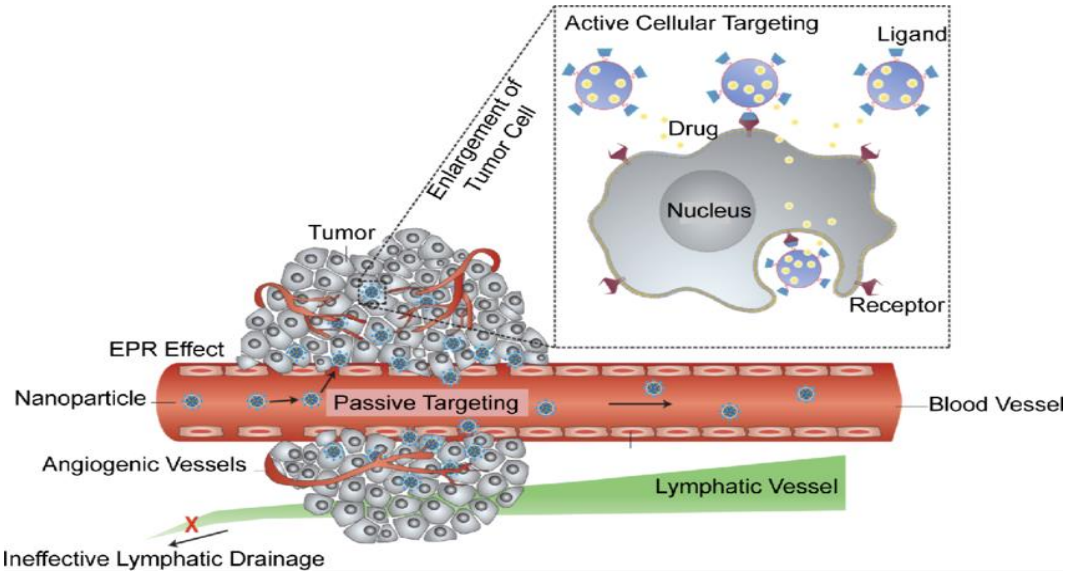

Figure 1-15: EPR effect and how NPs migrate to cancerous cells (Chinen *et al.*, 2015).

Since the normal tissue has intact vasculature, this achieves selectivity for NPs inside the tumour, but at the same time, these NPs must have dimensions smaller than the tumour gaps dimensions and larger than normal tissue pores dimensions. Added to the previous cause, defects in lymphatic drainage, which retain the drug inside the tumour for a long period, insufficient blood supply and slow venous return, all participate in this scenario (Blanco *et al.*, 2012). These defects help drug macromolecules to permeate through and accumulate in tumour tissues and not reside in normal tissues (Gu *et al.*, 2007; Yin, Liao and Fang, 2014).

Nevertheless, a limitation of passive targeting is that it does not achieve the desired accumulation and concentration in tumour cells, which leads to lower efficacy and systemic toxicity (Gu *et al.*, 2007). The delivery to certain tumours is difficult due to several reasons, such as lack of EPR effect because the permeability in blood vessels may not be the same throughout the tumour – particularly in solid tumours (Aslan *et al.*, 2013). Another cause is represented by high intra-tumoural osmotic pressure (Wang *et al.*, 2008). A solution to this problem is provided by ligands bound to NPs which specific receptors can recognize on the cell surface to achieve higher selectivity (active targeting) (Gmeiner and Ghosh, 2014; Ou *et al.*, 2018). This selective binding happens because molecules expressed by cancerous cells on their surfaces allow selective binding by nanoparticles with an appropriate ligand.

1.5.2.2. Active targeting

Targeting in cancer aims to get accurate and selective targeting to help in diagnosis and treatment (Bazak *et al.*, 2016). In addition to the fact that nanoparticles enhance

drug bioavailability, active targeting of them not only improves drug efficacy at the diseased tissue but also decreases off-target outcomes and participates in the expansion of new diagnostic tools (Fay and Scott, 2011). Using of NP for targeting medications, especially for cancer patients, must address specific issues, including how to target NP specifically to cancer cells, how to release medications inside the cancer cells and how to be excreted from the body, and finally how to avoid targeting normal tissues (Garcia-Bennett *et al.,* 2011). Targeting and localising drug conjugate can be attained by covering the nanoparticle surface with an extensive range of molecules (Fay and Scott, 2011). Attaching a molecule to a nanoparticle enables targeting the molecule to a cell that expresses a particular receptor (Gu *et al.*, 2007; Wang *et al.*, 2008; Sebastian, 2017). Using aptamers as an active targeting moiety is considered one of the efficient ways in nanoparticles targeting toward cancer cells. Aptamers are folded single-stranded oligonucleotide that fold into 3-dimensional structures and bind to specific target molecules, such as proteins, with high specificity and affinity (Keefe *et al*., 2010; Vivo-Llorca *et al.*, 2020). One of these aptamers that was applied with our studied drug, navitoclax, was MUC1 aptamer. MUC1 is transmembrane glycoprotein which belongs to mucin mucin family, which was studied with mesoporous Silica Nanoparticles for triple-negative breast cancer that has navitoclax resistance (Vivo-Llorca *et al.*, 2020). Active targeting will be discussed extensively in chapter 5.

1.5.3. Application of nanoparticles in ovarian cancer

Unfortunately, most chemotherapeutic agents are accompanied by several therapeutic drawbacks such as having a narrow therapeutic window, non-specific distribution when

given parenterally, developing resistance, and inducing unwanted side effects (Hascicek and Gun, 2017; Di Lorenzo *et al.*, 2018; Barani *et al.*, 2020). Thus, there were tremendous efforts which have been conducted to overcome these barriers by developing new treatment options. As such, several drug delivery systems and approaches have been developed, such as the nanotechnology approach. With their remarkable characteristics, the nanoparticles control the delivery of their contents and overcome the unwanted side effects by targeting their payload using passive and/or active targeting properties. Applying nanotechnology in ovarian cancer has gained importance day by day due to its remarkable and promising characteristics (Hascicek and Gun, 2017; Gupta *et al.*, 2019). In addition, it was demonstrated that applying nanotechnology helps to overcome the poor water solubility of several drugs (Gupta *et al.*, 2019). Application of nanotechnology in ovarian cancer is not only limited to deliver therapeutic agents such as chemotherapeutic agents (Hascicek and Gun, 2017) but also extended to incorporate imaging and diagnostic materials (Kafshdooz *et al.*, 2016; Di Lorenzo *et al.*, 2018; Barani *et al.*, 2020) and hence these systems are called “theranostics” nanotechnology (Engelberth *et al*., 2014). Several types of nanoparticles have been applied in ovarian cancer to deliver drugs such as liposomes, nanoparticles, micelles, dendrimers (Hascicek and Gun, 2017; Gupta *et al.*, 2019; Barani *et al.*, 2020), and polymers (Gupta *et al.*, 2019). Although the majority of nanomedicines are in the preclinical stage, some have been already approved, and others are now in clinical trials (Di Lorenzo *et al.*, 2018). The examples of the approved nanoparticles that are applied in ovarian cancer and are FDA approved are Doxil®, a liposomal formulation of doxorubicin, Genexol-PM®, a polymeric micellar formulation of paclitaxel (Di Lorenzo *et al.*, 2018). Abraxane, which is a nanoparticle bound albumin paclitaxel, entered the phase II clinical trials to be applied in ovarian cancer and this drug has

been approved by FDA to be applied in the treatment of small cell lung cancer, pancreatic adenocarcinoma, and metastatic breast cancer (Engelberth *et al*., 2014).

Aims and objectives

Aims

The work presented here seeks to improve the therapeutic index of navitoclax by encapsulating it into poly-allylamine-cholesteryl (PAA-ch$_5$) micelles. To achieve this aim mainly, several goals were set.

1. Previous work in our group used PAA-ch$_5$ polymer and other several comb-shaped polymers with different grafted groups. They demonstrated improvement in increasing the solubility of several hydrophobic drugs. Navitoclax, which is a BH3 mimetic that showed promising results in the treatment of ovarian cancer but has poor water-solubility and another problem of inducing thrombocytopenia that make its application limited. To resolve this, it was hypothesised that encapsulating navitoclax inside the PAA-ch$_5$ micelle core would increase its solubility. To this end, nanoparticles were prepared and how much drug loaded and released was determined (chapter 3). In addition, the physical characteristics of the formed nanoparticle with the stability profile were explored

2. Previous work in our group had revealed that several drugs that have been encapsulated inside the grafted polymers' cores showed higher cytotoxicity than the free drugs. This has been explained by the enhanced permeability and retention (EPR) effect, which permit the drug to get inside the cancerous cells more than the free drug, which in turn could increase the drug efficacy. To investigate this, the navitoclax was encapsulated in the PAA-ch$_5$ polymer (navitoclax-PAA-ch$_5$) and was compared with the free navitoclax (no PAA-ch$_5$) efficacy against ovarian cancer cell lines (chapter 5). Moreover, synergy between navitoclax and carboplatin

has been previously demonstrated by our group. Thus, the synergy between encapsulated navitoclax and carboplatin was also determined and compared to the activity of free navitoclax (chapter 5).

3. Active targeting can also be used to increase tumour uptake of nanoparticles. One method to achieve this is to attach folic acid (FA) to the encapsulated navitoclax polymer. Folic acid can bind to the folic acid receptors that are overexpressed on ovarian cancer cells. To investigate the potential for this to deliver navitoclax to ovarian tumours, folic acid was attached to the PAA-ch_5 polymer and prior to loading the nanoparticles with navitoclax. The loading and release of navitoclax was determined and the efficacy of the folate-tagged nanoparticles were evaluated both alone and in combination with carboplatin (chapter 6).

Chapter 2. Materials and methods

2.1. Materials

Table 2-1: The list of materials that were used in all experiments and the supplier's names.

	Material	supplier
1.	Acetic acid	Sigma-Aldrich Co., UK
2.	Acetonitrile	Sigma-Aldrich Co., UK
3.	Ammonium acetate	VWR international, UK
4.	Annexin V binding buffer	Miltenyi Biotec, Germany
5.	Annexin V fluorochrome	Miltenyi Biotec, Germany
6.	Anti-mouse IgG, HRP- linked secondary antibody	Cell signalling, UK
7.	Anti-rabbit IgG, HRP- linked secondary antibody	Cell signalling, UK
8.	Bicinchoninic acid Protein assay kit	Sigma-Aldrich Co., UK
9.	β-mercaptoethanol	Sigma-Aldrich Co., UK
10.	Bovine serum albumin (BSA)	Sigma-Aldrich Co., UK
11.	Carboplatin	Sigma-Aldrich Co., UK
12.	Caspase 3/7 reagent	Promega; Madison, USA
13.	4% Copper (II) sulphate pentahydrate solution	Sigma-Aldrich Co., UK
14.	Dialysis tubing membranes	Medical International Ltd, UK
15.	Dimethyl sulfoxide (DMSO)	Sigma-Aldrich Co., UK
16.	EDTA	Sigma-Aldrich Co., UK
17.	Ethanol	Sigma-Aldrich Co., UK
18.	Fetal bovine serum	Lonza, Switzerland
19.	Folic acid	Sigma-Aldrich Co., UK
20.	GAPDH primary antibody	Thermo-fisher scientific, USA
21.	0.45µm GDX PVDF filters	Whatman, UK
22.	Glycine	Sigma-Aldrich Co., UK
23.	HEPES	VWR international, UK
24.	Hydrochloric acid	Sigma-Aldrich Co., UK
25.	Leupeptin	Sigma-Aldrich Co., UK

26.	L-Glutamine	Lonza, Switzerland
27.	Methanol	Sigma-Aldrich Co., UK
28.	Navitoclax (ABT-263)	Adooq, UK
29.	NP40	Sigma-Aldrich Co., UK
30.	PARP primary antibody	Cell signalling, UK
31.	Penicillin streptomycin	Lonza, Switzerland
32.	Pepstatin	Sigma-Aldrich Co., UK
33.	Phenylmethanesulfonyl fluoride (PMSF)	Sigma-Aldrich Co., UK
34.	Phosphate buffer saline (PBS)	Lonza, Switzerland
35.	Poly(allylamine) Hydrochloride (PAA), (M.wt: 15 kDa)	Sigma-Aldrich Co., UK
36.	Poly (vinylidene difluoride) membrane (PVDF)	GE Healthcare Life Sciences, UK
37.	Prestained protein ladder (PageRuler Plus)	Thermo-fisher scientific, USA
38.	Propidium iodide (PI) solution	Miltenyi Biotec, Germany
39.	Roswell Park Memorial Institute medium (RPMI 1640)	Lonza, Switzerland
40.	SDS-Nupage sample buffer	Thermo-fisher scientific, USA
41.	Sodium chloride	Sigma-Aldrich Co., UK
42.	0.5% Sodium deoxycholate	Sigma-Aldrich Co., UK
43.	Sodium dodecyl sulphate	Sigma-Aldrich Co., UK
44.	0.4% sulforhodamine B (SRB)	Sigma-Aldrich Co., UK
45.	Tris Base	Sigma-Aldrich Co., UK
46.	4-20% Tris-Glycine (Nusep) polyacrylamide gradient gel	Thermo-fisher scientific, USA
47.	Tris hydrochloride	Sigma-Aldrich Co., UK

48.	Trypan blue	Sigma-Aldrich Co., UK
49.	0.01% Trypsin -EDTA	Lonza, Switzerland
50.	Tween-20	Fisher Bioreagents, UK
51.	Ultracyano 5 µm (50 x 3.0 mm) column	Restek Co., United states
52.	UptiLight HRP chemiluminescent substrate	Uptima, France

*The polymers were synthesised and characterised by the Hoskins research group prior to being passed to this project.

2.1.1. Ovarian Cancer Cell Lines

Table 2-2: Ovarian cancer cell lines used in our project and their origin

Ovarian cell line	Details
OVCAR-8	This cell line was attained from ovarian adenocarcinoma (Stordal *et al.*, 2013), January 2011, (Figure 2.1 (A)).
OVSAHO	This cell line was obtained from ovarian serous papillary adenocarcinoma (Yanagibashi *et al.*, 1997), September 2015, (Figure 2.1 (B)).

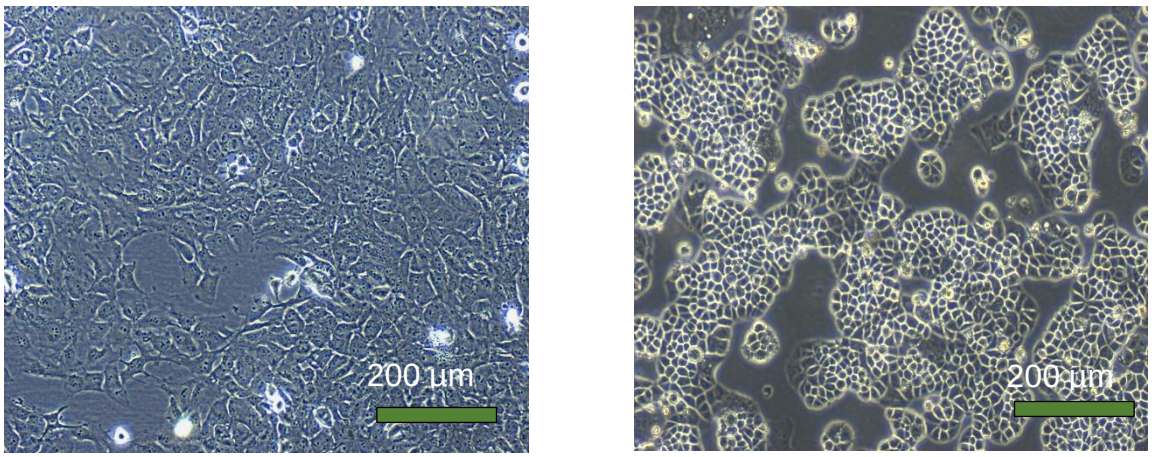

(A) (B)

Figure 2-1: Ovarian cancer cell lines that were applied. (A): OVCAR-8. (B): OVSAHO

2.2. Methods

2.2.1. Drug Loading

Polymers (PAA-ch$_5$ and PAA-ch$_5$-FA) were diluted in deionized water at a 1 mg/ml concentration before being sonicated using a probe sonicator (Soniprep 150 plus, MSE Co, MSS150.CX4.5) at room temperature for 10 minutes. Navitoclax (ABT-263) powder was added in 1:1 navitoclax: polymer weight ratios (% w: w), then the drug-polymer solution was also sonicated for 10 minutes. After that, the solutions were filtered using 0.45 µm syringe filters (with pre-filters) after being cooled at room temperature. The filtration goal is to remove any unsolubilised drug. The nanoaggregates that will form from this incorporation is represented in figure (2.2) below.

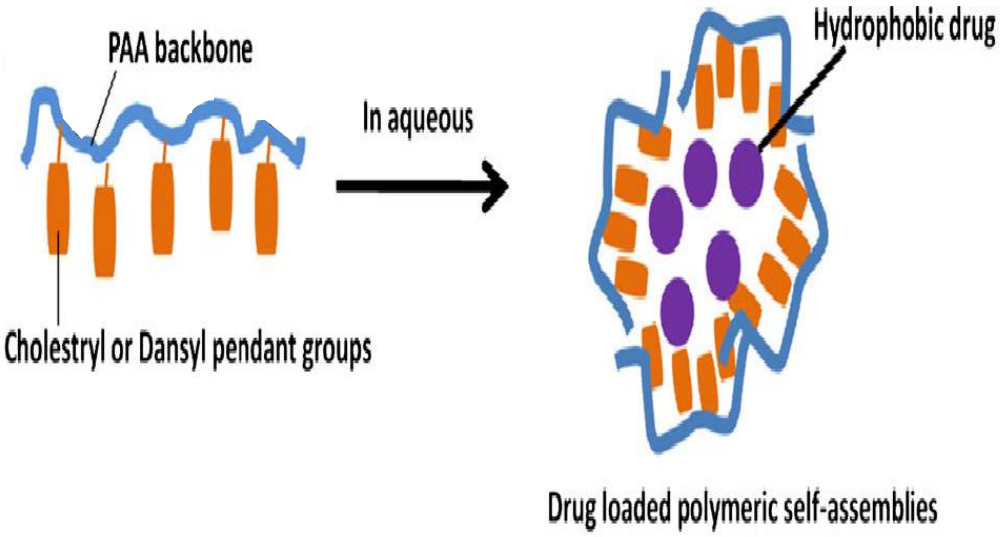

Figure 2-2: The self-assembly of PAA-ch_5 with the hydrophobic drug (Hoskins et al., 2011).

2.2.2. Detection of navitoclax, poly (allylamine)- ch5 (PAA-ch_5), poly (allylamine)- ch_5-folic acid (PAA- ch_5-FA) water solubility

Navitoclax (ABT-263) powder (4 mg) was added to 4 ml of deionized water (1 mg/ml) and sonicated for 10 minutes at 37 °C. PAA-ch_5 (4 mg), and PAA-ch_5-FA (4 mg) were also sonicated in deionized water (1 mg/ml, 4 ml) for 10 minutes at 37 °C. Solubility in water was measured using reversed phase high-performance liquid chromatography (RP-HPLC) (SHIMADZU, UK), wavelength 215 nm, ultracyano 5 µm (50 x 3.0 mm) column with mobile phase comprising 1 mM of ammonium acetate and 0.1% acetic acid in a mixture of methanol and water (95:5, v/v) and a flow rate 0.5 ml/min.

2.2.3. Quantification of encapsulated navitoclax

Reversed phase high-performance liquid chromatography (RP-HPLC) (SIMADZU, UK) with a wavelength of 215 nm was used with Column type: ultracyano 5 µm (50 x 3.0 mm) (Restek Co, United states), retention time was: 1.43 minutes, flow rate: 0.5 ml/minute. The mobile phase was 1 mM of ammonium acetate and 0.1% acetic acid in a mixture of methanol and water (95:5, v/v). The standard solution was carried out using a serial sequence of navitoclax concentrations (0.03125 mg/ml- 1 mg/ml), which was prepared by dilution navitoclax in ethanol. These concentrations were measured using HPLC and a calibration graph was constructed. For the sample solution, three samples of the navitoclax were loaded with PAA-ch_5 and PAA-ch_5-FA (as mentioned above). 0.5 ml of the solution was removed and was diluted in 0.5 ml of the eluent. The absorbance of this mixture was measured using HPLC under the same conditions. The area under the curve (AUC) that was obtained was substituted in the standard solution curve. The drug concentration inside the polymer was measured, and this concentration reflects the drug's solubility.

The loading capacity (%LC) and encapsulation efficiency (%EE) was calculated using the following equations

- % LC = (Drug determined by HPLC/ Polymer concentration) x 100%
- % EE = (Drug determined by HPLC/ Original drug concentration) x 100%

There is no definite value for %LC and %EE as in some papers it was found that these values can reach 200% and even more as for prednisolone, propofol and griseofulvin with $Dansyl_{10}$ (Hoskins *et al.*, 2011) and in some cases, it could be very small as with

BNIPDacot with PAA-ch5 (Hoskins *et al.*, 2010).However, the most important is the improvement in loading once compared with its original solubility.

2.2.4. Release method

Three samples of the formulation of navitoclax-PAA-ch_5 and navitoclax-PAA-ch_5-FA of (2 mL) were inserted inside dialysis tubing (MW cut off = 12-14 kDa) before being dialysed against phosphate buffer solution (5 ml) at 37 ^{o}C with stirring. 1 mL of the external PBS was pipetted and replaced by 1 mL of fresh PBS at various time points (up to 72 hours). As previously described, the drug concentration in PBS was determined using HPLC with the same protocol of drug loading. The release of navitoclax from the optimum formulation was calculated using the following equation

$$\% \text{ Drug release} = \frac{\text{Amount of drug released}}{\text{The initial amount of drug in optimum}} \times 100\%$$

2.2.5. Photon correlation spectroscopy

Polymeric nanoaggregates of PAA-ch_5, navitoclax-PAA-ch_5, PAA-ch_5-FA, and navitoclax-PAA-ch_5-FA were formed by probe sonication in distilled water before being filtered as mentioned before. The photon correlation spectrometer (Zetasizer Nano-ZS, Malvern Instruments, UK) was used to measure hydrodynamic diameters, zeta potential and polydispersity index (PDI) measurements. All measurements were analysed using screw-top glass vials at 25 °C, and it was conducted in triplicate then an average value was determined.

2.2.6. Freeze drying (lyophilization)

Four samples of navitoclax-PAA-ch_5 and navitoclax-PAA-ch_5-FA were freshly prepared before being frozen and then transferred to a freeze dryer (figure 2-3) for 72 hours to form freeze dried cakes. The experiment was conducted in triplicate. These samples were applied later in stability experiments.

Figure 2-3: Schematic presentation of the freeze dryer machine

2.2.7. Physical stability assay

Two formulations of navitoclax-PAA-ch_5 and navitoclax-PAA-ch_5-FA were prepared as solution forms and as freeze-dried forms. These formulations were stored in two different environments: at room temperature in dark bench and in fridge at 4 °C for total of four weeks. Each week, the liquid formulations were re-filtered. For the freeze-dried formulations, they were reconstituted and sonicated before filtered. All filtered samples

were analysed using HPLC to quantify the amount of navitoclax lost from the polymeric nanoaggregates. The samples were prepared in triplicates. The amount of drug remaining in formulation compared to its starting concentration was expressed as a percentage.

2.2.8. Cells used and growth, Drugs stock preparation

OVCAR-8 and OVSAHO cells were grown in the in RPMI-1640 culture media supplemented with 10% fetal bovine serum (FBS), 2mM of L-glutamine and 50 µg/ml (IU/ml) of penicillin-streptomycin. Each cell line was incubated in this RPMI-1640 in 5% CO_2 at 37 ºC until the cells became confluent. Navitoclax (ABT-263) was prepared as a solution of 20 mmol/L in DMSO (10 mg of navitoclax in 513 µl of DMSO). Of note, concentrations of DMSO between 0.1-0.5% according to our experience in the lab were seen to be safe for are not toxic to the cell lines used here, whereas 5% is very high and may lead to toxicity by dissolving the cell membrane.

For carboplatin, its stock solution was prepared in PBS of 13.5 mmol/L (5 mg of carboplatin in 998 µl of PBS). The folic acid stock solution was prepared in distilled water of 4.53 mmol/L (1 mg of folic acid in 500 µl of distilled water).

2.2.9. Seeding and harvesting

Cells were incubated in a culture medium in 5% CO_2 at 37 ºC until the cells became more than 70-80% confluent. After that, the growth medium was removed from cells, and then the cells were washed with PBS. Then, cells were trypsinized using 0.01% trypsin in PBS before being incubated for 3 min in 5% CO_2 at 37 ºC with shaking until

the cells were detached. After checking that detachment of the cells, the growth medium was added to stop the trypsin. Then, cells were collected using centrifugation (150 x g, 3 min) at room temperature. After that, the supernatant was removed, and the pellets were re-suspended using a growth medium before being transferred to a new flask (T25 or T75), which contained a suitable volume of growth medium. These cell pellets also were alternatively used for SRB proliferation assay and other assays. The haemocytometer was used to count the cells and to calculate the exact number of cells required for a specific experiment. After that, culture plates (96 well plates, 6-well plates, 12-well plates) were used to seed the cells in depending on the need for any experimental procedure.

2.2.10. Cryopreservation of adherent cell lines

OVCAR-8 and OVSAHO cells were collected as mentioned in the previous section. After that, the cells were collected as pellets using centrifuge (150 x g, 3 minutes). The supernatant was discarded, and the pellets were re-suspended in a freezing medium containing 10% DMSO (50 µl of DMSO in total of 500 µl of growth medium). 200 µl were put into cryovials before being frozen slowly for 24 hours to be inserted in racks in liquid nitrogen.

2.2.11. Thawing cells

Resuscitation of cells kept stored in liquid nitrogen was conducted by taking the preserved cryovials and then thawing them rapidly in the water bath at 37 °C. The liquid was transferred into a 15 ml tube that contains 5 ml of growth media. Cells were collected using centrifuge (150 x g, 3 minutes). After that, the supernatant was

removed, then, the cell pellets were mixed with a pre-warmed culture media before being transferred into a T25 flask. That flask was incubated for one day in the incubator in 5% CO2 at 37 ºC. After 24 hours, the growth medium was changed with a new fresh media.

2.2.12. Proliferation assay (Sulforhodamine B (SRB) assay)

Cells were collected by trypsinization as mentioned above and resuspended in growth medium (62,500 cells/ml OVSAHO, OVCAR-8 25,000 cells/ml), plated (80 µL) in 96-well plates and were incubated for 24 hours in 5% CO_2 at 37 ºC. On the next day, cells were treated with drugs (20 µL) with five times the desired final concentration, and then the plates were incubated for three days at 37 ºC / 5% CO_2. After three days, the culture medium was aspirated, and the cells were fixed by adding 100 µL of cold 10% trichloroacetic acid (TCA) before being placed on ice for 30 minutes. After that, the plates were rinsed five times in tap water in a bucket, then allowed to dry. After drying, 100 µL 0.4% sulforhodamine B (SRB) were added to stain the cells and left at room temperature for 30 minutes. Following that, SRB was removed, and the plate was washed three times with 100 µl of 1% acetic acid before being dried. Tris (10 mM) of 100µL was added to solubilize the SRB dye. The optical density was measured using a plate reader at a wavelength of 570nm. Finally, the data were analysed using GraphPad Prism 8 software. The Non-linear regression option was used to fit a four parameters Hill equation, and the IC_{50} of drugs was calculated. The normalization was calculated depending on the control absorbance reading. The mechanism of how SRB assay work is illustrated in figure (2.3).

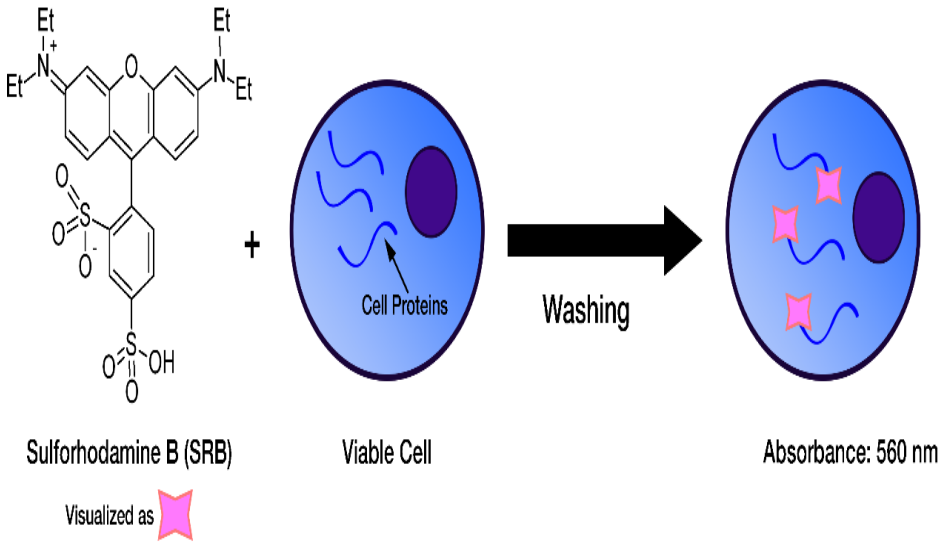

Figure 2-4: The mechanism of action of SRB dye assay, in which the SRB dye binds electrostatically to proteins basic amino acids in TCA-fixed viable cells (CEPHAM LIFE SCIENCES, 2019).

2.2.13. Caspase 3/7 activity assay

Caspase-Glo Assay was conducted to measure the apoptosis by quantifying the activity of executor caspases (caspase-3 and caspase-7). 25,000 cells/ml for OVCAR-8 and 62,500 cells/ml for OVSAHO in a volume of 80 µl were cultured in 96-well plates and were incubated for 24 hours in 5% CO_2 at 37 ºC. After 24 hours, cells were treated with different drugs as shown in table. After incubation for 48 hours, the activity of caspase 3/7 was carried out by adding 20 µl of caspase 3/7-reagent to each cell well, then the plate was protected from light using a foil cover, the plate was gently agitated, incubated at room temperature on a rocker for 30 minutes. Later, 100 µl from each well was transferred to an opaque-walled 96-well plate and the luminescence was measured using a microplate reader. The normalization in combination assay was calculated depending on the caspase 3/7 activity of carboplatin. Figure (2.4 (A, B))

shows the mechanism of action of caspase 3/7 assay and the assay procedure, respectively.

Table 2-3: Drugs with their final concentrations that were used in caspase 3/7 assay

Drug	Final drug concentration	Equivalent polymer concentration
Navitoclax-PAA-ch$_5$ (encapsulated form) (NP(N))	2.5 µM, 1 µM	15 µg/ml, 6 µg/ml
Navitoclax-PAA- ch$_5$-FA (encapsulated form) (NPF(N))	1 µM	20 µg/ml
Navitoclax	2.5 µM, 1 µM	----
PAA- ch$_5$ alone (NP(E))	15 µg/ml, 6 µg/ml	----
PAA-ch$_5$-FA (NPF(E))	20 µg/ml	----
Carboplatin	13 µM	----
A combination of NP(N) and carboplatin	1 µM/ 13 µM	6 µg/ml
A combination of NPF(N) and carboplatin	1 µM/ 13 µM	20 µg/ml
A combination of NP(E) and carboplatin	6 µg/ml/ 13 µM	----
A combination of NPF(E) and carboplatin	20 µg/ml/ 13 µM	----

This table shows the drugs that were used in caspase 3/7 assay and their final concentrations.

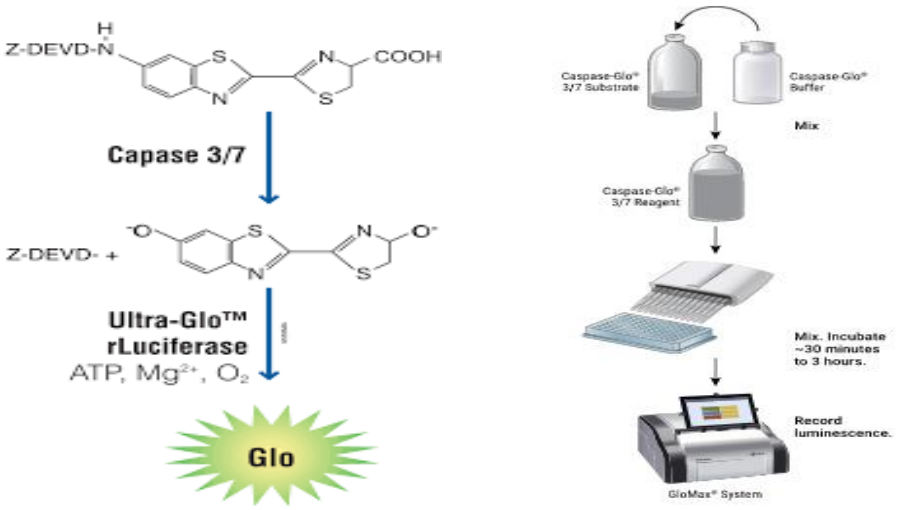

(A) (B)

Figure 2-5: (A) Caspase-3/7 cleavage of the luminogenic substrate containing the DEVD sequence. (B) Caspase-3/7 assay procedure (Promega, 2020).

2.2.14. Trypan blue assay

100,000 cells/well from either OVCAR-8 and OVSAHO were cultured in 12-well plates and incubated overnight. After 24 hours, drugs were added. PAA-ch_5 alone and PAA-ch_5-FA were applied to the cells with different final concentrations (1-500 µg/ml). NP(N) and navitoclax alone also NPF(N) and navitoclax alone were compared by adding the same final concentration of navitoclax (0.15-2.5 µM) and (0.2-1 µM), respectively. To get full navitoclax dose response curves another three final concentrations of 5 µM,10 µM, and 20 µM were applied. For the study of a combination of drugs, the drugs were added with final concentrations as in caspase assay.

After incubation for 72 hours, the supernatants were collected into 15 ml tubes, 200 µl of PBS were added to each well then, the PBS was added to the tubes. After that, cells were trypsinised to detach the adherent cells. Media was added to stop trypsinisation and added to the sample tubes before centrifugation (150 x g, 3 minutes). After that, the supernatant was discarded, and the pellets were re-suspended in 500 µl RPMI-1640 media. 15-30 µl of each sample was pipetted and mixed with an equal volume of trypan blue (0.4% in PBS). 10-20 µl was added to the haemocytometer to count the cells, and the cells were differentiated as dead cells (blue-stained) and live cells (exclude stain). At least 100 cells were counted for each sample in each experiment. Moreover, we used a hemocytometer and counted four or five different squares then got the mean of each count. Moreover, the experiments were performed separately in 3 different days. Also, each experiment was repeated three times using separate biological replicates. The investigator was not blinded to the identity of the samples. The percentage of viability and toxicity was calculated using following equations.

% cell viability = No. of cells alive / (No. of cells alive+ No. of dead cells)

% cell toxicity = No. of dead cells / (No. of cells alive+ No. of dead cells)

2.2.15. Bliss independence criterion

The Bliss independence principle, which was introduced by bliss in 1939, was used in trypan blue assay, annexin V/PI to determine the expected effect of the drug combination and compare it with the observed effect of the same drugs combination. This was used instead of the combination index formula which required a full dose response and determination of an IC_{50}, and it allows quantification of the synergy/antagonism between two drugs. The bliss independent criterion was calculated using the following equation:

$$E_{(x,y)} = E_{(x)} + E_{(y)} - E_{(x)} \times E_{(y)}$$

Where $E_{(x,y)}$ is the expected effect of the combination of the drugs X and Y, respectively. $E_{(x)}$ is the effect of drug x, and $E_{(y)}$ is the effect of drug y. The paired t-test was used to compare the expected effect of the drug combination calculated using the Bliss independence criterion and the observed drug effect determined in the experiment.

2.2.16. Western blot assay

2.2.16.1. Preparation of cell lysates

100,000 cells/well from both OVCAR-8 and OVSAHO were cultured in 12-well plates before being incubated overnight. After 24 hours, drugs were added the same in trypan

blue assay and caspase assay. After incubation for 48 hours, the supernatant was collected. Trypsin was added to each well to detach the adherent cells, media was added to stop trypsinisation and both were added to the corresponding supernatant before being centrifuged (150 x g, 3 minutes). After that, the growth medium was aspirated and the precipitated pellets were washed with cold PBS before being centrifuged again (250 x g, 3 minutes, 4ºC). The supernatant was discarded, and the pellets lysed with100 µl RIPA (Radio-Immunoprecipitation Assay) buffer (0.5% sodium deoxycholate, 20 mM HEPES, 2 mM EDTA, 150 mM sodium chloride, and 1% NP40), supplemented with 10 µM pepstatin, 120 µM leupeptin, and 1 mM phenylmethanesulfonyl fluoride (PMSF). After mixing, the samples were centrifuged (15000 RPM, 10 minutes, 4 ºC). Later, the supernatant was collected and kept frozen at -80 ºC before analysis using Bicinchoninic acid Protein assay (BCA) and western blotting.

2.2.16.2. Bicinchoninic acid Protein assay (BCA)

Standard samples were prepared of eight different concentrations of Bovine serum albumin (BSA, 0- 2 mg /ml). The BCA reagent was prepared by adding 4% copper (II) sulphate pentahydrate solution to the Bicinchoninic acid Protein assay kit solution in a ratio of 1:50. From the latter prepared solution, 100 µL was added to the wells in 96-well plates that contained 10 µL of the BSA standards or protein lysates, then incubated for 30 minutes at 37ºC. The BioTek Synergy 2 multi-mode microplate reader was used to measure the optical density at a wavelength of 570nm. A standard calibration curve was conducted on the protein standard from the absorbance readings

of the BSA standard and then were analyzed using linear regression. Figure (2.5) shows the mechanism of action of BCA assay.

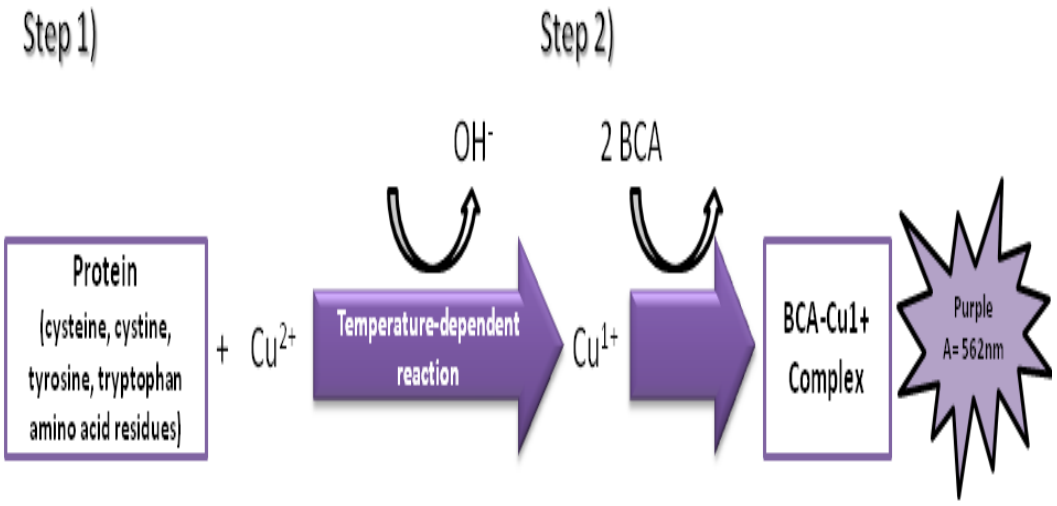

Figure 2-6: Mechanism of action of BCA assay (Microamaze, 2015).

2.2.16.3. Proteins loading, transferring, and reading

Running buffer comprised of 14.4 g/L glycine, 3 g/L grams Tris, 1 g/L sodium dodecyl sulphate; Transfer buffer comprised of 14.4 g/L glycine, 3 g/L Tris base, and 0.75 g/L sodium dodecyl sulphate and 20% methanol. The TBST was prepared using 6.7 g/L Tris base, 70.2 g/L grams Tris hydrochloride (pH 7.4), 10 ml Tween-20, 87 g/L NaCl, pH 7.0-7.2.

From each protein sample, that was measured using the BCA assay, 10 µg was mixed with 5 µl of SDS-Nupage sample buffer (Invitrogen) containing 5% β-mercaptoethanol and incubated at 80 ºC for 15 minutes. During that, the 4-20% Tris-Glycine (Nusep) polyacrylamide gradient gel was washed two to three times with the running buffer

before being inserted into the tank. After that, the samples were loaded into the gel wells with a prestained protein ladder (PageRuler Plus), which was loaded on the first well of each gel for estimating the size of each detected protein. The running buffer was added to the tank until it covered the gels completely. After filling the tank and attaching the electrodes, the power supply was set at 200 V for 40 minutes.

After completion, the gel was removed carefully and was covered with poly (vinylidene difluoride) (PVDF) membrane and sponges. The separated proteins were then electro-transferred onto using cold transfer buffer solution (230 mA, 30 V, for 1 hour). After the transfer was completed, the PVDF membrane was blocked by soaking it in 5% blocking milk solution in TBST for 1 hour at room temperature. The PVDF membrane was incubated with the primary antibody (PARP, Cell Signalling Technology) or (GAPDH, Thermo-fisher scientific) in TBST/ 5% milk with 1/2000 dilution for PARP and GAPDH antibodies overnight s at 4°C. On the next day, the PVDF membrane was washed three times with TBST, then incubated with 1:1000 HRP-conjugated anti-rabbit or anti-mouse antibodies, at room temperature with gentle rocking. After that, the PVDF was washed in TBST three times. UptiLight HRP chemiluminescent substrate was applied to detect the immuno-reactive bands in the membrane using FluorChem M Imager.

2.2.17. Cellular uptake

OVCAR-8 and OVSAHO were seeded in 12-well plates at a density of 100,000 cells/well. They were incubated overnight with 5% CO_2 at 37 °C. After 24 hours, navitoclax with a final concentration of (2.5 µM) and NP(N) with also a final concentration of (2.5 µM) were added to each well separately also navitoclax with a final concentration of (1 µm) and NPF(N) with also a final concentration of (1 µM) were

added to each well separately and incubated for different time frames 4 hours, 24 hours, and 72 hours. After the incubation, the media was aspirated, and the treated cells were washed with phosphate buffer solution (PBS) three times. Trypsin 0.01% of 500 µl was added to each well to detach the cells. After that, fresh media was added to stop the trypsin. The suspension of cells was centrifuged (170 x g, 3 minutes). The supernatant was discarded, and the pellet was resuspended before the cells were counted. 100,000 viable cells of each cell line were then transferred into new tubes and the tubes were centrifuged (170 x g, 3 minutes). The supernatant was removed, and the pellets were resuspended using 1 ml of sterilized water. After that, the tubes were put in vortexed gently for 30 seconds. Then, the tubes were centrifuged again (170 x g, 3 minutes) before water was aspirated completely, and the pellet was resuspended again with 1 ml of the mobile phase before being measured through the HPLC. The concentration of navitoclax alone and in combination with PAA-ch_5 or PAA-ch_5-FA were measured at 215 nm and analysed by using HPLC. All experiments were carried out in triplicate.

2.2.18. Measurement of annexin V/PI labelling

One marker of apoptosis is the appearance of phosphatidylserine proteins (PS) on the cellular surface, and this can be detected by the binding of annexin V to these PS molecules on the cellular surface. As such, this assay is applied to detect viable and apoptotic cells. In this protocol, cells were seeded and treated the same way as the trypan blue assays. After incubation for 48 hours, cells were washed with 1 ml of 1× annexin V binding buffer. After that, the cells were centrifuged (300 x g, 10 minutes). The supernatant was discarded, and the cells were re-suspended gently with 100 µl of 1× annexin V binding buffer before 10 µL of annexin V fluorochrome was added and

the formed solution was then mixed gently again. This mixture was kept in the dark for 15 minutes at room temperature. After that, the cells were rewashed with 1 ml of 1× annexin V binding buffer before being collected by centrifugation (300 x g, 10 minutes). The supernatant was aspirated, and the cells were resuspended in 500 µl of 1× annexin V binding buffer. Before analysis by flow cytometry, 1 µg/ml of PI solution was added to detect dead cells. The mechanism of action of annexin V/PI assay is illustrated in figure (2.6).

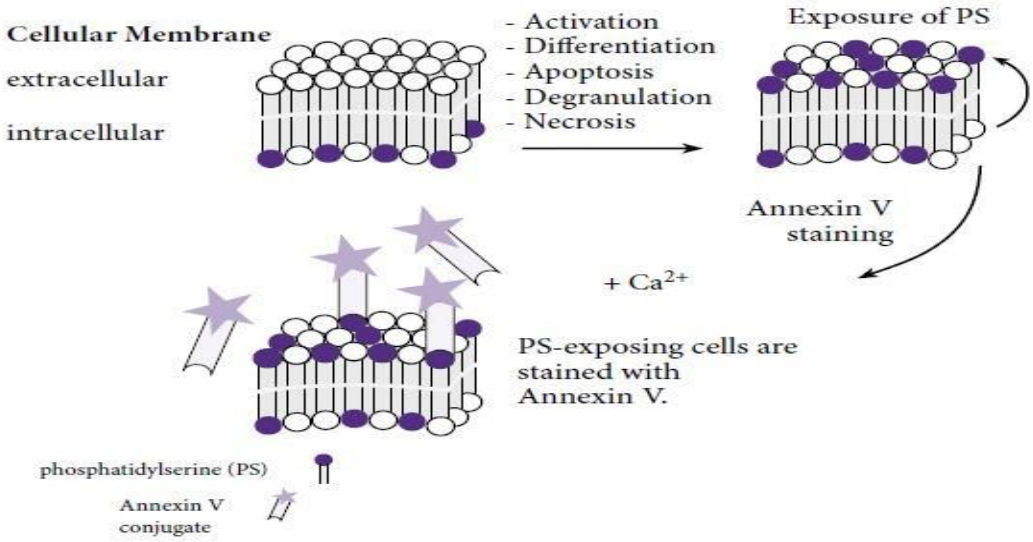

Figure 2-7: mechanism of action for annexin V/PI staining.

2.2.19. Effect of folic acid competition on cellular toxicity

The cell that was chosen in this assay was OVSAHO because it showed a significant sensitivity to navitoclax-PAA-ch$_5$-FA and the literatures showed that it has a high folic acid receptor expression on its surface when compared with other ovarian cancer cell lines. OVSAHO cells (80 µL) were seeded in 96-well plates (62,500 cells/ml) and were incubated for 24 hours in 5% CO_2 at 37 ºC. On the next day, cells were treated with 20 µL of a serial dilution of folic acid (0.78125-200 µM) with five times the desired final

concentration, and then the plates were incubated for three days at 37 ºC / 5% CO_2. After 72 hours, the medium was aspirated, and the same steps followed in proliferation assay using SRB assay was followed. The experiment was conducted in triplicate.

After determination that that a concentration of 0.1 mM folic acid was not toxic, OVSAHO cells were treated with the combinations of the drug either alone or with folic acid to block folate receptor mediated endocytosis. OVSAHO cells of 100,000 cells/ well were seeded on 12 well plate and incubated for one day. After 24 hours, and before 30 minutes from adding the drugs, folic acid with a final concentration of 0.1 mM was added on specified wells, (figure 2.7). After 48 hours, the cells were analysed by staining with trypan blue as described before. The experiment was conducted in a triplicate.

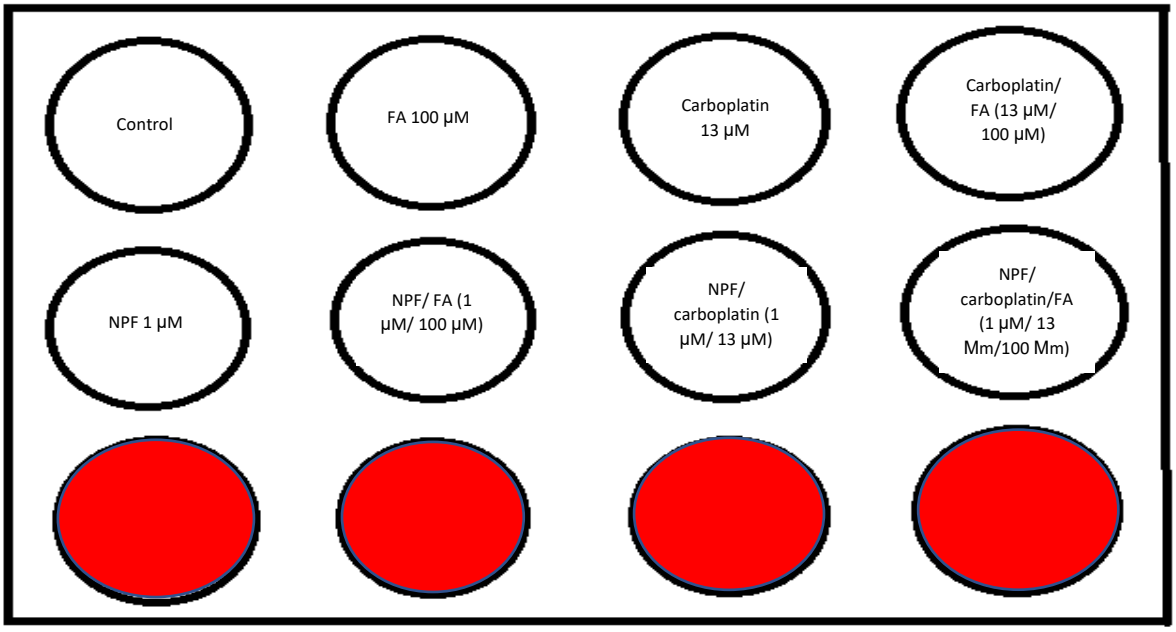

Figure 2-8: Schematic representation for the 12-well plate that was applied to conduct folic acid competition assay.

2.2.20. Statistical analysis

Graphpad Prism software version 8 was used to analyse data from cell growth assays and cytotoxicity assays. Nonlinear regression was used fit a 4-parameter Hill equation sigmoidal dose-response curve. From this the concentration that is needed to kill 50% (IC_{50}) of the cells was determined. Sample means were compared statistically using t-test, ANOVA test (one-way and two-way) followed by Tukey's *post hoc* test. This was applied to determine if there are statistically differences between the means of the different experimented groups.

Chapter 3. Formulation and analysis of navitoclax polymer complexes

3.1. Introduction

One of the most widely used graft polymer backbones is poly(allylamine) (PAA) (Hoskins *et al.*, 2011), which is a water-soluble, cationic, and long-chain polymer (Thompson *et al.*, 2008; Hoskins *et al.*, 2010; Alsuraifi *et al.*, 2018). This PAA has been used clinically as an oral phosphate binder, and the thiolated form has been reported to increase permeability within the intestines (Hoskins *et al.*, 2010; Hoskins *et al.*, 2011). Recently, the use of PAA as the hydrophilic backbone of the amphiphilic comb-shaped polymer has been reported (Hoskins *et al.*, 2012). As with other amphiphilic polymers, this polymer can form self-assemblies once put in the aqueous media as the hydrophobic grafted groups aggregate and shield themselves against the aqueous media. These nanoaggregates have been studied as universal drug carriers for various water-insoluble drugs, including anticancer medications such as paclitaxel and etoposide (Hoskins *et al.*, 2010; Al Ameri *et al.*, 2020).

The PAA amphiphiles have been grafted with various hydrophobic pendant groups (Thompson *et al.*, 2008; Hoskins *et al.*, 2012), which can significantly impact the polymer characteristics and the nanoaggregates formed in the aqueous environment (Thompson *et al.*, 2008). Thompson *et al*. started the grafting of PAA by adding palmitoyl, cetyl, and cholesteryl groups with different molar ratios to the PAA backbone (Thompson *et al.*, 2008). They reported that adding quaternary ammonium ion is responsible for decreasing the size of the formed self-assemblies and increasing their overall water solubility (Thompson *et al.*, 2008; Hoskins *et al.*, 2012). Later Hoskins and her group grafted the PAA with different types and level of hydrophobic groups such as 9-fluorenylmethoxy (fmoc), dimethylamino- 1-naphthalenesulfonyl (Dansyl),

naphthalene, and cholesteryl moieties, to increase the loading of lipophilic drugs and hence, increase their water solubility (Hoskins *et al.*, 2011). Surprisingly, it was reported that the hydrophobic pendant groups are responsible for decreasing the cytotoxic effect of the polymer on cells (Hoskins *et al.*, 2012). Fmoc, dansyl, and naphthalene are common aromatic moieties that possess planar architectures. Of note, these compounds have inherent fluorescent properties, which are related to the presence of the conjugated aromatic ring systems. As such, these aromatic groups avoid the need to attach external fluorescent tags, and thus this can give a more precise representation of its fate *in vivo*. In addition, they have a role in forming self-assemblies to carry hydrophobic drugs (Hoskins *et al.*, 2012). The limitation of using fmoc and naphthalene is that they have flat stereochemistry, which will lead to π-π stacking, and thus leads to the formation of excimers. Accordingly, this limits the payload at higher concentrations in the inner core because these excimers prevent the core from expanding (Hoskins *et al.*, 2011; Hoskins *et al.*, 2012). This limitation was explained later when it was reported that the naphthalene and fmoc moieties have two CAC values (Hoskins *et al.*, 2012). Although dansyl has an aromatic structure like fmoc and naphthalene, the presence of the N, N-dimethylamino side chain prevents the stacking interactions as it gives rise to a 3-dimensional (3-D) structure (Hoskins *et al.*, 2011).

Several hydrophobic drugs have been used with the PAA with different pendant groups to see the effect of this polymer in increasing their water solubility and the changes in physical characteristics for both the drug and the polymer itself has been studied. These model drugs were propofol, griseofulvin, and prednisolone (Hoskins *et al.*, 2011; Barnett *et al.*, 2013), and bisnaphthalimidopropyldiaaminooctane (BNIPDaoct)

(Hoskins *et al.*, 2010). Moreover, Barnett *et al*. synthesised and evaluated a new class of poly(allylamine) (PAA) polymer grafted with oxadiazole pendant group using a 5% molar ratio. Since this pendant group has thiol group, this can enhance the attachment of hybrid iron oxide-gold nanoparticles (HNPs) by dative covalent bonding (Barnett *et al.*, 2013). The polymeric amphiphiles with HNPs have been reported to be used as a dual vehicle for both drugs and imaging agents. The model hydrophobic drug used with that polymer was Paclitaxel (PTX), as it has poor water solubility (Barnett *et al.*, 2013). Furthermore, they reported that there was also a successful encapsulation of BNIPDaoct in the PAA self-assembly in both PAA-Ox5 and PAA-Ox5-HNP, which led to an increment in the cytotoxicity of this anticancer drug on BxPC-3 pancreatic adenocarcinoma cells (Barnett *et al.*, 2013).

For the cholesterol pendant group, its grafting resulted in superior drug loading within the PAA nanoaggregates, possible due to its high tendency to form nanoaggregates even at low molar grafting (Hoskins *et al.*, 2012). Importantly, cholesteryl group possesses unique characteristics that give it an advantage over other pendant groups such as being biodegradable, biocompatible and its ability to act as a permeability enhancer (Zhou *et al.*, 2009). Furthermore, cholesterol, which is a sterol compound (Hoskins *et al.*, 2011; Hoskins *et al.*, 2012), is an integral part of the cell membrane that plays a pivotal role in multiple biological pathways such as cellular migration and cellular adhesion (Zhou *et al.*, 2009; Hoskins *et al.*, 2012; Yusa, 2012; Yang *et al.*, 2019). Thus, this makes cholesterol very important in highly proliferative cells such as cancer cells (Cerqueira *et al.*, 2016). Significantly, cholesterol moiety has been reported to induce cytotoxicity and this was demonstrated by Xu *et al.* when they used cholesterol as a hydrophobic cap on poly(2-methacryloyloxyethyl phosphorylcholine)

(Xu *et al.*, 2005). Furthermore, other than the cellular function of cholesterol, it participates in vitamin D, steroid hormones, and bile salt synthesis (Cerqueira *et al.*, 2016).

The cholesterol, once added into self-assemblies of the amphiphilic comb-shaped polymer, gives a chance for hydrophobic drugs and hydrophilic drugs to be incorporated as it can form a vesicular bilayer structure (Hoskins *et al.*, 2012). Although several model drugs and pendant groups were studied, it was found that the cholesteryl modified polymer gave a higher encapsulation capacity when compared with the polymer alone (Zhou *et al.*, 2009). Notably, using cholesterol as a pendant group gives the self-assemblies unique optical characteristic (Wang *et al.*, 2011). Although it was reported that even at low molar grafting, it could form self-assemblies in a liquid environment (Zhou *et al.*, 2009; Yusa, 2012), the higher cholesterol grafting is accompanied by higher core-shell stability of the formed self-assembly (Zhou *et al.*, 2009).

3.2. Factors affect nanoaggregates

Several factors affect the self-assembly of nanoaggregates, including the type of hydrophilic segment, the type of hydrophobic monomers, their sequence, and their molar grafting percentage (Yusa, 2012). The drug loading capacity of the amphiphilic polymers is affected by several factors, and these parameters include drug physicochemical properties, the type of hydrophobic pendant groups, and the ratio of hydrophobic block versus the hydrophilic blocks (Hoskins *et al.*, 2012). It has been reported that if the level of hydrophobic modification has increased, this would lead to

a higher lipophilic content. Accordingly, this causes a more robust interaction with the drug particles, which leads to higher encapsulation efficacy (Hoskins *et al.*, 2012). Other properties that can affect the loading of hydrophobic molecules include the drug feeding ratio (Thompson *et al.*, 2008; Hoskins *et al.*, 2012; Hussein and Youssry, 2018) and the polymer concentrations (Hussein and Youssry, 2018), which are determinant factors as they can affect not only the loading capacity but also the size and the polydispersity of the formed micelles. However, this is not totally true as there is a limit to which the polymer cannot load more drug particles in its core and decrease in loading capacity (Hussein and Youssry, 2018). Furthermore, it was demonstrated that the miscibility or the compatibility between the drug and the polymer is also very important in drug loading (Hoskins *et al.*, 2011; Hoskins *et al.*, 2012; Hussein and Youssry, 2018). Moreover, the length of the hydrophilic backbone also has a higher impact on increasing the hydrophobic drug solubility as it can encapsulate higher drug quantities and large drug molecules without affecting the hydrophobic-hydrophobic interactions that are responsible for shielding the core. However, this is only true up to a limit as it was found that the molecular weight of PAA above 900 kDa, even though it can carry higher cargo, leads to a large nanoaggregate which limits their application to cancer therapy, although they can be applied in other fields where the size is not a determinant (Al Ameri *et al.*, 2020).

Since loading is essential to achieve improvement in the solubilisation, loading will be of lesser importance if the cargo will stay entrapped in the nanoaggregate core and not released (Al Ameri *et al.*, 2020). The release of the hydrophobic drugs from the amphiphilic polymer core depends on several factors, including desorption of the polymer nanoparticles' surface, combined diffusion/ degradation process and the

drug's diffusion from polymer nanoparticles. In addition, the polymer molecular weight and drug loading have a crucial role in drug release. It was reported that the high molecular weight of the polymer can potentially entrap the drug inside its core compared with the low molecular weight. Although it was found that the polymers with high molecular weight have a higher loading capability, high stability but, at the same time, a prolonged-release which limits their applications in cancer treatment and thus the PAA with the molecular weight of 15 kDa is the most widely used (Al Ameri *et al.*, 2020).

The Critical Aggregation Concentration (CAC) is defined as the lowest concentration required to form polymeric self-assemblies in the aqueous media (Hoskins *et al.*, 2012). The polymeric micelles are a perfect alternative for the traditional surfactants as they have lower CAC (Movassaghian *et al*., 2015; Hussein and Youssry, 2018). The lower CAC means better stability *in vivo* as there is resistance to the dilution the polymers can face and thus minimise the premature release (Hoskins *et al.,* 2012; Hussein and Youssry, 2018). The CAC for the amphiphilic comb-shaped polymers is affected by several parameters such as the hydrophobic pendant group lengths, the level of molar grafting, the molecular weight of the polymeric backbone, the type of the grafted hydrophobic pendant groups, and the stereochemistry of the hydrophobic pendant groups (Hoskins *et al.,* 2012), (Figure 3.1).

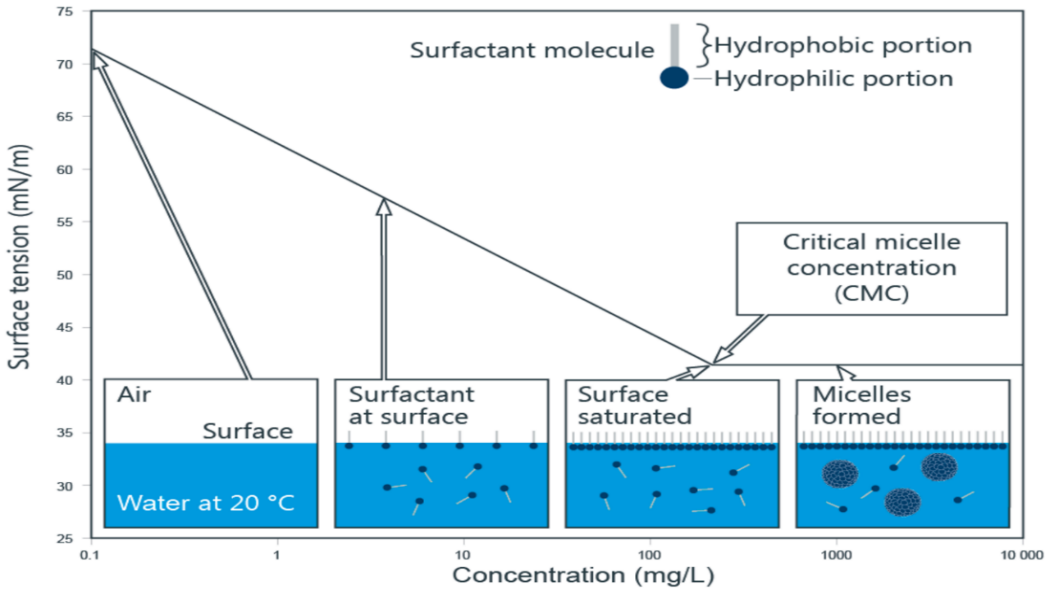

Figure 3-1: Critical micelle concentration and surface concentration (*Critical micelle concentration (CMC) and surfactant concentration | KRÜSS Scientific*, n.d)

3.3. Nano-aggregate formation

Nowadays, there is no universal incorporation method used in drug-polymer systems, which means that there is a need to find a suitable preparation method for each lipophilic drug to be incorporated into a polymer and forming nano aggregates. Thus, several engineering studies are required to improve this technology. The incorporation methods used to form nano aggregates from hydrophobic drugs and polymers are fundamental not only in determining the physical loading efficiencies of the drug particles but also on the micelle size and size distribution (polydispersity) (Hussein and Youssry, 2018). Several methods can be used to encapsulate the hydrophobic drugs inside the polymeric micelles' cores (Hoskins *et al.*, 2012; Hussein and Youssry, 2018). These methods include solvent evaporation, probe sonication, dialysis, and oil/water emulsion (Hussein and Youssry, 2018). In the dialysis method, the drug and the polymer are dissolved in a mixture of organic solvent and water. The solution is placed

onto a dialysis bag that drives the formation of self-assemblies from the polymeric parts with the lipophilic drug upon exchanging water and the solvent out of the dialysis bag. Later, removing the excess free drug is carried out using a syringe filter (0.45 μm). Importantly, there is an advantage in forming nano aggregates in this method. In the solvent evaporation, both the hydrophobic drugs and polymers are dissolved in organic solvents. The pressure is used to evaporate the solvent and to form the nano aggregation, and then the residue will be reconstituted with water. However, the residual organic solvent in these techniques could be toxic and harmful, especially if applied *in vivo.* (Hoskins *et al.*, 2012).

The probe sonication method is a revolutionary technique that is simple, quick and allows for self-assemblies of the lipophilic drug with comb-shaped polymers. In this method, the polymeric amphiphiles form aggregates when put in the aqueous media before the hydrophobic drugs being added, which encourages the drugs to be encapsulated in the self-assembly's core. The excess drug is filtered through a syringe filter, the same as in the evaporation method. The advantageous property of this method over the evaporation technique is that there is a high safety profile for this technique because of not using an organic solvent (Hoskins *et al.*, 2012). Furthermore, sonication effectively reduced the formed micellar size (Hussein and Youssry, 2018), (Figure 3.2).

Although the Microfluidic technology (MF), which is a new technology, has improved the formulation of nanoparticles (Meng *et al.*, 2019), at present, there is no superiority of any preparation method over another in any polymer-drug system. As such, there is

a need for more scientific and engineering studies to significantly develop the incorporation technology (Hussein and Youssry, 2018).

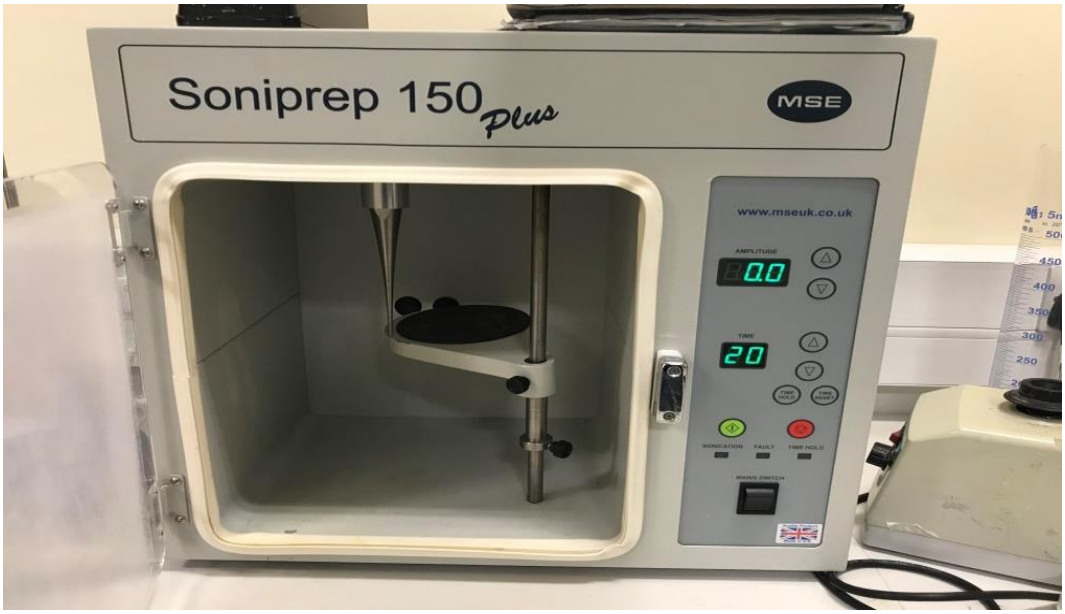

Figure 3-2: Schematic figure of the sonication machine (soniprep).

3.4. Nano-aggregate characterisation

The formation of nanoparticles with a therapeutic efficacy requires appropriate characterisation of these nanoparticles before they can be used (Bhattacharjee, 2016). These characterisations include particle size, surface charge (zeta potential), and polydispersity index (PDI) (Agrawal and Patel, 2011; Bhattacharjee, 2016). This characterisation of nanoparticles has a pivotal role in predicting the nano-drug delivery systems performance in both *in vitro* and *in vivo*. These characteristics affect the nano-drug delivery systems' efficacy, safety, and stability (Agrawal and Patel, 2011). These characteristics are measured using photon correlation spectroscopy (PCS) and

transmission electron microscopy which are used to determine the shape and the size of nanoparticles.

Tyndall (1868) was the first one who experimented with light-scattering for colloidal suspensions. Further experiments followed this until Einstein established the Brownian motion theory in 1905, which elucidated the molecular motion of the particles. Pecora, Pike, Cummins, and others were the first who found the modern dynamic light scattering (DLS) instrument. PCS, also known as dynamic light scattering (DLS), is a great tool that is non-invasive and non-destructive that is used to study the behaviour of the molecules in a solution, (Figure (3.3, A)). The mechanism of action for PCS depends on light scattering. The samples are exposed to a light beam at a specific wavelength, and then light scatters in all directions depending on the size and shape of macromolecules. Since there is a relationship between particle displacement and time, the speed of particles will vary, as small particles will move faster than large particles, and thus the particle size can be measured depending on their speed of motion. Accordingly, the signals that appeared are recorded by specific detectors (Stetefeld *et al*., 2016), (Figure 3.3, B). The PCS application is not limited to study the homogeneity of nucleic acids but extended to include the study of proteins, protein-small molecules interaction, carbohydrates, and nanoparticles (Stetefeld *et al*., 2016).

(A)

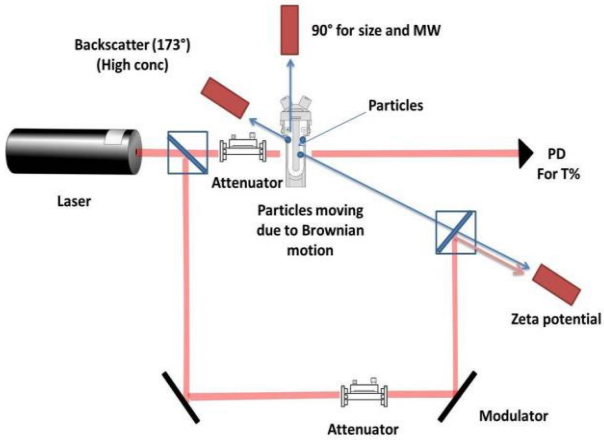

(B)

Figure 3-3: (A) Zetasizer machine. (B) Schematic diagram of how PCS machine works.

Zeta potential (ζ), or the surface charge, which is also called electro-kinetic potential, is an indicator of the overall attraction or repulsion between particles (Khoshnevisan and Barkhi, 2015). It is used to measure the electrical charge of the nanoparticles surfaces in comparison with the outer solution's charge (Ruiz-Cabello *et al.*, 2014). The measurement of zeta potential is exerted initially by measuring the electrophoretic mobility, which is then transferred into zeta potential (Agrawal and Patel, 2011). Its measurement can indicate the nanoparticle colloidal dispersion stability (Agrawal and Patel, 2011; Khoshnevisan and Barkhi, 2015).

3.5. Quantification of Drug Loading

Chromatography, in general, is an important technique that is applied for several purposes, such as purification, identification, and separation of different mixture components. The main principle of chromatography is to separate the mixture

components depending on the distribution of these components between two phases: a stationary and a mobile phase (Coskun, 2016). The movement of the analytes in the mobile phase through the stationary phase is determined by several factors, such as the composition of stationary and mobile phases and the separation temperature (Lech, 2018). Since the mobile phase could be gas or fluid and helps the mixture molecules be transported in; the stable phase (stationary phase) could be fluid or solid (Coskun, 2016). Various chromatography types are available nowadays. These include: Thin-layer chromatography (TLC), Ion exchange chromatography (IEC), Gas chromatography (G.C.), Liquid chromatography (L.C.), and High-performance liquid chromatography (HPLC) (Coskun, 2016).

HPLC separates molecules depending on their distribution between the mobile and stationary phases (Jared, 2015). Its application is not confined to the pharmaceutical field, but extended to include biotechnology, food industries, environment, polymers applications (Sundaram *et al.*, 2009; Malviya *et al.*, 2010; Dong, 2019). Additionally, HPLC is applied in drug discovery, development, and measuring the extent of a drug in a mixture and its release a system (Kazakevich and LoBrutto, 2007). Figure (3.4, A), represents a schematic diagram of the HPLC system (Czaplicki, 2013).

(A)

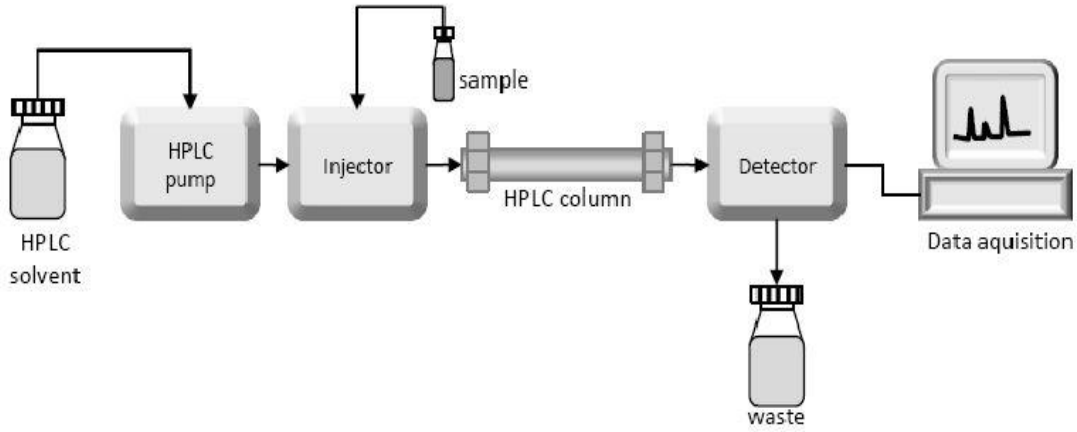

(B)

Figure 3-4: (A) schematic diagram of HPLC (Czaplicki, 2013). (B) RP-HPLC machine

3.6. Aims

1. To encapsulate navitoclax in the PAA-ch$_5$ polymer, exploring if this will lead to a successful encapsulation and determine if this improves the solubility of navitoclax.
2. Determine optimal drug: polymer feed ratios and different polymer concentrations for navitoclax encapsulation and optimise the loading efficiency.

3. Determine the release profile of the encapsulated navitoclax under the sink condition.
4. Determine the physical stability for the encapsulated form of navitoclax using different formulations (liquid and freeze-dried cakes) with different storage conditions.

3.7. Results

3.7.1. Detection of navitoclax, PAA-ch$_5$ using HPLC

To confirm the poor solubility of navitoclax, its powder was added to deionized water with a 1:1 ratio. In addition, the PAA-ch$_5$ was also diluted in water with a ratio of 1:1 and both samples were analysed using HPLC with the conditions described in the methodology section. The HPLC analysis of navitoclax failed to identify a single peak and reflecting the poor solubility of the drug, (Figure (3.5, A)). The PAA-ch$_5$ amphiphile in water was also run on the HPLC and the results showed no peaks at these specific conditions, (Figure (3.5, B)). The rationale behind testing the polymer on its own was to detect any peak that could appear at a similar retention time and as navitoclax and interfere with its detection

(A)

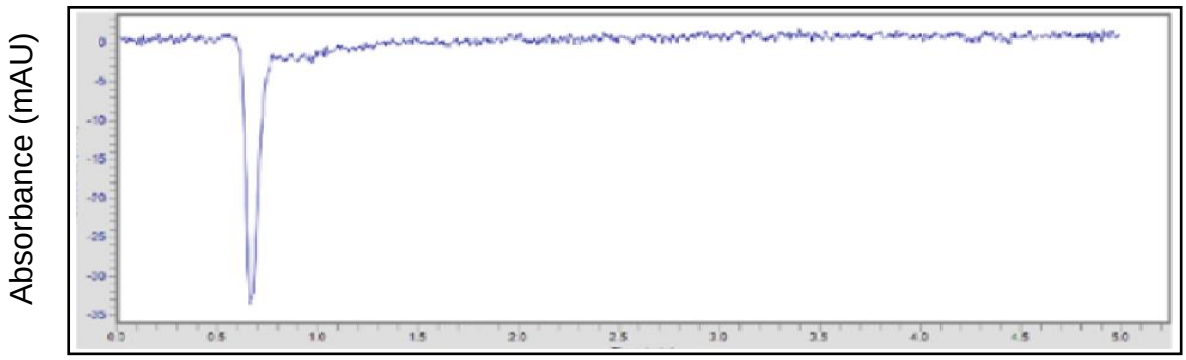

(B)

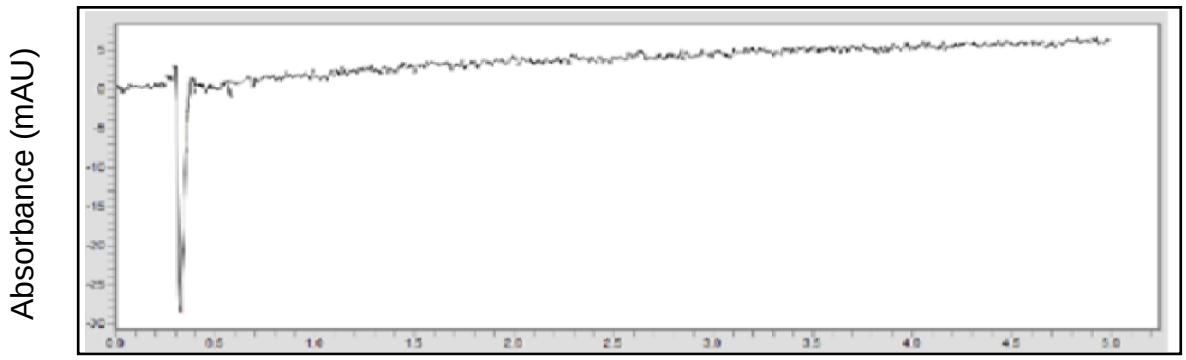

Figure 3-5: Navitoclax and PAA-ch$_5$ water solubility detection by HPLC

(A) This figure shows that there is no peak apparent by HPLC at any retention time after adding navitoclax to water. (B) This figure shows that there is no peak appeared in HPLC at any retention time after adding the polymer (PAA-ch$_5$) in water. (n=1)

3.7.2. Standard calibration curve construction

A standard curve was constructed to allow analysis of navitoclax by HPLC. After dissolving navitoclax in an organic solvent (ethanol) to obtain a range of concentrations (0.03125-1 mg/ml), the samples were analyzed by HPLC. The peaks appeared at a

retention time of 1.43 minute in proportion to the concentration of navitoclax, (Figure 3.6, A). After calculation the area under the curve for the peaks one by one, a calibration curve was instructed, ($y = 5 \times 10^6 x + 106316$, $R^2=0.9998$), (Figure 3.6, B). This equation was subsequently used to calculate the concentration of navitoclax that has been encapsulated in the PAA-ch_5 polymer.

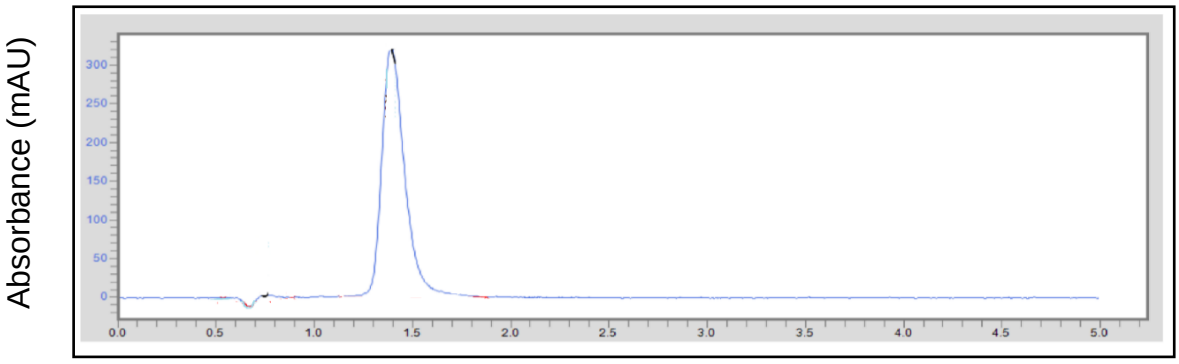

(A)

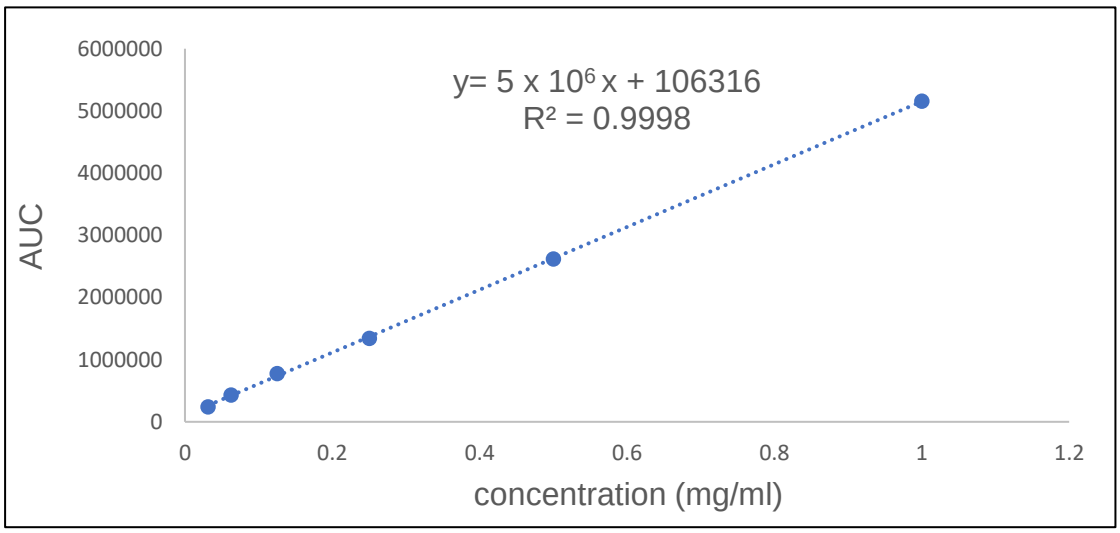

(B)

Figure 3-6: Navitoclax standard curve construction

(A)This figure shows a peak of navitoclax at concentration of 0.06125 mg/ml, this shows that the retention time is 1.43 minutes, which means any peak appeared at this time is related to the navitoclax. (B) Standard calibration curve for navitoclax with its equation. (n=3)

3.7.3. Navitoclax quantification

After the standard curve was constructed, navitoclax powder was added to the PAA-ch_5, before being prob sonicated and filtered. The formed samples, which represent nanoparticles of navitoclax and PAA-ch_5 were measured with the HPLC using the same conditions in the methodology section. The PAA-ch_5 appeared white cloudy before adding the drug to it. However, after adding the drug and filtering the sample, the solution was clear. All samples showed a peak at 1.43 minutes corresponding to the retention time of navitoclax and demonstrating that navitoclax was successfully solubilised in PAA-ch_5 polymer. The navitoclax concentration was highly improved after encapsulation within the PAA-ch_5 amphiphile with around a 100-fold improvement in its aqueous solubility, (Figure (3.7, B)). Figure (3.7, A) shows the navitoclax peak that was encapsulated in the PAA-ch_5 polymer as nanoaggregates using the HPLC.

(A)

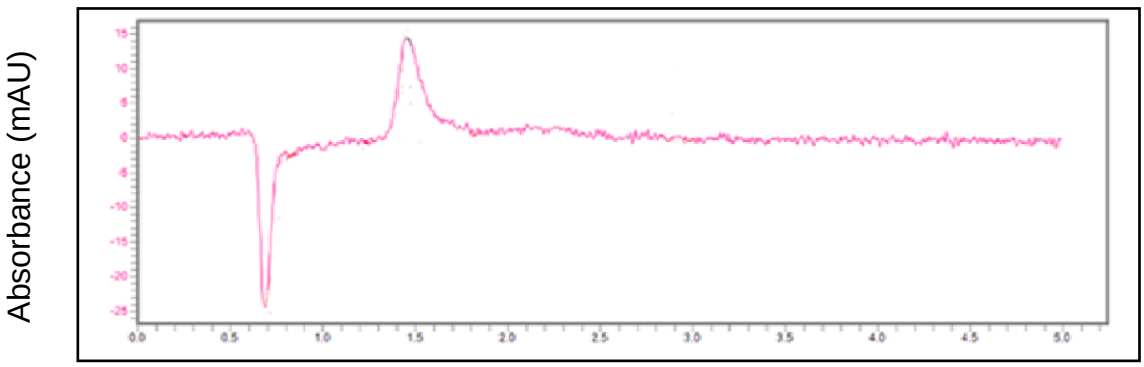

(B)

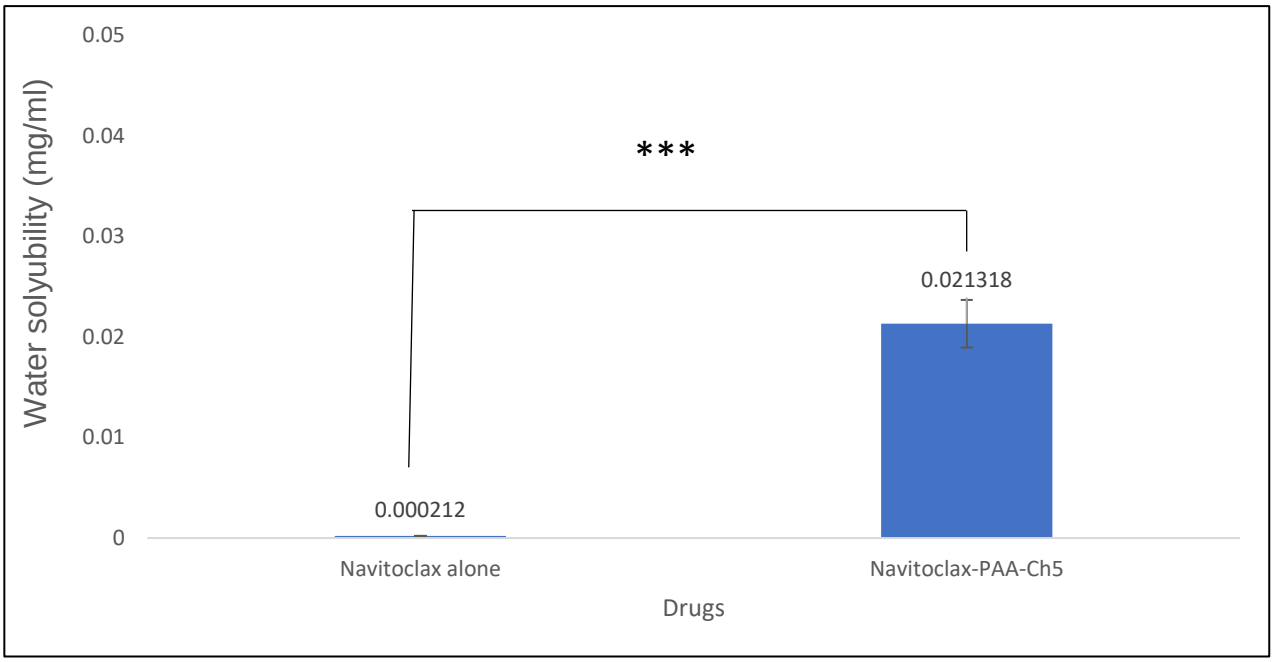

Figure 3-7: Quantification of encapsulated navitoclax inside the PAA-ch$_5$ core

(A)This figure shows a navitoclax-PAA-ch$_5$ sample, which shows a peak at the same retention time of navitoclax standard. (B) This figure represents the maximum concentration of navitoclax that has been encapsulated inside the PAA-ch$_5$ core. The concentration of navitoclax encapsulated was 21.5 µM. (*(***): p<0.001;* data were analysed using paired *t-test)*. Results (mean ± S.D, n=3).

3.7.4. Effect of changing the drug: polymer ratio on loading capacity

Since it was reported the changing in feeding ratio has a positive impact on the hydrophobic loading in the micellar core, the solubility of navitoclax in water when it was loaded into PAA-ch$_5$ was investigated by increasing the feeding ratio of the drug using a fixed polymer concentration. Three different ratios from navitoclax: polymer of 1:1, 5:1, and 10:1 were tested. The ratio of drug to the polymer affected the navitoclax loading and its water solubility, with encapsulated navitoclax concentration increase once the ratios were increased from 1:1 to 5:1 up to 10:1, respectively, (Figure 3.8). The effect of increasing navitoclax: polymer ratio on navitoclax encapsulation and its

effect on loading capacity (%LC) and encapsulation efficacy (%EE) is presented in table (3-1).

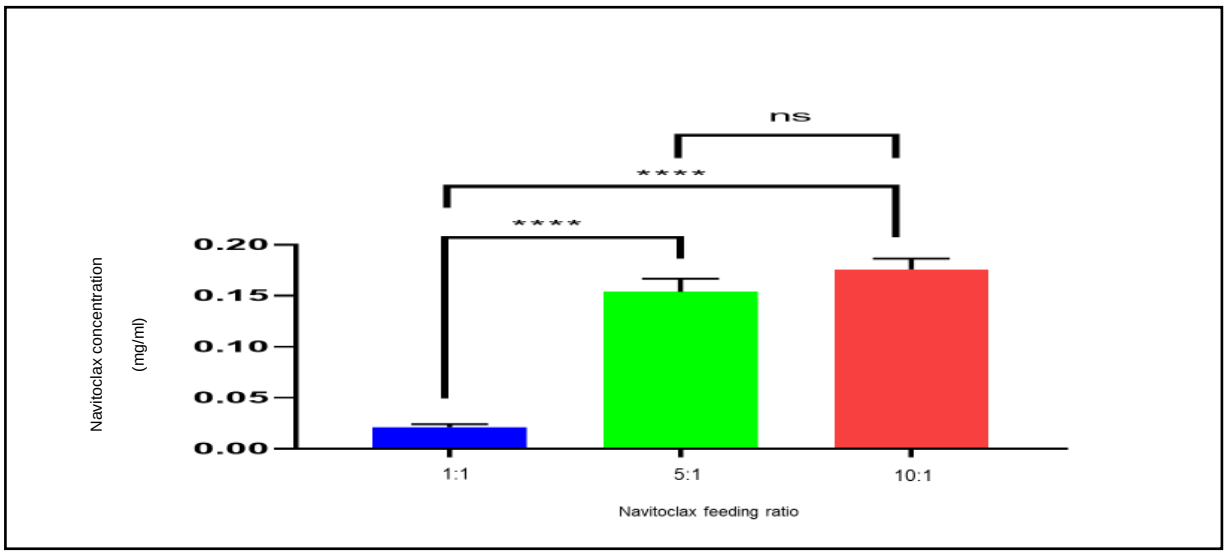

Figure 3-8: Effect of drug ratio on navitoclax encapsulation

This figure shows the effect of using different drug ratios with the fixed polymer concentration. An increment in drug: polymer ratio from 1:1 to 5:1 until 10:1 increases navitoclax encapsulation significantly. (*(****): p<0.0001, (ns): non-significant;* statistical analysis was performed using One-way ANOVA). Results (mean ± S.D, n=3).

Table 3-1: The effect changing navitoclax ratios on navitoclax loading capacity and encapsulation efficacy

Different drug ratio Navitoclax: PAA- Ch_5	Water solubility (mg/ml) Mean	Standard deviation	% LC	% EE
1:1	0.021	0.002	2.13 %	2.13%
5:1	0.154	0.011	15.38 %	3.08 %
10:1	0.176	0.009	17.58 %	1.76 %

This table shows the effect of changing the navitoclax: PAA-ch_5 ratios on navitoclax encapsulation. (%LC): loading capacity and (%EE): encapsulation efficacy for all ratios were also represented. Results (mean ± S.D, n=3).

3.7.5. Effect of changing polymer concentration on the loading capacity

Increasing the polymer concentrations has also been shown in the literature to increase drug solubilisation. Three different polymer concentrations have been selected with a fixed drug ratio. The fixed ratio of navitoclax that was chosen was 1:1, and the three difference PAA-ch_5 concentrations were 1 mg/ml, 3 mg/ml, and 6 mg/ml. The results showed improved navitoclax loading and its water solubility by increasing the polymer concentration even though the same ratio was used. The navitoclax loading was increased significantly by increasing the polymer concentrations, (Figure (3.9). The effect of increasing polymer concentration, with fixed ratio (drug: polymer), on navitoclax encapsulation and its effect on loading capacity (%LC) and encapsulation efficacy (%EE) is presented in table (3-2).

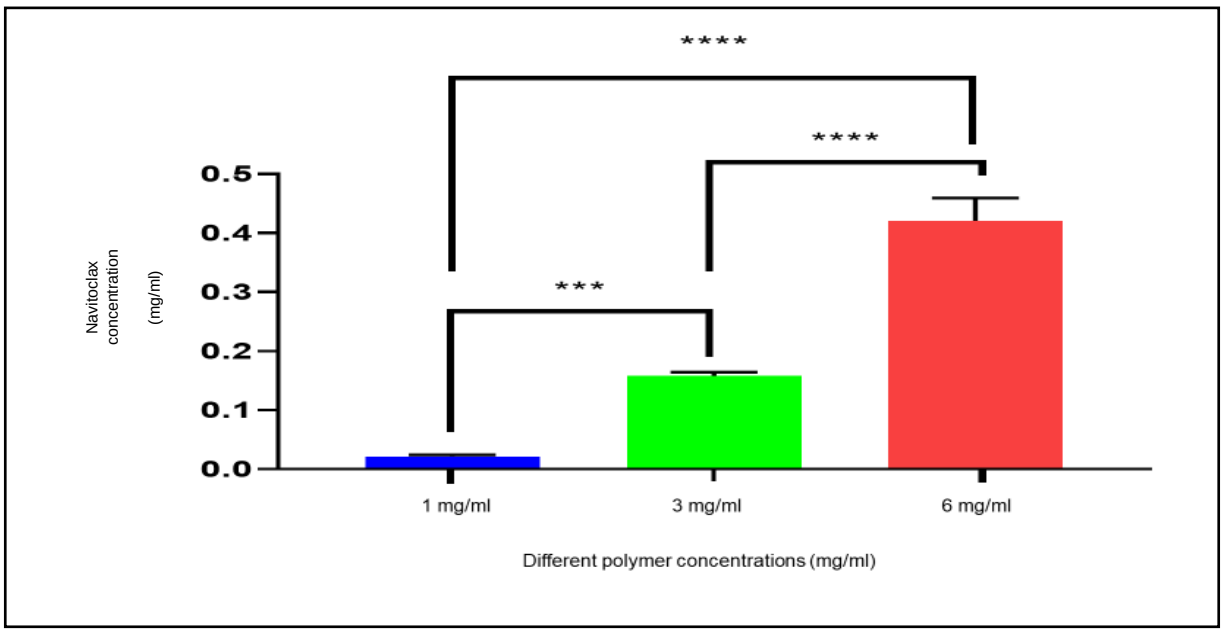

Figure 3-9: Effect of changing PAA-ch$_5$ concentration on navitoclax encapsulation

This figure shows the effect of using fixed drug ratio with the different polymer concentration. An increment in polymer concentration from 1 mg/ml to 3 mg/ml up to 6 mg/ml increases navitoclax encapsulation significantly. (*(***): p<0.001, (****): p<0.0001;* statistical analysis was examined using One-way ANOVA). Results (mean ± S.D, n=3).

Table 3-2: The effect changing PAA-ch$_5$ concentration on navitoclax loading capacity and encapsulation efficacy

Different polymer concentrations with fixed drug ratio	Water solubility (mg/ml) Mean	Standard deviation	% LC	%EE
1 mg/ml	0.021	0.002	2.13 %	2.13%
3 mg/ml	0.158	0.005	5.27 %	5.27 %
6 mg/ml	0.42	0.032	7.00 %	7.00 %

This table shows the effect of changing the PAA-ch$_5$ concentration on navitoclax encapsulation. (%LC): loading capacity and (%EE): encapsulation efficacy for concentrations were also represented. Results (mean ± S.D, n=3).

3.7.6. Nano-aggregate characterisation

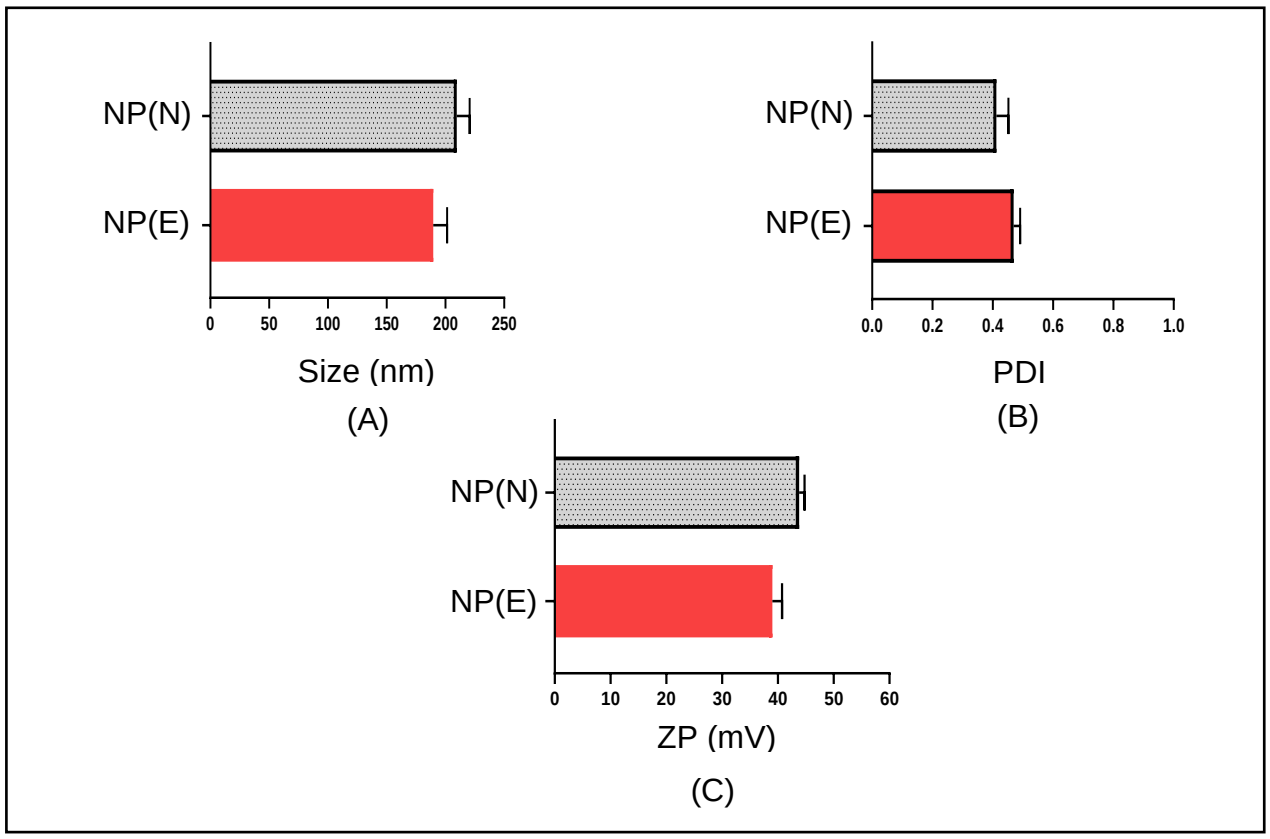

Figure 3-10: The physical characteristics for both the polymer alone and the navitoclax-PAA-ch$_5$.

These three figures show the physical characteristics for both the polymer alone (NP(E)) and the navitoclax-PAA-ch$_5$ (NP(N)). (A) The difference in size of the polymer before and after adding navitoclax. (B) The particles polydispersity of both the polymer and the encapsulated navitoclax in the polymer. (c) The surface charge for both the polymer alone and the encapsulated navitoclax in the polymer. Results (mean ± S.D, n=3).

The zetasizer was used to measure the physical characteristics of the PAA-ch$_5$ (empty polymer) and the loaded navitoclax with the polymer. These include size, polydispersion index, and zeta potential what were evaluated. Figure (3.10, A) shows that the size of the micelles was increased when the drug was added. For the polydispersion index (PDI), it showed that after adding navitoclax, the micellar dispersion was improved, with a slight decrease in the PDI, (Figure (3.10, B)). In

(Figure (3.10, C)), analysis also showed that there was no significant difference in the zeta potential after encapsulation of navitoclax, which means that there was a successful encapsulation that did not affect the polymer surface positively charge.

3.7.7. Drug release

Since the drug release from its delivery vehicle inside the body is the desired outcome, the release of navitoclax from the PAA-ch$_5$ core was tested. The concentration of navitoclax chosen for the release study was 0.0213 mg/ml, which has been achieved by taking a ratio of 1:1 from navitoclax: PAA-ch$_5$. Release was measured in dialysis tube tin PBS for 72 hours. The maximum release percentage that was achieved was 12% after 72 hours, and one-third of this release happened within the first 5 minutes, and around 10% release happened in the first 6 hours, (Figure 3.11). The release was measured at 37 ^{o}C under stirring.

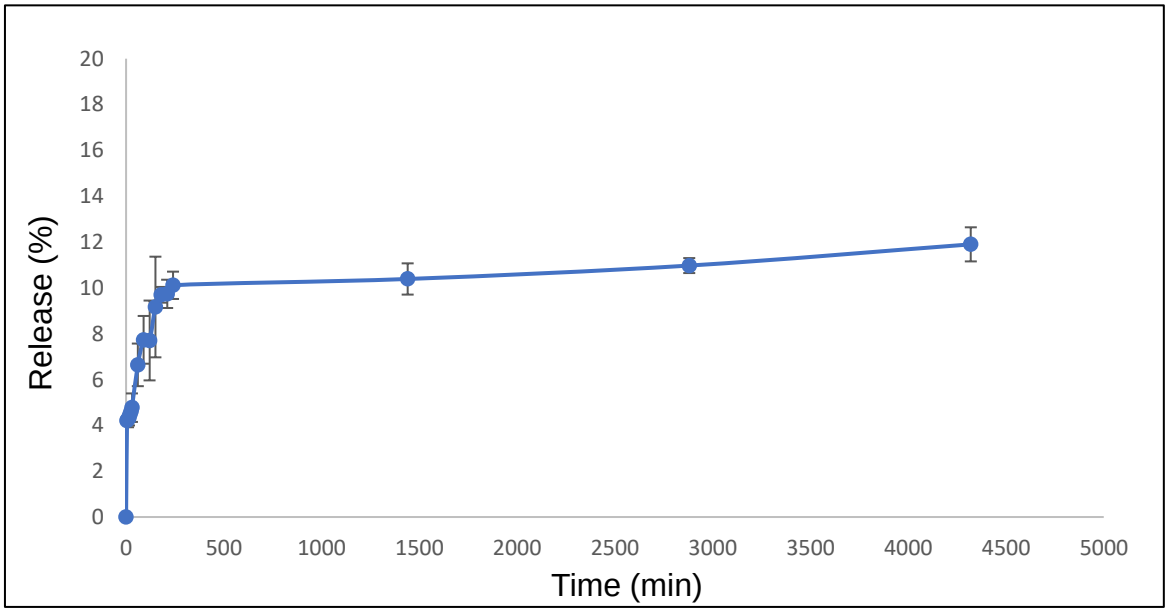

Figure 3-11: Navitoclax release from PAA-ch5 core.

This figure shows the release percentage of navitoclax-PAA-ch5 from the PAA-ch$_5$ polymer in PBS. That release did not exceed 12% of the drug encapsulated after 72 hours. Results (mean ± S.D, n=3).

3.7.8. Formulation Stability

Since stability is considered an essential physical characteristic for any formulation, the navitoclax-PAA-ch_5 formulation samples were prepared in two different states (liquid state and freeze-dried cakes). Samples were prepared and were divided equally as freeze-dried and liquid forms. Furthermore, the samples were also kept in two different conditions: in the fridge at 4 °C and in dark cabinets at room temperature. The samples were assessed weekly for a total of four weeks to measure the percentage of drug lost during storage.

Both freeze-dried forms are more stable than their counterparts in the liquid form for the whole four weeks period, (Figure 3.12). Although there was a gradual loss of navitoclax from the micellar core when the samples were freeze-dried, these sampled could preserve around 85% of the encapsulated navitoclax at 4°C and at room temperature. This was better than the liquid samples that were stored at room temperature or at 4°C. Furthermore, for the liquid samples the cold temperature showed a better navitoclax encapsulation at the end of the four weeks than those kept at room temperature. However, temperature had no significant effect on the freeze-dried forms. Accordingly, the freeze-dried forms and cold temperature are the best environments to preserve this type of nano-formulations.

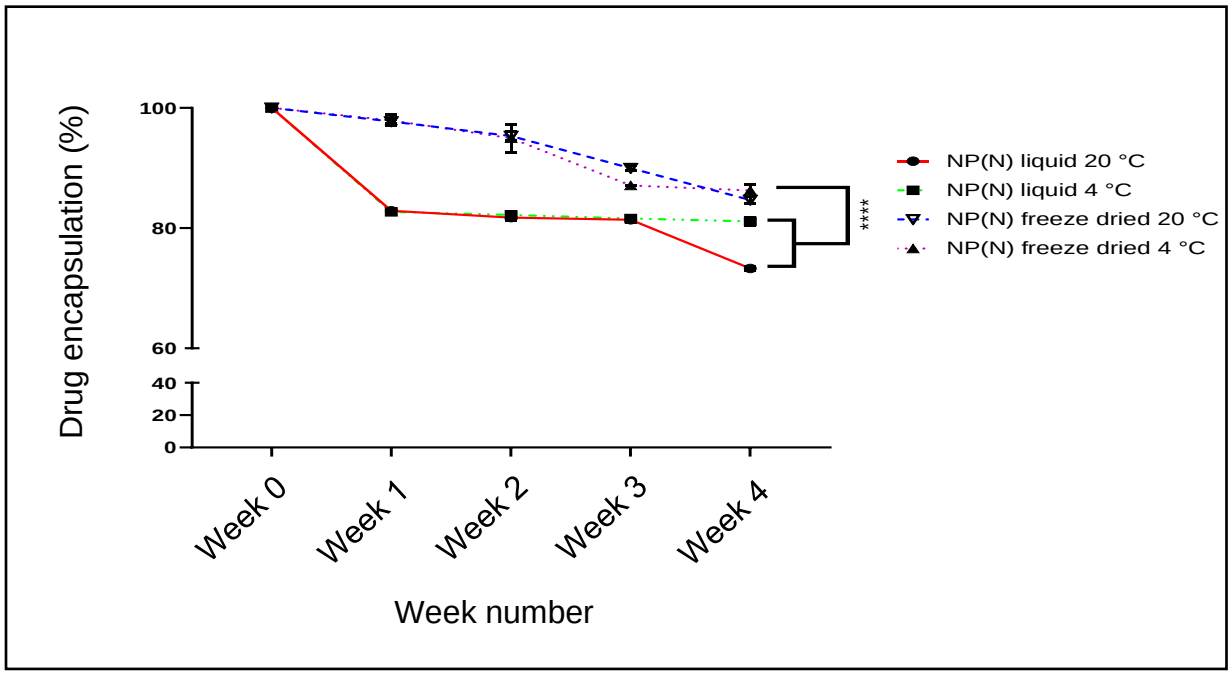

Figure 3-12: Physical stability for navitoclax nanoparticles with PAA-ch$_5$ polymer

Physical stability test for Navitoclax-PAA-ch$_5$ (NP(N)) at 4 ^{o}C and 20 ^{o}C in the form of liquid and freeze dried, over 4 weeks-period. There is a significant difference between the freeze-dried formulation at 4°C compared with both liquid formulations. (*(****): p<0.0001*; statistical analysis was examined using Two-way ANOVA). Results (mean ± S.D, n=3).

3.8. Discussion

Using amphiphilic graft polymers to increase drug solubility represents a revolution in biomedical sciences (Barnett *et al.*, 2013). The self-assemblies that are formed from these polymers, once put in the aqueous media, are considered universal drug delivery systems as they can carry the hydrophobic cargo, including hydrophobic drugs. This ideal drug delivery happens because of the remarkable properties these nanoaggregates have, which potentiate their application in carrying the hydrophobic drugs and increase their water solubility (Hoskins *et al.*, 2012).

One of these well-known comb-shaped polymers is the poly (allylamine) polymer (PAA) which can bind several pendant groups and showed interesting results giving an increase in the solubility of several drugs, including anticancer medications (Hoskins *et al.*, 2012). One of these efficient pendant groups that are grafted on PAA polymer is the cholesteryl group (ch). This group, besides its notable characteristics, showed an efficient loading efficiency for several drugs. The comb-shaped polymer of PAA with the cholesteryl pendant group was successfully fabricated by Thompson *et al.* (Thompson *et al.*, 2008) before being furtherly studied by Hoskins and her group. One of the essential properties of this polymer with molar grafting of 5% (PAA-ch_5) is that it has the lowest critical aggregation (CAC) when compared with other pendant groups with 0.02 mg/ml (Hoskins *et al.*, 2010). Hence, this means that it can form self-assemblies at lower polymer concentration and increase the payload encapsulation in its core (Thompson *et al.*, 2008). The other characteristic of being non-toxic at a lower concentration makes it an ideal carrier for drugs to be applied *in vivo* (Hoskins *et al.*, 2010).

Navitoclax, like other hydrophobic drugs, has issues with poor solubility and low bioavailability which can decrease its efficacy; in addition it has a significant side effect of causing thrombocytopenia (Tolcher *et al.*, 2015). Several trials have been carried out to improve the navitoclax therapeutic index and encapsulate it in nanoparticles either alone (Chen *et al.*, 2016) or in combination with other drugs (Ding *et al.*, 2020; Vivo-Llorca *et al.*, 2020). Figure (3.13) represents the proposed mechanism of how navitoclax was encapsulated in the PAA-ch_5 micellar core.

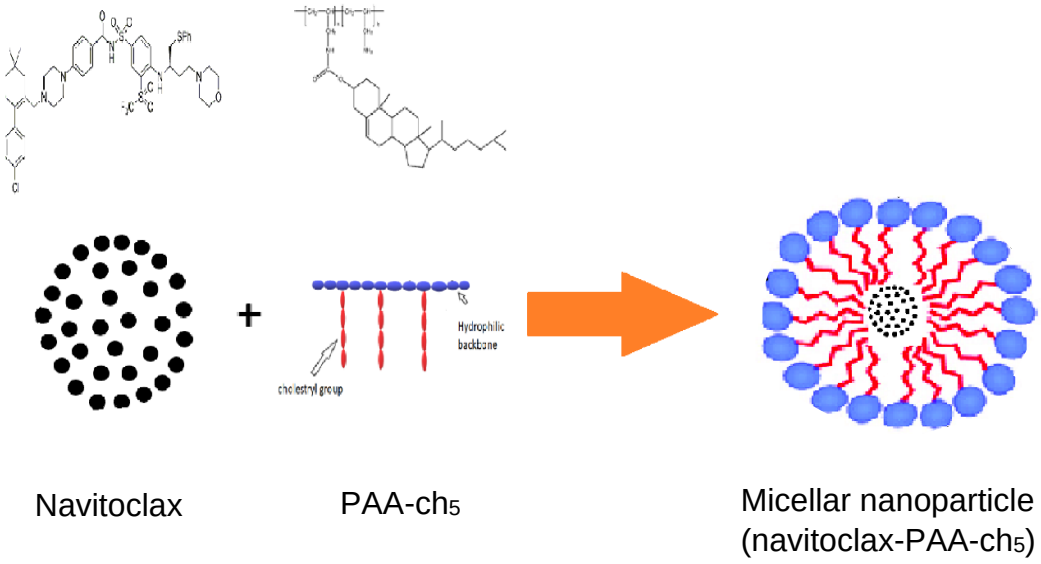

Navitoclax PAA-ch$_5$ Micellar nanoparticle (navitoclax-PAA-ch$_5$)

Figure 3-13: Schematic presentation of the navitoclax encapsulation in the core of the PAA-ch$_5$ core to form a polymeric micelle

The navitoclax encapsulation in the polymeric core was dependent on the method that was carried out by Hoskins et al. (Hoskins *et al.*, 2011). In which, navitoclax was added to PAA-ch$_5$ of 1 mg/ml with a (1:1 drug: polymer) ratio. The formulation was sonicated and then filtered to remove the excess drug. Before filtration, some of the drug droplets appeared as white clumped particles on the formulation surface, and the appearance of the formulation was still cloudy, but after filtration, the formulation got clearer with no visible drug particles in the final solution. This appearance was identical to what has been explored when BNIPDaoct added to the same polymer, and its undissolved particles were removed by filtration. As such, this could indicate that the unremoved drug particles have been dissolved in the polymeric cores (Hoskins *et al.*, 2010). Figure (3.14, B) shows how the navitoclax-PAA-ch$_5$ formulation appeared as a clear colourless solution compared with the polymer alone, (Figure (3.14, A)).

(A)

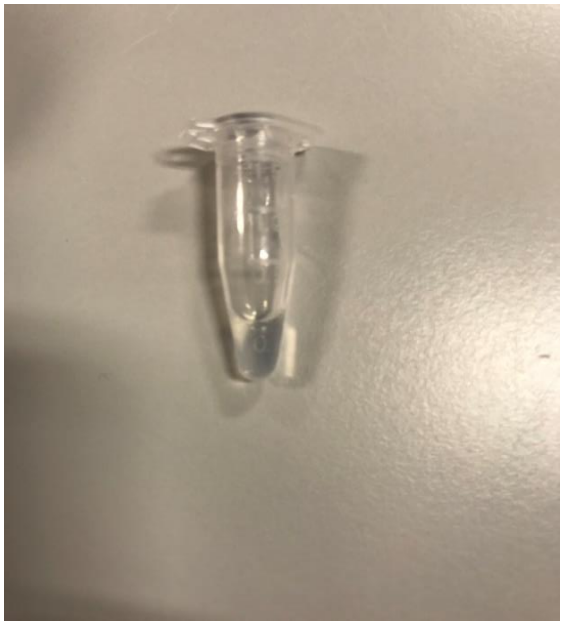

(B)

Figure 3-14: Schematic presentation of both (A) PAA-ch_5 alone (B) Navitoclax-PAA-ch_5

Significantly, there was around a 100-fold improvement in navitoclax solubility in water when it was encapsulated in PAA-ch_5 and this solubility improvement was consistent with the results reported for propofol, griseofulvin, prednisolone (Hoskins *et al.*, 2011), and BNIPdaoct (Hoskins *et al*., 2010). However, the loading efficacy was very low, and this could be related to the higher hydrophobicity of navitoclax. Despite all of that, the intended goal of increasing navitoclax solubility has been achieved providing a new carrier for navitoclax. Moreover, this can give a new era for this drug to be applied parenterally.

The loading of any hydrophobic drugs is affected by several parameters including the drug feeding concentration, the polymer concentration, the partition coefficient, and the compatibility between the drug and the micellar core (Hussein and Youssry, 2018). For approving the drug feeding concentration, different drug to polymer ratios have been taken of 1:1, 5:1, and 10:1 by taking a fixed polymer concentration of 1 mg/ml. The results of a 10:1 feeding ratio achieved an increment in navitoclax solubility up to 800-fold, which is a significant improvement. That significant improvement was likely to have occurred because the higher drug concentration allows for a higher degree of hydrophobic-hydrophobic interactions, and hence increment in drug particles encapsulation and higher drug solubilisation as what was experienced (Du *et al.*, 2009).

The other parameter investigated were varying the polymer concentrations with a fixed drug to polymer ratio. The results showed the highest encapsulation when 6 mg/ml of the polymer was used, and it showed a navitoclax concentration of 0.4 mg/ml, which is equivalent to a 2100-fold increment in navitoclax solubility. These results were consistent with what have been demonstrated by Zafar *et al*. who used the same polymer, PAA-ch_5, and found the effect of increasing the polymer concentration in increasing the solubility of thieno [2,3-b]pyridines derivative (Zafar *et al.*, 2018). This increase in solubility is likely to occur because when the polymer concentration increases more micelles are present in the solution. Once the drug particles have been added, this could increase the chance of the drug becoming encapsulated and show increased solubility. Although other studies have explored drug ratios of 5:1 and 10:1 and were the polymer concentrations of 3 mg/ml and 6 mg/ml were used, the cost of navitoclax made this prohibitive.

After quantifying the navitoclax loading inside the polymeric role and there was a need to confirm a successful encapsulation of navitoclax inside the hydrophobic core of the PAA-ch_5 polymer. The physical characteristics of the self-assemblies were examined to help predict the fate of encapsulated drugs. The size of the formed nanoaggregates is an important parameter because size affects retention of the particles in the cancerous tissue by the EPR effect (Hoskins *et al.*, 2010; Gao *et al.*, 2013; Hussein and Youssry, 2018). Whereas the hydrodynamic size of the PAA-ch_5 of 1 mg/ml was close to the results in previous researchers for the same polymer (Thompson *et al.*, 2008; Hoskins *et al.*, 2010; Zafar *et al.*, 2018), the size for the nanoaggregates of the drug encapsulated in that polymer was increased slightly. This increment in the micellar size is likely to have happened because of the core expansion since hydrophobic molecules resided in the polymer core (Hoskins *et al.*, 2010; Zafar *et al.*, 2018). Although it has previously been found that the ideal size is 100-200 nm (Jin *et al.*, 2016), the size of the formed nanoparticles was close to 200 nm. Thus, it is likely that this small size of the formed nanoparticles will have prolong circulation time which permit the nanoparticles to be internalised in the tumour tissue through EPR effect and avoid these nanoaggregates from being cleared by macrophages (Jin *et al.*, 2016). Moreover, it was demonstrated that the endothelial gap holes in the tumour blood vessels are 50~500 nanometers (Jin *et al.*, 2016), and since the formed nanoparticles from navitoclax with the PAA-ch_5 was in that range, the formed nanoparticles are likely to enter the tumour tissue selectively and reside there.

Zeta potential, which reflects the surface charge, has been demonstrated to be a crucial parameter. Since the zeta potential is directly correlated with the stability, the values for both the polymer and the encapsulated particles (>30 mV) are considered

highly stable and are not likely to aggregate (Bhattacharjee, 2016; Jin *et al.*, 2016; Poy *et al.*, 2018). The results did not show significant change in surface charge between the polymer itself and the self-assembly of the navitoclax with the polymer, and this is a good indication as this means that there was a successful encapsulation, the drug particles became fully shielded from the surrounding environment, and no complexation happened between the drug and the polymer (Alsuraifi *et al.*, 2018). Furthermore, the positive charge for the formed nanoparticles allows for electrostatic interaction between them and the negative charge for the cellular membrane of cancer cells, allowing for better internalisation (Jin *et al.*, 2016).

The PDI index for both the polymer alone and the nanoaggregates were comparable. The PDI values are between 0 and 1, and as where 1 represents unwanted polydispersion of the micelles in the solution; 0 represents a uniformity of the micelles in the solution. Although the PDI observed of approximately 0.4 is slight above a value of 0.3 which is postulated to be desirable, any value between 0.08-0.7 still represents an acceptable mid-range distribution (Trang Le *et al*., 2020). However, it is also noteworthy that encapsulation of the drug improved the PDI marginally.

Drug release is a critical factor in the development of any drug delivery systems. The drug release from the micellar core to reach the target site is the intended goal of any delivery system and can predict the drug destiny in vivo (Hussein and Youssry, 2018). It was reported that if the drug molecules remain stacked in the micellar core and the micelles do not dissociate, this leads to a non-ideal delivery system. Thus, it is essential to study the release kinetics of the drug from the micelles. If the drug is formulated to be given orally, it must resist the premature release and withstand the extreme dilution

(sink condition) (Hussein and Youssry, 2018). The release kinetics are affected by several factors such as the compatibility between the micelle core and drug molecules, polarity of the hydrophobic groups, micellar size and length, and the amount of drug-loaded (Hussein and Youssry, 2018).

The release of navitoclax was examined for 72 hours using PBS by taking samples with different time frames. The release showed a plateau in release after 6 hours. The release from the PAA-ch$_5$ core was not that high, and only 12% of the drug was released. This was close to the percentage achieved for navitoclax when formulated with mPEG-PDPA, which showed only 16.6% of navitoclax release at a pH of 7.4 (Ding *et al.*, 2020).

The low release rate could be due to several causes, as the concentration of drug loaded was very low as the ration was applied was 1:1 which had a loading of 0.0213 mg/ml, this low concentration allows the grafted hydrophobic moiety to be highly bound to the drug in its core and prevent it from being released outside. This is consistent with what happened with a thieno [2,3-b]pyridine derivative, which was encapsulated in the same polymer and showed release of no more than 20% (Zafar *et al.*, 2018) and with BNIPDaoct when it was internalised in the PAA-ox5, which showed only 25% release (M. Barnett 2013). Another explanation is that navitoclax has a very high Log P of 7.77 (*Navitoclax drugbank*, 2018). Since Log P represents the partition coefficient which is very important in determining the drug water solubility, a higher value means that the drug particles tend to reside in the micellar lipophilic core and not to leave it to the hydrophilic media (Hussein and Youssry, 2018). Despite all of that, the low release also could represent an advantage for the encapsulated hydrophobic drug because it

may promote cellular uptake (Chen *et al.*, 2016). Furthermore, this means that the drug encapsulated in the polymer could offer an extended-release profile which may be desirable to provide prolonged drug exposure, which can be advantageous for not causing side effects and decreasing the frequency of drug administration. Yet, the release has to be further examined using a different drug: polymer ratios to identify those which show a higher encapsulation. In addition, the release also has to be determined using culture media to synchronise the environmental media to that the encapsulated drug will face *in vivo*. However, the shortage of time because of the pandemic and the higher price of the drug prevented us from further investigating the complete release picture for navitoclax. Moreover, the release was not assessed with freeze dried samples.

The stability of the formulation is one of the determinant factors that affect drug release (Heurtault *et al.*, 2003). The stability is variable from one formulation to another, and the environmental factors play a pivotal role in the formulation stability, including chemical and physical factors. As such, various conditions the formulations are exposed to for stability prediction, and one of these is making freeze-drying (Abdelwahed *et al.*, 2006). It was found that the polymer physical characteristics can affect stability as it was found that the higher the hydrophobic ratio is associated with a tighter inner core, high stability and low release (Hussein and Youssry, 2018).

It was postulated from the physical stability assay that the best environment that preserves the navitoclax content was the cold temperature and as freeze-dried cakes. This could be due to the fact that in the liquid media, there will be an increase in the

self-assembly of particles, and this forces them to release their content more rapidly. In contrast, the decrease in temperature may preserve the electrostatic bonding integrity and prevent the drug particles from being detached from the micellar core. Nevertheless, these interesting stability results, they have to be further expanded by doing this experiment in several conditions to get a full picture about the drug stability such as performing investigations at 37 °C to mimic body temperature.

3.9. Conclusion

This chapter showed the potential of the PAA-ch_5 amphiphiles in improving navitoclax's aqueous solubility. The results showed a successful encapsulation of navitoclax inside the polymeric core, which was confirmed by measuring the physical characteristics of the formed nanoaggregates of size, zeta potential, and PDI. The increment in the water solubility from negligible solubility was increased 100-fold and even more by using different ratios. This may represent a revolution that can help in drug formulation and decrease its side effects. Furthermore, the new formulation showed an extended release over 72 hours. Regarding the physical stability for the new formulation, it was high when it was as freeze-dried cakes and the importance of low temperature on preserving the overall drug stability.

Chapter 4. The cytotoxicity of the navitoclax-PAA-ch$_5$ and its combination with Carboplatin

4.1. Introduction

It is already known that the cell fate depends on the balance between anti-apoptotic and pro-apoptotic proteins, which all belong to the BCL-2 family proteins. The evasion of apoptosis, which is in large part related to overexpression of the anti-apoptotic BCL-2 family, is responsible for undesirable outcomes. These include cancer initiation, drug resistance, and disease progression. As such, this makes management of the apoptosis escaping a tempting target for cancer drug development (Kaefer *et al.*, 2014; Ashkenazi *et al.*, 2017). Although the evasion of apoptosis is mainly attributed to pro-survival protein overexpression, deregulation of pro-apoptotic proteins also contributes to the evasion of apoptosis. Examples of the proteins that are deregulated are the effector pro-apoptotic proteins BAX and/or BAK in addition to PUMA, BIM ("BH3-only" apoptosis activator proteins). Of note, deregulation of these proteins has been reported in several cancer cell types (Delbridge and Strasser, 2015). Consequently, this idea led to proposals to discover drugs that can induce apoptosis in cancer cells and overcome the problem of apoptosis evasion (Finlay *et al.*, 2017; Pfeffer and Singh, 2018).

Of all the pro-survival proteins, it was found that BCL-X_L and MCL-1, are mainly amplified in several cancer types. Notably, it was demonstrated that when the expression of the genes encoding these proteins were knocked down, more cancerous cells were killed (Delbridge and Strasser, 2015). For ovarian cancer, it was reported that one of the leading causes of the treatment failure is overexpression of the anti-apoptotic BCL-2 proteins family, mainly BCL-X_L, which is known to have an anti-apoptotic effect in solid tumours and some haematological tumours (Ashkenazi *et al.*, 2017). High expression of BCL-X_L has been attributed to drug resistance (Siddiqui *et*

al., 2015), especially paclitaxel resistance (Wong *et al.*, 2012). Furthermore, it has been associated with short disease-free intervals (Brotin *et al.*, 2010).

4.2. The road to invention BH3 mimetics

The first attempt to inhibit the BCL-2 family was BCL-2 anti-sense therapy. Oblimersen sodium, which is one of these anti-sense therapies, causes a breakdown in BCL-2 mRNA and has been evaluated in clinical trials for several malignancies. However, it was not approved by the FDA as it could not show survival improvement in phase III clinical trials (Masood *et al.*, 2011; Davids and Letai, 2012). Another treatment method was the development of antibodies that inhibit BCL-2 activity, but unfortunately, they also showed several limitations including poor results in clinical trials and short half-life of anti-sense therapies because of enzymatic degradation (Masood *et al.,* 2011). In addition to the BCl-2 family, several other targets have been proposed to overcome the evasion of apoptosis. These include direct targets drugs, targeting the inhibitor of apoptotic proteins (IAPs) and indirect targets, including *p53,* micro-RNA, and homologous recombination DNA repair (Binju *et al.*, 2019).

The structure of anti-apoptotic BCL-2 family proteins has been studied and it was shown that there is a hydrophobic cleft where pro-apoptotic BCl-2 family “BH3-only” proteins bind to stimulate apoptosis. (BH3-only refers to the fact that these proteins only possess the BH3 homology domain found in other Bcl-2 family members). This led to the idea to create small molecules that can bind to these grooves, inhibiting their ability to sequester pro-apoptotic proteins and restoring apoptosis (Certo *et al.*, 2006). A combination of nuclear magnetic resonance (NMR) screening and structure-based

drug design was used to discover the first BH3mimetics (Ashkenazi *et al.*, 2017). These BH3 mimetics work as sensitisers and inhibit the pro-survival proteins (Villalobos-Ortiz *et al.*, 2019; Cerella *et al*., 2020). Examples of these are ABT-737 and its orally bioavailable analogue ABT-263 drugs. These drugs bind the same the pro-survival proteins as the pro-apoptotic BAD BH3 protein and thus they are called BAD-like BH3 mimetics (Davids and Letai, 2012; Wong *et al.*, 2012; Billard, 2013). Nevertheless, a challenge in the design of BH3 mimetics was that the binding sites for these drugs are large, shallow, and lipophilic. So far, six BH3-mimetic drugs have reached the clinic with only the BCL-2 inhibitor, venetoclax (ABT-199), currently approved (Merino *et al.*, 2018).

4.3. BH3 mimetic drugs

4.3.1. ABT-737

The first BH3 mimetic was ABT-737 which was developed by Abbott laboratories in collaboration with Idun (Merino *et al.*, 2018). This drug has a high affinity toward BCL-2, BCL-X_L, and BCL-W, but not MCL-1 or A1 (Wong *et al.*, 2012; Billard, 2013; Delbridge and Strasser, 2015; Merino *et al.*, 2018). In addition, this drug induces apoptosis *in vitro* using BAX/BAK dependent apoptosis. Although this drug inhibits specific pro-survival BCL-2 proteins, the release of BH3-only proteins from the anti-apoptotic BCL-2 protein can lead to inhibition of other BCL-2 family such as A1 and MCL-1, BCl-2 family members that ABT-737 does not bind to directly, thus indirectly inducing apoptosis (Billard, 2013; Delbridge and Strasser, 2015).

ABT-737 is mainly active in hematological malignancies, but less potent in solid tumours (Nakajima and Tanaka, 2016). Furthermore, it was shown to have anti-tumour activity as a single agent in preclinical models of small-cell lung carcinoma (SCLC) and lymphoma (Ashkenazi *et al.*, 2017). Despite being found to have a modest cytotoxic effect, when given in combination with carboplatin, it reduced tumour growth and decreased the time needed to induce apoptosis (Jain and Meyer-Hermann, 2011). However, the poor bioavailability and physicochemical properties represented an obstacle for clinical use of ABT-737 (Nakajima and Tanaka, 2016; Mohamad Anuar *et al.*, 2020). Accordingly, this led to the invention of navitoclax.

4.3.2. Navitoclax (ABT-263)

4.3.2.1. Introduction to navitoclax

ABT-263 has a similar structure and the exact mechanism of action as its predecessor ABT-737 by binding with a high affinity to BCL-2 and BCL-X_L and with a lower affinity for MCL-1(Choo *et al.*, 2014; Ashkenazi *et al.*, 2017; Timucin *et al.,* 2018), but it has better oral bioavailability compared to ABT-737 (Tolcher *et al.*, 2015). However, navitoclax itself still has only moderate bioavailability and poor water solubility (Choo *et al.*, 2014; Tolcher *et al.*, 2015). It was developed to be used in tablet formulation in clinical trials (Tolcher *et al.*, 2015).

Preclinical studies demonstrated that navitoclax inhibits tumour growth when used as a single agent against chronic lymphocytic leukaemia (CLL) and follicular lymphoma (FL) (Ashkenazi *et al.*, 2017). In preclinical studies, navitoclax is active when used as monotherapy and as a combination with standard care agents (Ashkenazi *et al.*, 2017;

Adams and Cory, 2018). Consequently, that gave a rationale to use it in patients and it became the first BH3 mimetic to enter clinical trials (Adams and Cory, 2018). It was evaluated in several clinical trials targeting different liquid and solid tumours (Vivo-Llorca *et al.*, 2020). Indeed, it showed excellent results in B cell malignancies in both phase I and phase II clinical studies (Ashkenazi *et al.*, 2017). Importantly, this drug shows a pharmacokinetic profile as it reached peak plasma concentration (Cmax) within around 9 hours, while the elimination half-life ($t_{1/2}$) is approximately 17 hours (Xiong H. *et al.*, 2014; Kim *et al.*, 2020). Importantly, its pharmacokinetic parameters were not affected by giving concomitantly with chemotherapeutic drugs (Kim *et al.*, 2020).

4.3.2.2. Application of navitoclax in fibrotic diseases and with senescent cells

Once fibroblasts are differentiated to myofibroblasts, they tend to survive and escape apoptosis. The mitochondria will be targeted by pro-apoptotic proteins and thus they express anti-apoptotic proteins such as BCL-X_L to survive. Since navitoclax has been shown to induce apoptosis in multiple cell types, including cancer cells, it has been proposed to cause myofibroblast apoptosis. Accordingly, navitoclax is considered a potent drug in treating the conditions associated with high myofibroblasts function and thus slowing down the progression of fibrotic diseases (Mohamad Anuar *et al.*, 2020). The diseases that are associated with myofibroblast persistent function and navitoclax has shown promising results are pulmonary fibrosis (Pan *et al.*, 2017), liver fibrosis (cirrhosis) (Moncsek *et al.*, 2018), and cardiac fibrosis (Walaszczyk *et al.*, 2019), in addition to the cardiovascular diseases such as myocardial infarction, atherosclerosis, and stroke (Mohamad Anuar *et al.*, 2020). Moreover, other than their application in

fibrotic diseases, and from all of the drugs used to treat senescent cells, the ABT-263, in addition to ABT-737, became the gold standard as senolytic agents (Guerrero *et al.*, 2020; He *et al.*, 2020).

4.3.2.3. Problems that face navitoclax

Despite the promising results that have been demonstrated using navitoclax in cancer treatment, unfortunately, navitoclax was found to induce unwanted side effects such as temporary decreases in platelet counts in both animal studies and in patients (Thrombocytopenia) as a result of inhibiting BCL-X_L (Ashkenazi *et al.*, 2017; Adams and Cory, 2018). In addition to thrombocytopenia, navitoclax is also associated with neutropenia, which is also due to inhibition of anti-apoptotic BCL-2 (Ashkenazi *et al.*, 2017), gastrointestinal disorders (vomiting, diarrhoea, nausea), fatigue, anaemia (Timucin *et al.,* 2018; Mohamad Anuar *et al.*, 2020), lymphocytopenia, an increase in aminotransferases, and infection (Mohamad Anuar *et al.*, 2020).

One of the problems that can face the use of navitoclax in cancer, other than thrombocytopenia, is that some cancer cells have high levels of the anti-apoptotic protein MCL-1 which is not inhibited by navitoclax with high affinity (Boiani *et al.*, 2013). MCL-1 itself is expressed in some ovarian cancer cells, as is BCL-X_L (Abed *et al.*, 2016). Therefore, it represents a resistance factor for navitoclax and some chemotherapeutic agents (Ashkenazi *et al.*, 2017). Thus, even if cancer cells are initially sensitive to navitoclax they may become resistant if MCL-1 is overexpressed in response to therapy. However, this problem can potentially be solved by the administration of navitoclax in combination with drugs that can inhibit MCL-1 function (Adams, 2012). Several efforts are underway to invent small molecules that can inhibit

MCL-1 and recently new highly potent inhibitors have been found to cause tumour regression *in vivo* (Ashkenazi *et al.*, 2017).

4.4. Thrombocytopenia

Platelets are parts of blood cells, and their primary function is to heal wounds and maintain hemostasis; thus, they have to be highly regulated. Platelets are synthesised from bone marrow megakaryocytes and released into the blood circulation. The life span of platelets ranges from 7-10 days and their normal count is 150,000–450,000 platelets/µl of blood. Thrombocytopenia is defined as a condition in which platelets count dropped below 150,000 platelets/µl, and hence it is associated with a fatal consequence (haemorrhage). Drug-induced thrombocytopenia (DIT) is a term that describes thrombocytopenia is related to medication. This can be induced in two ways either centrally, by affecting megakaryocytes and decrease platelets release, or peripherally by increasing platelets clearance from blood circulation (De Silva and Kim, 2018).

Mason *et al*. (2007) demonstrated that the life-span of platelets is determined by a balance between pro-apoptotic protein, BAK, and antiapoptotic protein, BCL-X_L, which prevents apoptosis (Mason *et al.*, 2007). Apoptosis, which normally happens for platelets, occurs because the BCL-X_L level decrease over time faster than the pro-apoptotic proteins that they sequester, a “molecular clock” regulating cell death (Vogler *et al.*, 2011). Although ABT-737 and ABT-263 are associated with dose-dependent thrombocytopenia within hours of treatment, they are not associated with a decrement in platelets production (Davids and Letai, 2012; Billard, 2013; Delbridge and Strasser, 2015; Mohamad Anuar *et al.*, 2020). Fortunately, this problem is considered a

reversible problem that can potentially be tolerated and which has a well-defined mechanistic basis (Mohamad Anuar *et al.*, 2020). One way to manage DIT induced by navitoclax is by starting with a small lead-in dose before using higher doses. As such, this will allow the bone marrow to recover and produce more platelets and manage the thrombocytopenia (Kipps *et al.*, 2015).

4.5. New BH3 drugs era

4.5.1. Venetolcax

Venetoclax (ABT-199, Venclexta®) is a selective BCL-2 inhibitor (Juin *et al.*, 2013; Ashkenazi *et al.*, 2017; Adams and Cory, 2018), which was approved by FDA in 2016 (Billard, 2013; Perini *et al.*, 2018). It was reported that venetoclax binds to BCL-2 with high affinity but only binds BCL-X_L, BCL-W and MCL-1 with low affinity (Billard, 2013; Choo *et al.*, 2014). Accordingly, the selective inhibition of BCL-2 avoids thrombocytopenia and spares the circulating platelets (Delbridge and Strasser, 2015). In contrast, the selectivity for BCL-2 also means that the over-expression of MCL-1 protein or multiple BCL2 members represent barriers for venetoclax efficacy (Merino *et al.*, 2018; Cerella *et al.*, 2020). Compared with ABT-263 or ABT-737, ABT-199 was not effective in BCL-X_L dependant cancer cells such as ovarian cancer because of its poor affinity for BCL-X_L (Souers *et al.*, 2013).

It was reported that venetoclax has other mechanism of action in inducing apoptosis as it is able to induce apoptosis through BAX/BAK activation (Billard, 2013; Ashkenazi *et al.*, 2017). Surprisingly, recent findings show that venetoclax prevents mitochondrial respiration regardless of BCL-2 expression (Cerella *et al*., 2020). The invention of

venetoclax represents a revolution in BH3 mimetics application as it was found to have good anti-tumour activity (Vaillant *et al.*, 2013; Touzeau *et al.*, 2014), and it has been applied to the treatment of acute myelocytic leukemia (AML) and in CLL patients who cannot tolerate harsh chemotherapy effect (Merino *et al.*, 2018; Cerella *et al.*, 2020). In addition, the pharmacokinetic profile for venetoclax has shown that it can reach the peak plasma concentration within 4-8 hours and it has a safety profile represented by manageable side effects (Konopleva *et al.*, 2017). This drug was used as a single agent or in combination with other anticancer drugs, and it has been applied in both *in vitro* and xenograft *in vivo* (Davids and Letai, 2012; Nakajima and Tanaka, 2016; Ashkenazi *et al.*, 2017; Merino *et al.*, 2018; Cerella *et al.*, 2020). Unfortunately, this drug is associated with several side effects, such as a decrease in mature B and T cells and early T cell progenitors, respiratory tract infections, and neutropenia (Cerella *et al*., 2020).

4.5.2. WEHI-539

The fact that BCL-X_L is the dominant anti-apoptotic BCL-2 family member in some cancers, including ovarian cancer, requires a BH3-mimetic that has suitable affinity for BCL-X_L to treat this disease (Abed *et al.,* 2016). As a result, novel BCL-X_L inhibitors were sought. This led to the invention of WEHI-539, which binds and antagonises BCL-X_L. The selectivity of this compound comes from its binding to the P2 hydrophobic groove of BCL-X_L (Juin *et al.*, 2013). Significantly, WEHI-539 has a 400-fold higher affinity to BCL-X_L than other BH-3 mimetics (Lessene *et al.*, 2013) and it does not efficiently inhibit BCL-2 nor BCL-W. Notably, WEHI-539 has shown a synergistic effect with carboplatin, similar to ABT-737. However, since its mechanism depends on inhibition of BCL-X_L selectivity, this means that it also has the potential to induce

thrombocytopenia (Abed *et al.*, 2016). Figure (4.1) represents the chemical structures of aforementioned BH3 mimetics and table (4-1) shows the BH3 mimetics that have been invented until now.

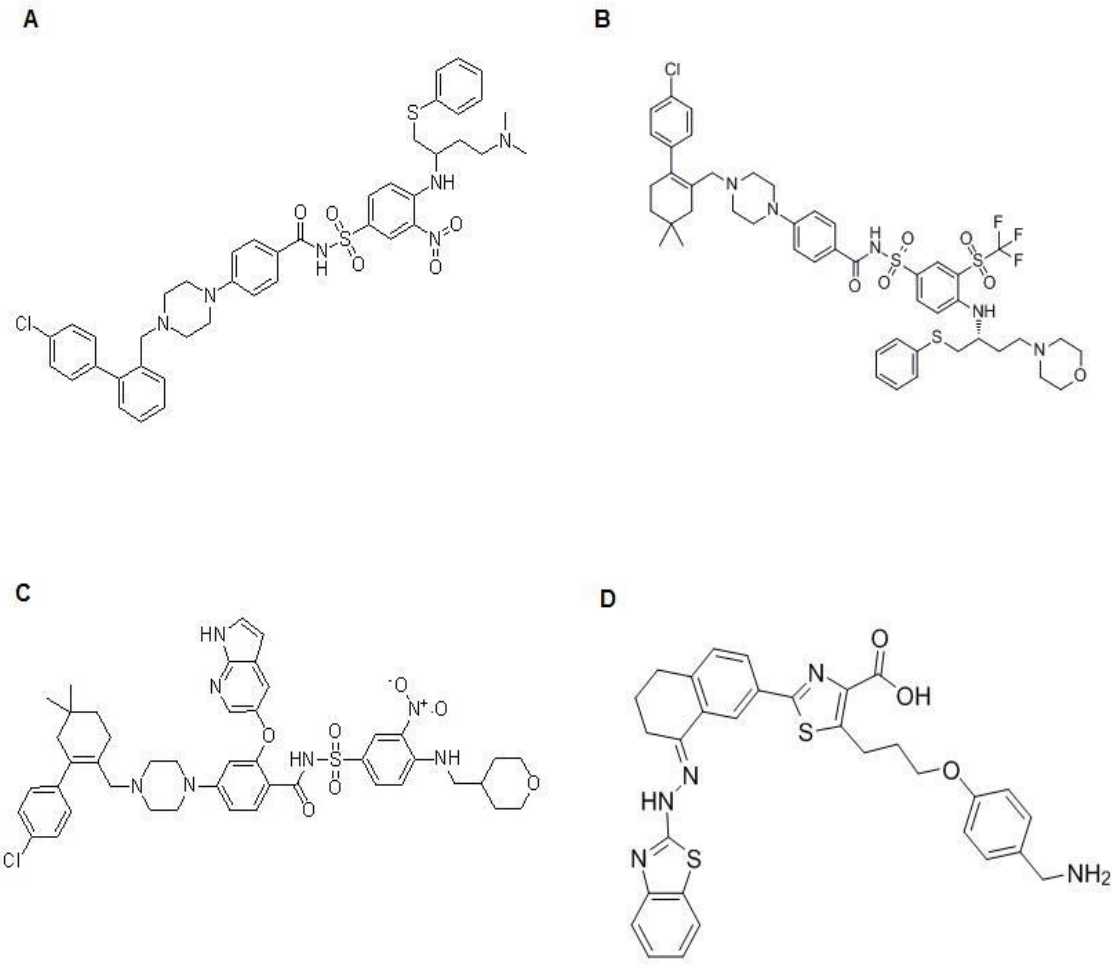

.

Figure 4-1: Some BH3 mimetic drugs chemical structures.

(A) ABT-737 (Erlanson *et al.*, 2016), (B) navitoclax (Erlanson *et al.*, 2016), (C) venetoclax (Erlanson *et al.*, 2016), (D) WEHI-539 (Lessene et al., 2013).

Table 4-1: Small molecules that inhibit the BCL-2 family (BH3 mimetics) and their targets.

Compound	Targets	References
BCL-2 inhibitors		
ABT-737	BCL-2, BCL-X_L and BCL-W	(Wong *et al.*, 2012; Billard, 2013; Delbridge and Strasser, 2015; *Ashkenazi et al., 2017;* Merino *et al.*, 2018)
Navitoclax (ABT-263)	BCL-2, BCL-X_L and BCL-W	*(*Nakajima and Tanaka, 2016; *Ashkenazi et al., 2017*; Moncsek *et al.*, 2018*;* Cerella *et al*., 2020)
BM-1197	BCL-2 and BCL-X_L	*(Ashkenazi et al., 2017)*
S44563	BCL-2 and BCL-X_L	*(Ashkenazi et al., 2017)*
BCL2-32	BCL-2 and BCL-X_L	*(Ashkenazi et al., 2017)*
AZD4320	BCL-2 and BCL-X_L	*(Ashkenazi et al., 2017)*
Venetoclax (ABT-199)	BCL-2	(Billard, 2013; *Ashkenazi et al., 2017;* Cerella *et al*., 2020)
S55746 (BCL201)	BCL-2	*(Ashkenazi et al., 2017)*
GX15-070 (Obatoclax)	All antiapoptotic BCL-2 family proteins	(Billard, 2013; Nakajima and Tanaka, 2016)

Gossypol (AT-101)	BCL-2, BCL-X_L, and MCL-1	(Billard, 2013)
TW-37	All of the antiapoptotic BCL-2 family proteins	(Binju *et al.*, 2019)
BI-97D6	BCL-2, BCL-X_L, MCL-1, BCL-2A1	(Billard, 2013)
S1 derivative	BCL-2, BCL-X_L, MCL-1	(Billard, 2013)
Polyquinolines	BCL-2, BCL-X_L, MCL-1, BCL-2A1	(Billard, 2013)
BH3-M6	BCL-2, BCL-X_L, MCL-1	(Billard, 2013)
BIM SAHB	BCL-X_L, BCL-W, MCL-1, BCL-2A1	(Billard, 2013)
BI97C1 (sabutoclax)	BCL-2, BCL-X_L, BCL-2A1, MCL-1	(Nakajima and Tanaka, 2016)
*BCL-X*L *inhibitors*		
WEHI-539	BCL-X_L	(Nakajima and Tanaka,2016; *Ashkenazi et al., 2017;* Merino *et al.*, 2018)
A-1155463	BCL-X_L	*(Ashkenazi et al., 2017;* Merino *et al.*, 2018*;* Cerella *et al*., 2020)
A-1331852	BCL-X_L	*(Ashkenazi et al., 2017;* Merino *et al.*, 2018;

		Moncsek *et al.*, 2018; Cerella *et al*., 2020*)*
BXI-61, BXI-72	BCL-X_L	(Nakajima and Tanaka, 2016)
MCL1 inhibitors		
UMI-77	MCL1	(Nakajima and Tanaka, 2016; *Ashkenazi et al., 2017)*
Compound 9	MCL1	*(Ashkenazi et al., 2017)*
A-1210477	MCL1	*(Ashkenazi et al., 2017;* Cerella *et al*., 2020)
Compound 34	MCL1	*(Ashkenazi et al., 2017)*
S63845	MCL1	*(Ashkenazi et al., 2017;* Merino *et al.*, 2018*;* Cerella *et al*., 2020)
AMG176	MCL1	*(Ashkenazi et al., 2017;* Merino *et al.*, 2018*;* Cerella *et al*., 2020)
MIM 1	MCL1	(Billard, 2013)
S64315/MIK665	MCL1	(Merino *et al.*, 2018; Cerella *et al*., 2020
AZD5991	MCL1	(Merino *et al.*, 2018; Cerella *et al*., 2020)

A-1210477	MCL1	(Moncsek *et al.*, 2018)
Maritoclax	MCL-1	(Billard, 2013)
JY-1-106	MCL-1, BCL-X_L	(Nakajima and Tanaka, 2016)
AM-8621	MCL1	(Cerella *et al*., 2020)
VU661013	MCL1	(Cerella *et al*., 2020)
BAX activator		
BAM 7	BAX	(Billard, 2013)

4.6. BH3 profiling

Whereas specific cancers depend on single antiapoptotic proteins such as lymphomas and leukemias, other cancer cells, such as solid tumours, are dependent on multiple antiapoptotic BCL-2 proteins. Accordingly, assays that can detect the pro-survival proteins which are essential to sustain tumour cells are crucial to predict the efficacy of BH3 mimetics. By predicting the BH3 mimetics that a tumour is most dependant on, in principle the most effective BH3 mimetic can be chosen to treat a patient. One method to do this is ‘‘dynamic BH3 profiling’’ (Merino *et al.*, 2018). This method relies on using peptides from the BH3 domain of the BH3 only proteins (Cerella *et al*., 2020). In this method, the mitochondria are isolated and exposed to these different peptides from different BH3 only proteins, and the apoptosis assessed by cytochrome C release (Villalobos-Ortiz *et al.*, 2019; Cerella *et al*., 2020). Mitochondrial outer membrane polarization (MOMP) is measured using a fluorescent probe (JC-1,5,5′,6,6′-tetrachloro-1,1′,3,3′-tetraethylbenzimidazolocarbo-cyanine iodide or

tetramethylrhodamine, TMRE). The identification of the BH3 only proteins that induce MOMP and knowledge of the specificity of the BH3 only proteins for Bcl-2 family proteins, allows the dependency on particular Bcl-2 family inhibitors to be identified (Cerella *et al*., 2020). This can help to identify the patients who will respond to a BH3 mimetic that targets the relevant Bcl-2 family protein and also will be helpful in identifying who are eligible to take a combination regimen of one of the BH3 mimetics and MCL-1 inhibitors (Zervantonakis *et al.*, 2017).

4.7. Combination of BH3 mimetics with chemotherapy

Ovarian cancer, like other cancers, is a heterogenic disease that characteristically develops drug resistance. This means a single drug is not likely to be sufficient, and there is a need to discover a drug combination that overcomes resistance. As such, there is a rationale for giving several drugs that can target several pathways, potentially synergistically, to overcome resistance and improve therapeutic efficacy (Zhou *et al.*, 2019; Ding *et al.*, 2020). Unexpectedly, BH3 mimetics are not efficient in inducing apoptosis by themselves, especially in non-primed cells (see below), and they need activation of pro-apoptotic BH3 only proteins. Accordingly, combining BH3 mimetics with chemotherapeutic agents could be beneficial, and the previous research has shown better efficacy and fewer adverse effects (Delbridge and Strasser, 2015).

The term ‘primed for death’ describes cells that have high load of BH3-only proteins, requiring higher expression of anti-apoptotic proteins levels for cells to survive; this means that cells are near to death and any additional stress, such as chemotherapy or radiation, provides a pro-apoptotic stress that kills cells. Thus, in primed cells,

oncogenic stress that increases BH3-only proteins is countered by the high expression of anti-apoptotic proteins, and any additional pro-apoptotic stimuli that increases pro-apoptotic proteins or decreases anti-apoptotic proteins leads to liberation of BH3-only proteins that induce BAX and BAK activation. On the other side, in non-primed cells, there is a low BH3-only proteins load that cannot neutralize the anti-apoptotic proteins and using chemotherapeutic agents or BH3-mimetics will not have the desired effect of producing an excess of expressed anti-apoptotic proteins. Consequently, one of the obstacles to successful treatment that faces chemotherapeutic agents and BH3 mimetics is when they face cells that are not primed for death (Lopez and Tait, 2015), (Figure (4.2) .

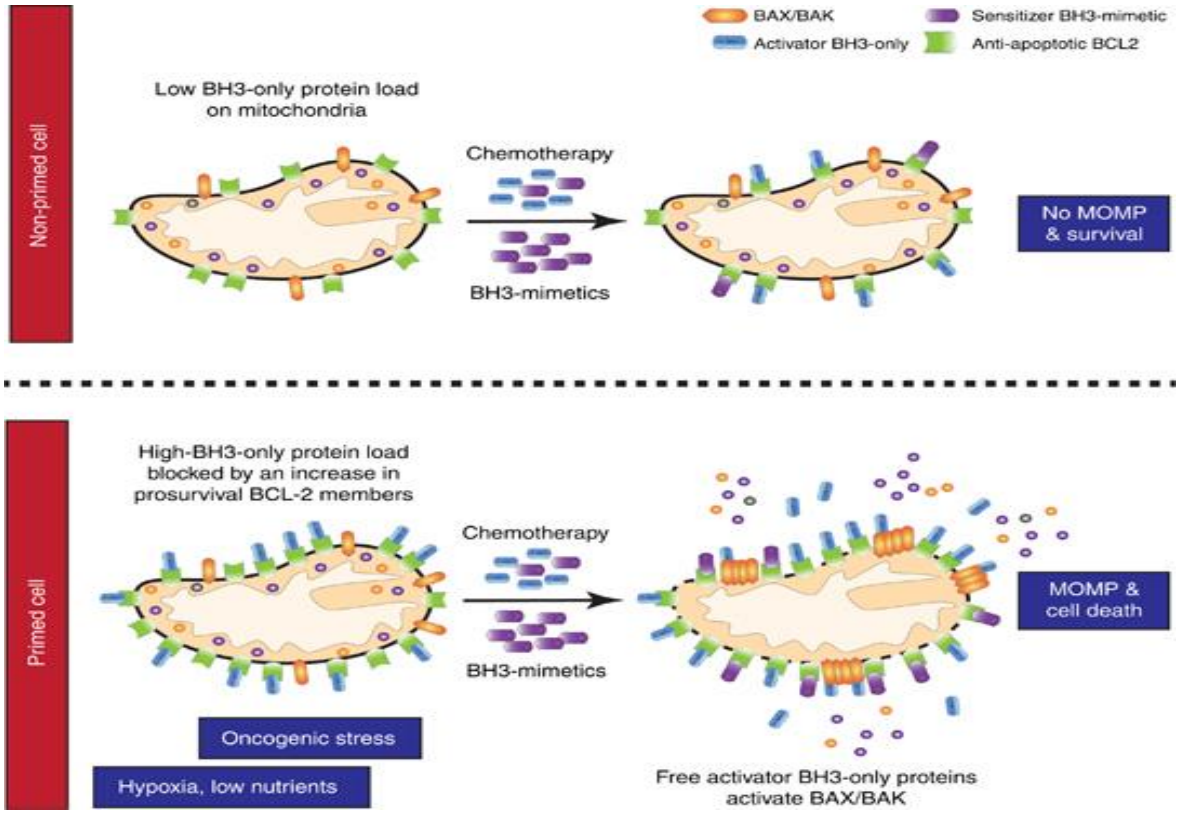

Figure 4-2: Mitochondrial priming model

The top image represents the non-primed cells, in which mitochondria have low BH3-only proteins and hence allow the anti-apoptotic survival BCL-2 proteins to sequester the pro-apoptotic BH3-only proteins resulting from cytotoxic chemotherapy or BH3-mimetic treatment. The bottom panel shows the primed cancer cells, in which any stresses can lead to a high BH3-only protein load blocked by a compensatory increase in anti-apoptotic BCL-2 members. Accordingly, any pro-apoptotic stimuli, either by chemotherapy or BH3 mimetics, result in excess activator BH3-only proteins that cause BAX/BAK activation, MOMP and cellular death (Lopez and Tait, 2015).

Since It was found that the high level of BCL-X_L is accompanied by poor chemotherapy response in ovarian cancer patients (Binju *et al.*, 2019), inhibition of BCL-X_L in combination with chemotherapy may be useful in ovarian cancer treatment (Witham *et al.*, 2007). ABT-737 was found to increase the sensitivity of ovarian cancer, especially when combined with carboplatin (Witham *et al.*, 2007; Stamelos *et al.*, 2013). It was

proposed that prior treatment with carboplatin primes cells to become sensitive to ABT-737, as after DNA damage the cells depends on BCL-X_L to survive. Therefore, treatment with ABT-737 with or after carboplatin is the best regimen to maximise the synergy between both drugs and this has been confirmed by modelling studies (Jain and Meyer-Hermann, 2011).

The success of the combination between ABT-737 and carboplatin led to the evaluation of navitoclax and carboplatin combination in the treatment of ovarian cancer. Significantly, it was reported that there is a synergy between navitoclax and carboplatin. However, both navitoclax and carboplatin cause thrombocytopenia. This represents a barrier to clinical application of this combination, but fortunately, paclitaxel is known to decrease the effect of carboplatin on platelets. This led to the proposal of adding paclitaxel in combination with navitoclax and carboplatin (Stamelos *et al.*, 2013). Moreover, Stamelos *et al*. (2013) showed that paclitaxel augmented the activity of navitoclax combined with carboplatin *in vitro,* which gave a rationale to be used in combination with them in clinical trials for ovarian cancer treatment to avoid thrombocytopenia (Stamelos *et al.*, 2013).

Prior to that, Wong *et al*. (2012) studied several combinations of navitoclax with paclitaxel or gemcitabine that have been tested on 27 ovarian cancer-derived cell lines. It was reported that navitoclax combined with paclitaxel resulted in inhibition of growth and showed a synergistic effect of killing, not just an additive effect (Wong *et al.*, 2012). In addition, it was found that navitoclax accelerates apoptosis in cells, especially during the mitotic arrest that is known to be induced by paclitaxel (Shi *et al.*, 2011).

The combination of navitoclax with other drugs, including chemotherapeutic agents, has been extensively studied in several cancers, not limited to ovarian cancer, such as breast cancer cells (Merino *et al.*, 2018), NSCLC (Merino *et al.*, 2018), solid-tumour xenograft models (Wong *et al.*, 2012; Timucin *et al.,* 2018; Mohamad Anuar *et al.*, 2020), and lymphoid malignancies (Mohamad Anuar *et al.*, 2020). These include a combination of navitoclax with benzimidazoles (Mohamad Anuar *et al.*, 2020), vemurafenib (Mohamad Anuar *et al.*, 2020); vorinostat (Nakajima *et al.*, 2016), dasatinib (Kivioja *et al.*, 2019), rituximab (Kipps *et al.*, 2015), either bendamustine alone or bendamustine with rituximab (Ackler *et al.*, 2012).

Consequently, because of the ovarian cancer dependence on BCL-X_L for their survival and to resist the chemotherapeutic agents, the use of BCL-X_L inhibitors in the treatment is not a choice but almost mandatory to eradicate these tumour cells. However, platelets depend on these BCL-X_L proteins for their survival and cause thrombocytopenia (Afreen *et al.*, 2020). Of the BCL-X_L inhibitors, navitoclax is the most studied BCL-X_L inhibitors studied that has reached clinical studies. One way to overcome these issues is to reformulate navitoclax to improve its therapeutic index. Since it has been demonstrated that encapsulation of drugs in nanoparticles, including those comprised of PAA-ch_5, could enhance their selectivity toward cancer cells, encapsulation of navitoclax inside comb shaped PAA-ch_5 polymer could provide one means to achieve this.

4.8. Aims and goals

1. Evaluate the cytotoxicity of the PAA-ch$_5$ polymer on both ovarian cancer cell lines (OVCAR-8 and OVSAHO) to identify non-toxic concentrations for use in subsequent experiments.
2. Compare the activity of both free drug and encapsulated navitoclax on several cell lines.
3. Evaluate the activity of combinations of carboplatin with encapsulated navitoclax.

4.9. Results

4.9.1. Evaluation of the PAA-ch$_5$ toxicity

4.9.1.1. Evaluation of PAA-ch5 cytotoxicity using SRB assay and troubleshooting

Navitoclax was successfully encapsulated inside the PAA-ch$_5$ polymer (chapter 3). Prior to evaluating the cytotoxicity towards cancer cells of the encapsulated navitoclax to free navitoclax, the toxicity of the polymer alone was first determined. Ovarian cancer cells OVCAR-8 and OVSAHO were exposed to a range of concentrations of PAA-ch$_5$ (0.0625-320 µg/ml), and relative cell number was investigated by staining with SRB. Unexpectedly, at the higher concentrations of PAA-ch$_5$, the absorbance measured following staining with SRB increased above control values, rather than decreased, (Figure (4.5)). Assessment of the cells by microscopy (Figure (4.3), (4.4)) did not show any obvious increase in cell number. The increase in absorbance was also observed when cells were omitted, and media alone used, (Figure (4.6)). This suggested the SRB dye interacted with the polymer at high concentrations. Several experiments were performed to overcome the problem, including filtration of the polymer and extensive PBS washing but all were unsuccessful. Moreover, the MTT assay was conducted, and the polymer also interfered with that assay. Thus, it was not possible to use the SRB method or any light absorbance assay to assess the activity of the PAA-ch$_5$ nanoparticles when used at high concentrations.

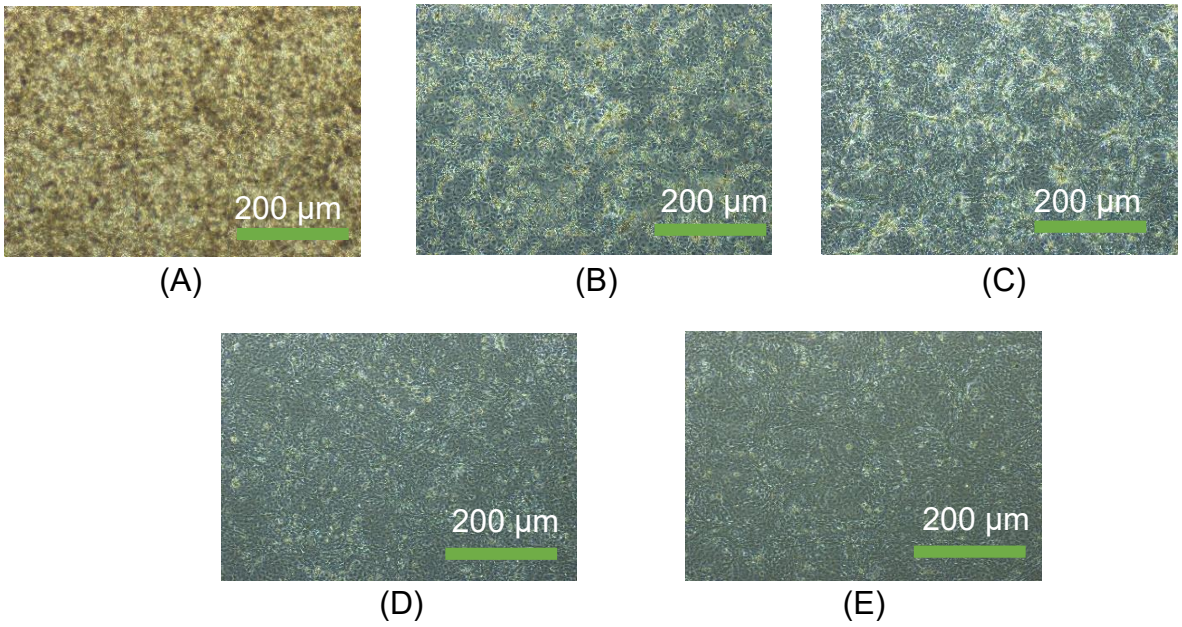

Figure 4-3: Morphological appearance of OVCAR-8 cells treated with PAA-ch$_5$

These figures represent the cytotoxicity of several PAA-ch$_5$ (NP(E)) concentrations on OVCAR-8 after 48 hours. (A) 250 µg/ml (B) 30 µg/ml (C) 15 µg/ml (D) 1 µg/ml (E) control. (n=3)

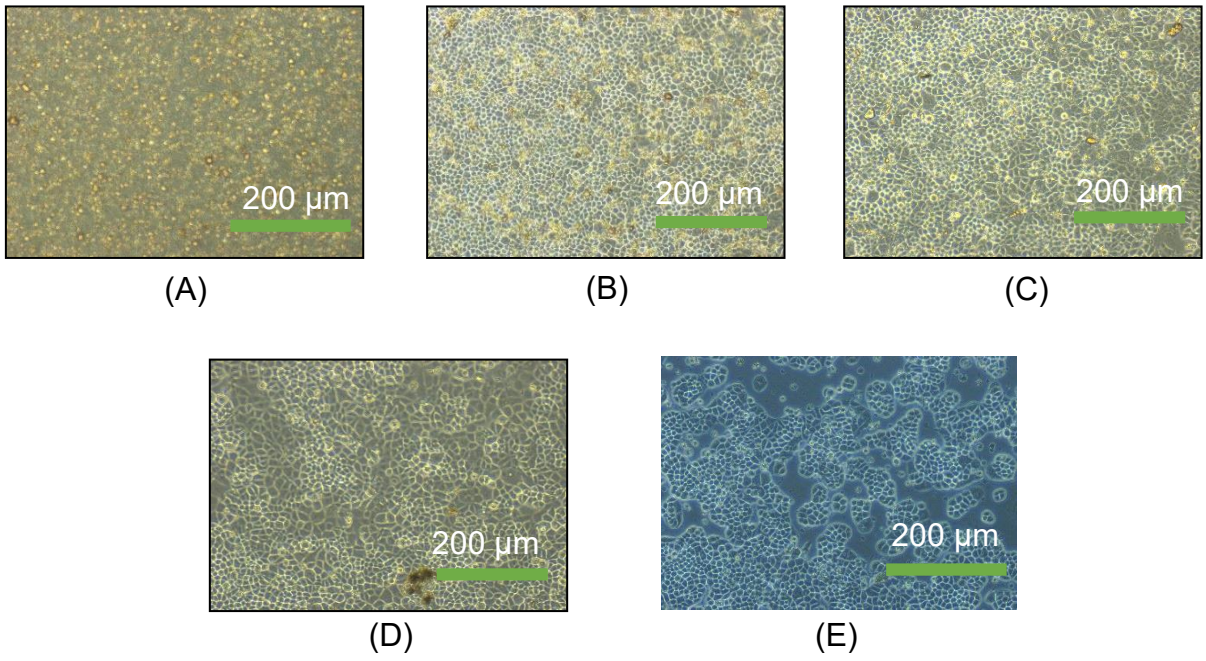

Figure 4-4: Morphological appearance of OVSAHO cells treated with PAA-ch$_5$

These figures represent the cytotoxicity of several PAA-ch$_5$ (NP(E)) concentrations on OVSAHO after 48 hours. (A) 250 µg/ml (B) 30 µg/ml (C) 15 µg/ml (D) 1 µg/ml (E) control. (n=3)

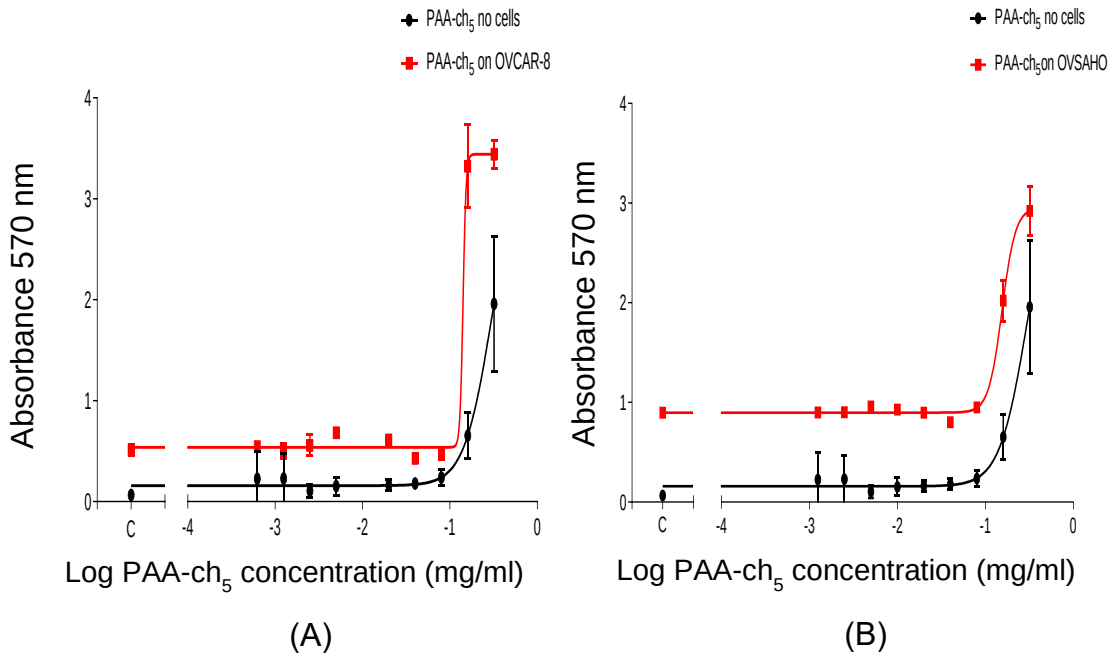

Figure 4-5: SRB assay for PAA-ch$_5$ on OVCAR-8 and OVSAHO

These figures show the PAA-ch$_5$ toxicity using SRB assay on (A) OVCAR-8 and (B) OVSAHO. It represents a correlation between the concentration and the absorption as high concentration gives higher absorbance then the absorbance was fixed with changing the concentration. This means that there could be an incompatibility between the PAA-ch$_5$ polymer and the SRB dye. Results (mean ± S.D, n=3).

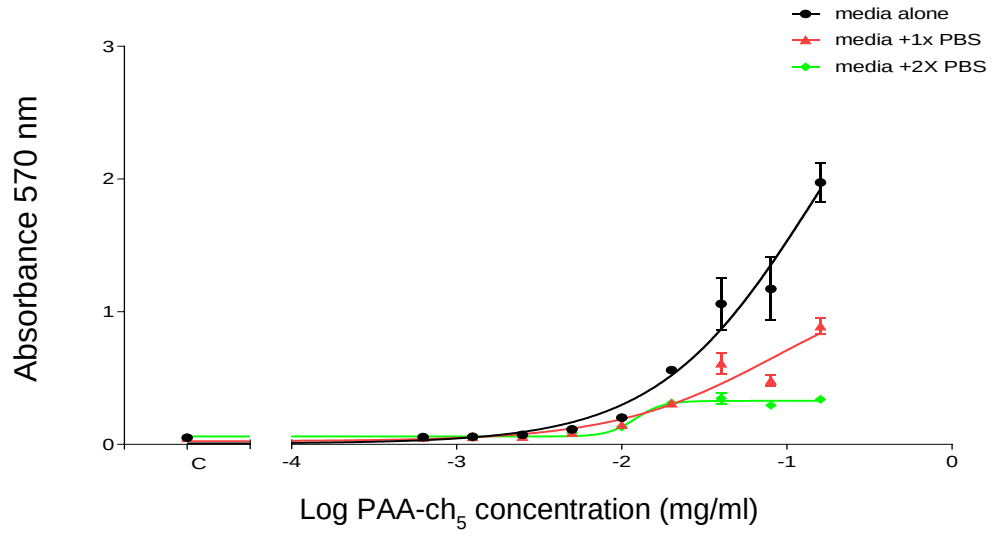

Figure 4-6: SRB assay for PAA-ch$_5$ on media

This figure shows the effect of PAA-ch$_5$ on growth media using SRB assay. The results were consistent for the one on the cells also as there was increasing the absorbance when using higher polymer concentrations even no cells inside. PBS was used to wash the well 1-time or 2-times before adding the SRB dye. None of these processes prevented the polymer form interfering with the assay. Results (mean ± S.D, n=3).

4.9.1.2. Detection of PAA-ch$_5$ toxicity using trypan blue assay

To explore the cytotoxic effect of the PAA-ch$_5$ using a different method, the trypan blue exclusion assay was employed, using a range of concentrations of PAA-ch$_5$ concentration (1-500 µg/ml). PAA-ch$_5$ inhibited the proliferation of OVCAR-8 cells (IC_{50} =28.57 ± 0.37 µg/ml) and OVSAHO cells (IC_{50}=38.36 ± 2.3 µg/ml), consistent with the morphological assessment of the cells by microscopy. Figure (4.7) shows the dose response of PAA-ch$_5$ on both ovarian cancer cell lines. At concentrations above 15 µg/ml the polymer was cytotoxic.

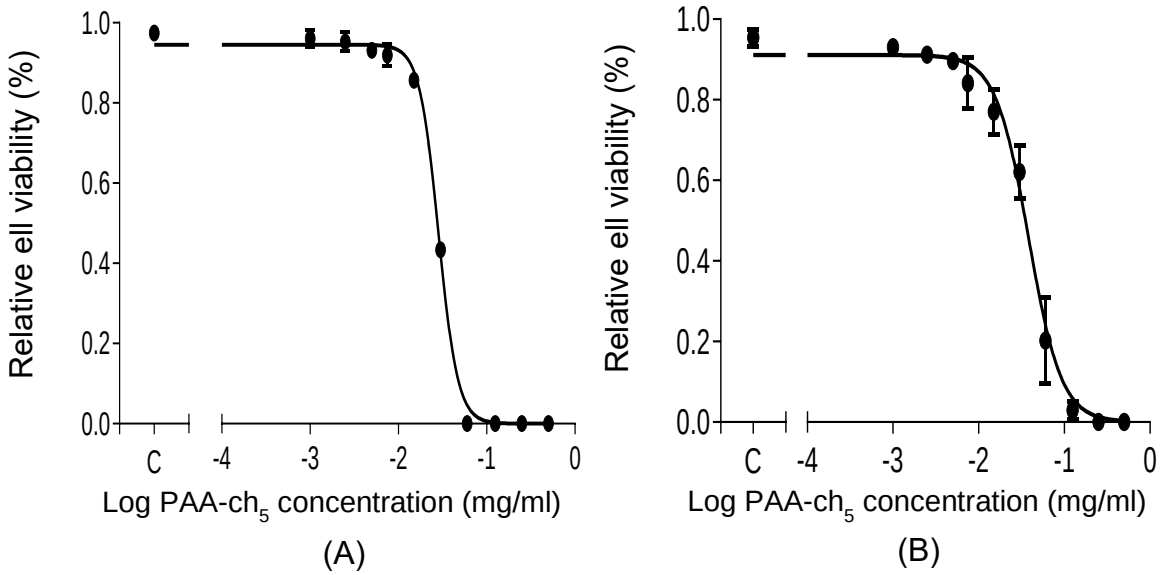

Figure 4-7: PAA-ch$_5$ cytotoxicity using trypan blue assay

These figures show the cytotoxicity of PAA-ch$_5$ (NP(E)) on (A) OVCAR-8 and (B) OVSAHO using trypan blue assay. From this we use the concentration of 15 µg/ml as non-toxic concentration as it allows a viability of more than 80%. Results (mean ± S.D, n=3).

4.9.2. Cytotoxicity of the Navitoclax-PAA-ch5 versus navitoclax

4.9.2.1. Trypan blue assay

A maximum concentration of 15 µg/ml of PAA-ch_5 was selected for further studies because this was the highest concentration that had negligible cytotoxic effect. Using the nanoparticles loaded with navitoclax at a ratio of 5:1 meant a maximum encapsulated navitoclax concertation of approximately 2.5 µM could be tested. Serial dilutions of NP(N) containing 0.15-2.5 µM encapsulated navitoclax, and corresponding concentrations of free navitoclax were tested using both OVCAR-8 and OVSAHO cells in the trypan blue assay. The nanoaggregates of navitoclax/PAA-ch_5 inhibited the growth of cultures of both OVSAHO and OVCAR-8 cells. However, the maximum concentration tested was not able to fully inhibit cell growth and an IC_{50} could not be determined. Nevertheless, at the two highest concentrations tested it was clear that in both cell lines the encapsulated navitoclax was more potent than the free navitoclax, (Figure (4.10)). These results were corroborated by microscopy, which confirmed the larger effect of the encapsulated navitoclax (tested at 2.5 µM, (Figure (4.8 (A and C))) and free navitoclax (tested at 2.5 µM, (Figure (4.8 (B and D))). For comparison, the activity of free navitoclax was also measured in the SRB assay, which in the absence of the polymer posed less limitations on the concentration of navitoclax that could be tested. In these assays, navitoclax inhibited the growth of cultures of both cell lines with comparable potencies, (Figure (4.9)).

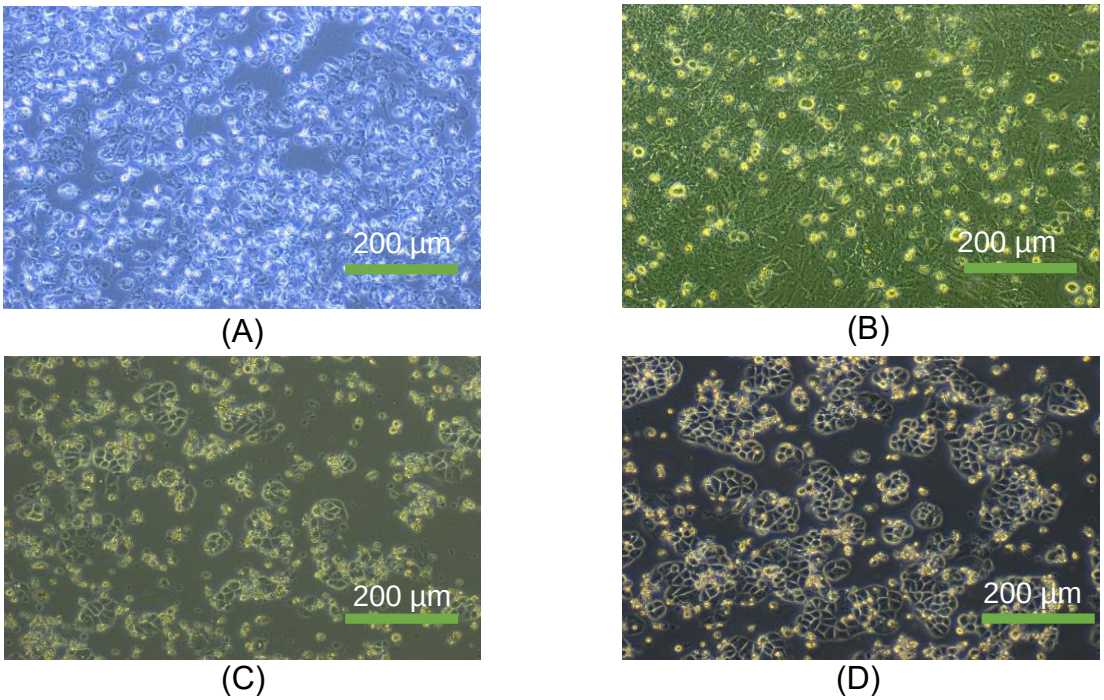

Figure 4-8: Morphological appearance of both OVCAR-8 and OVSAHO after being treated with NP(N) and free navitoclax

These figures show the cytotoxicity of both navitoclax-PAA-ch$_5$ (NP(N)) and navitoclax alone with final concentration of navitoclax of 2.5 µM which is equivalent to PAA-ch$_5$ final concentration of 15 µg/ml after 48 hours. (A) Navitoclax-PAA-ch$_5$ (NP(N)) on OVCAR-8 (B) Navitoclax on OVCAR-8. (C) Navitoclax-PAA-ch$_5$ (NP(N)) on OVSAHO (D) Navitoclax on OVSAHO. (n=1).

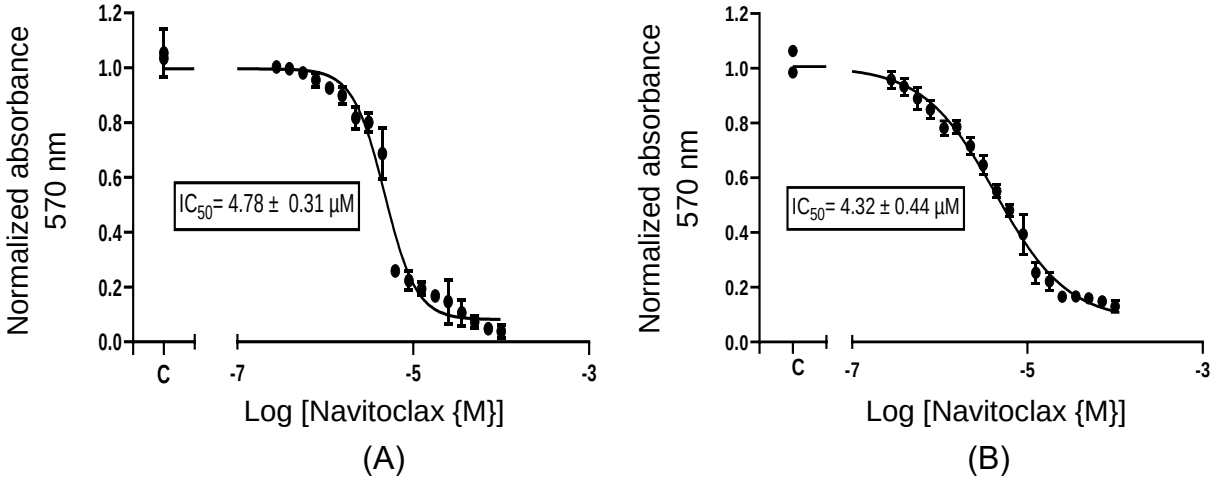

Figure 4-9: Cytotoxicity of Navitoclax on OVCAR-8 and OVSAHO using SRB assay

These figures show the cytotoxicity of dose response curve for navitoclax with final highest concentration of 100 µM using SRB assay on both (A) OVCAR-8 (B) OVSAHO. Results (mean ± S.D, n=3).

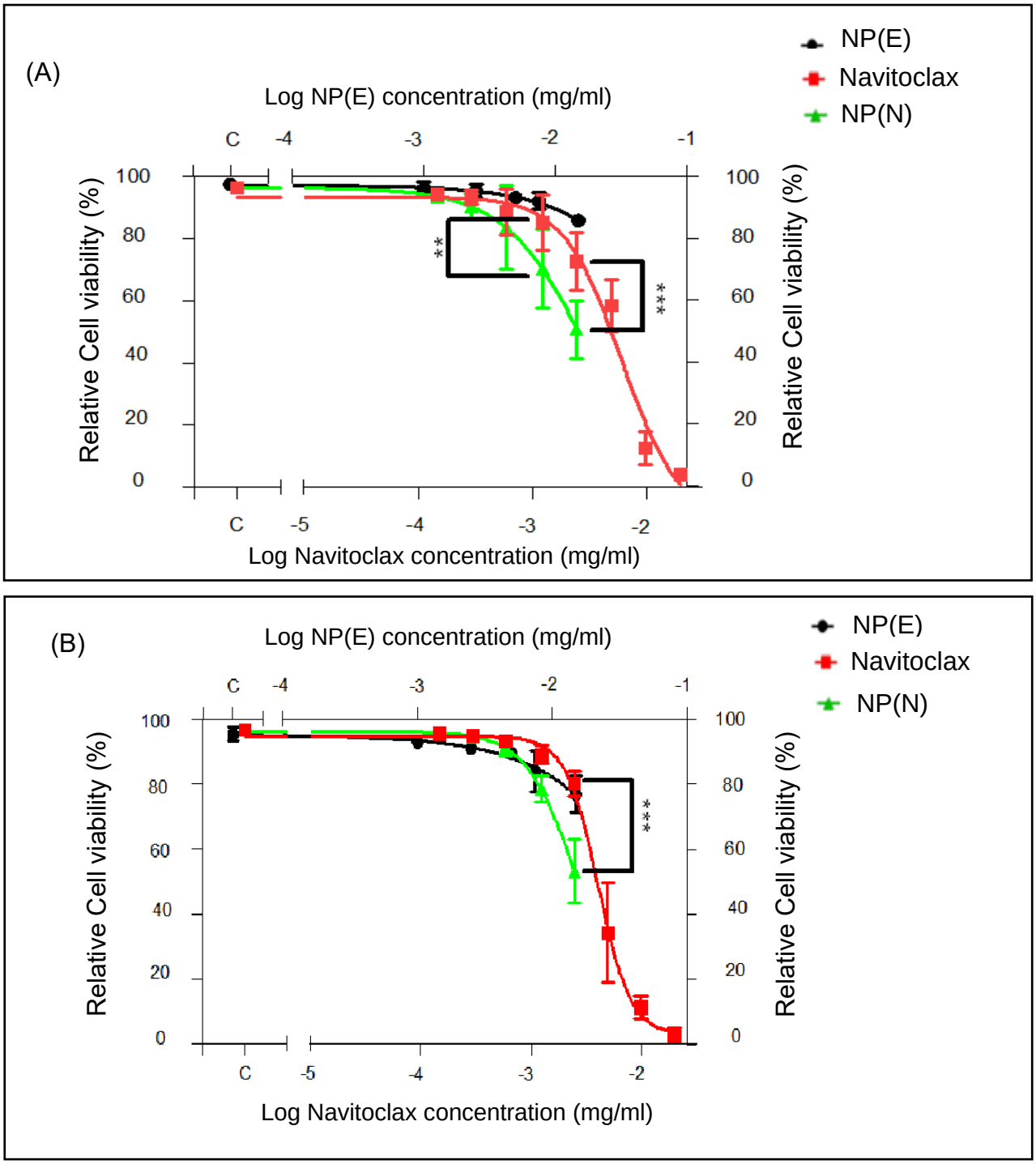

Figure 4-10: Cytotoxicity of NP(N) and Navitoclax on OVCAR-8 and OVSAHO using trypan blue assay

These figures show the cytotoxicity of both navitoclax-PAA-ch$_5$ (NP(N)), navitoclax alone, and PAA-ch$_5$ using trypan blue assay on (A) OVCAR-8 and (B) OVSAHO with serial concentrations of encapsulated navitoclax of (0.15-2.5 µM) which corresponds with PAA-ch$_5$ (NP(E)) final concentration of 15 µg/ml. A serial concentration of free navitoclax of (0.15-20 µM) and empty nanoparticle of (1-15 µg/ml) are also presented. There is a significant difference between both navitoclax formulations in higher doses. (*(**): $P \leq 0.01$; (***): $P \leq 0.001$*; data were analysed using One-way ANOVA). Results (mean ± S.D, n=3).

4.9.2.2. Caspase 3/7 assay

The activation of the caspase cascade is considered a crucial step in apoptosis initiation and so can be used as an additional means to characterize the cytotoxic activity of a drug. Cells were exposed to a non-toxic concentration of the polymer (15 µg/mL, “NP (E)”), free navitoclax (2.5 µM) or the encapsulated navitoclax (containing both agents at the same concentration, NP(N”)). The polymer alone had negligible effect on caspase- 3/7 activity, whereas navitoclax increased caspase 3/7 activity. The encapsulated navitoclax increased caspase 3/7 activity significantly more than the free navitoclax. Figure (4.11) shows caspase 3/7 activity of NP(N), navitoclax, and PAA-ch_5 on both ovarian cancer cell lines.

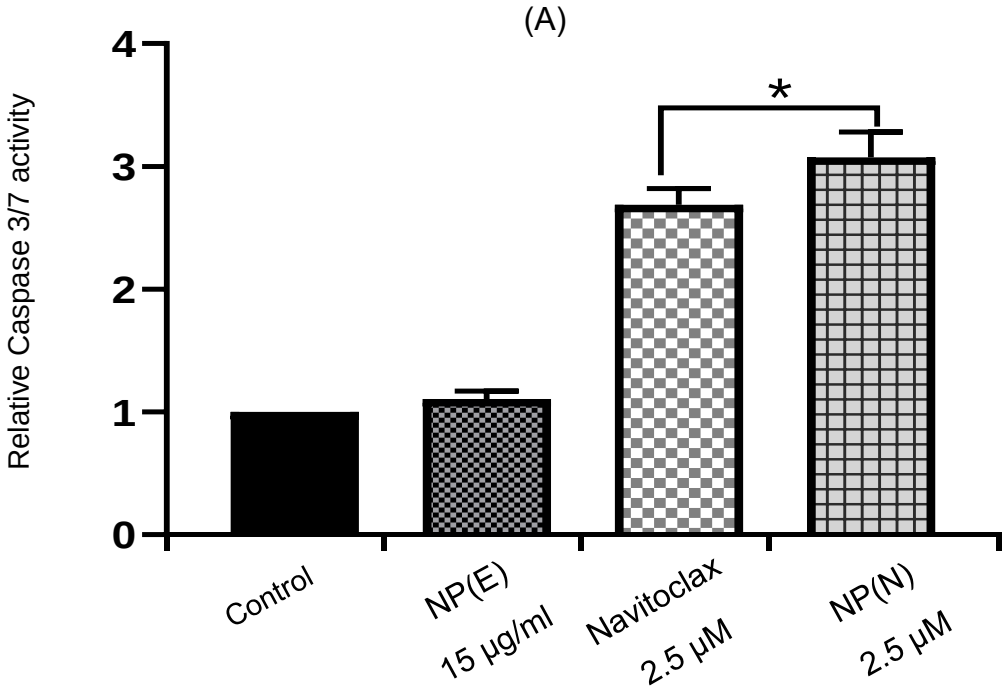

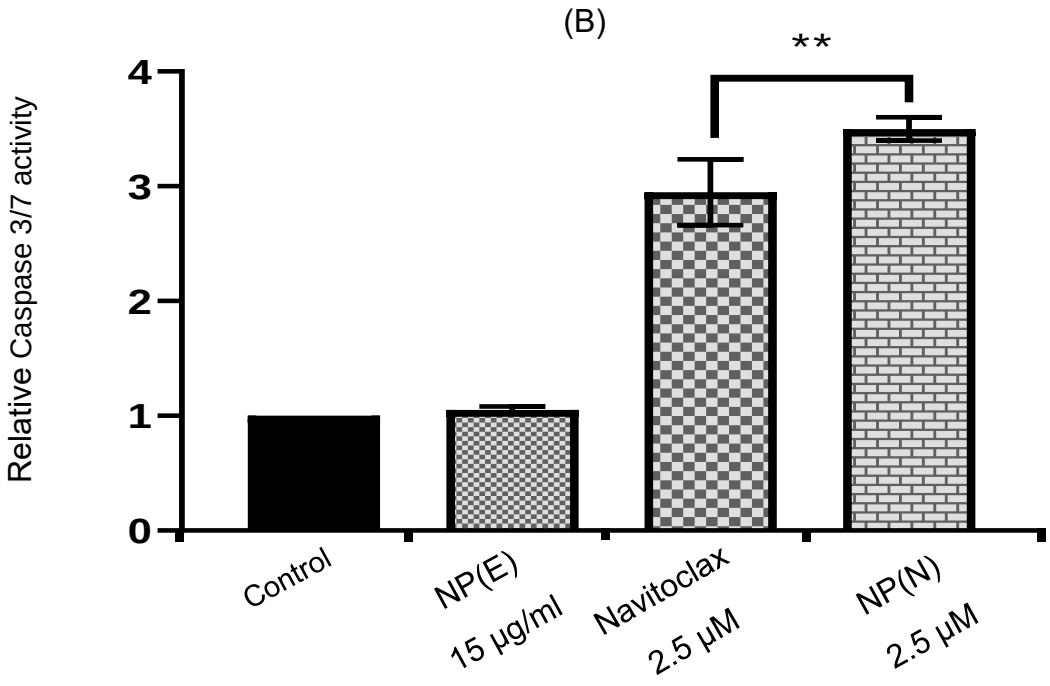

Figure 4-11: Cytotoxicity of NP(N), Navitoclax, and PAA-ch$_5$ on OVCAR-8 and OVSAHO using caspase 3/7 assay

These figures represent the cytotoxicity of both navitoclax-PAA-ch$_5$ and navitoclax alone on both (A) OVCAR-8 and (B) OVSAHO, using caspase 3/7 assay with a final concentration of navitoclax of 2.5 µM and with highest concentration to PAA-ch$_5$ of 15 µg/ml. The results appeared as a relative caspase 3/7 activity compared to the control samples. There is a significant difference between both navitoclax formulations. ((*): $P< 0.05$; (**): $P \leq 0.01$; data were analysed using One-way ANOVA). Results (mean ± S.D, n=3).

4.9.3. Drug uptake

To confirm these results, a drug uptake assay was conducted. The previous assays showed a higher effect of NP(N) than the free navitoclax, and this was not accompanied by any toxic effect of the polymer on these cells. In this assay, both navitoclax formulations of 2.5 µM were added to the OVCAR-8 and OVSAHO cells and the navitoclax taken up measured after 4, 24 and 72 hours. The concentration of navitoclax was measured using the HPLC. No difference in intracellular navitoclax concentration which was measured after 4-hours, but after 24- and 72-hours exposure

there was a significantly higher concentration in OVSAHO and OVCAR-8 cells exposed to the encapsulated navitoclax than to the free navitoclax, (Figure (4.12)).

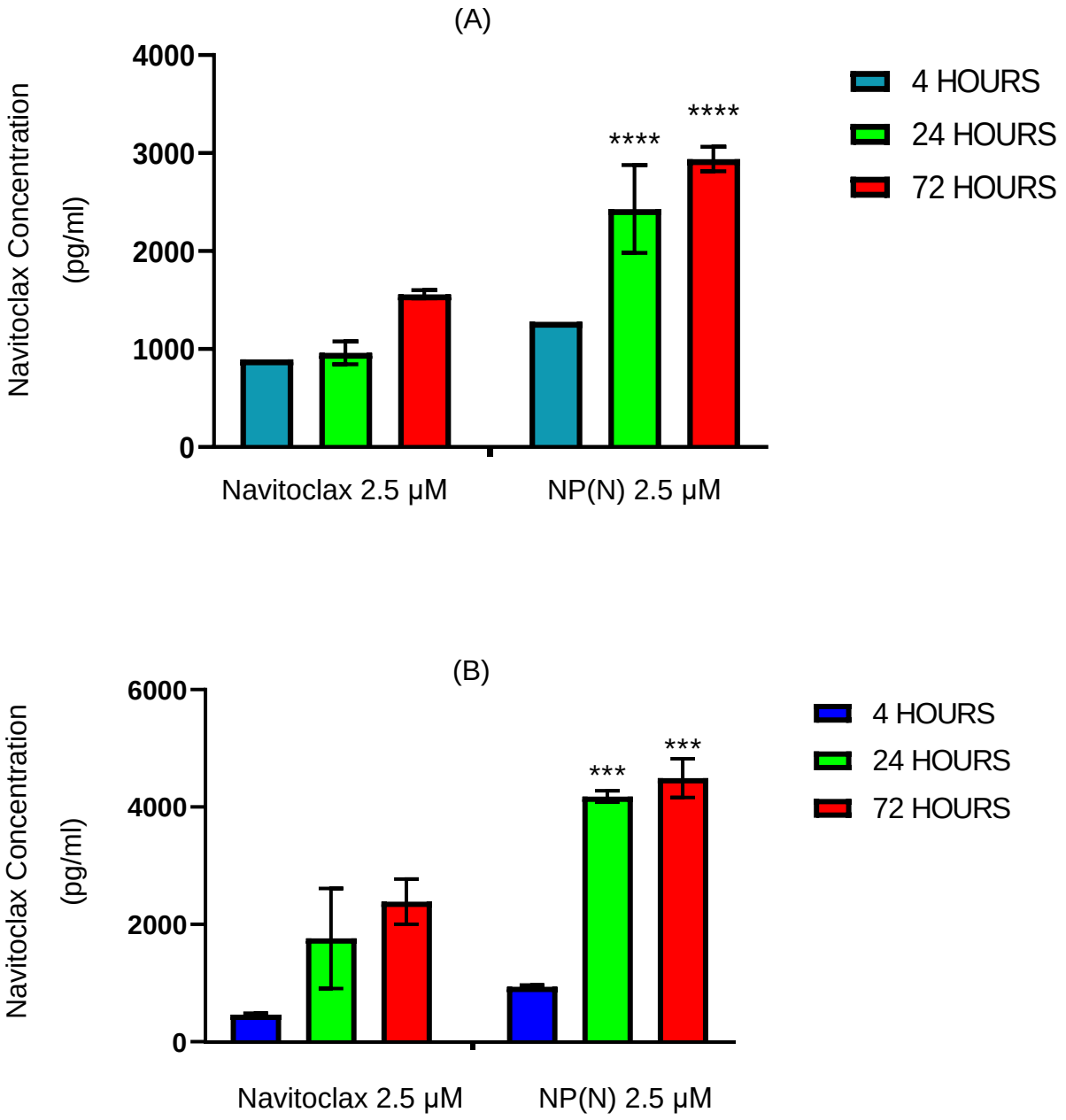

Figure 4-12: Navitoclax uptake for OVCAR-8 and OVSAHO after NP(N) and navitoclax administration in different time frames

These figures represent the drug uptake of both NP(N) and navitoclax alone with a final concentration of 2.5 µM on both (A) OVCAR-8 and (B) OVSAHO. There is a significant difference between both navitoclax formulations at 24 and 72 hours. ((***): $P \leq 0.001$, (****): $P \leq 0.0001$; data were analysed using Two-way ANOVA). Results (mean ± S.D, n=3).

4.9.4. Combination assays

Previous work has shown the synergy between BCL-X_L inhibitors and carboplatin in ovarian cancer cell lines. Prior to testing this with the encapsulated navitoclax, the toxicity of carboplatin was first determined using the SRB assay (Figure (4.13)). Carboplatin showed reasonably comparable potencies in both cell lines. For simplicity, studies with the nanoparticles were performed using a concentration of carboplatin of 13 µM with both cell lines. The final concentration of navitoclax in these subsequent experiments was slightly reduced (to 1µM) (20% of navitoclax IC_{50}) compared to the previous experiments because of the additional effect of the carboplatin. The concentration of PAA-ch_5 was also reduced to 6 µg/ml. Combinations of free or encapsulated navitoclax were subsequently tested in trypan blue, caspase 3/7, PARP cleavage using western blot assay, and Annexin/PI assays. In addition, the morphological appearance of the cells was also monitored, (Figure (4.14) and (4.15)).

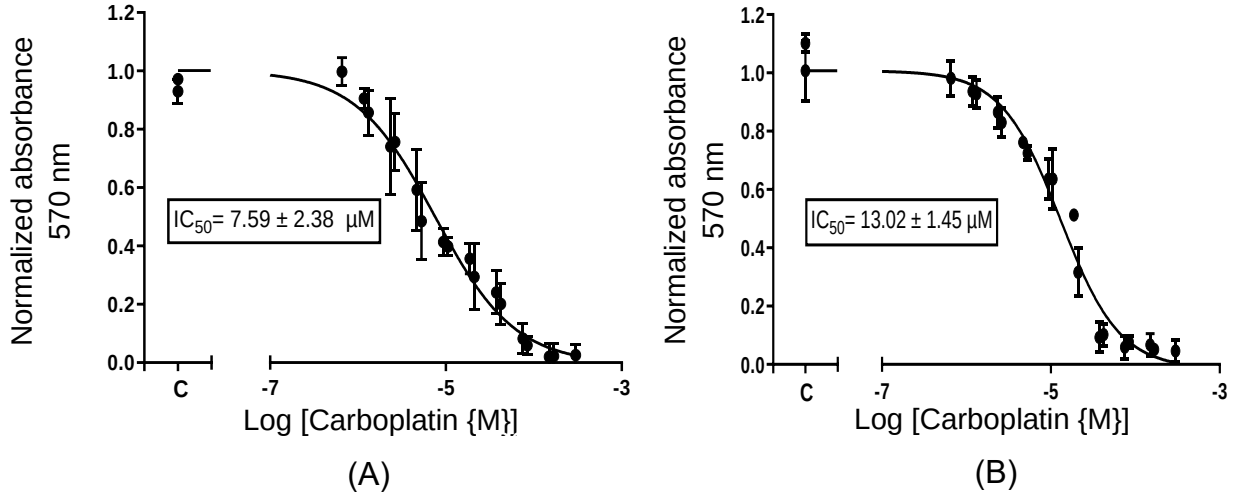

Figure 4-13: Cytotoxicity of carboplatin on OVCAR-8 and OVSAHO using SRB assay

These figures represent the cytotoxicity of carboplatin with final highest concentration of 300 µM on both (A) OVCAR-8 (B) OVSAHO. Results (mean ± S.D, n=3).

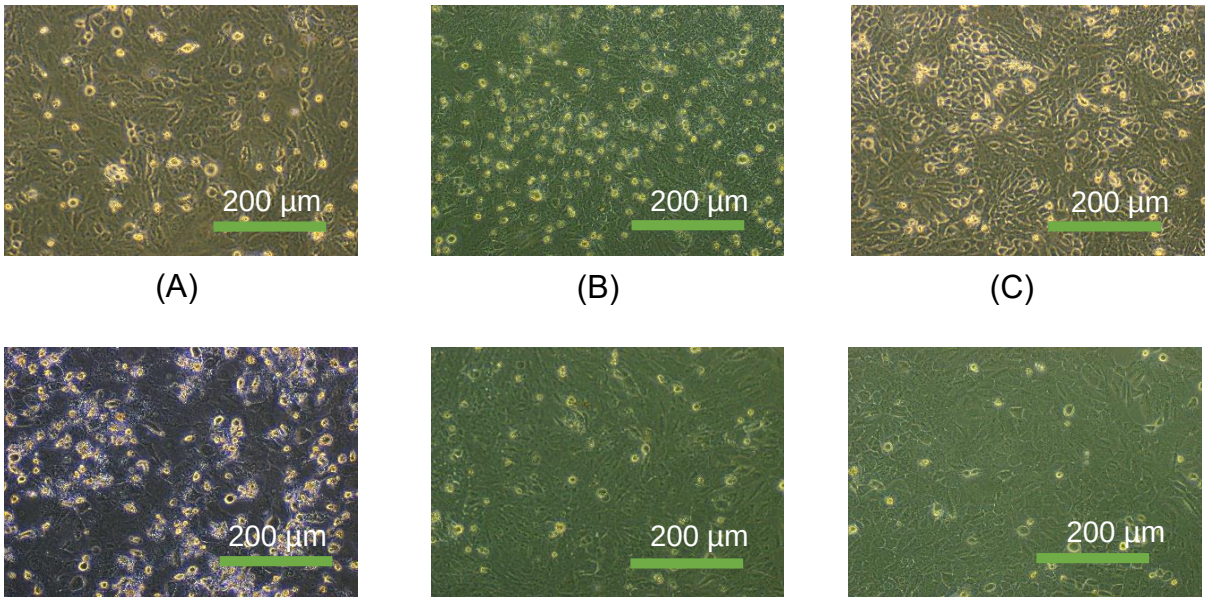

(A) (B) (C)

(D) (E) (F)

Figure 4-14: Morphological appearance of OVCAR-8 cells treated with several drugs combinations

These figures represent the cytotoxicity effect of several drugs on their own and in combinations on OVCAR-8 after 48 hours. (A) navitoclax alone 1 µM (B) navitoclax+ carboplatin 1 µM/13 µM (C) Navitoclax-PAA (NP(N)) 1 µM (D) Navitoclax-PAA (NP(N)) + carboplatin 1 µM/13 µM (E) PAA (NP(E)) 6 µg/ml (F) control. (n=2).

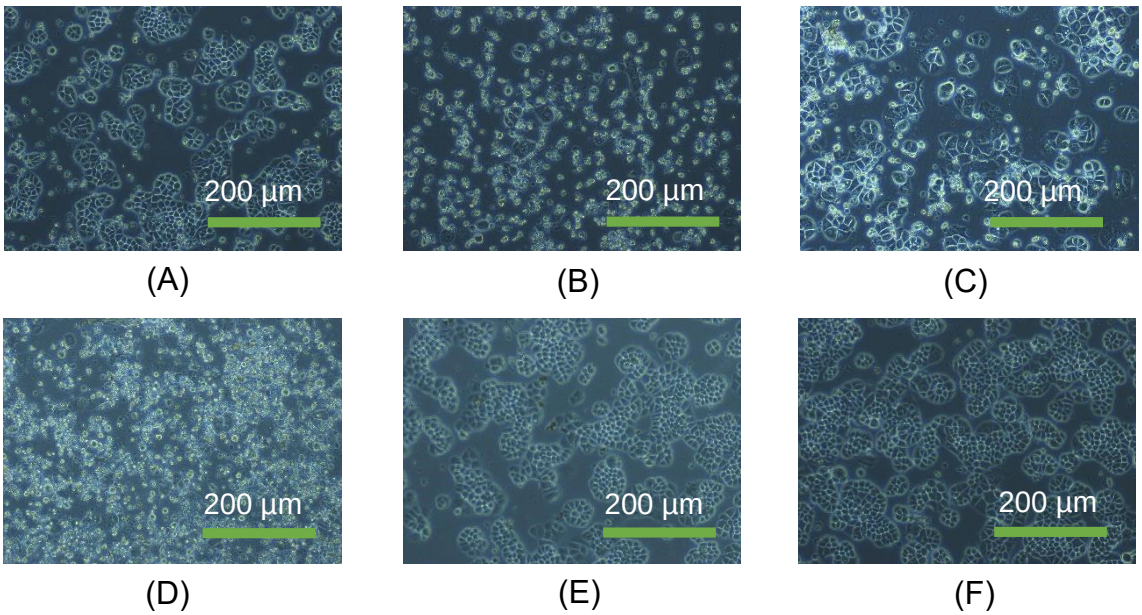

(A) (B) (C)

(D) (E) (F)

Figure 4-15: Morphological appearance of OVSAHO cells treated with several drug combinations

These figures represent the cytotoxicity effect of several drugs on their own and in combinations on OVSAHO after 48 hours. (A) navitoclax alone 1 µM (B) navitoclax+ carboplatin 1 µM/13 µM (C) Navitoclax-PAA (NP(N)) 1 µM (D) Navitoclax-PAA (NP(N)) + carboplatin 1 µM/13 µM (E) PAA (NP(E)) 6 µg/ml (F) control. (n=2).

4.9.4.1. Trypan Blue

When OVSAHO cells were exposed to the carboplatin or encapsulated navitoclax, there was an evident increase in cell death. However, when cells were exposed to carboplatin and free navitoclax or carboplatin and encapsulated navitoclax, the number of dead cells was significantly more than would have been expected from the Bliss independence criterion, if the drugs had acted additively. Unexpected, empty nanoparticles also augmented the cell death induced by carboplatin, although to a lesser extent than those containing navitoclax (Figure (4.17)). Similar results were obtained with OVCAR-8 cells (Figure 4.16).

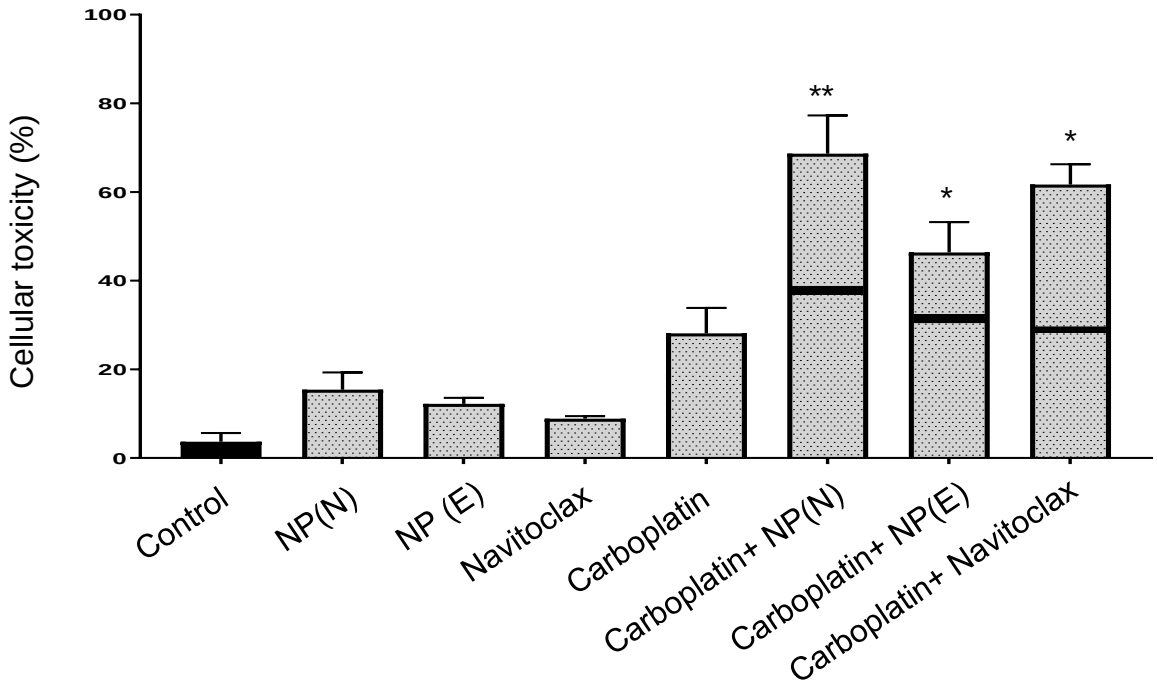

Figure 4-16: The effect of Navitoclax-PAA and navitoclax alone when given in combination with carboplatin on OVCAR-8 using trypan blue assay

The indicated cell was exposed to 13 μM carboplatin, 1 μM NP(N), 1 μM navitoclax, 6 μg/ml NP(E) for 72h. Cytotoxicity was determined using trypan blue assay. The data are represented in relative to the live cells after being treated with several drugs as single and in combinations. The expected effect of the combination was calculated using the Bliss independence criterion and represented as black horizontal lines. There is a significant difference with the calculated additive effect but no significant difference between the encapsulated navitoclax with carboplatin and the free navitoclax with carboplatin. *((*): $P \leq 0.05$, (**): $P \leq 0.01$;* data were analysed using *paired t-test).* Results (mean ± S.D, n=4).

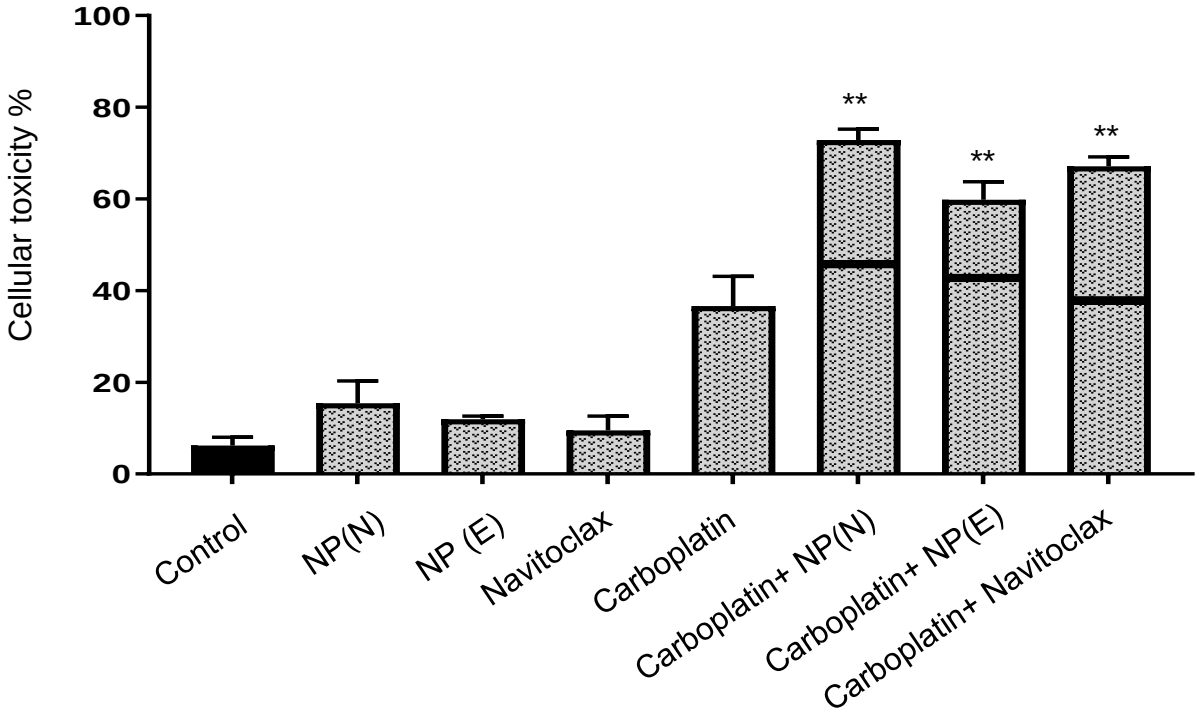

Figure 4-17: The effect of Navitoclax-PAA and navitoclax alone when given in combination with carboplatin on OVSAHO using trypan blue assay

The indicated cell was exposed to 13 μM carboplatin, 1 μM NP(N), 1 μM navitoclax, 6 μg/ml NP(E) for 72h. Cytotoxicity was determined using trypan blue assay. The data are represented in relative to the live cells after being treated with several drugs as single and in combinations. The expected effect of the combination was calculated using the Bliss independence criterion and represented as black horizontal lines. There is a significant difference with the calculated additive effect but no significant difference between the encapsulated navitoclax with carboplatin and the free navitoclax with carboplatin. *((**): P ≤ 0.01;* data were analysed using *paired t-test).* Results (mean ± S.D, n=4).

4.9.4.2. Caspase assay

To confirm these results the effect of the combination on caspase activity were also measured. There was no significant increase in caspase 3/7 activity in OVSAHO cells caused by the polymer, free or encapsulated navitoclax NP(N), and NP(E) relative to the carboplatin caspase activity. In contrast, carboplatin caspase 3/7 activity was augmented by the inclusion of either free or encapsulated navitoclax (Figure (4.18, B)). Similar results were observed with OVCAR-8 cells, (Figure (4.17, A)).

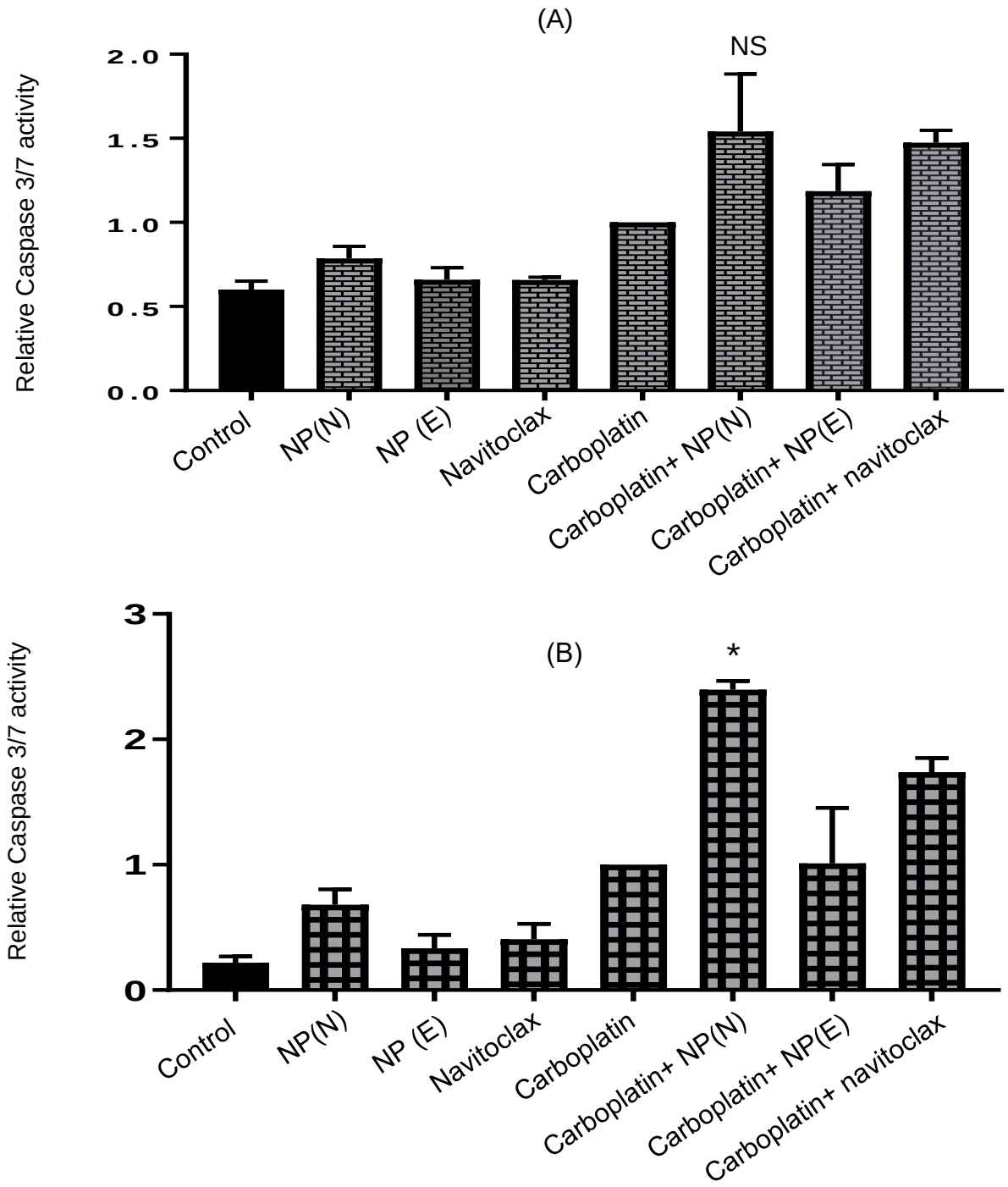

Figure 4-18: The effect of Navitoclax-PAA and navitoclax alone when given in combination with carboplatin on (A) OVCAR-8 and (B) OVSAHO using caspase 3/7 assay

The indicated cell lines (A) OVCAR-8 and (B) OVSAHO were exposed to 13 μM carboplatin, 1 μM NP(N), 1 μM navitoclax, 6 μg/ml NP(E) for 48h. Cell death was determined using relative caspase 3/7 activity. The data are expressed as a relative caspase 3/7 activity compared to the one of carboplatin treated samples. There is significant difference in caspase 3/7 activity between the combination of carboplatin with encapsulated navitoclax and the combination of carboplatin with free navitoclax in OVSAHO but not in OVCAR-8. *((*): $P \leq 0.05$, (NS): Not significant; data were analysed using One-way ANOVA).* Results (mean ± S.D, n=3).

4.9.4.3. PARP-cleavage assay

To confirm apoptosis induction by an additional method, PARP cleavage was assessed by western blotting. Poly (ADP-ribose) polymerase-1 (PARP-1)'s normal function is to repair DNA damage, but it is cleaved by caspases during apoptosis. The blot showed cleavage of PARP-1 protein (116 KDa) into 89 KDa PARP-1 fragments. In OVSAHO, although free navitoclax did not cause cleavage of PARP, this was observed with the addition of carboplatin alone. The empty nanoparticles also did not cause PARP cleavage. On the other hand, encapsulated navitoclax on its own showed more PARP cleavage when compared with the previous mentioned drugs. Significantly, the combination of carboplatin with encapsulated navitoclax showed a significant PARP cleavage once compared with the ones that were induced by combination of carboplatin with either navitoclax or empty nanoparticles, (Figure (4.19, B)). The OVCAR-8 blot showed the same results except the PARP cleavage for free navitoclax was less prominent than that in OVSAHO blot, (Figure (4.19, A)). The cleaved and uncleaved PARP were quantified using Alphaview software and their ratios were determined to calculate the proportion of PARP cleavage that had taken place. This ratiometric analysis has the advantage that it does not require identical protein levels in each sample, which may be hard to control due to cell death induced by the drugs. The GAPDH protein was applied as a standard protein for both cell lines. GAPDH is considered a housekeeping gene and consequently widely used as loading control, its main role is in glycolysis to catalyze the oxidative phosphorylation of glyceraldehyde-3-phosphate.

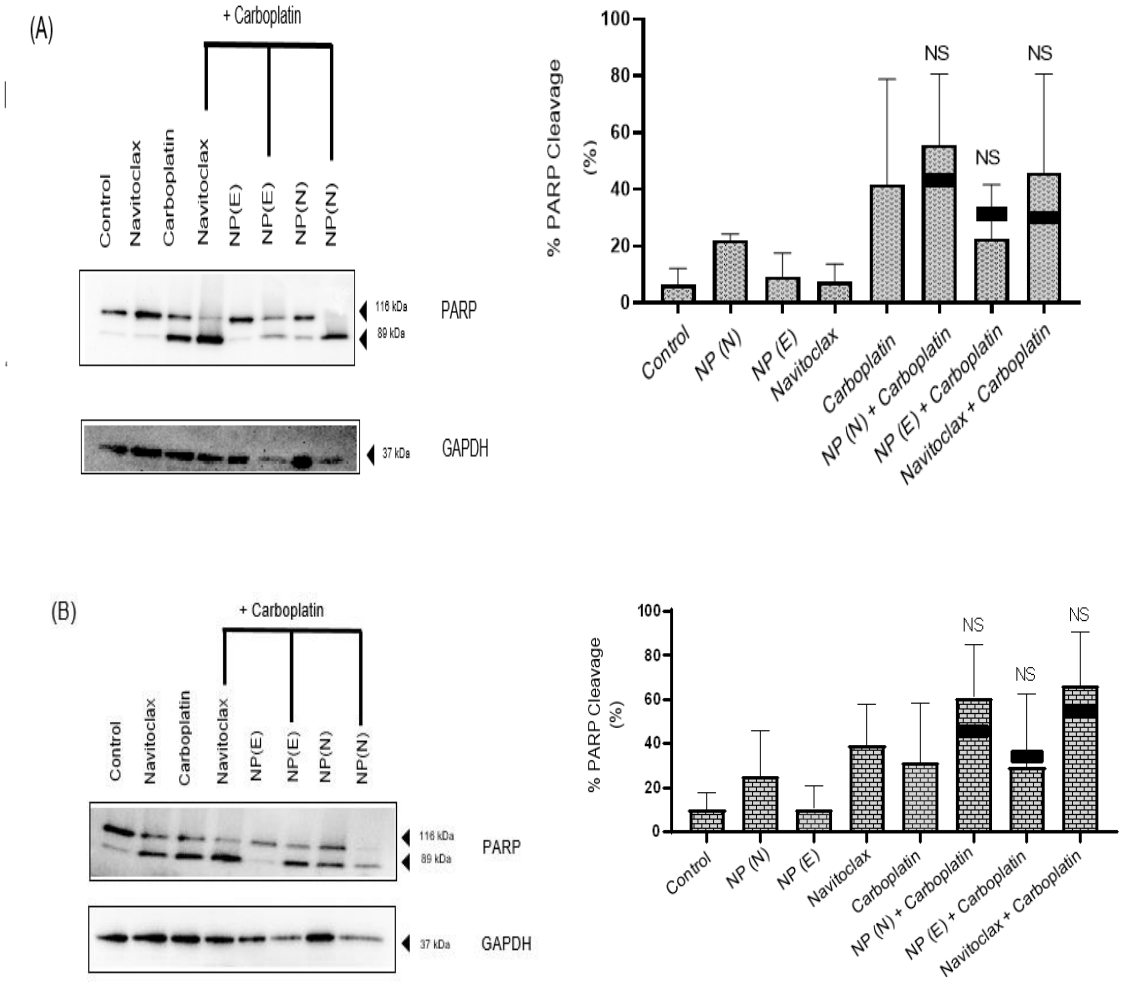

Figure 4-19: Effect of several drug combinations with carboplatin on PARP cleavage using western blot assay

The indicated cell lines (A) OVCAR-8 and (B) OVSAHO were exposed to 13 μM carboplatin, 1 μM NP(N), 1 μM navitoclax, 6 μg/ml NP(E) alone and in combinations for 48 hours. The results showed the protein expression for all the drugs used using western blot assay. The GAPDH expressed the standard protein in each cell line. Although there was significant variation between samples in the total protein (as shown by the loading control), interpretation of the data is not affected because it is the ratio of cleaved PARP to uncleaved PARP that is an indicator of apoptosis. The expected effect of the combination was calculated using the Bliss independence criterion and represented as black horizontal lines. There is no significant difference with the calculated additive effect and no significant difference between the encapsulated navitoclax with carboplatin and the free navitoclax with carboplatin. *((NS): non-significant;* data were analysed using *paired t-test).* Results (mean ± S.D, n=3).

4.9.4.4. Annexin V/PI assay

The annexin V/PI assay was conducted to further assess apoptosis triggered by the same combination of drugs previously mentioned. This assay characterizes cellular death (necrosis, early apoptosis, late apoptosis) depending on the phosphatidyl serine (PS) translocation from the inner to the outer surface of the plasma membrane that occurs during apoptosis, thereby exposing PS to the external cellular environment. Staining with both PI and annexin V (which detects phosphatidyl serine) is an indication of late cellular apoptosis. This assay was carried out using OVCAR-8, not OVSAHO, because of difficulties in detaching the cells and getting sufficient numbers of single cells for flow cytometry. The results showed no significant toxicity of the free navitoclax nor the empty nanoparticles. In contrast, the NP (N) did not show significant cellular toxicity although it was modestly higher than that for free navitoclax and empty nanoparticles. However, the combination of carboplatin with NP(N) was slightly higher than that with navitoclax and higher than that with empty nanoparticles, (Figure (4.20), Figure (4.21)). In all combinations, the number of dead cells was significantly more than would have been expected from the Bliss independence criterion, if the drugs had acted additively, (Figure, 4.22).

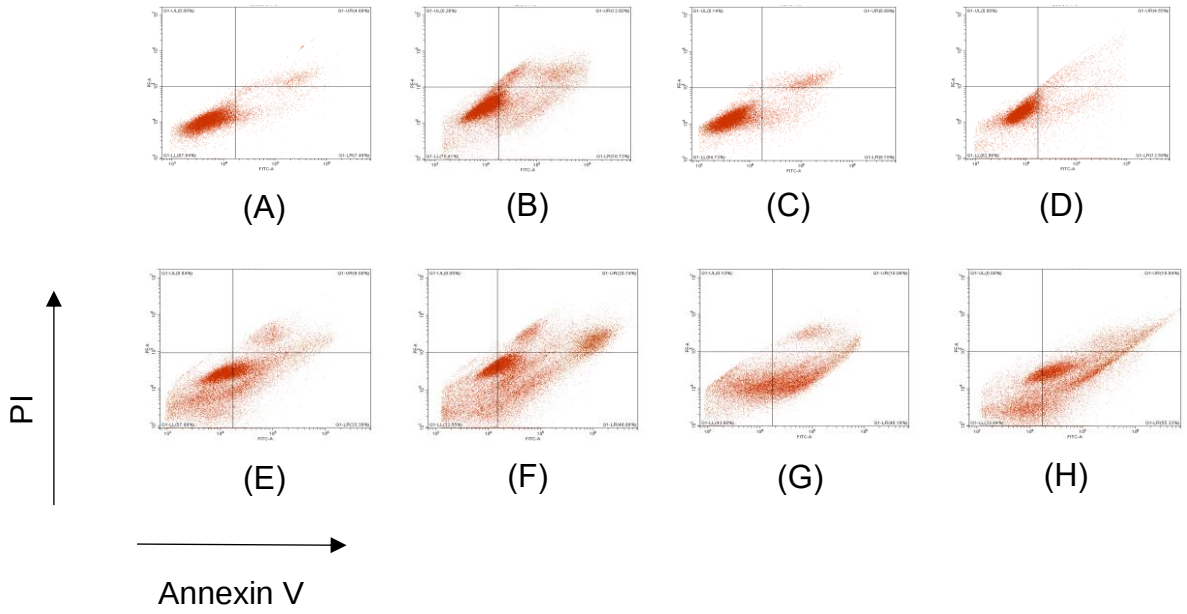

Figure 4-20: Flow-cytometry images for different drug combinations

These figures represent the cytotoxicity of several drugs on their own and in combination with carboplatin on OVCAR-8 cells after 48h. (A) Control (B) NP(N) (C) Navitoclax (D) NP(E) (E) Carboplatin (F) NP(N)-Carboplatin (G) NP(E)-Carboplatin (H) Navitoclax-Carboplatin. (n=3).

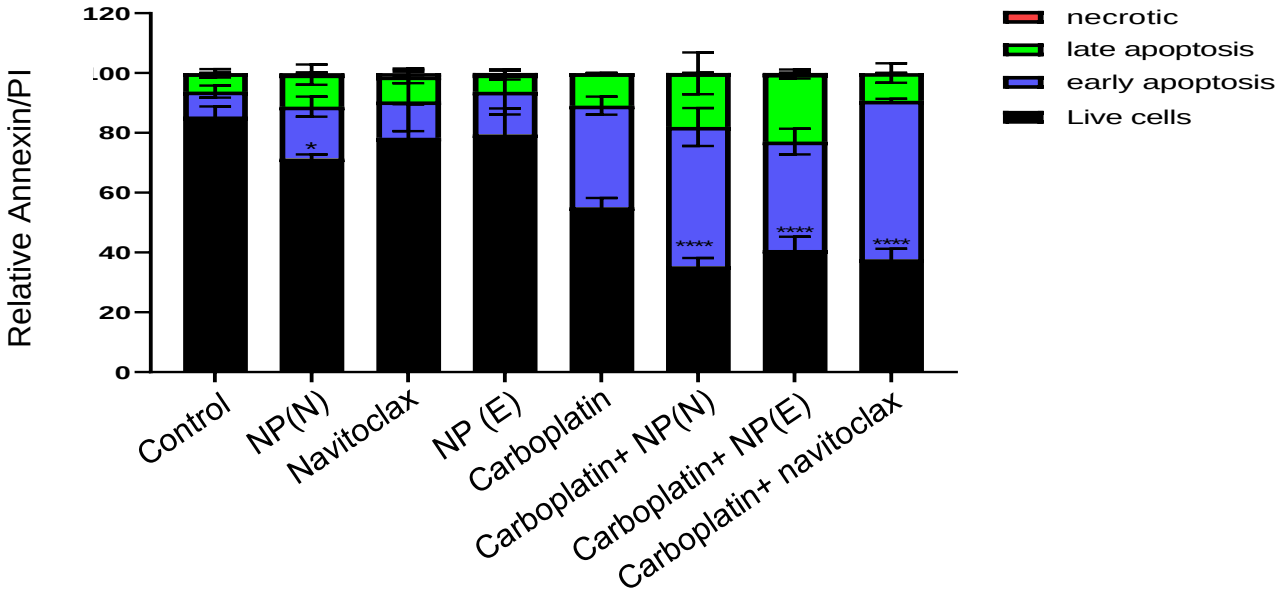

Figure 4-21: Relative Annexin V/PI activity for OVCAR-8 using several drug combinations

The indicated cell was exposed to 13 µM carboplatin, 1 µM NP(N), 1 µM navitoclax, 6 µg/ml NP(E) for 48h. Cytotoxicity was determined by Annexin V/PI assay and cells were labelled with annexin V and propidium iodide and measured by flow cytometry. The results are expressed as a fraction of that measured in control cells which showed significant difference in all combinations. ((*): *P ≤ 0.05, (****): P ≤ 0.0001*; data were analysed using Two-way ANOVA). Results (mean ± S.D, n=3).

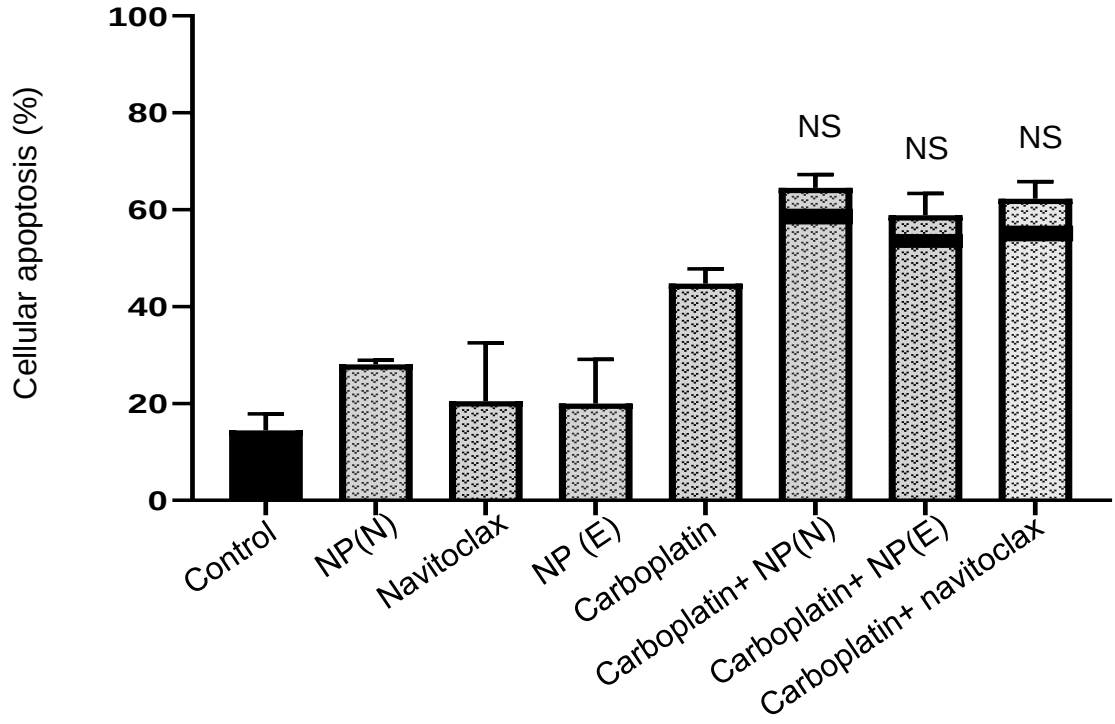

Figure 4-22: Cellular apoptosis for OVCAR-8 using several drug combinations using annexin V/PI assay

The indicated cell was exposed to 13 μM carboplatin. 1 μM NP(N), 1 μM navitoclax, 6 μg/ml NP(E) for 48h. Cytotoxicity was determined by Annexin V/PI assay. The results are expressed as a fraction of that measured in control cells. The Bliss independence criterion was used to calculate the expected effect of the combination and the results are express as solid horizontal black lines on the bar chart. There is no significant difference with the calculated additive effect and no significant difference between the encapsulated navitoclax with carboplatin and the free navitoclax with carboplatin. (*(NS): Not significant,* data were analysed using paired t-test*).* Results (mean ± S.D, n=3).

4.10. Discussion

The evasion of apoptosis due to overexpression of anti-apoptotic BCL-2 family members is one of the leading causes of chemotherapy resistance (Pfeffer and Singh, 2018). These family of proteins are also responsible for the progression of the disease. One of the best solutions to overcome this obstacle was the development of the BH3 mimetics that resemble the sensitiser BH3 only proteins and thus induce apoptosis (Cerella *et al*., 2020). Navitoclax, which is one of these BH3 mimetics, inhibits several

BCL-2 family proteins, including BCL-X_L and BCL-2. The importance of navitoclax came from its oral bioavailability and because it has entered the phase I and phase II clinical trials (Ashkenazi *et al.*, 2017). Ovarian cancer mainly depends on BCL-X_L. Our group has previously demonstrated that navitoclax potentiates the cell death that carboplatin induces. However, clinical success with navitoclax has been hindered as it causes mechanism-dependant thrombocytopenia by inhibiting BCL-X_L in platelets. Unfortunately, strategies are needed to target navitoclax to ovarian cancer cells to overcome this (Abed *et al.,* 2016). Here, the formulation of navitoclax in nanoparticles was investigated to achieve this.

The encapsulation of navitoclax and other BH3 mimetics, in general, is not a new method. The application of BH3 mimetics with nanoparticles as delivery systems has previously shown promising results (Ding *et al.*, 2020). Furthermore, the encapsulation of BH3 mimetics inside the nanoparticles improved their targeting toward cancer cells, achieved a decrease in the incidence of unwanted side effects and improved their physical characteristics in general. Examples of the application of some BH3 mimetics with nanoparticles include the encapsulation of ABT-737 with PEGylated polymeric nanoparticles (NPs) (Schmid *et al.*, 2014), the encapsulation of venetoclax and S63845 (MCL-1 inhibitor) using nanoparticles (Tannan *et al.*, 2021), and encapsulation of navitoclax with doxorubicin with ultra pH-sensitive nanovesicle based on polyethylene glycol-poly(diisopropylamino) ethyl methacrylate (mPEG-PDPA) (Ding *et al.*, 2020).

The application of poly(allylamine) polymer on ovarian cancer cell lines, and in particular to encapsulate navitoclax, has not investigated before. However, Hoskins

and her group studied this type of polymers widely with the cholesteryl pendant group and other pendant groups on pancreatic cancer cell lines. The rationale behind using this type of polymer as mentioned before, is because of its ability to form nanoaggregates in water which can carry hydrophobic drugs including anticancer drugs (Al Ameri *et al.*, 2020), in addition to its ability to increase the drug uptake inside the cancer cells through endocytosis (Zafar *et al.*, 2018). Yet, there was a need to examine the polymer toxicity on OVCAR-8 and OVSAHO first by using different cytotoxicity assays before examining navitoclax nanoparticles. Significantly, it has been documented that although this type of polymer was designed to carry drugs, it possesses inherent toxicity (Alsuraifi *et al.*, 2018). This cytotoxicity of this polymer is likely to be due to the primary amine groups it has on its backbone, and grafting this polymer by pendant groups, such as cholesteryl, can decrease the cytotoxic effect of the polymer on cells as the primary amines are modified (Alsuraifi *et al.*, 2018).

The first cytotoxicity assay that was used was the SRB assay since this technique is a quantitative, simple, cheap, reproducible, colorimetric, technically easy and allows reasonably high throughput which facilitates the quantitative assessment of drug combinations. The polymer was tested with different concentrations of polymer (0.0000625- 0.32 mg/ml), but the results were extraordinary and divergent from the morphological appearance of cells when examined under the microscope. The ambiguity of the results came from the absorbance readings that have been recorded as the higher polymer concentrations and which showed a higher light absorbance. Unfortunately, this also happened when the polymer was tested on media alone without any cells seeded. Several attempts to overcome the problem were

investigated, including washing and filtering the polymer. However, all these trials failed.

This suggests that high concentrations of polymer bind the SRB dye giving rise to the high absorbance readings. Notably, the higher concentrations of polymer had a cloudy opaque appearance which is consistent of what has been reported by Thompson *et al.* who studied this polymer for the first time and mentioned that this polymer with a cholesterol grafting with 5% (PAA-ch_5) has an opaque cloudy appearance (Thompson *et al.*, 2008). This suggests particulate polymer may bind the SRB dye and thus giving this unusual increment in light absorbances at high polymer concentrations, (Figure 4.23).

Figure 4-23: Interference between SRB dye and the high PAA-ch_5 concentrations

96-well plated for ovcar-8 cells treated with different PAA-ch_5 concentrations. The blue arrow showed the well that contain cells that were treated with PAA-ch_5 with a final concentration of 0.5 mg/ml and how a dark violet layer appeared after SRB dye was added and washed

To overcome this problem, the trypan blue assay was used as an alternative. Both cells were treated with a range of polymer concentrations (0.001- 0.5 mg/ml) and for both cells, and this assay allowed the toxicity of the polymer to be determined. The slightly higher IC_{50} for OVSAHO (38.36 ± 2.3 µg/ml) compared with the one for OVCAR-8 (28.57 ± 0.37 µg/ml) could be because the OVCAR-8 cells have a higher growth rate when compared with OVSAHO.

The SRB assay could be used, however, to confirm the cytotoxicity of free navitoclax. The results for the OVCAR-8 cell line were close to the results reported by Stamelos *et al*. (Stamelos *et al.*, 2013). OVSAHO cells were not tested by Stamelos *et al.* but showed a slightly higher sensitivity to navitoclax toxicity when compared with OVCAR-8. This may be due to the low expression of the anti-apoptotic BCL-2 protein (MCL-1), which represents a barrier for navitoclax efficacy, and thus this gave higher navitoclax toxicity on OVSAHO. However, the anti-apoptotic BCL-X_L and BCL-2 proteins in OVSAHO are slightly highly expressed than OVCAR-8. As such, this can elucidate the negative impact of MCL-1 on ovarian cancer cells and making them resistant to anticancer drugs. Furthermore, these results were consistent with previous results in which ABT-737, the navitoclax parent drug, showed a higher cytotoxicity in OVSAHO compared with OVCAR-8 cells (Abed *et al*., 2016).

For the nanoparticles containing navitoclax, the feeding ratio of drug: polymer that showed a higher navitoclax loading concentration without consuming a large quantity of the drug was the ratio of 5:1 of navitoclax: PAA-ch_5. When the non-toxic polymer concentration of 15 µg/mL was used, that corresponded to 2.5 µM navitoclax.

Interestingly, the nanoparticular that encapsulated navitoclax tested at this concentration were twice as effective as free navitoclax when tested in both OVSAHO and OVCAR-8 cell lines. This increase in toxicity is likely to be due to an improvement in the intracellular concentration of navitoclax achieved by encapsulation.

It has been demonstrated that free drug particles can enter the cells through tight junctions, diffusion and through specific transporters (Alsuraifi *et al.*, 2018). Accordingly, nanoparticle application represents one solution for this obstacle as it was reported that the self-assemblies could enhance the *in vitro* cellular uptake for encapsulated or conjugated drugs such as anticancer drugs (Barnett *et al.*, 2013). Drug accumulation studies showed that almost twice the intracellular concentration of navitoclax was achieved with the nanoparticular navitoclax than with the free navitoclax. This may be due to increased permeability as a result of endocytosis of the particles (Zafar *et al.*, 2018). It may also be due to reduced efflux because this has also been shown to be reduced by encapsulation (Esim *et al.*, 2020). Thus, these results were consistent with what has been achieved by Zafar *et al*. (2018), who reported an improvement in drug solubility and enhancement in drug cytotoxicity when a thieno [2,3-b]pyridine derivative was encapsulated in the same polymer (Zafar *et al.*, 2018).

Several experiments were performed to confirm that the cellular toxicity caused by the nanoparticles was due, as expected, to apoptosis. Again, the navitoclax nanoaggregates were tested at the concentration at which the polymer on its own was not cytotoxic. For both cell lines, the results were consistent with the trypan blue assay.

There was a larger increase in caspase 3/7 activity obtained with the encapsulated navitoclax than with navitoclax alone. As expected, the polymer alone had minimal effect on caspase activity confirming that the increase in caspase activity was not due to the polymer alone. Similarly, when apoptosis was measured by flow cytometry to quantify externalization of phosphatidylserine, there were slightly more apoptotic cells in the samples treated with the encapsulated navitoclax than the free navitoclax.

Navitoclax on its own did not cause a substantial amount of apoptosis. This suggested that the cells were “not primed for death” most likely due to the high expression of the anti-apoptotic BCL-X_L protein compared to BH3-only proteins. However, when carboplatin was administered concomitantly with navitoclax, significant synergistic toxicity was observed. This likely occurs because carboplatin leads to the production of BH3-only proteins that neutralize the overexpressed BCL-X_L proteins and transfer the cells from being “not primed for death” to be “primed for death”. Accordingly, once navitoclax was administered, it was sufficient to block the other BCL-X_L anti-apoptotic proteins and cause significant cellular death.

Our group has previously shown synergy between ABT-737 or navitoclax with carboplatin (Witham et al., 2007; Stamelos et al., 2013). In ovarian cancer cells, inhibition of BCL-X_L is mandatory to produce a synergistic effect between a BH3 mimetic and carboplatin (Abed *et al*., 2016). These interesting results, in addition to the higher efficacy of the encapsulated navitoclax form, encouraged us to use the new formulation form and combine it with carboplatin and determine if the nanoparticles loaded with navitoclax can augment the carboplatin cytotoxicity. Various assays with

different targets were used to evaluate this including caspase 3/7 assay, PARP cleavage assay, and annexin V/PI labelling. In all of these assays, synergy was observed between both free navitoclax or encapsulated navitoclax with carboplatin. Importantly, the effect of the encapsulated navitoclax combination was greater than that achieved with the free navitoclax. This is also likely to result from the enhanced uptake of navitoclax caused by encapsulation and the effect of the polymer in increasing the permeability. Of note, it would have been desirable to measure a combination index to confirm synergy, but that would have required higher throughput than the trypan blue assay and is what we would have done if the SRB assay had worked.

It has been reported that carboplatin, which has a hydrophilic structure suffers from low uptake by cancer cells (Sadhukha and Prabha, 2014; Ming *et al.*, 2017). Notably, several trials have been undertaken to encapsulate carboplatin using nanoparticles to increase its uptake and thus its cellular toxicity (Ming *et al.*, 2017; Poy *et al.*, 2018; Trang Le *et al.*, 2020). Herein, the nanoparticles even though they had encapsulated navitoclax inside their core, might also entrap carboplatin particles between their hydrophilic backbones and thus increase carboplatin internalisation and higher toxicity. In support of this, the empty nanoparticles, even at very low concentrations, showed synergy with carboplatin, However, this has to be further investigated.

Since thrombocytopenia represents a hurdle to the clinical use of navitoclax, the next logical step would have been to evaluate whether the improved uptake of navitoclax brought about by encapsulation improved the therapeutic window for navitoclax, by

determining in animal studies whether and anti-tumour effect could be obtained without significant thrombocytopenia. However, that was not feasible due to the effect of the COVID-19 pandemic as we were planning to examine both navitoclax formulations on platelets both *in vitro* and *in vivo*. Previous literature results showed that administration of ABT-737 as a nanoparticle was efficient in decreasing the thrombocytopenia problem (Schmid *et al.*, 2014). Another successful trial was carried out by formulating navitoclax into a prodrug named a galacto-conjugation of navitoclax (Nav-Gal), which reduced the drug-induced thrombocytopenia and increase the selectivity of navitoclax toward cancer cells that have senescent cells (González-Gualda *et al.*, 2020).

4.11. Conclusion

The results that have been achieved in this chapter were auspicious as there was an improvement in navitoclax cellular toxicity once encapsulated in the nanoparticle. This improvement in cellular toxicity is related to enhancing the accumulation of navitoclax in the cancerous cells. Furthermore, this new navitoclax formulation improved the synergy obtained between carboplatin and navitoclax suggesting it may increase the drug's therapeutic window. However, it is possible that further improvements in the targeting of the nanoparticles to cancer cells is possible and this is the subject of Chapter 5.

Chapter 5. Folate targeting of PAA-ch5 nanoparticles loaded with navitoclax

5.1. Introduction

The application of nanoparticles represents one of the successful platforms that has been used for drug delivery (Yoo *et al.*, 2019). Indeed, this is because nanoparticles can offer several advantages over some traditional therapies by improving specificity, stability, prolonged and controlled release, solubility, bioavailability, as well as the ability to deliver a high payload and to overcome the resistance (Zheng *et al.*, 2015; Behera and Padhi, 2020). Nevertheless, they are associated with several drawbacks and one of the significant obstacles to utilize nanoparticles *in vivo* is their poor localisation to its intended target site, such as the cancerous tissue (Krystofiak *et al.*, 2012). Notably, there are several factors that play a determinant role in nanoparticles targeting, including their physicochemical properties, surface functionalisation, and the pathophysiological properties of the tumour microenvironment. Thus, enormous progress has taken place to allow the application of nanoparticles to cancer therapy. This has included improved targeting (Bazak *et al.*, 2016; Attia *et al.*, 2019) and enhancements in pharmacokinetic profiles (Patel *et al.*, 2018; Attia *et al.*, 2019). Accordingly, this makes these targeted nanoparticles ideal delivery systems and makes them superior to conventional therapies (Bazak *et al.*, 2016). Nowadays, there are two kinds of targeted drug delivery systems; passive targeted drug delivery is based on the enhanced permeability and retention effect (EPR effect) while active targeted drug delivery (smart drug delivery) is based on ligands binding to a receptor in the target tissue (Clemons *et al.*, 2018; Yoo *et al.*, 2019).

Although nanoparticles can be retained preferentially in tumour tissue compared with healthy cells due to the EPR effect serves, active targeting can still improve the

nanoparticles delivery (Tarudji and Kievit, 2020). Surprisingly, it has been found that the actively targeted nanoparticles may accumulate preferentially in tumours by the EPR effect and this is further enhanced by the active targeting which improves the nanoparticle distribution through the tumour cells and increasing the internalisation of the nanoparticles (Tarudji and Kievit, 2020). Thus, active targeting may provide additional benefits even in tumours where the EPR effect occurs. For example, doxorubicin, which has no issues in tissue penetration and passive targeting is sufficient to achieve the desired effect, active targeting can increase its accumulation in tumour tissue and decrease systemic toxicity in highly perfused organs such as liver, kidneys, and heart (Attia *et al.*, 2019). Importantly, in tumours that do not have an EPR effect, such as small metastatic tumours, some hematological malignancies, and circulating tumour cells, active targeting is beneficial for nanoparticle targeting (Tarudji and Kievit, 2020). Yet, the choice between active and passive targeting relies on the characteristics of the tumour cells, as well as the chemical nature of the drug.

5.2. Nanoparticles active targeting

Cancer cells are often characterised by the expression of various receptors on their surfaces that differ in number or in type from those on normal cells (Behera and Padhi, 2020). One method to improve the retention of nanoparticles and their therapeutic payload to tumours is by conjugating nanoparticles to molecules that bind these receptors (Cheung *et al.*, 2016; Clemons *et al.*, 2018; Tsolou *et al.*, 2020). As such, an extensive range of ligands have been considered as targeting moieties (Fay and Scott, 2011; Blanco *et al.*, 2012). The term “magic bullet” was introduced in the twentieth

century and it is tempting to speculate that functionalized nanoparticles might represent exactly that (Bazak et al., 2016).

Targeting nanoparticles of cancer tissues offers several advantages including decreased systemic toxicity (Krystofiak *et al.*, 2012; Anarjan, 2019), increasing the drug release in the targeted tissue site (Anarjan, 2019), bypassing the activity of multidrug resistance (MDR) transporters and poly-glycoproteins (PGP) which pump anticancer drugs out of the cancer cells, and reducing the dose of drug required (Bazak *et al.*, 2016; Anarjan, 2019). Moreover, active targeting can decreases the frequency of drug administration and cause smaller fluctuations in drug concentration between doses (Behera and Padhi, 2020). However, these actively targeted NPs have not been approved clinically and although some have entered phase 1 and phase 2 and showed efficacy and safety, none has yet entered a phase 3 trial (Tarudji and Kievit, 2020).

5.3. Ligands

There are several factors which play a determinant role when selecting targeting ligands. These include not only the ligand properties but also the nanoparticle surface chemistry, and receptor's expression profile (Attia *et al.*, 2019). Moreover, the affinity of the active targeting moieties to their specific receptors is also a determinant factor and the interactions must be very strong which can depend on ionic interactions, van der Waals, hydrophobic effect, and hydrogen bond interactions (Tarudji and Kievit, 2020). Several classes of ligand have been used including antibodies, antibody fragments, aptamers, proteins and peptides (e.g. transferrin) small molecules (e.g. folic acid) (Gmeiner and Ghosh, 2014; Bazak *et al.*, 2016; Anarjan, 2019; Tarudji and Kievit, 2020; Yoo *et al.*, 2019), B12 (Tarudji and Kievit, 2020), Hyaluronic acid (HA) (Tarudji

and Kievit, 2020; Yoo *et al.*, 2019), and carbohydrates (Yoo *et al.*, 2019). Figure (5.1) represents the most well-known moieties and molecules that are utilized in nanoparticles active targeting.

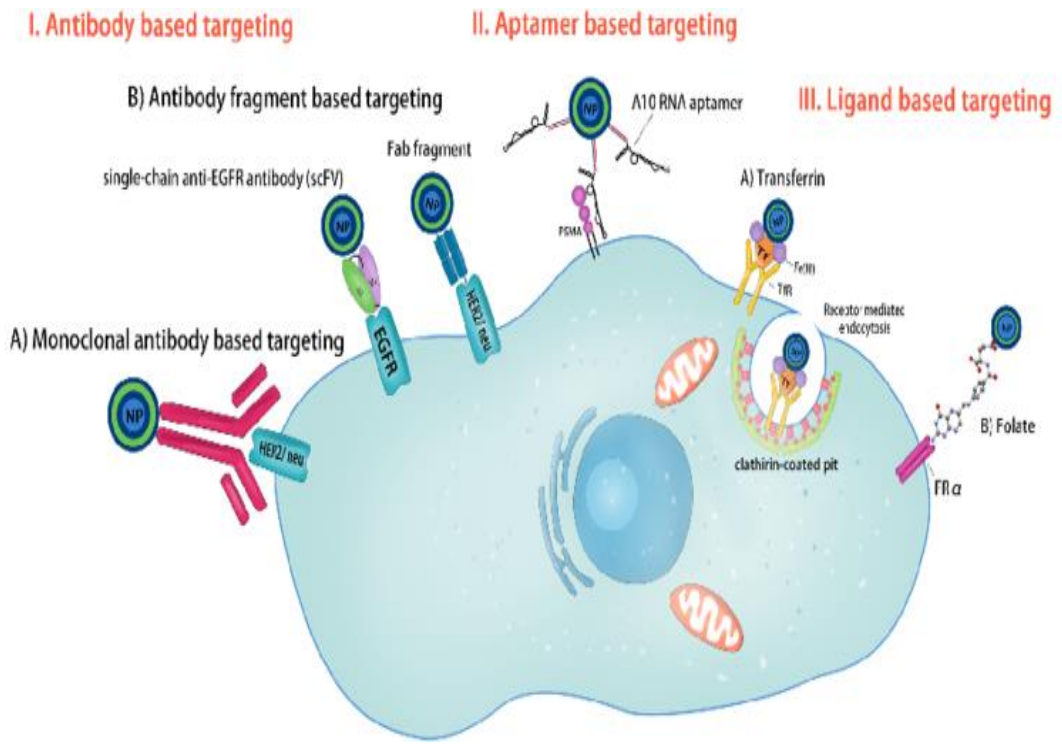

Figure 5-1: Active targeting using different moieties and molecules (Bazak et al., 2016).

5.4. Folic acid

Folate (vitamin B9) is a 441 Da water-soluble vitamin used as one-carbon donor that is crucial for any eukaryotic cells for purines and pyrimidines synthesis (Bartouskova *et al*., 2015; Bazak *et al.*, 2016; Cheung *et al.*, 2016; Fernández *et al*., 2018; Anarjan, 2019; Tamura *et al.*, 2020). Folic acid shows advantages over other targeting ligands by being stable (Bazak *et al.*, 2016; Anarjan, 2019), inexpensive, easy to conjugate,

non-immunogenic and it has a higher affinity for folate receptors in tumour cells (Bazak *et al.*, 2016; Fernández *et al*., 2018; Tarudji and Kievit, 2020). Furthermore, it has superiority of being internalised through endocytic vesicles in the process of receptor-mediated endocytosis, (Figure (5.2)) (Bazak *et al.*, 2016; Anarjan, 2019; Yoo *et al.*, 2019; Tamura *et al.*, 2020). However, being a vitamin it has the disadvantage that excess folate in the body might compete with targeted NP (Tarudji and Kievit, 2020). Moreover, folic acid particles on the surface of NPs can lead to self-assembly and formation of dimers, trimers and even tetramers (Blanco *et al.*, 2012). This means that there must be further modification to achieve more targeting selectivity (Gu *et al.*, 2007).

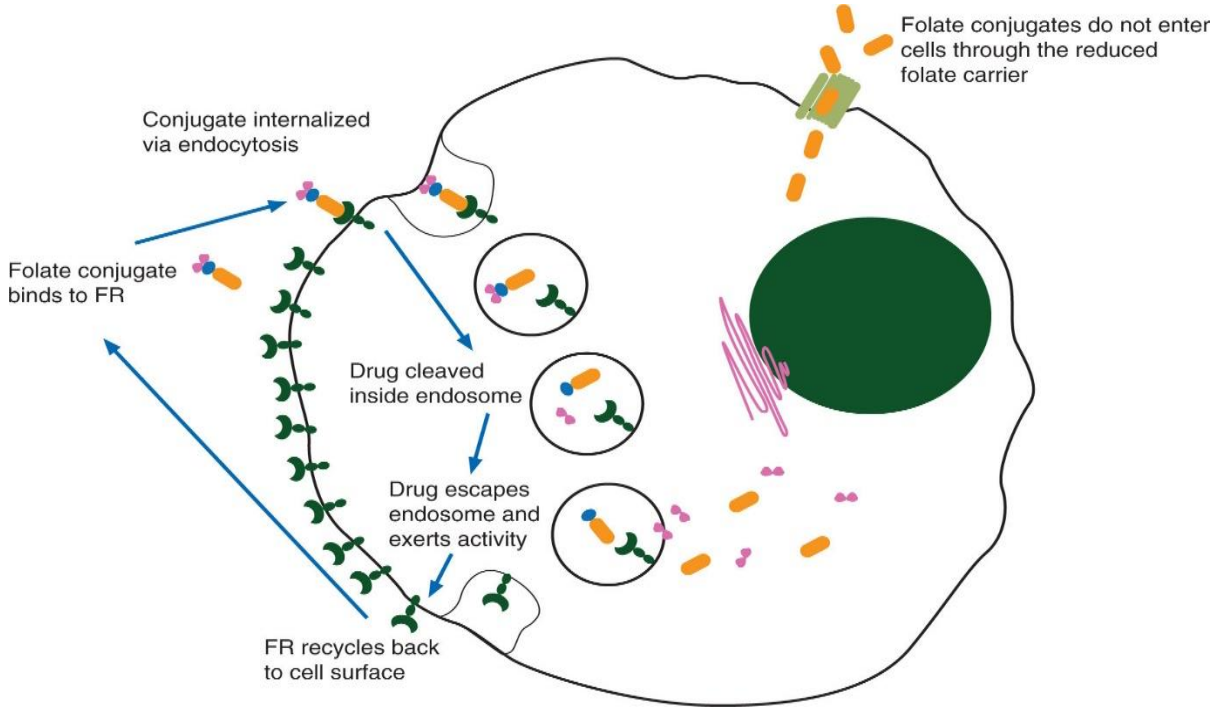

Figure 5-2: Receptor mediated endocytosis mechanism (Ledermann et al., 2015)

5.5. Folate receptors

It has been reported that the folic acid uptake happens through two different receptors, either low-affinity-reduced folate carriers, which are expressed in all cells, or high-affinity glycosylphosphatidyl-inositol-linked (GPI) folate receptors (FR), which are expressed in limited cell types (Krystofiak *et al.*, 2012; Marchetti *et al.*, 2014; Bazak *et al.*, 2016; Cheung *et al.*, 2016). Whereas the reduced folate carriers are responsible for the uptake of folic acid and the reduced form of folic acid (Bazak *et al.*, 2016), the folate receptors are responsible for transporting folic acid, as well as folate-linked nanoconjugates (Bazak *et al.*, 2016).

Folate receptors are glycosylphosphatidylinositol (GPI)-anchored receptors that bind folic acid with high affinity (KD ~1nM). These genes responsible for this protein expression are located on chromosome 11q13 (O'Shannessy *et al.*, 2015). Significantly, FR transport folic acid and the folic acid targeted molecules into the cell via receptor-mediated endocytosis. In addition, using folate receptors to deliver chemotherapeutic agents in cancer cells follows a "trojan horse" approach (Gu *et al.*, 2007; Garcia-Bennett *et al.,* 2011; Blanco *et al.*, 2012). Of note, the FR is not in direct contact with the blood circulation as they are localised on the apical surface of polarised epithelium in normal cells, but in the cancerous cells, they lose their polarisation and make these folate receptors accessible to blood circulation, (Figure (5.3)) (Krystofiak *et al.*, 2012; Kurosaki *et al.*, 2016; Fernández *et al*., 2018). Since these folate receptors are highly expressed in several malignant and leukemic cells, placing them in direct contact with the folic acid targeted nanoparticles in the blood circulation (Bazak *et al.*, 2016). Therefore, this makes folic acid targeting a promising

platform to decrease toxicity toward normal tissues (Bazak *et al.*, 2016; Zaidan *et al.*, 2017).

While all FR have a high affinity to folate, there is a difference between the FR subtypes distribution. There are three main subtypes of folate receptors expressed on cells, termed FRα (also called FR1), FRβ, and FRγ (Wu *et al.*, 2017). There is another subtype, FRδ, which is less well characterized (O'Shannessy *et al.*, 2015). The FRγ is a secreted protein and it lacks the GPI component, making it freely soluble (Cheung *et al.*, 2016; Ledermann et al., 2015; Fernández *et al*., 2018). For FR-β, it has a relatively lower affinity for folic acid and is expressed predominantly in normal hematopoietic cells as well as malignant hematopoietic cells and activated macrophages (Marchetti *et al.*, 2014; Fernández *et al*., 2018; Anarjan, 2019).

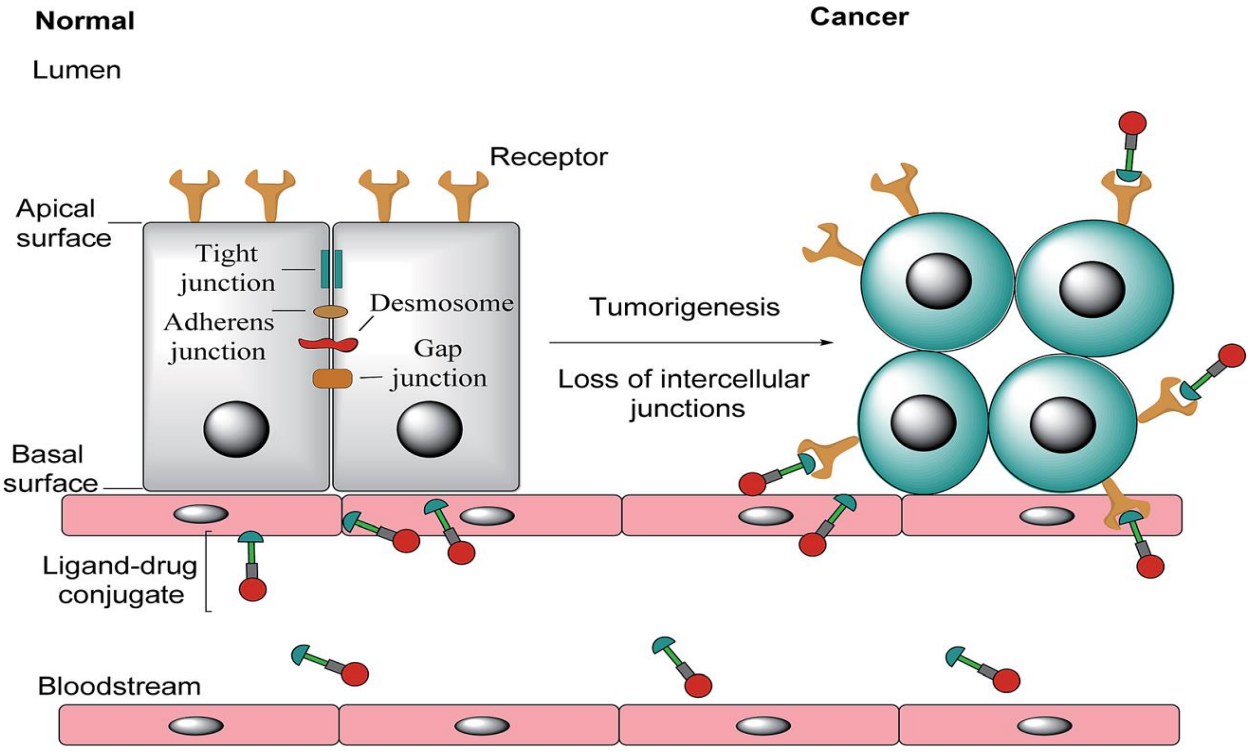

Figure 5-3: Normal and cancer apical surfaces distribution of folic acid receptors (Fernández et al., 2018)

5.5.1. Folate receptor alpha

Folate receptor-alpha (FRA) is a glycosylphosphatidylinositol (GPI) anchored membrane protein (Kalli *et al.*, 2008; Kurosaki *et al.*, 2016; Hulin-Curtis *et al.*, 2020). This FRA is a 38- to 40-kDa molecule encoded by the *FOLR1* gene (Kurosaki *et al.*, 2016). FRA shows limited normal tissue distribution, with expression restricted to the apical surfaces in specific epithelia such as in the proximal kidney tubules, choroid plexus, fallopian tube, submandibular salivary, uterus, epididymis, acinar cells of the breast, bronchial gland, trophoblasts of the placenta, and type I and type II pneumocytes in the lung (Basal *et al.*, 2009; Marchetti *et al.*, 2014; Cheung *et al.*, 2016; Patel *et al.*, 2018). In contrast, this receptor is widely expressed in 40% of human cancers (Bazak *et al.*, 2016; Tarudji and Kievit, 2020), such as the cancers of the breast, ovarian, prostate, colon, lung, kidney, myeloid, head and neck cancers, human nasopharyngeal carcinoma, and brain cancers (Krystofiak *et al.*, 2012; Marchetti *et al.*, 2014; Cheung *et al.*, 2016; Wu *et al.*, 2017; Anarjan, 2019). Moreover, it was demonstrated that this receptor, as other FR, is associated with cancer growth, tumour stage and grade and with poor overall survival (Hulin-Curtis *et al.*, 2020). Interestingly, it has been reported that elevated FRA expression is associated with negative prognostic factors for chemotherapy resistance (Marchetti *et al.*, 2014). Therefore, this makes the FRA a promising target to permit the internalisation of the folic acid conjugated drugs and nanoparticles specifically into tumour cells (Kalli *et al.*, 2008).

5.6. FRA in ovarian cancer

The FRA, is overexpressed in approximately 90% of cases of ovarian cancer (Marchetti *et al.*, 2014; Hekman *et al.*, 2017) at a level 10- to 100- fold higher than in kidneys, lung, and breast epithelial cells (Kalli *et al.*, 2008; Patel *et al.*, 2018). In addition, it was reported that its expression is associated with EOC histological stage and grade (Cheung *et al.*, 2016). Importantly, it has been demonstrated that the *FOLR1* overexpression in EOC supports the theory that EOC is derived from fallopian fimbriae as it has been found that its overexpression is associated with overexpression of other genes, including *MUC16*, *MSLN*, and *WFDC2* which are not significantly expressed in normal ovarian tissue but they are overexpressed in fallopian tubes (O'Shannessy *et al.*, 2015). Surprisingly, FRA is not appreciably altered in tumour tissue after chemotherapy, making this receptor an ideal target for both therapies and imaging applications (Hekman *et al.*, 2017).

5.7. Drugs targeting FRA

Since FRA overexpression is associated with increased folic acid uptake and higher tumour growth (Norton et al., 2020), FRA inhibition can significantly decrease the proliferation of cancer cells (Kalli *et al.*, 2008; Norton *et al.*, 2020). Accordingly, several therapies that target FRA have been developed and these include FRA engineered chimeric antigen receptor (CAR), monoclonal antibodies, drug conjugates (Norton *et al.*, 2020), vaccine-based approach (Kalli *et al.*, 2008; Cheung *et al.*, 2016; Norton *et al.*, 2020), virus oncolytic therapy (Cheung *et al.*, 2016), and nanoparticles (Kalli *et al.*, 2008). From these platforms, the main two basic strategies that have been widely investigated include either antifolate receptor antibodies or small molecule–drug

conjugates (SMDCs) (Marchetti *et al.*, 2014; Bartouskova *et al*., 2015; Ledermann *et al*., 2015; Fernández *et al*., 2018; Patel *et al.*, 2018).

The farletuzumab (MORab003) (Cheung *et al.*, 2016; Fernández *et al*., 2018) is a monoclonal antibody (mAb) with high affinity toward FRA (Bartouskova *et al*., 2015) and has a synergistic effect with taxanes (Marchetti *et al.*, 2014; Bartouskova *et al*., 2015). Notably, farletuzumab does not inhibit folate binding to its receptor or prevent internalisation through the receptor. Rather, its mechanism of action depends on killing tumour cells by complement-dependent cytotoxicity (CDC) and antibody-dependent cellular cytotoxicity (ADCC), inhibition of Lyn kinase-substrate phosphorylation, and sustained tumour cell autophagy (Cheung *et al.*, 2016; Fernández *et al*., 2018).

Unlike anti-FRA antibodies, drugs conjugated to folate can be targeted to tissues expressing both FRA and FRB; this permits targeting tumours that are low in FRA but high in FRB, such as the tumours that are infiltrated by large numbers of tumour-associated macrophages (Marchetti *et al.*, 2014; Cheung *et al.*, 2016). Although several chemotherapeutic agents have been linked to a folate moiety, the one that showed most successful results was vintafolide (Marchetti *et al.*, 2014). Vintafolide (EC145) is a water-soluble FRA targeted drug conjugate and it is comprised of folate moiety, which is linked with a peptide spacer to a chemotherapeutic drug (desacetyl vinblastine monohydrazide (DAVLBH)) (Marchetti *et al.*, 2014; Ledermann *et al*., 2015; Fernández *et al*., 2018). DAVLBH belongs to the vinca alkaloid chemotherapy family that affect microtubule function. Vintafolide enters the cell through receptor-mediated endocytosis and the drug is released inside the cell (Ledermann *et al*., 2015). Other SMDC includes EC0225, BMS-753493 (Epofolate), EC0489, EC1456, IMGN853,

and DM4 (Cheung *et al.*, 2016). However, none of these drugs have been approved for clinical use (Marchetti *et al.*, 2014; Patel *et al.*, 2018). Nevertheless, it is possible this setback may be overcome by exploring synergistic effects with other drugs (Bartouskova *et al*., 2015).

Although the work in the previous chapter showed that navitoclax was successfully encapsulation in PAA-ch$_5$ nanoparticles there is still a concern that the nanoparticles could cause thrombocytopenia. This might be ameliorated by conjugating the nanoparticles to folate. This could enhance the therapeutic index for navitoclax, making its use clinically viable.

5.8. Aims

1. To encapsulate navitoclax in the PAA-ch$_5$-FA polymer and determine if this improves the solubility of navitoclax.
2. Determine optimal drug: polymer feed ratios and different polymer concentrations for navitoclax encapsulation and optimise the loading efficiency.
3. Determine the release profile of the encapsulated navitoclax under sink conditions.
4. Determine the physical stability for the encapsulated form of navitoclax using different formulations (liquid and freeze-dried cakes) with different storage conditions.
5. Evaluate the cytotoxicity of the PAA-ch$_5$-FA polymer on both ovarian cancer cell lines to identify non-toxic concentrations for use in

subsequent experiments, comparing the activity of both free drug and encapsulated navitoclax on several cell lines.

6. Evaluate the activity of combinations of carboplatin with encapsulated navitoclax.

5.9. Results

5.9.1. Detection of PAA-ch$_5$-FA using HPLC

The PAA-ch$_5$-FA was analysed using HPLC as mentioned in the methodology section. As with PAA-ch$_5$, the HPLC data showed no peaks that could interfere with the detection of navitoclax, figure (5.4).

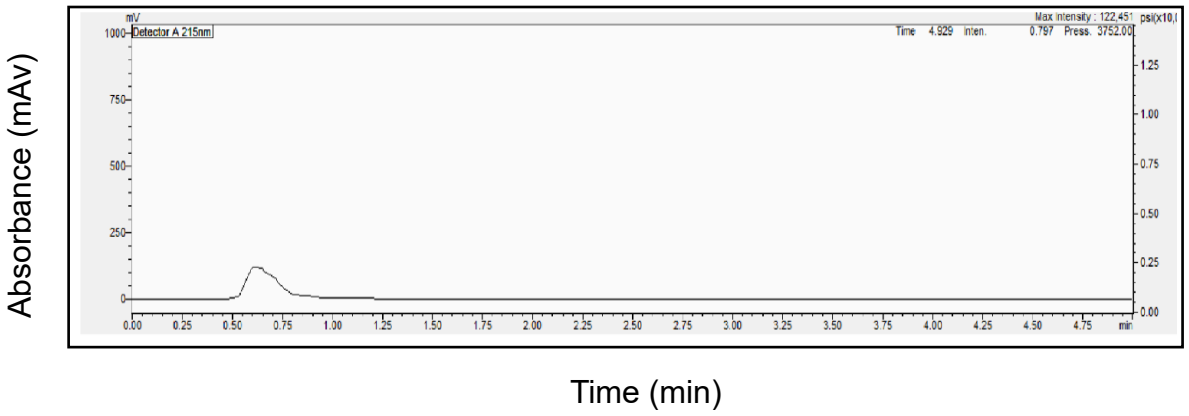

Figure 5-4: PAA-ch$_5$-FA water solubility detection by HPLC

This figure shows that there is no peak apparent by HPLC analysis at any retention time after adding the polymer (PAA- ch$_5$-FA) in water.

5.9.2. Navitoclax quantification

Navitoclax powder was added to the PAA-ch$_5$-FA with a ratio of 1:1 drug: polymer, before being sonicated and filtered. The PAA-ch$_5$-FA appeared yellow and opaque before adding the drug to it. However, after adding the drug and filtering the sample, the solution was clear and faintly yellow. The samples were analysed by HPLC. All samples showed a peak at 1.43 minutes corresponding to the retention time of navitoclax and demonstrating that navitoclax was successfully encapsulated in PAA-ch$_5$-FA polymer, (Figure (5.5, A)). The navitoclax solubility within the PAA-ch$_5$-FA amphiphile was improved approximately a 60-fold, (Figure (5.5, B)).

(A)

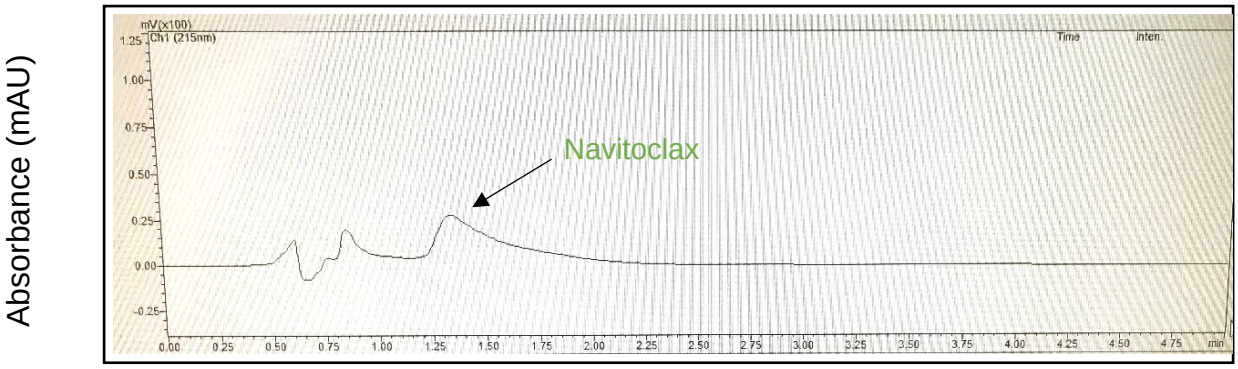

(B)

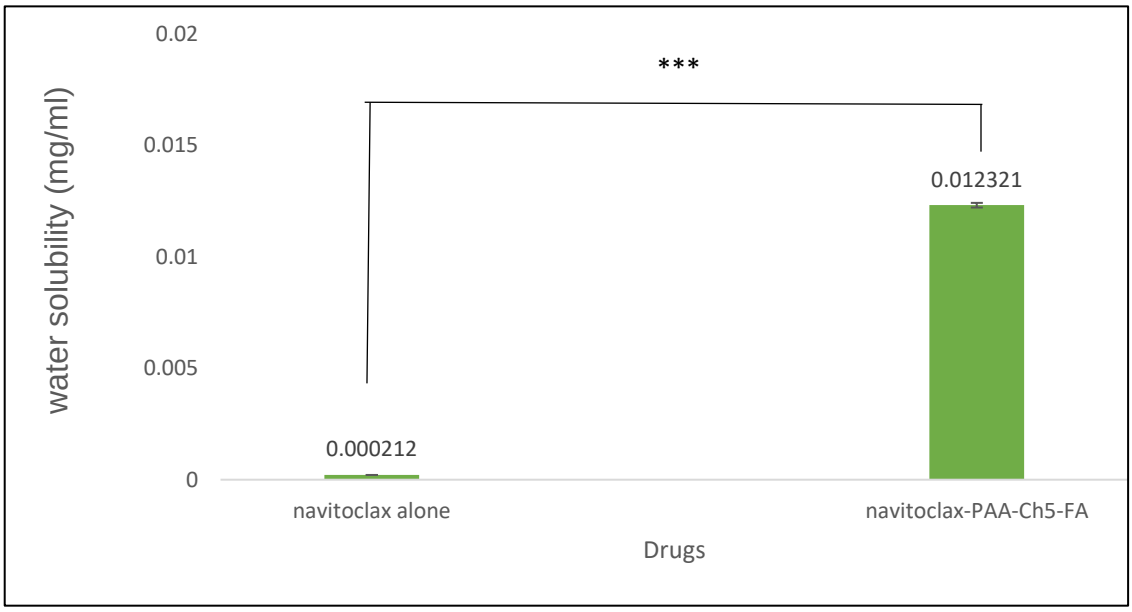

Figure 5-5: Quantification of encapsulated navitoclax inside the PAA-ch$_5$-FA core

(A)This figure shows a navitoclax-PAA-ch$_5$-FA sample, which shows a peak at the same retention time of navitoclax standard. (B) This figure represents the maximum concentration of navitoclax that has been encapsulated inside the PAA-ch$_5$-FA core. The concentration of navitoclax encapsulated was 12.61 µM. (*(***): p<0.001;* data were analyzed using paired t-test). Results (mean ± S.D, n=3).

5.9.3. Effect of changing the drug: polymer ratio on loading capacity

Changing in feeding ratio can have a positive effect on the hydrophobic loading in the self-assembly nanoparticles. As such, navitoclax loading was assessed with different feeding ratios of navitoclax: polymer of 1:1, 5:1, and 10:1. The higher feed ratios significantly improved navitoclax loading and its water solubility, (Figure (5.6)). The effect of increasing navitoclax: PAA-ch$_5$-FA ratio on navitoclax encapsulation concentration and its effect on loading capacity (%LC) and encapsulation efficacy (%EE) is presented in table (5-1).

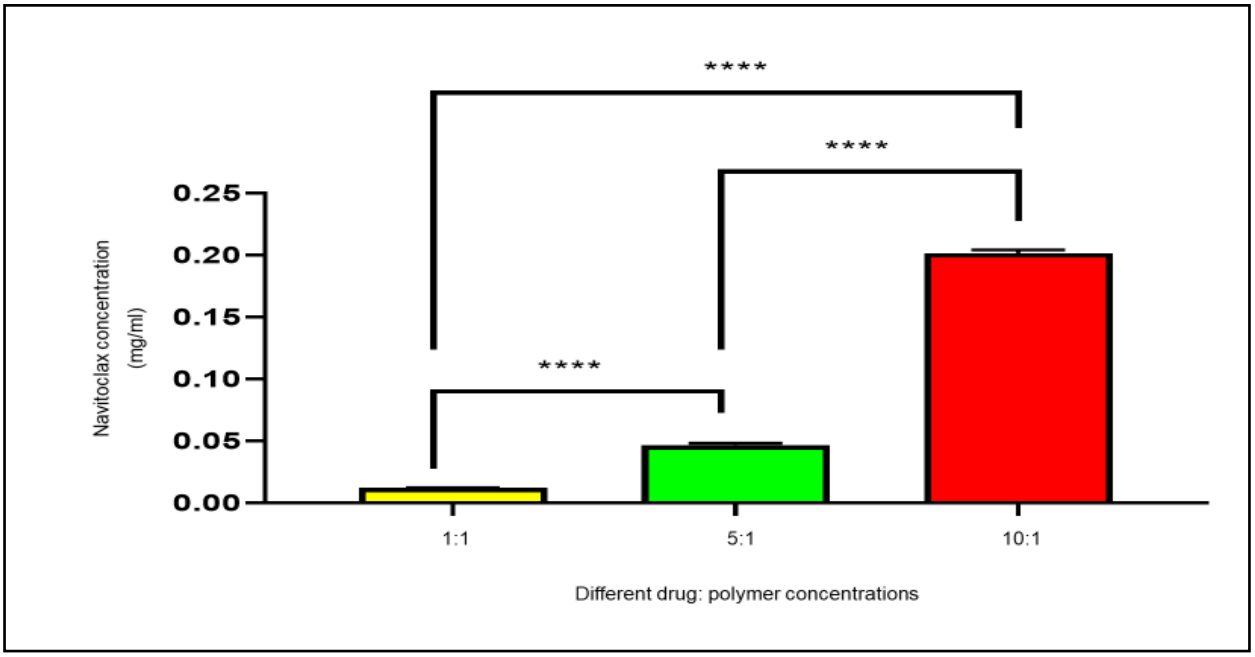

Figure 5-6: Effect of increasing (drug: polymer) ratio on navitoclax encapsulation

This figure shows the effect of using different drug ratios with the same PAA-ch$_5$-FA polymer concentration. The 5:1 and 10:1 ratio gave concentrations corresponding to 48 µM, 207 µM navitoclax, respectively. There is a significant difference between all ratios that were used. (*(****): p<0.0001;* the statistical analysis was performed using One-way ANOVA). Results (mean ± S.D, n=3).

Table 5-1: The effect changing navitoclax ratios on navitoclax loading capacity and encapsulation efficacy

Different drug ratio **Navitoclax: PAA-** Ch$_5$	**Water solubility (mg/ml)** **Mean**	**Standard deviation**	**% LC**	**% EE**
1:1	0.012	0.0001	1.23 %	1.23%
5:1	0.047	0.002	4.67 %	0.94 %
10:1	0.202	0.003	20.2 %	2.2 %

This table shows the effect of changing the navitoclax: PAA-ch$_5$-FA ratio on navitoclax loading. (%LC): loading capacity and (%EE): encapsulation efficacy for all ratios were also represented. Results (mean ± S.D, n=3).

5.9.4. Effect of changing polymer concentration on the loading capacity

Three different polymer concentrations were also tested using a fixed drug ratio. The three difference PAA-ch$_5$-FA concentrations were 1 mg/ml, 3 mg/ml, and 6 mg/ml and the fixed ratio of navitoclax: PAA-ch$_5$-FA to 1:1. Although the same ratio was used, the results showed improved navitoclax encapsulation by increasing the polymer concentration, (Figure (5.7)). Table (5-2) shows the effect of increasing PAA-ch$_5$-FA concentration using fixed navitoclax: polymer ratio on navitoclax encapsulation concentration and its effect on loading capacity (%LC) and encapsulation efficacy (%EE).

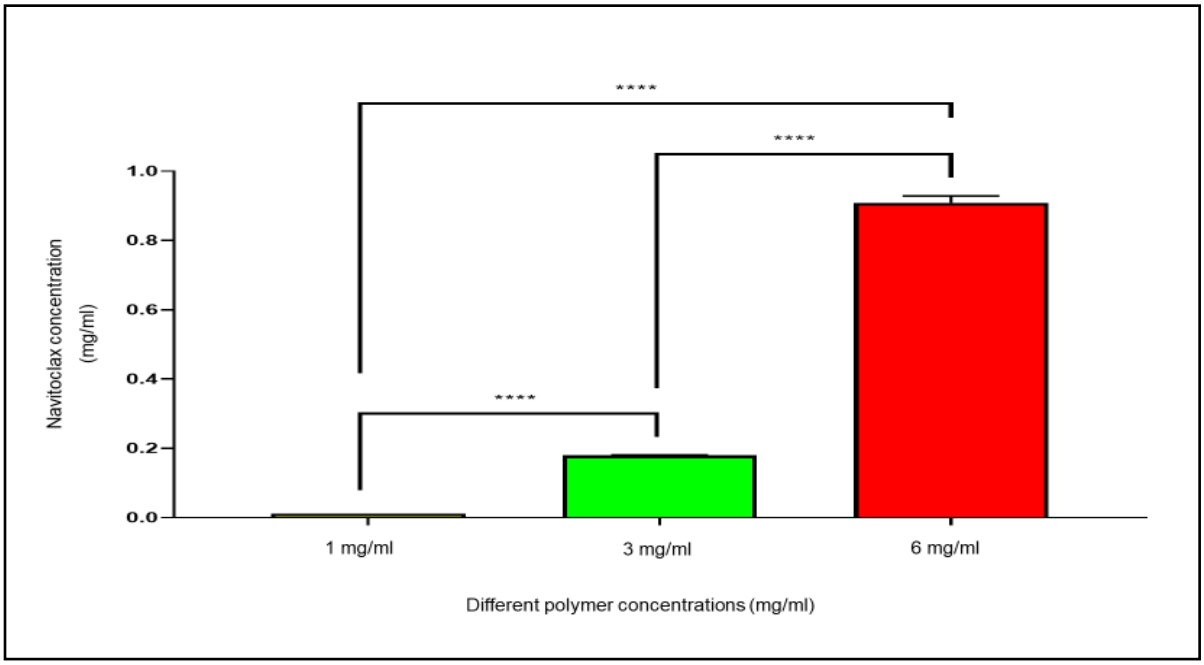

Figure 5-7: Effect of changing PAA-ch$_5$-FA concentration on navitoclax encapsulation

This figure shows the effect of using fixed drug ratio with the different polymer concentration, it shows that the increment in polymer concentration is associated with higher navitoclax encapsulation. The higher loading concentration achieved with 6 mg/ml of the polymer which achieved 75-fold higher navitoclax concentration once compared with polymer concentration of 1 mg/ml. There is a significant difference between the polymer concentrations that were used. (*(****): p<0.0001;* statistical analysis was examined using One-way ANOVA). Results (mean ± S.D, n=3).

Table 5-2: The effect changing PAA-ch$_5$-FA concentration on navitoclax loading capacity and encapsulation efficacy

Different polymer concentrations	Water solubility (mg/ml) Mean	Standard deviation	% LC	%EE
1 mg/ml	0.012	0.0001	1.23 %	1.23%
3 mg/ml	0.18	0.002	5.99 %	5.99 %
6 mg/ml	0.91	0.02	15.2 %	15.2 %

This table shows the effect of changing the polymer concentrations using fixed navitoclax: polymer ratio on navitoclax loading. (%LC): loading capacity and (%EE): encapsulation efficacy for concentrations were also represented. Results (mean ± S.D, n=3).

5.9.5. Nano-aggregate characterization

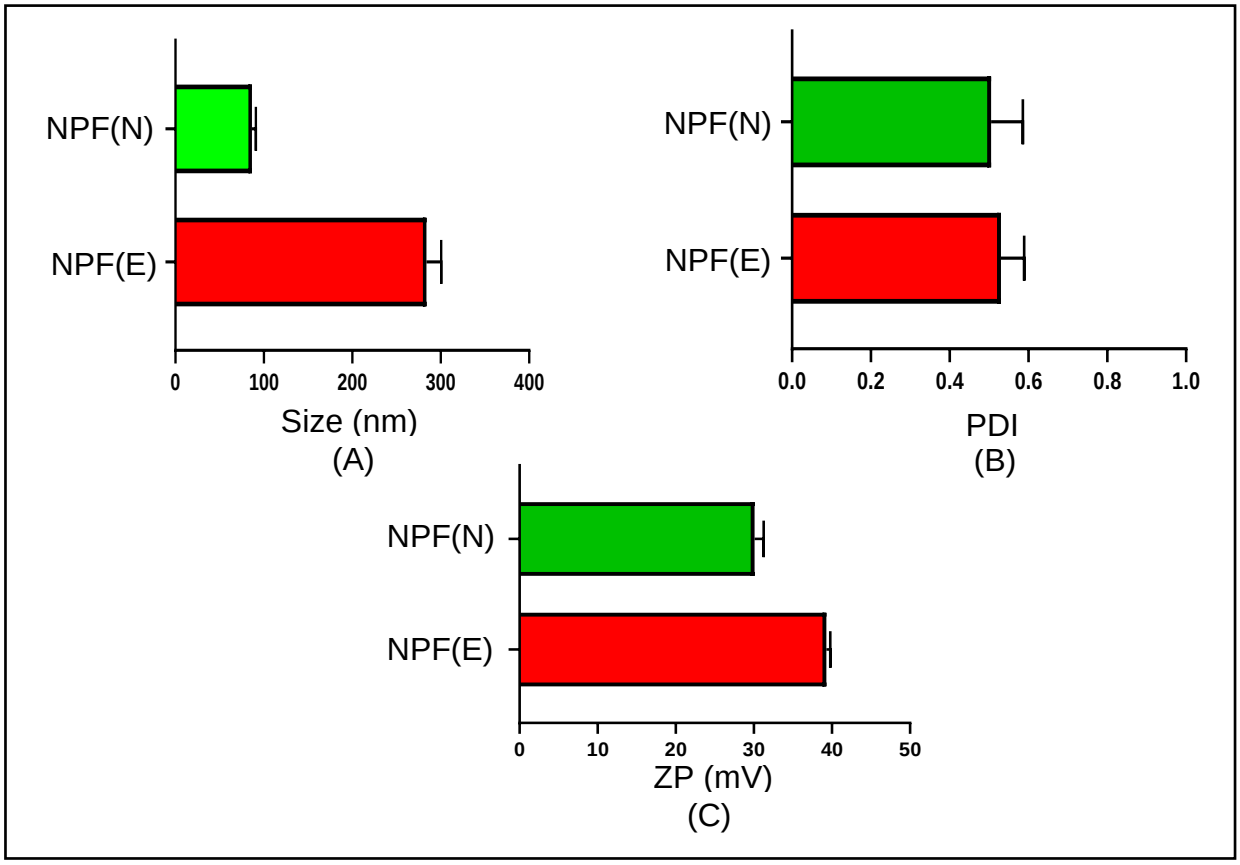

Figure 5-8: The physical characteristics for both the polymer alone and the navitoclax-PAA-ch$_5$-FA

These three figures show the physical characteristics for both the polymer alone (NPF(E)) and the navitoclax-PAA-ch$_5$-FA (NPF(N)). (A) shows the difference in size of the polymer before and after adding navitoclax. (B) The particles polydispersity of both the polymer and the encapsulated navitoclax in the polymer core. (c) The surface charge for both the polymer alone and the encapsulated navitoclax. Results (mean ± S.D, n=3).

The physical properties of PAA-ch$_5$-FA (empty polymer) and the loaded navitoclax with the polymer were assessed on a zetasizer to determine size, polydispersion index, and zeta potential. The size of the micelles was unexpectedly smaller when the drug was added (Figure (5.8, A)). The polydispersion index (PDI) showed that after adding navitoclax, the micellar dispersion was slightly improved, with a slight decrease in the PDI, (Figure (5.8, B)). However, there was no significant difference in the zeta potential after encapsulation of navitoclax, which means that encapsulation did not affect the polymer surface positively charge, (Figure (5.8, C)).

5.9.6. Drug release

Considering that the drug release from its delivery vehicle inside the body is the desired outcome, the release of navitoclax from the PAA-ch$_5$-FA core was tested. The concentration of navitoclax chosen to study the release was 0.012 mg/ml, which has been achieved by taking a ratio of 1:1 from navitoclax: PAA-ch$_5$-FA. Only a fraction of the navitoclax was release over 72 hours, and the majority of this occured in the first 6 hours, (Figure (5.9)).

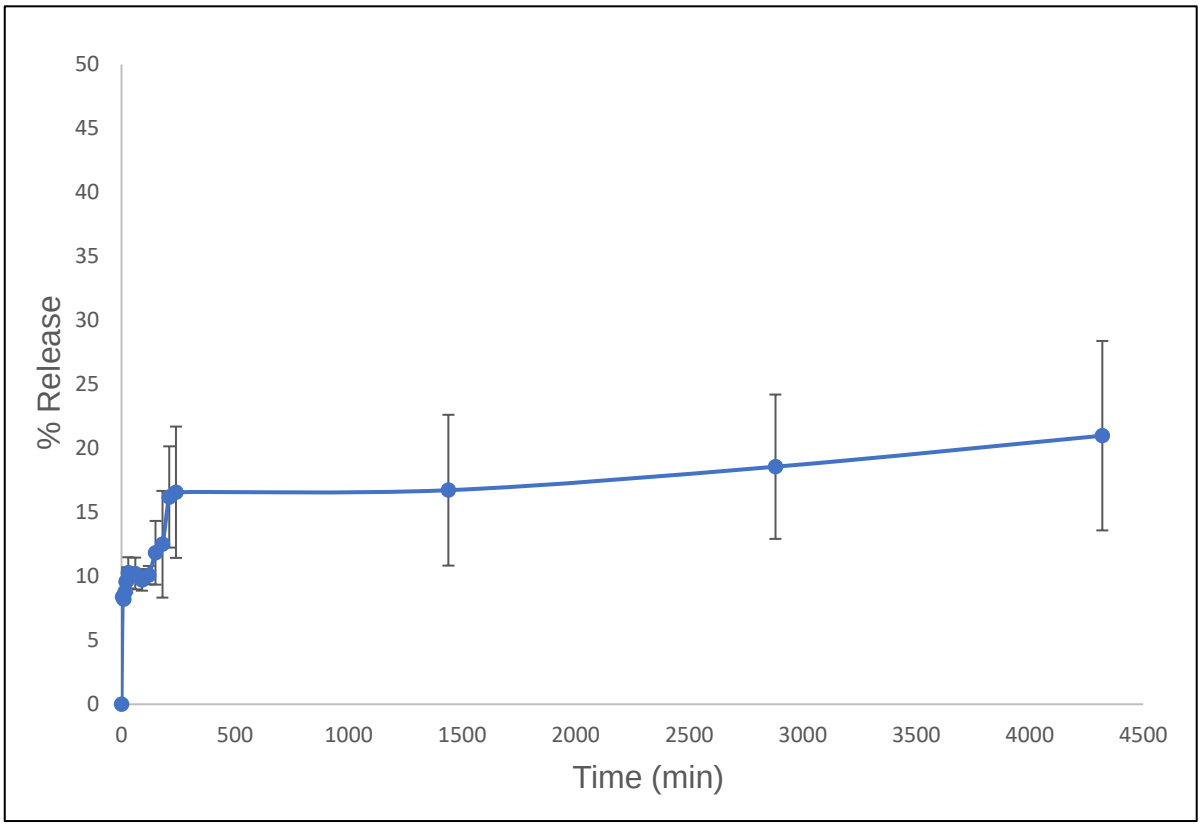

Figure 5-9: Navitoclax release from PAA-ch5-FA core.

This figure shows the release percentage of navitoclax-PAA-ch$_5$-FA from the PAA ch$_5$-FA polymer core in PBS. The release did not exceed 21% with 50% of this release happened as an initial burst in the first 5 minutes. Results (mean ± S.D, n=3).

5.9.7. Formulation Stability

Since stability is considered an essential physical characteristic for any formulation, the navitoclax-PAA-ch$_5$-FA formulation samples were prepared in two different states (liquid state and freeze-dried cakes). Samples were prepared and were divided equally as freeze-dried and liquid forms. Furthermore, the samples were also kept in two different conditions: in the fridge at 4 °C and in dark cabinets at room temperature. The samples were assessed weekly for a total of four weeks to measure the percentage of drug lost during storage.

Both freeze-dried forms were more stable than their counterparts in liquid form for the whole four weeks period, (Figure (5.10)). Although there was a sharp loss of 20% of the navitoclax from the micellar core when the samples were freeze-dried in the first week, these sampled could preserve the majority of the encapsulated navitoclax at room temperature, and at 4°C. Importantly, this was better than the liquid samples that were stored at room temperature or at 4°C. However, storage of liquid samples at 4°C maintained better navitoclax encapsulation than liquid samples at room temperature.

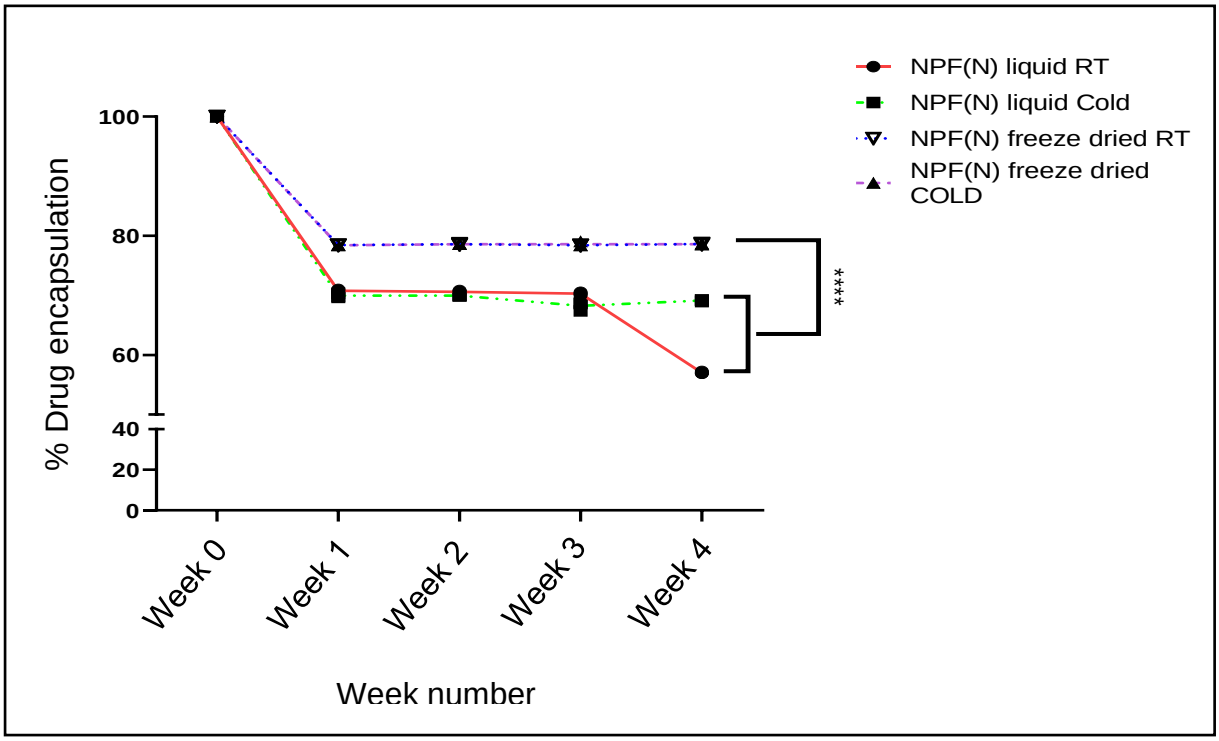

Figure 5-10: Physical stability for navitoclax nanoparticles with PAA-ch$_5$-FA polymer

Physical stability test for Navitoclax-PAA-ch$_5$-FA (NPF(N)) at 4 ^{o}C and 20 ^{o}C in the form of liquid and freeze-dried form over 4 weeks-period. There is a significant difference between the freeze-dried formulation at 4°C compared with both liquid formulations. ((****): *p<0.0001*; statistical analysis was examined using Two-way ANOVA). Results (mean ± S.D, n=3).

5.9.8. Detection of the PAA-ch5-FA toxicity

The cytotoxicity of PAA-ch$_5$-FA was explored using trypan blue assay, but not with SRB or other light absorbance assays to avoid the interference issues noted with PAA-ch$_5$. A range of PAA-ch$_5$-FA concentrations (1-500 µg/ml) were used. The results showed inhibition of OVCAR-8 (IC_{50}=37.15± 1.53 µg/ml) and OVSAHO (IC_{50}=71.87 ± 1.33 µg/ml) viability by the polymer alone, (Figure (5.13)). The results were compatible with the morphological appearance of both cells lines, (Figure (5.11), (5.12)). In both cell lines a maximum concentration of 20 µg/ml could be used without toxicity, suggesting that this was a suitable concentration for further experiments.

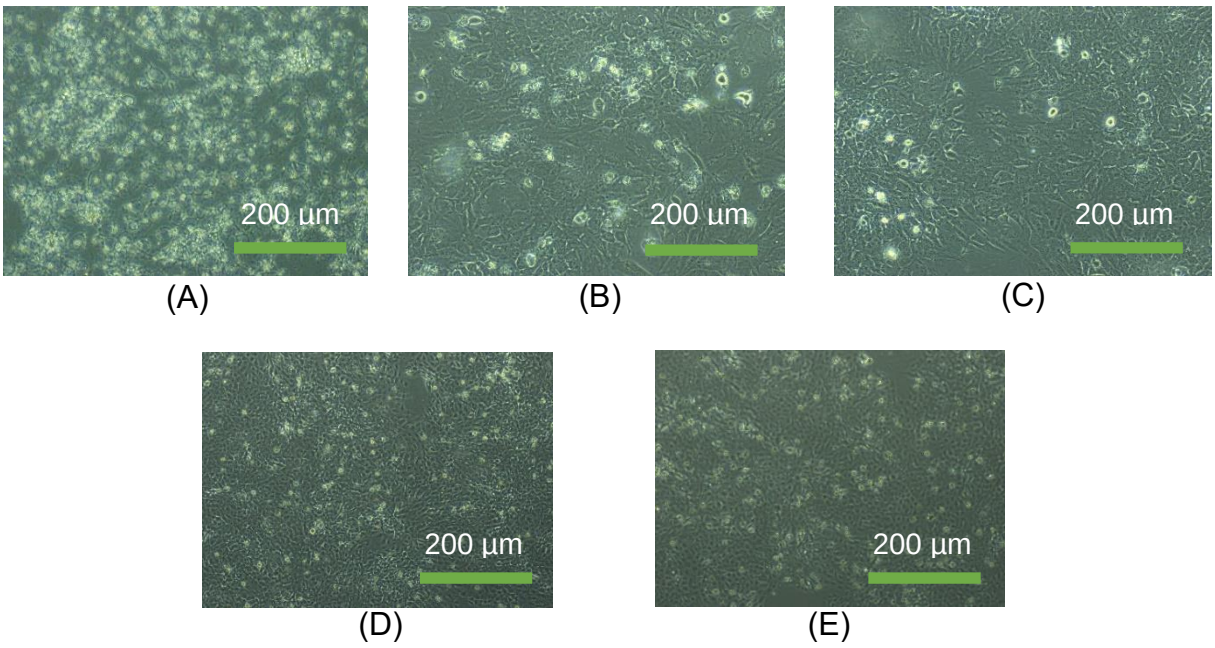

Figure 5-11: Morphological appearance of OVCAR-8 cells treated with PAA-ch$_5$-FA

These figures show the cytotoxicity of several PAA-ch$_5$-FA (NPF(E)) concentrations on OVCAR-8 after 48 hours. (A) 250 µg/ml (B) 30 µg/ml (C) 15 µg/ml (D) 1 µg/ml (E) control. (n=1).

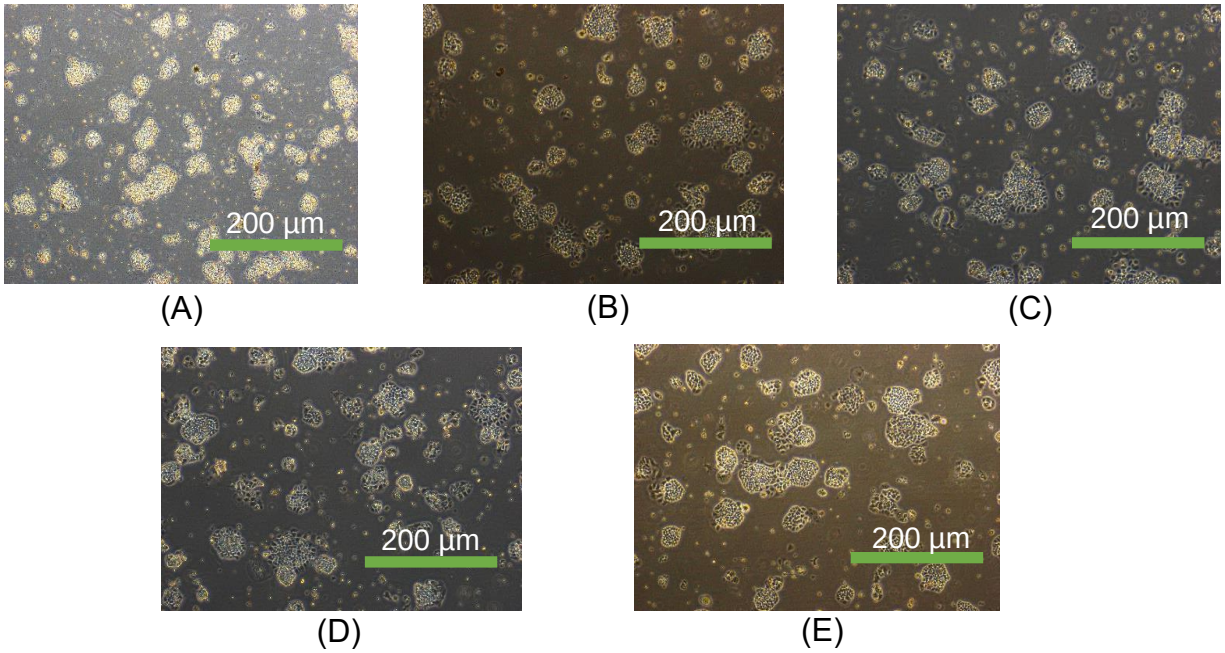

Figure 5-12: Morphological appearance of OVSAHO cells treated with PAA-ch$_5$-FA

These figures show the cytotoxicity of several PAA-ch$_5$-FA (NPF(E)) concentrations on OVSAHO after 48 hours. (A) 250 µg/ml (B) 30 µg/ml (C) 15 µg/ml (D) 1 µg/ml (E) control. (n=1)

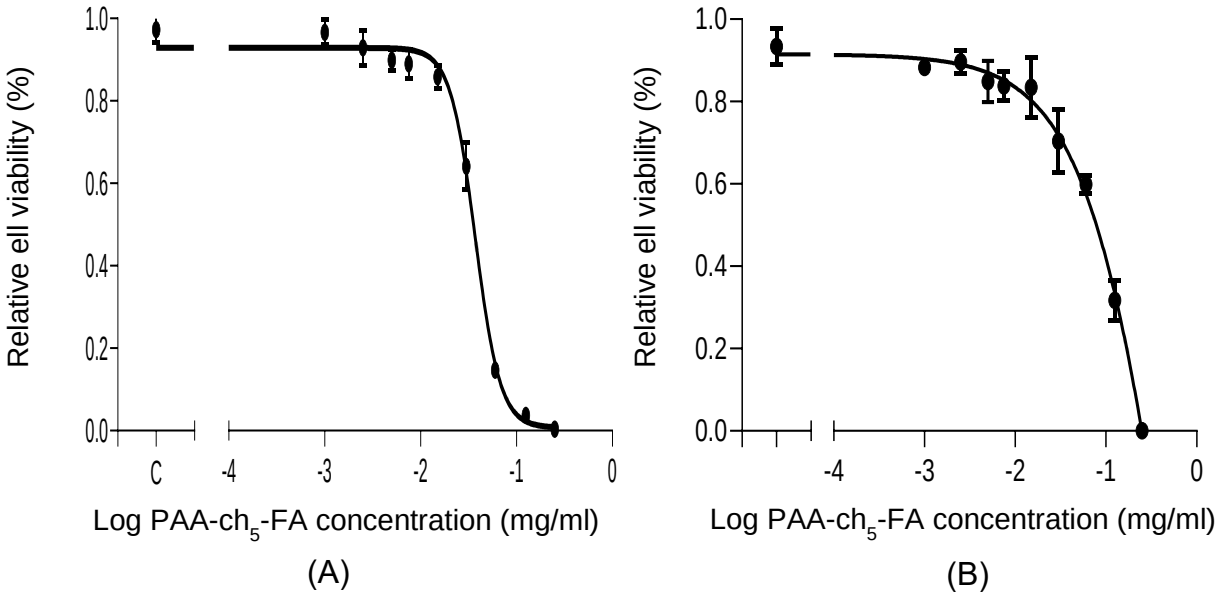

Figure 5-13: PAA-ch$_5$-FA cytotoxicity using trypan blue assay

These figures show the cytotoxicity of PAA-ch$_5$-FA (NPF(E)) on (A) OVCAR-8 and (B) OVSAHO using trypan blue assay. From this we use the concentration of 20 µg/ml as non-toxic concentration as it allows a viability of more than 80%. Results (mean ± S.D, n=3).

5.9.9. Cytotoxicity of the Navitoclax-PAA-Ch5-FA versus navitoclax

5.9.9.1. Trypan blue assay

A maximum concentration of 20 µg/ml of PAA-ch$_5$-FA was selected for further studies as this was the highest concentration that had a negligible cytotoxic effect. Using the nanoparticles loaded with navitoclax at a ratio of 5:1, which corresponded to a maximum encapsulated navitoclax concertation of approximately 1 µM that could be tested, cytotoxicity was evaluated in both OVCAR-8 and OVSAHO cells using the trypan blue assay. The nanoparticles of navitoclax inhibited the growth of cultures of both OVCAR-8 and OVSAHO cells. However, the maximum concentration that could be tested was not able to fully inhibit cell growth and IC_{50} could not be determined. In OVCAR-8 cells at the two highest concentrations tested, it was clear that the

encapsulated navitoclax was more potent than the free navitoclax, (Figure (5.15, A)). In contrast, in OVSAHO, all tested concentrations of encapsulated navitoclax showed significance improved activity when compared with free navitoclax at a corresponding concentration (Figure (5.15, B)). These results were corroborated by microscopy, which confirmed the larger effect of the encapsulated navitoclax (tested at 1 µM, (Figure (5.14 (A and C))) than free navitoclax (tested at 1 µM, (Figure (5.14 (B and D))).

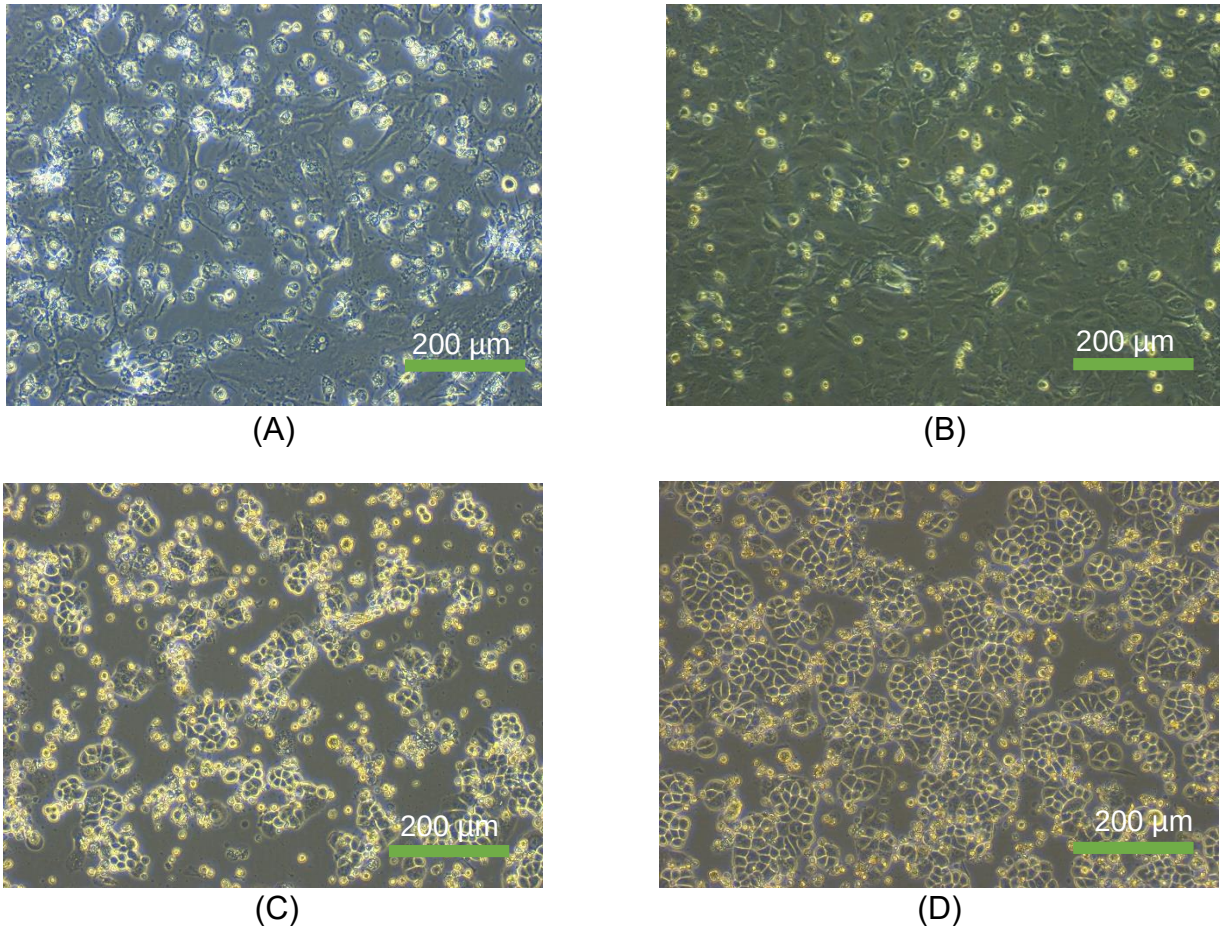

Figure 5-14: Morphological appearance of both OVCAR-8 and OVSAHO after being treated with NPF(N) and Navitoclax

These figures show the cytotoxicity of both navitoclax-PAA-ch$_5$-FA (NPF(N)) and navitoclax alone after 48 hours using a final concentration of navitoclax of 1 µM which is equivalent to PAA-ch$_5$-FA final concentration of 20 µg/ml. (A) Navitoclax-PAA-ch5-FA (NPF(N)) on OVCAR-8 (B) Navitoclax on OVCAR-8. (C) Navitoclax-PAA-ch$_5$-FA (NPF(N)) on OVSAHO (D) Navitoclax on OVSAHO. (n=3)

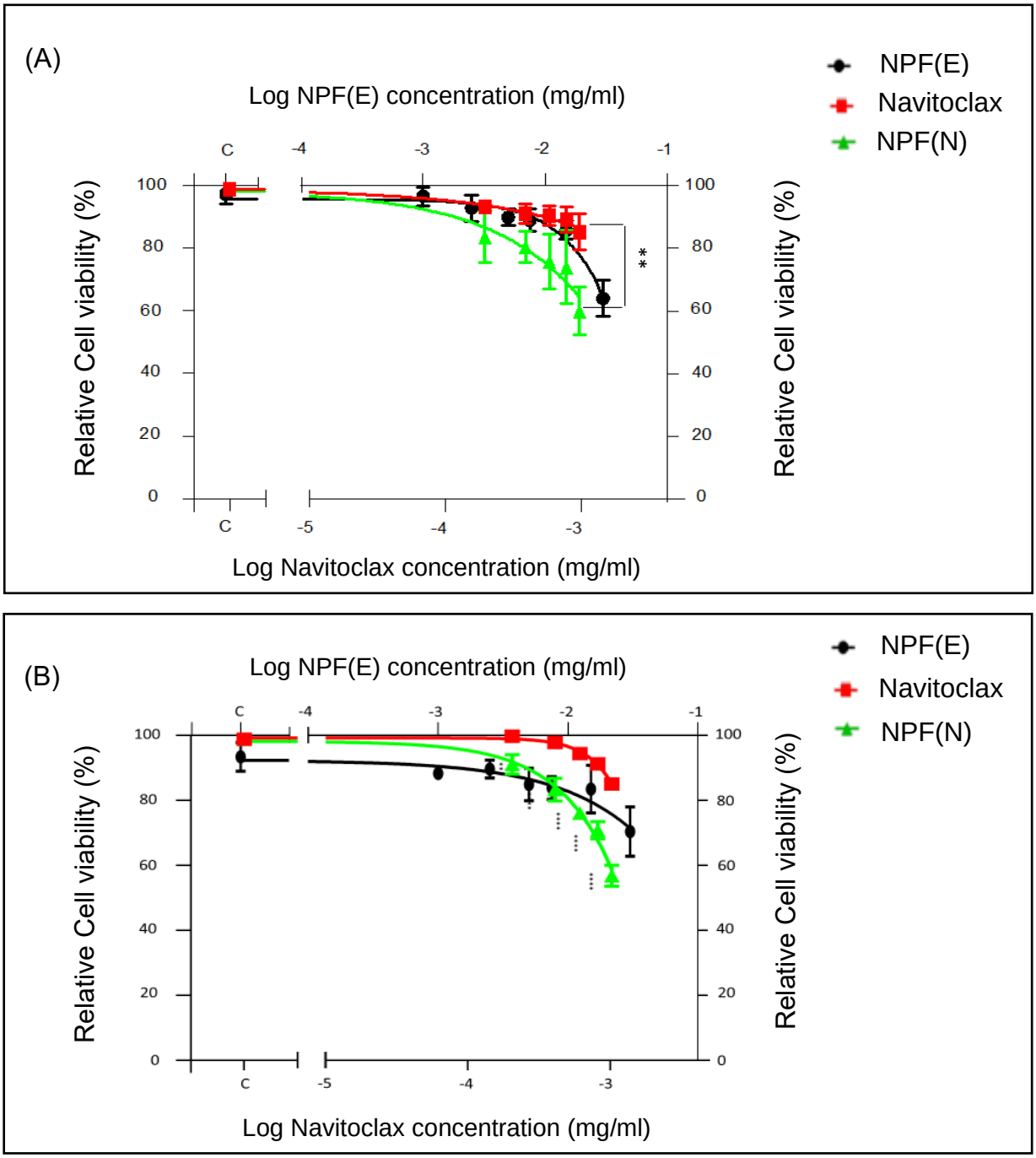

Figure 5-15: Cytotoxicity of NPF(N) and Navitoclax on OVCAR-8 and OVSAHO using trypan blue assay

These figures show the cytotoxicity of both navitoclax-PAA-ch$_5$-FA (NPF(N)) and navitoclax alone assessed using the trypan blue assay on (A) OVCAR-8 and (B) OVSAHO cells using a range of concentrations of navitoclax (0.2-1) µM. The maximum concentration of PAA-ch$_5$-FA (NPF(E)) was 20 µg/ml. A serial concentration of empty nanoparticle of (1-30 µg/ml) was also tested. There is a significant difference between both navitoclax formulations at different concentrations. (*(**): $P \leq 0.01$, (****): $P \leq 0.0001$*; data were analyzed using Two-way ANOVA). Results (mean ± S.D, n=3).

5.9.10. Caspase 3/7 assay

Since the intrinsic apoptosis pathway depends on the activation of caspase cascade, the caspase 3/7 assay could be utilized as an additional means to characterize the cytotoxic activity of a drug. In this assay, cells were exposed to both navitoclax formulations (the encapsulated navitoclax, “NPF(N)”, (1 µM navitoclax) or free navitoclax, (1 µM)) and a non-toxic concentration of the polymer (20 µg/mL, “NPF (E)”). The nanoparticles without navitoclax have an insignificant effect on caspase- 3/7 activity. Encapsulated navitoclax increased caspase 3/7 activity significantly more than the free navitoclax. Figure (5.16) shows caspase 3/7 activity of NPF(N), Navitoclax, and PAA-ch$_5$-FA on both ovarian cancer cell lines.

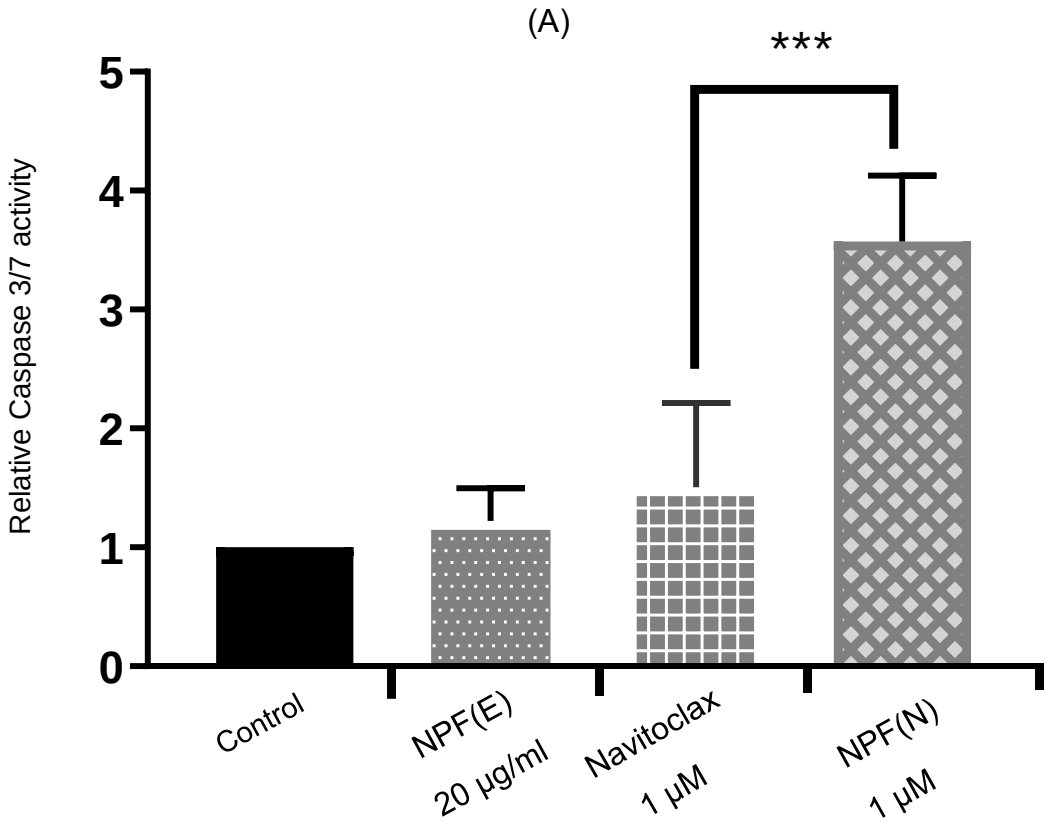

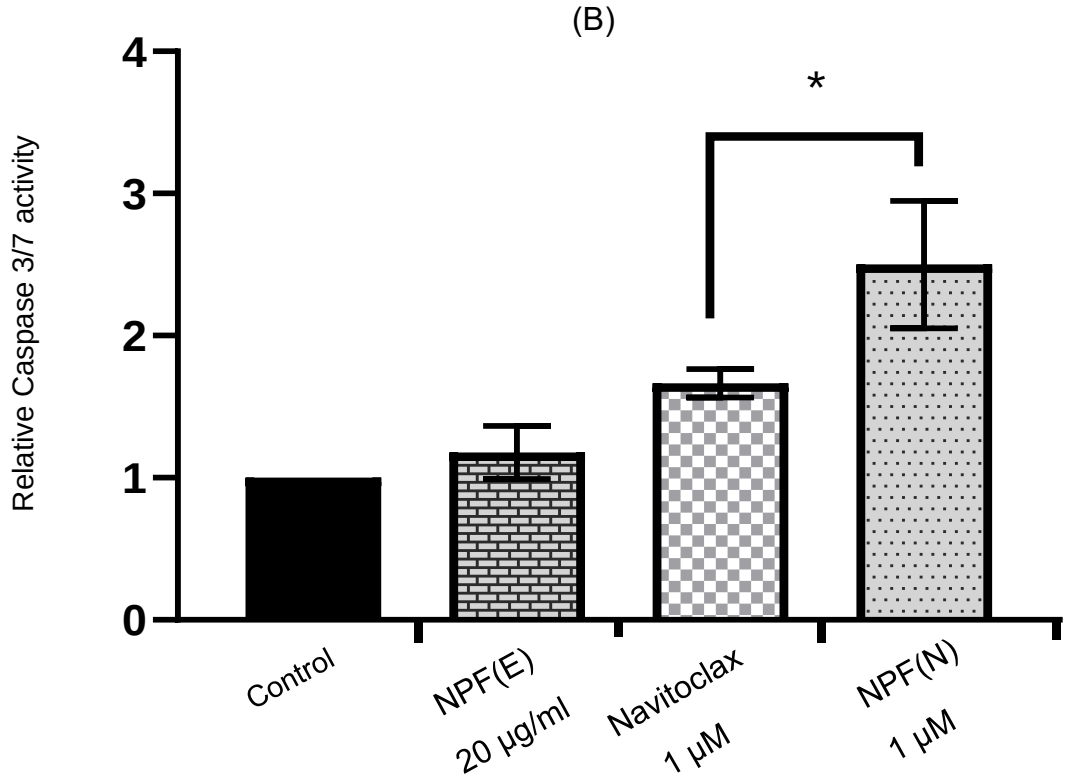

Figure 5-16: Cytotoxicity of NPF(N), Navitoclax, and PAA-ch$_5$-FA on OVCAR-8 and OVSAHO using caspase 3/7 assay

These figures show the effect of navitoclax-PAA-ch$_5$-FA nanoparticles (NPF(N)), free navitoclax and the nanoparticles without navitoclax (NPF(E)) alone assessed using a caspase 3/7 assay with final concentration of navitoclax of 1 µM and PAA-ch$_5$-FA (NPF(E)) of 20 µg/ml on both (A) OVCAR-8 and (B) OVSAHO. The results appeared as a relative caspase 3/7 activity compared to the control samples. There is a significant difference between both navitoclax formulations. (*(*) P< 0.05; (***): P ≤ 0.001*; data were analysed using One-way ANOVA). Results (mean ± S.D, n=3).

5.9.11. Drug uptake

Drug uptake assay was conducted to confirm the previous results. In this assay, both navitoclax formulations of 1 µM were added to the OVCAR-8 and OVSAHO cells and the navitoclax concentrations taken up into cells were measured after 4, 24 and 72 hours by HPLC. Importantly, significant increases in intracellular navitoclax concentration appeared at all time intervals in both OVSAHO and OVCAR-8 cells when

they were exposed to the encapsulated navitoclax compared to the free navitoclax, (Figure (5.17)).

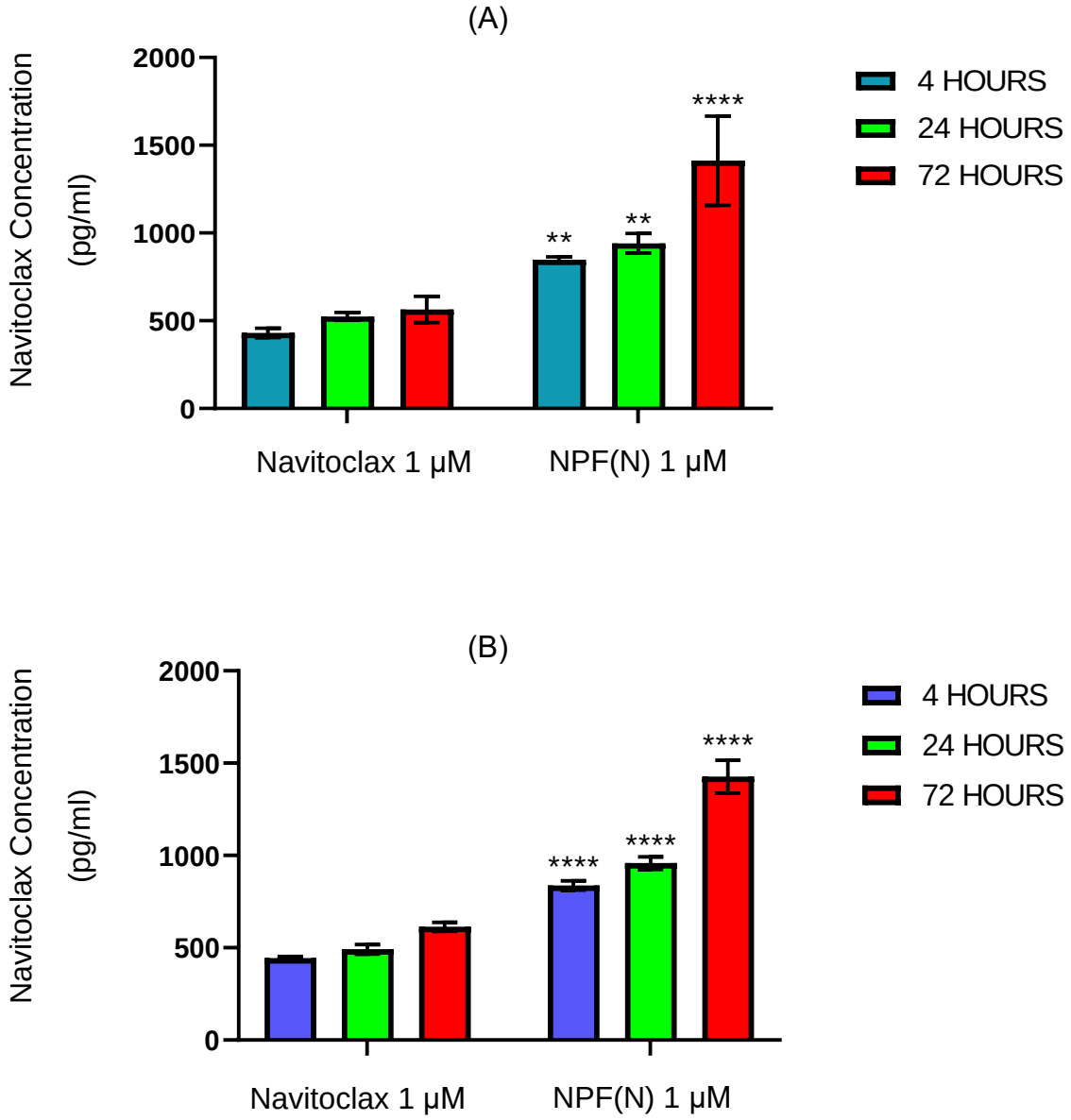

Figure 5-17: Navitoclax uptake for OVCAR-8 and OVSAHO after NPF(N) and navitoclax administration in different time frames

These figures show the drug uptake of both NPF(N) and navitoclax alone (final concentration of 1 µM) on both (A) OVCAR-8 and (B) OVSAHO. There is a significant difference between both navitoclax formulations at various time points of 4 hours, 24 hours and 72 hours. (*(**): $P \leq 0.01$, (****): $P \leq 0.0001$*; data were analyzed using Two-way ANOVA). Results (mean ± S.D, n=3).

5.9.12. Combination assays

Previous work has shown the synergy between BCL-X_L inhibitors and carboplatin in ovarian cancer cell lines (Abed *et al*., 2016). Moreover, the NP(N) showed synergy with carboplatin (chapter 4). Combinations of carboplatin with free or encapsulated navitoclax were subsequently tested in trypan blue, caspase 3/7, PARP cleavage using western blot assay, and Annexin/PI assays. In addition, the morphological appearance of the cells was also gathered, (Figure (5.18) and (5.19)). The final concentration of navitoclax in these experiments was (1µM) as this corresponded to the maximum concentration of polymer (20 µg/ml) that could be used without causing cytotoxic effects.

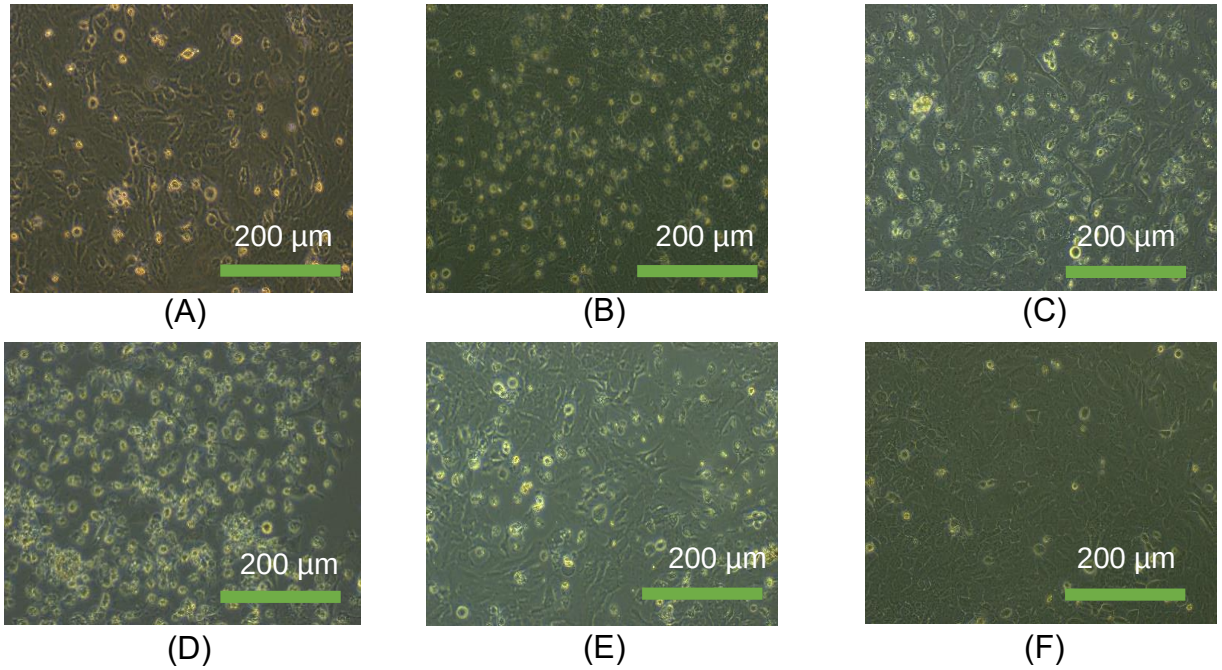

Figure 5-18: Morphological appearance of OVCAR-8 cells treated with several drugs combination

These figures represent the cytotoxicity effect of several drugs on their own and in combinations on OVCAR-8 cells after 48 hours exposure. (A) navitoclax alone 1 µM (B) navitoclax+ carboplatin 1 µM/13 µM (C) Navitoclax-PAA-ch_5-FA (NPF(N)) 1 µM (D) Navitoclax- PAA-ch_5-FA (NPF(N)) + carboplatin 1 µM/13 µM (E) PAA-ch_5-FA (NPF(E)) 20 µg/ml (F) control. (n=2)

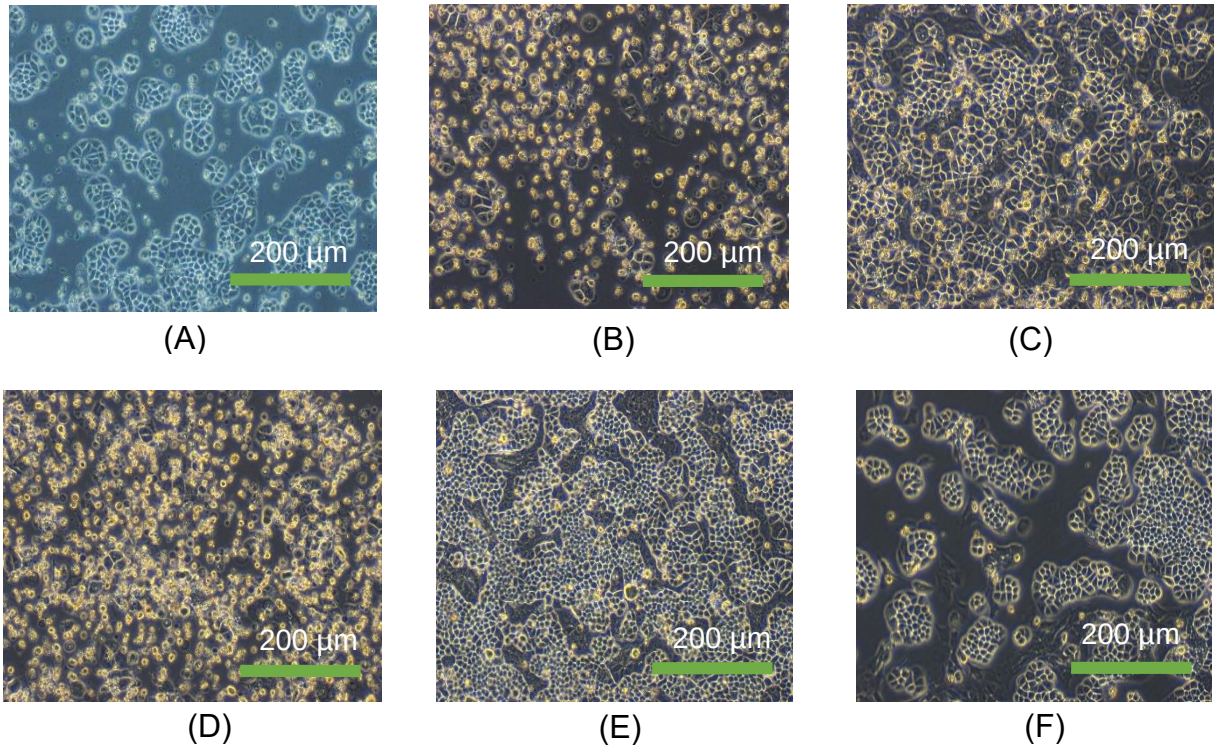

Figure 5-19: Morphological appearance of OVSAHO cells treated with several drugs combination

These figures represent the cytotoxicity effect of several drugs on their own and in combination on OVSAHO cells after 48 hours exposure. (A) navitoclax alone 1 µM (B) navitoclax+ carboplatin 1 µM/13 µM (C) Navitoclax-PAA-ch_5-FA (NPF(N)) 1 µM (D) Navitoclax- PAA-ch_5-FA (NPF(N)) + carboplatin 1 µM/13 µM (E) PAA-ch_5-FA (NPF(E)) 20 µg/ml (F) control. (n=2).

5.9.12.1. Trypan Blue

When OVCAR-8 cells were exposed to the carboplatin or encapsulated navitoclax, there was an evident increase in cell death. Furthermore, the cytotoxicity of these two drugs were almost the same. However, when cells were exposed to a combination of carboplatin and free navitoclax or carboplatin and encapsulated navitoclax, the number of dead cells was significantly more than would have been expected from the Bliss independence criterion, if the drugs had acted additively. As expected, empty

nanoparticles had an effect when combined with carboplatin which was not significantly different from the additive effect predicted by the Bliss independent criterion (Figure (5.20)). In OVSAHO cells, similar results were obtained with the exception that there was a modest supra-additive effect when empty nanoparticles and carboplatin were combined showed minor augmentation not as in OVCAR-8. However, this augmentation was less than that obtained with nanoparticles containing navitoclax, (Figure (5.21)).

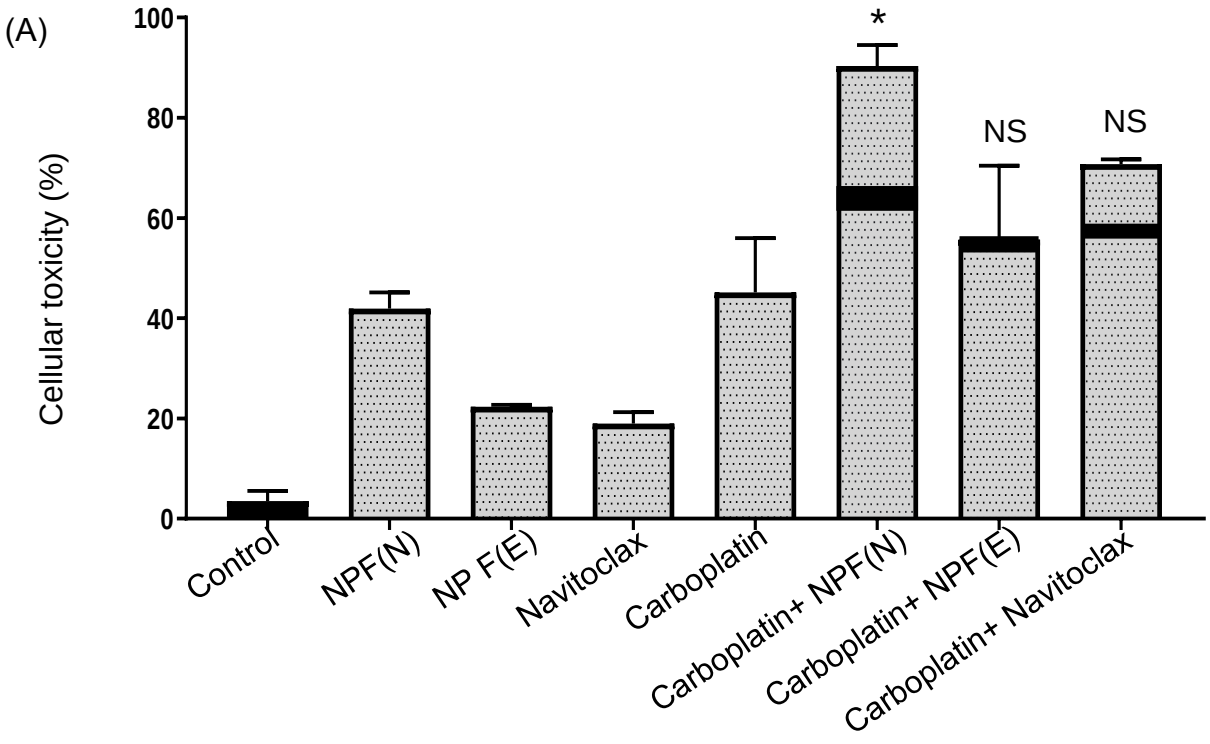

Figure 5-20: The effect of Navitoclax-PAA-ch5-FA and navitoclax alone when given in combination with carboplatin on OVCAR-8 using trypan blue assay

The indicated cells were treated with 13 μM carboplatin, 1 μM NPF(N), 1 μM navitoclax, 20 μg/ml NPF(E) for 72h cytotoxicity was determined using trypan blue assay. The data are represented in relative to the live cells after being treated with several drugs as single and in combinations. The expected effect of the combination was calculated using the Bliss independence criterion and represented as black horizontal lines and significantly different to the calculated additive effect for the encapsulated navitoclax with carboplatin. Moreover, there is a significant difference between the encapsulated navitoclax with carboplatin and the free navitoclax with carboplatin. (*(*): $P \leq 0.05$,* data were analysed using paired t-test*).* Results (mean ± S.D, n=3).

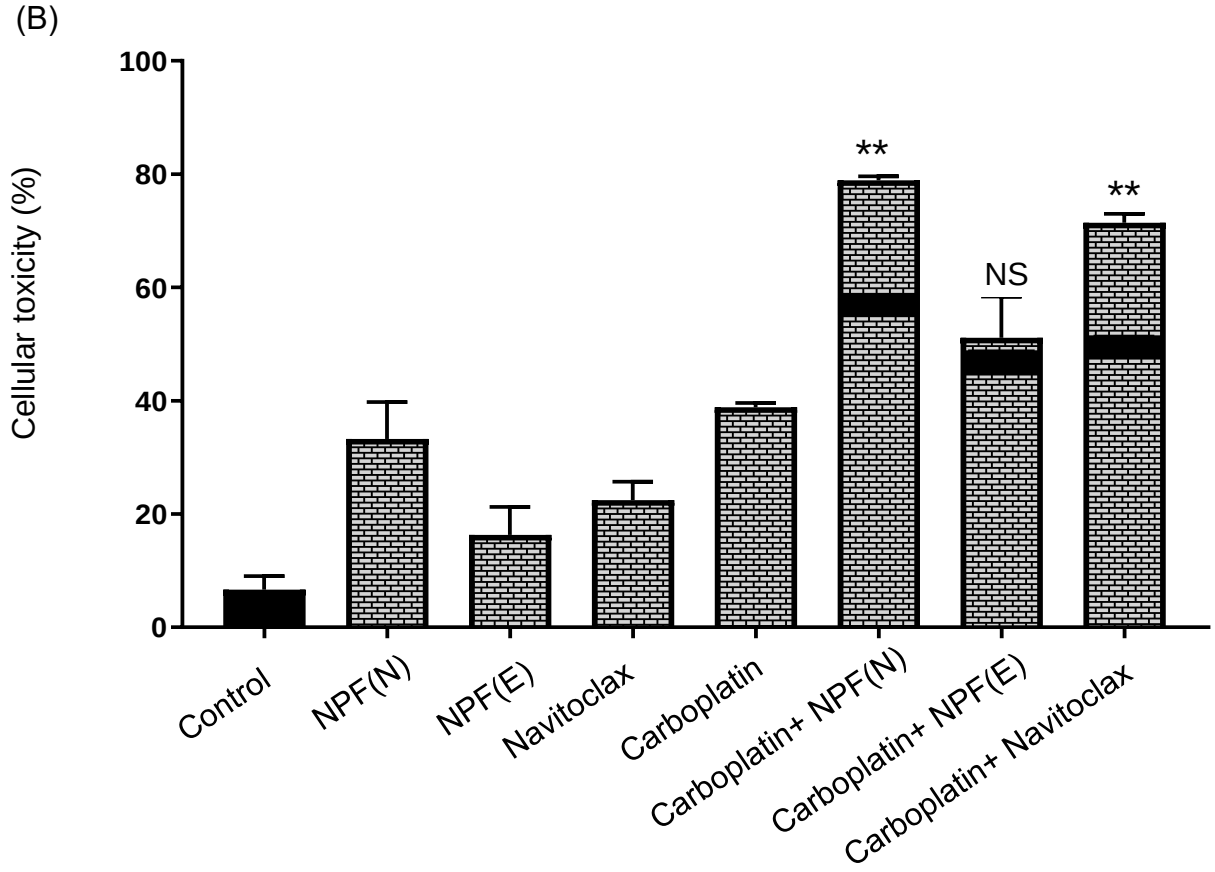

Figure 5-21: The effect of Navitoclax-PAA-ch5-FA and navitoclax alone when given in combination with carboplatin on OVSAHO using trypan blue assay

The indicated cells were treated with 13 μM carboplatin, 1 μM NPF(N), 1 μM navitoclax, 20 μg/ml NPF(E) for 72h cytotoxicity was determined using trypan blue assay. The data are represented in relative to the live cells after being treated with several drugs as single and in combinations. The expected effect of the combination was calculated using the Bliss independence criterion and represented as black horizontal lines and significantly different to the calculated additive effect for the encapsulated navitoclax and free navitoclax with carboplatin. Moreover, there is a significant difference between the encapsulated navitoclax with carboplatin and the free navitoclax with carboplatin. (*(NS): Not significant, (**): P ≤ 0.01,* data were analysed using paired t-test*).* Results (mean ± S.D, n=3).

5.9.12.2. Caspase 3/7 assay

Caspase 3/7 assay was used to confirm the previous results. There was no significant increase in caspase-3/7 activity in OVCAR-8 cells caused by free navitoclax and NPF(E) but there was a significant increase for encapsulated navitoclax (NPF(N))

relative to the carboplatin caspase activity. However, the caspase 3/7 activity stimulated by carboplatin was augmented by the inclusion of free navitoclax, and this was increased further when encapsulated navitoclax was used. In contrast, there was no augmentation for the empty nanoparticles when added to carboplatin (Figure (5.22)). Similar results were observed with OVSAHO cells (Figure (5.23)).

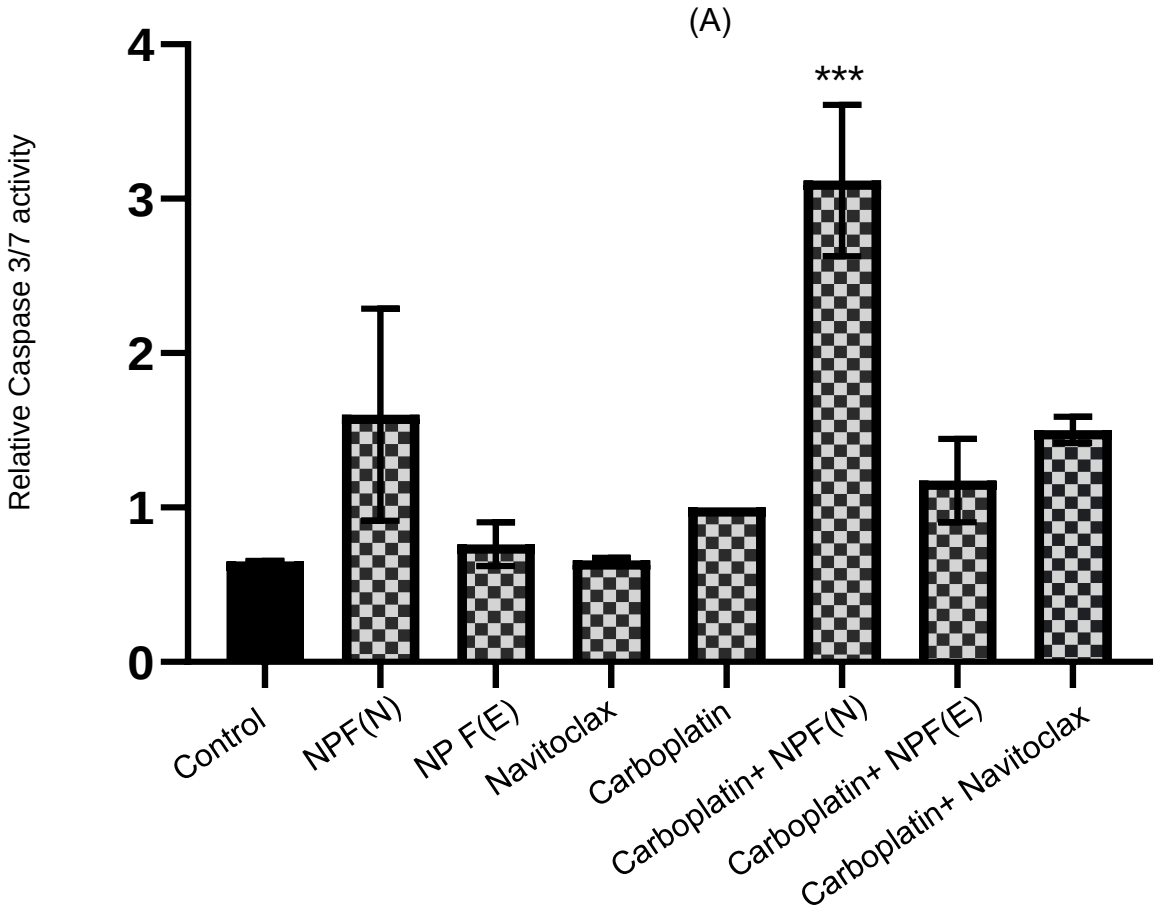

Figure 5-22: The effect of Navitoclax-PAA and navitoclax alone when given in combination with carboplatin on OVCAR-8 using caspase 3/7 assay

The indicated cells were exposed to 13 μM carboplatin, 1 μM NPF(N), 1 μM navitoclax, 20 μg/ml NPF(E) for 48h. Cell death was determined using relative caspase3/7 activity. The data are expressed as a relative caspase 3/7 activity compared to the one of carboplatin treated samples. There is significant difference in caspase 3/7 activity between the combination of carboplatin with encapsulated navitoclax and the combination of carboplatin with free navitoclax. *((***): $P \leq 0.001$*; data were analyzed using One-way ANOVA). Results (mean ± S.D, n=3).

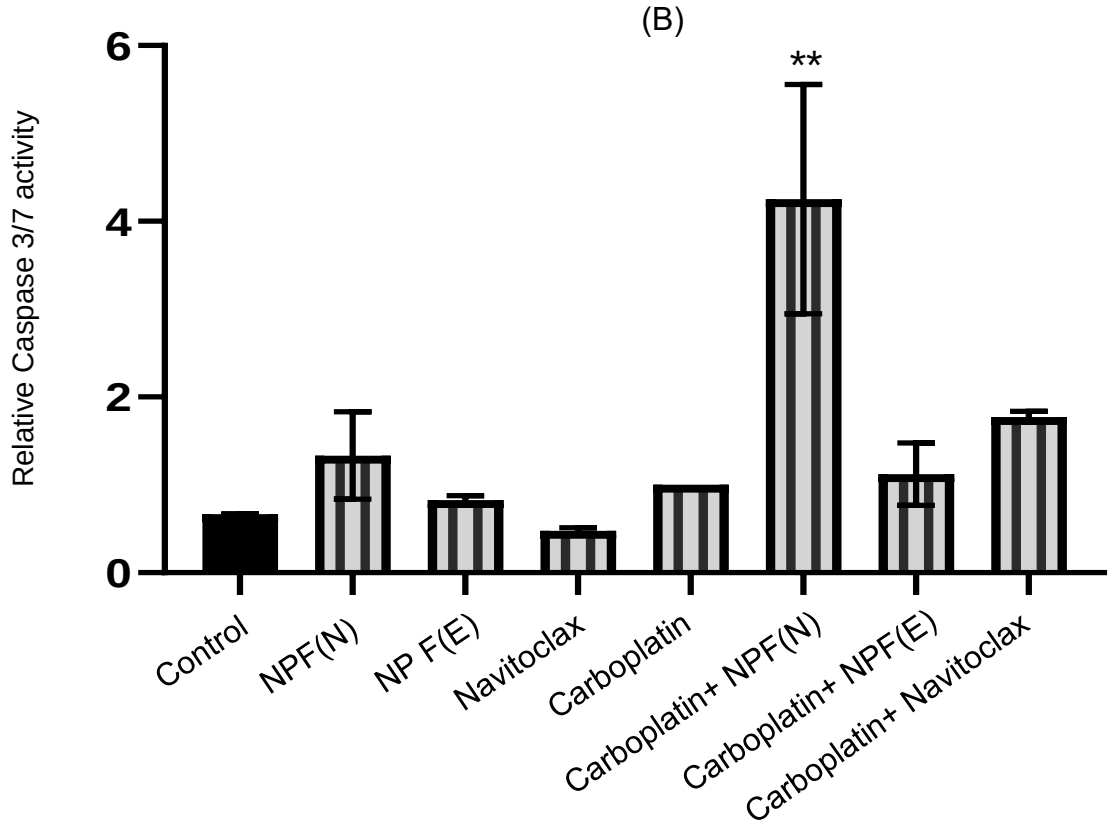

Figure 5-23: The effect of Navitoclax-PAA and navitoclax alone when given in combination with carboplatin on OVSAHO using caspase 3/7 assay

The indicated cells were exposed to 13 μM carboplatin, 1 μM (N), 1 μM navitoclax, 20 μg/ml NPF(E) for 48h. Cell death was determined using relative caspase 3/7 activity. The data are expressed as a relative caspase 3/7 activity compared to the one of carboplatin treated samples. There is significant difference in caspase 3/7 activity between the combination of carboplatin with encapsulated navitoclax and the combination of carboplatin with free navitoclax. *((**): $P \leq 0.01$*; data were analyzed using One-way ANOVA). Results (mean ± S.D, n=3).

5.9.12.3. PARP-cleavage assay

PARP cleavage measured by western blotting was used to confirm apoptosis induction by the drug combinations. In OVCAR-8, although neither free navitoclax nor the empty nanoparticles caused cleavage of PARP, this was observed with the addition of carboplatin alone. Encapsulated navitoclax on its own showed more PARP cleavage when compared with the previously mentioned drugs and even close to that observed

with carboplatin on its own. Significantly, the combination of carboplatin with encapsulated navitoclax showed a significant PARP cleavage when compared to that induced by combination of carboplatin with either navitoclax or empty nanoparticles. The cleaved and uncleaved PARP were quantified using Alphaview software and their ratios were determined to calculate the proportion of PARP cleavage that had taken place. This ratiometric analysis has the advantage that it does not require identical protein levels in each sample, which may be hard to control due to cell death induced by the drugs. GAPDH was used as a loading control for both cell lines, (Figure (5.24)).

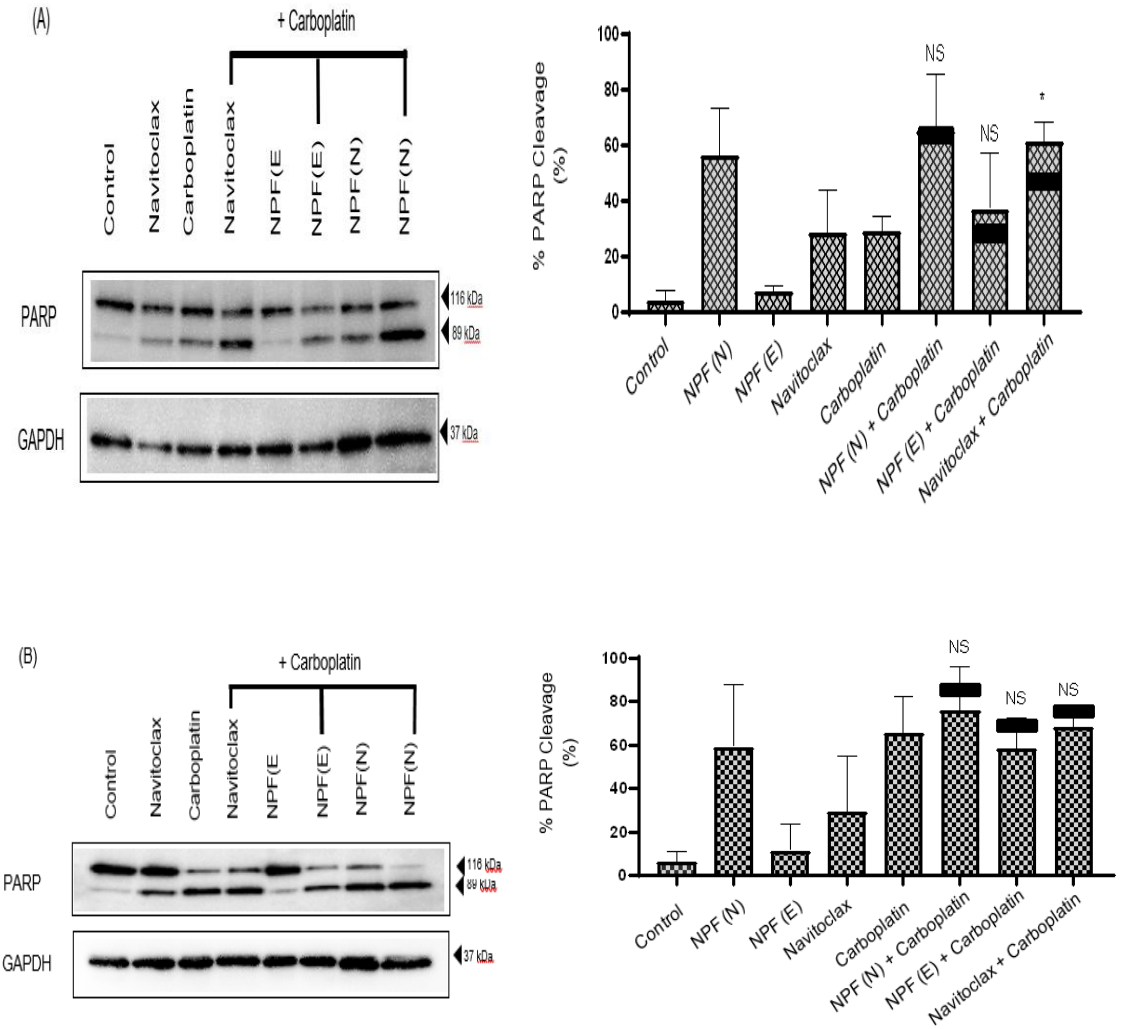

Figure 5-24: Effect of several drug combinations with carboplatin on PARP cleavage using western blot assay

The indicated cell lines (A) OVCAR-8 and (B) OVSAHO were exposed to 13 μM carboplatin,1 μM NPF(N), 1 μM navitoclax, 20 μg/ml NPF(E) alone and in combinations for 48 hours. The results showed the protein expression for all the drugs used using western blot assay. The GAPDH expressed the standard protein in each cell line. Although there was significant variation between samples in the total protein (as shown by the loading control), interpretation of the data is not affected because it is the ratio of cleaved PARP to uncleaved PARP that is an indicator of apoptosis. The expected effect of the combination was calculated using the Bliss independence criterion and represented as black horizontal lines. There is no significant difference with the calculated additive effect except for the free navitoclax with carboplatin in OVCAR-8 cell line and no significant difference between the encapsulated navitoclax with carboplatin and the free navitoclax with carboplatin. *((*): P ≤ 0.05 (NS): non-significant;* data were analysed using *paired t-test).* Results (mean ± S.D, n=3).

5.9.12.4. Annexin V/PI assay

To have a more complete picture of cellular death (necrosis, early apoptosis, late apoptosis), the annexin V/PI assay was conducted to study the effect of the drugs and their combinations. This assay was carried out using OVCAR-8, not OVSAHO, because of time constraints and also because the addition of NPF(E) and the NPF(N) to the OVSAHO cells make them hard to detach and obtain a single cell suspension with an adequate number of cells that was suitable for analysis by flow cytometry. The results with OVCAR-8 cells were consistent with those of the previous assays. The results showed no significant toxicity of the free empty nanoparticles or the navitoclax. In contrast, the NPF (N) showed significant cellular toxicity which was even slightly higher than that of carboplatin on its own. The activity of the combination of carboplatin with NPF(N) was higher than that with navitoclax and higher than that with empty nanoparticles, (Figure (5.26)). When compared to the additive effect predicted by the Bliss independence criterion, the combinations containing carboplatin and navitoclax

(free and encapsulated) showed significantly synergistic effect, while the empty nanoparticles with carboplatin did not, (Figure (5.27)). Figure (5.25) shows the flow cytometry images for all drugs that were tested on their own or in combination with carboplatin.

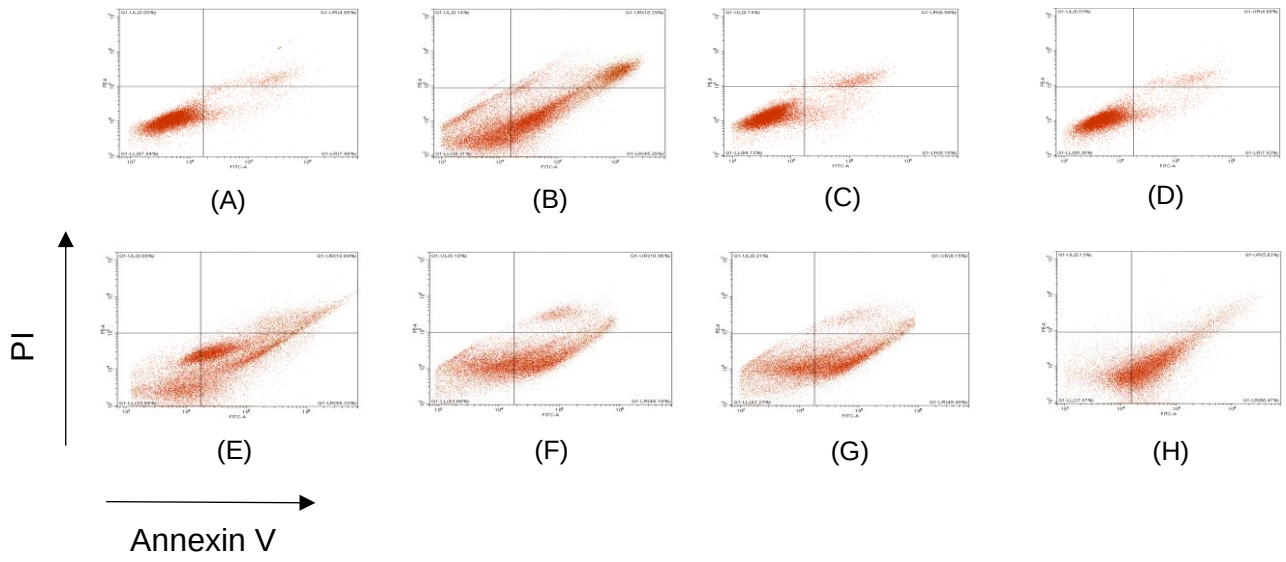

Figure 5-25: Flow-cytometry images for different drug combinations

These figures represent the cytotoxicity of several drugs alone and as combinations on OVCAR-8 after 48h. (A) Control (B) NPF(N) (C) Navitoclax (D) NPF(E) (E) Carboplatin (F) Navitoclax-Carboplatin (G) NPF(E)-Carboplatin (H) NPF(N)-Carboplatin. (n=3).

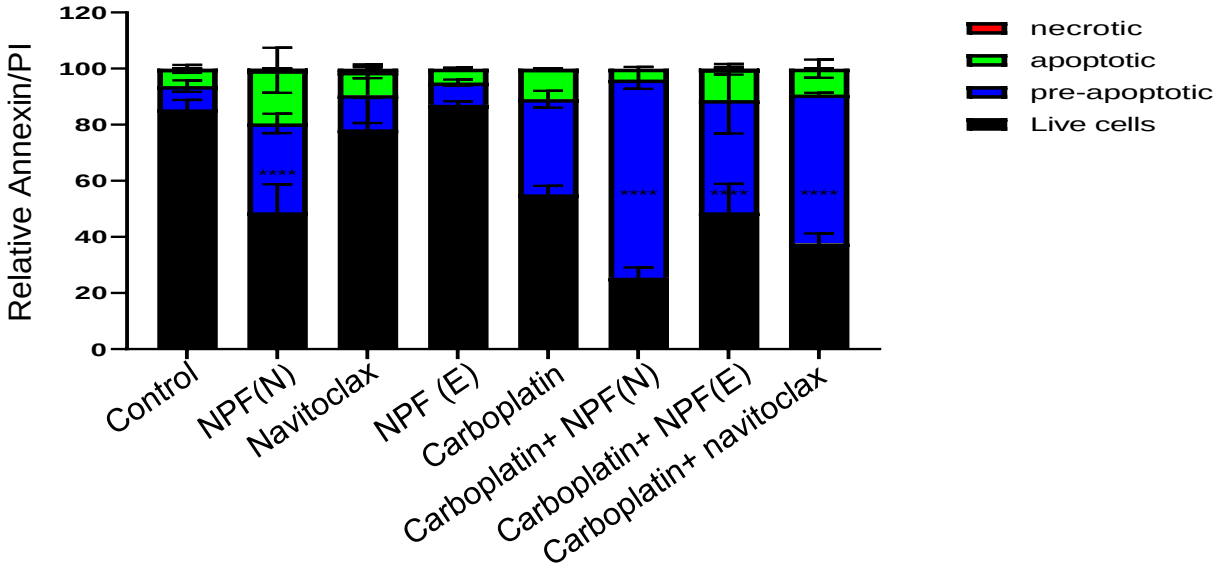

Figure 5-26: Relative Annexin V/PI activity for OVCAR-8 using several drug combinations

The indicated cell was exposed to 13 µM carboplatin, 1 µM NPF(N), 1 µM navitoclax, 6 µg/ml NPF(E) for 48h. Cytotoxicity was determined by Annexin V/PI assay and cells were labelled with annexin V and propidium iodide and measured by flow cytometry. The results are expressed as a fraction of that measured in control cells which showed significant difference in all combinations. (*(****): $P \leq 0.0001$*; data were analysed using Two-way ANOVA). Results (mean ± S.D, n=3).

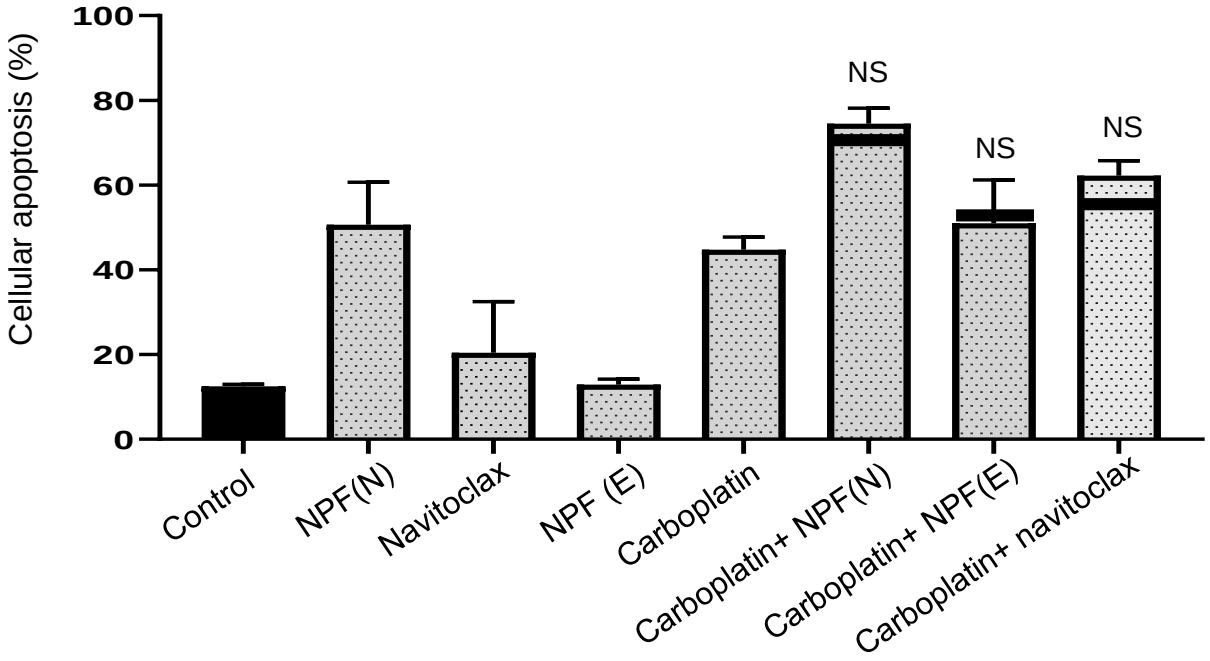

Figure 5-27: Cellular apoptosis for OVCAR-8 using several drug combinations using annexin V/PI assay

The indicated cell was exposed to 13 µM carboplatin, 1 µM NPF(N), 1 µM navitoclax, 6 µg/ml NPF(E) for 48h. Cytotoxicity was determined by Annexin V/PI assay. The results are expressed as a fraction of that measured in control cells. The Bliss independence criterion was used to calculate the expected effect of the combination and the results are express as solid horizontal black lines on the bar chart. There is no significant difference with the calculated additive effect and no significant difference between the encapsulated navitoclax with carboplatin and the free navitoclax with carboplatin. (*(NS): Not significant,* data were analyzed using paired t-test*).* Results (mean ± S.D, n=3).

5.9.13. Competition assay

To provide evidence that the effect of the folate-labelled nanoparticles depended on uptake by folate receptors, excess free folate was added to block receptor-mediated endocytosis. The ovarian cancer cell line used in this assay was OVSAHO, not OVCAR-8, because OVSAHO show high expression of FRA (Haddad *et al*., n.d). In a preliminary SRB assay to measure cell growth, the toxicity of free folate was evaluated, and none observed up to a final concentration of 200 µM, (Figure (5.28)). Accordingly,

in subsequent experiments FA was added at a concentration of 100 µM 30 minutes before adding the NPF(N) alone or in combination with carboplatin. The cells were treated with these drugs with and without pre-treatment with folic acid. As expected, there was no effect of folate on control samples or samples treated with carboplatin. However, folate reduced the toxicity of NPF(N), and of the combination of NPF(N) and Carboplatin, (Figure (5.29)).

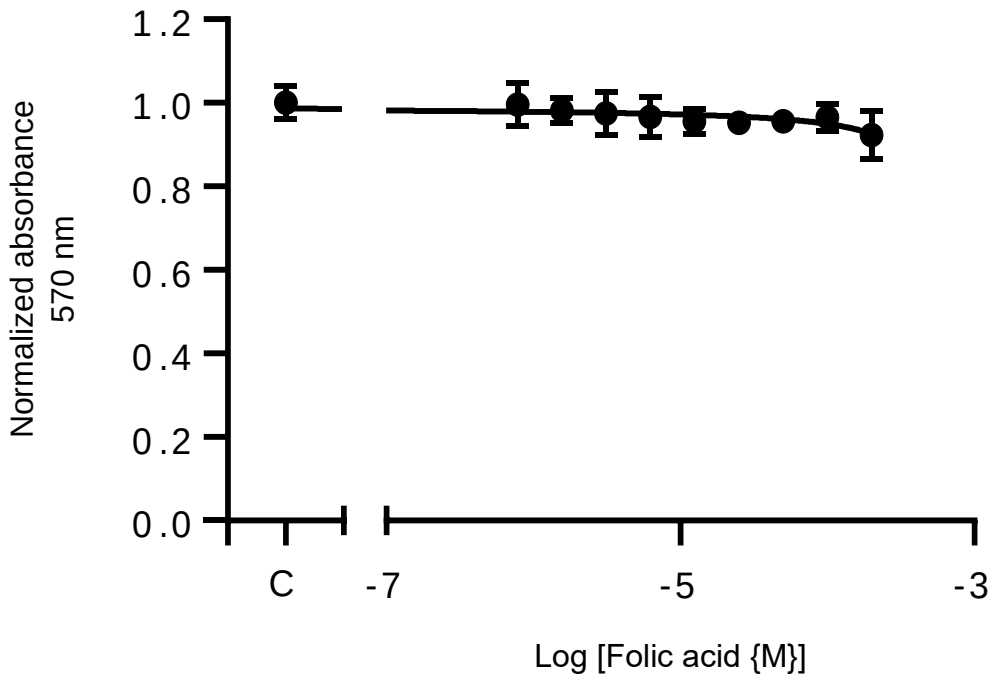

Figure 5-28: Cytotoxicity of Folic acid on OVSAHO using SRB assay

This figure shows the cytotoxicity of dose response curve for folic acid with final highest concentration of 200 µM using SRB assay on OVSAHO cell line. Results (mean ± S.D, n=3).

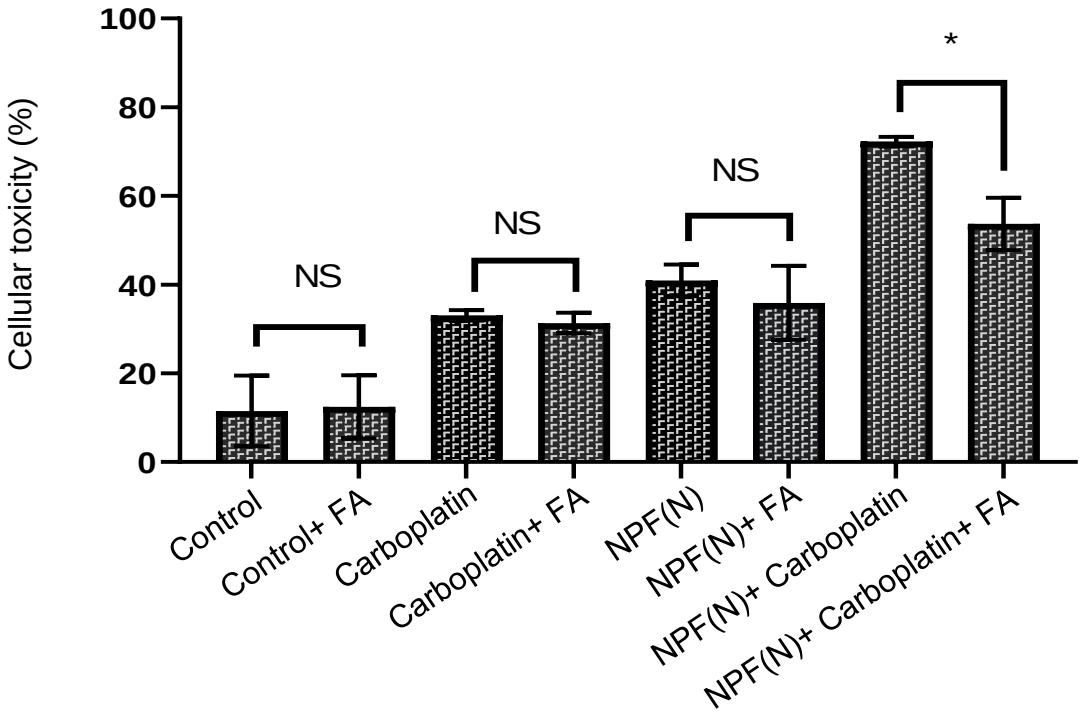

Figure 5-29: *The* effect of folic acid addition when given in combination with several drugs on OVSAHO using Trypan blue assay

The indicated cell was exposed to 13 µM carboplatin, 1 µM NPF(N), folic acid (FA) 100 µM for 48h. Cell death was determined by trypan blue assay. The data are expressed as a fraction of the number of live cells that were measured after exposure to drug. The significance appeared in one group when encapsulated navitoclax was combined with carboplatin. (*(NS): not significant, (*): P ≤ 0.05;* data were analyzed using One-way ANOVA*).* Results (mean ± S.D, n=3).

5.10. Discussion

Drug targeting to the specific site of action is considered a big challenge in any drug delivery system. Thus, several trials have been examined to find the best method in drug targeting (Zaidan *et al.*, 2017). Although multiple trials have shown promising results, there is still no universal method that is efficient for delivering all drugs (Attia *et al.*, 2019). Using nanoparticles as a drug delivery system is considered an ideal platform when compared with conventional therapies (Behera and Padhi, 2020). However, when they are used in treating cancerous tissues, passive targeting has

failed to achieve a sufficient localisation (Krystofiak *et al.*, 2012). The active targeting method has been developed to overcome the passive targeting drawbacks (Yin *et al.*, 2014). In this study, active targeting using folate has been explored.

Encapsulating navitoclax in actively targeted nanoparticles is not new, as previous researchers tried using this to improve its water solubility and cytotoxicity. One of these was the encapsulation of navitoclax and S63845 (MCL-1 inhibitor) in mesoporous silica nanoparticles targeted with a MUC1-targeting aptamer, which showed induction of apoptosis, resolving navitoclax resistance and decreased the problem of thrombocytopenia (Vivo-Llorca *et al.*, 2020). Navitoclax was also encapsulated in nanoliposomes, and these nanoparticles were grafted with FH peptide and this FH peptide is a small peptide isolated by phage display. This peptide targets explicitly cancer-associated fibroblasts (CAFs) in the tumour. The formed nanoparticles showed increment in navitoclax water solubility, and they induced apoptosis in CAFs (Chen *et al.*, 2016).

Herein, nanoaggregates of navitoclax with PAA-ch$_5$-FA, were prepared affording a 60-fold improvement in navitoclax solubility. Although the folate provides the advantage of active targeting, the increase in solubility was less than that achieved with the PAA-ch$_5$ without folic acid (chapter 3). The reason behind the decrease in the navitoclax loading is likely to be related to the hydrophilicity nature of the folic acid moiety, which might destabilize hydrophobic-hydrophobic interactions in micellar core. This is consistent with what happened with cabazitaxel; its loading capacity decreased once encapsulated in the folic acid targeted nanoparticles compared to non-folate targeted nanoparticles (Meng *et al.*, 2019).

Several parameters affect drug loading, including the polymer concentration and the drug feed concentration, the compatibility between the drug and the micellar core, and the partition coefficient (Hussein and Youssry, 2018). Here a 10:1 (drug: polymer) ratio substantially improved solubilization of navitoclax. This may reflect a higher degree of hydrophobic-hydrophobic between the polymer and the drug (Du *et al.*, 2009). On the other hand, the increment in polymer concentration also showed improvement in loading capacity because this increased the number of formed micelles and thus more navitoclax encapsulation.

The physical characteristics of the formed self-assemblies were also characterized. The size of the nanoaggregates is an essential parameter to consider as they have to be in an ideal dimensions (50-500 nm) to permeate through tumour blood vessels fenestrations to reach the intended site of action (Jin *et al.*, 2016). They should not be less than 50 nm to eliminate renal clearance and not large micelles which will be detected by the RES (Hoskins *et al.*, 2010; Gao *et al.*, 2013; Hussein and Youssry, 2018). The hydrodynamic size of the empty polymer was larger than the one that was not folate targeted (chapter 3). This is probably because the hydrophilicity of folic acid molecules and the week hydrophobic-hydrophobic interactions make micellar expansion larger than that of the micelles of PAA-ch$_5$. Unexpectedly, inclusion of navitoclax decreased the size of the nanoparticles. This is the opposite of what has been found with ursolic acid (Jin *et al.*, 2016) and with cabazitaxel (Meng *et al.*, 2019), where there was an increment in the size of the nanoparticles once drugs were encapsulated in folic acid targeted nanoparticles. The decrease in size is hard to explain, but it could be due to that after adding the navitoclax, there was a micellar

expansion to reach a size larger than that of the filter pores and once filtered the large micelles were removed.

As reported, having a zeta potential above 30 mV reflects highly stable particles (Poy *et al.*, 2018). The empty nanoparticles and encapsulated navitoclax showed zeta potential values above 30 mV, suggesting highly stable nanoaggregates. In addition, the positive charge of the nanoparticles may allow for electrostatic interaction with the negatively charged cell membrane of cancer cells, allowing for better internalisation (Jin *et al.*, 2016). Moreover, the non-significant change in zeta potential between polymer before and after being encapsulated with navitoclax is a good indication as this means that there was a successful encapsulation and no complexation between the drug and the polymer (Alsuraifi *et al.*, 2018). Although the polydispersity index showed no uniform dispersion of the micelles before and after adding navitoclax, it still represents an acceptable mid-range distribution (Trang Le *et al*., 2020). Thus, the physical characteristics of the folate-tagged nanoparticles containing navitoclax were encouraging.

Since navitoclax must be released from the polymer core to reach its site of action, this was also measured. This can help predict the drug fate *in vivo* (Hussein and Youssry, 2018). The release of navitoclax was disappointing, with only 21% of the drug being released. However, it was still higher than that for the navitoclax with the PAA-ch$_5$ (chapter 3). This may be because the folic acid moieties have a role in decreasing navitoclax encapsulation because of the weak interactions in the micellar core, allowing the navitoclax to leave the micellar core more easily than the PAA-ch$_5$. The low release could be due to several causes such as poor solubility, and the high log P

for navitoclax (Hussein and Youssry, 2018). Furthermore, the concentration of navitoclax that has been tested was very low. However, this low release could represent an advantage by providing extended-release (Chen *et al.*, 2016). This should be further investigated using high feeding ratios, using different environments other than PBS but the high drug price prevented us from proceeding in these experiments. Moreover, the release was not assessed with freeze dried samples. The physical stability of the new formulation was also assessed. Although there was a burst loss of navitoclax from all formulations in the first week, the results showed that the best environment that preserves the navitoclax content was the cold temperature in as freeze-dried cakes.

Using folic acid-targeted poly(allylamine) polymer with ovarian cancer cell lines or any other cancer cells has not been used before. Hence, there was a need to examine the polymer toxicity. The cytotoxicity for this polymer is due to the primary amine groups it has on its backbone, and grafting this polymer by pendant groups, such as cholesteryl, can decrease the cytotoxic effect of the polymer on cells as this functionalizes the primary amines (Alsuraifi *et al.*, 2018). Accordingly, targeting the PAA-ch$_5$ polymer with FA will also reduce the number of primary amines and decrease the inherent toxicity of the polymer. As expected, the polymer showed toxicity on both cell lines, although this was somewhat less than that of PAA-ch$_5$. Toxicity was marginally grater with OVCAR-8 cells than with OVSAHO cells. The non-toxic concentration of PAA-ch$_5$-FA (80-90 % viability) was 20 µg/ml and this concentration correspond to 1 µM of encapsulated navitoclax. The nanoparticles containing navitoclax showed a three-fold increment in cytotoxicity compared to free navitoclax. This increment in cellular toxicity is likely related to the receptor-mediated endocytosis through FRA receptors and thus

a higher drug uptake and higher cytotoxicity (Jin *et al.*, 2016). These results were consistent with what has been found with an increase in cytotoxicity of folate-targeted nanoparticles for anticancer drugs on different cell lines such as cabazitaxel on HeLa and A549 cells (Meng *et al.*, 2019), with doxorubicin on MCF-7 cells (Zheng *et al.*, 2015), with docetaxel on SKOV3 cells (Barani *et al.*, 2020), and with paclitaxel and carboplatin that were encapsulated together (Gupta *et al.*, 2019). Moreover, the drug uptake assay showed that navitoclax nanoparticles increased intracellular concentration of navitoclax almost three-fold compared to free navitoclax. This could be due to increased permeability from the polymer itself and/or the effect of receptor mediated endocytosis. Furthermore, the targeted nanoparticles have been found by others to decrease the drug efflux (Bazak *et al.*, 2016; Anarjan, 2019) and this may contribute to the higher concentrations observed here. This was also observed when camptothecin drug delivery that was enhanced through receptor-mediated endocytosis using folate targeted nanoparticles (Behera and Padhi, 2020).

Several cellular toxicity assays have been conducted to confirm that the cellular toxicity of NPF(N) happened through apoptosis. A higher caspase- 3/7 activity was observed with NPF(N) than with navitoclax alone. The polymer alone had negligible effect. This was consistent with Ursolic acid which was encapsulated in folic acid targeted nanoparticles and also activated caspase 3/7 in MCF-7 cells (Jin *et al.*, 2016). Moreover, the flow cytometry showed similar results as there were more apoptotic cells in the samples treated with the NPF(N) than the free navitoclax. The encapsulated navitoclax was even able to induce more apoptosis than carboplatin on its own.

Our group has previously shown synergy between ABT-737 or navitoclax with carboplatin (Witham *et al*., 2007; Stamelos *et al*., 2013). In addition, the promising results obtained in chapter 4 from combination of NP(N) with carboplatin, led us to explore if the NPF(N) could augment the carboplatin cytotoxicity. Several assays with different targets were performed to determine if there is a synergistic interaction between carboplatin and the encapsulated navitoclax. All of the assays showed significant synergy, with different extents, between both navitoclax formulations with carboplatin, and this was more marked with NPF(N) than with free navitoclax. This is likely due to higher drug uptake as a result of the folate-targeting. The difference in Bliss independent synergism magnitude between the trypan blue and the flow cytometry could be due to the fact that the trypan blue assay measures dead cells, whereas annexin V/PI staining discriminates necrotic, pre-apoptotic and apoptotic cells. Alternatively, there may be error in the compensation matrix used to analyse the flow data. It would have been desirable to solidify these observations by determining a combination index to confirm that synergy, but this would require a full dose response curve to determine the IC_{50}. This was precluded by the toxicity of the polymer itself and the low throughput of the trypan blue assay.

Although the previous results were promising, the original plans to evaluate the newly developed targeted nanoparticles with navitoclax on platelets was not feasible due to constraints imposed by the COVID-19 pandemic. Nonetheless, there are several promising results from previous literature which predict that the use of folate-targeted nanoparticles will widen the navitoclax therapeutic window and decrease the possibility of thrombocytopenia. These include the results found by Vivo-Llorca *et al*., who found that when navitoclax was encapsulated in nanoparticles actively targeted with a MUC1-

targeting aptamer, there was a decrease in thrombocytopenia and this represented a revolution in improving the navitoclax therapeutic index (Vivo-Llorca *et al.*, 2020). Furthermore, Ledermann *et al.* demonstrated interesting results who showed that the platelets have no FRA expression on their surfaces, favouring selectivity toward ovarian cancer cells (Ledermann *et al*., 2015). Nevertheless, testing of this new formulation is mandatory to detect its effect on platelets by using several in vitro and in vivo assays.

In order to confirm that the uptake happens through receptor-mediated endocytosis, the folic acid-FRA competition assay was conducted (Jin *et al.*, 2016; Muralidharan *et al.*, 2016; Meng *et al.*, 2019; Tsolou *et al.*, 2020). Choosing of OVSAHO instead of OVCAR-8 as it has been found that OVSAHO, in addition to OVKATE cell line, show the highly expression of FOLR1 when compared with other ovarian cancer cell lines, while in OVCAR-8, it does not express more than one-third of that FOLR1 expression on OVSAHO cell line. Of note, it has been found that the concentration of folic acid on nanoparticles surface plays a determinant role in the binding affinity to FRA and it has been reported that these folic acid moieties on nanoparticles have to overcome the competition of normal folic acid levels (Patel *et al.*, 2018; Tarudji and Kievit, 2020). Here, the administration of folic acid at non-toxic doses was used to determine if the activity of the folate-tagged nanoparticles was dependent on folate receptors. Although there was no significant decrease in cytotoxicity after administration of NPF(N) with and without folic acid, the combination of NPF(N) with carboplatin showed a significantly lower cytotoxic effect when this combination was given after administered folic acid. This gave an indication that the uptake of NPF(N) uptake was dependent on receptor medicated endocytosis, as has been demonstrated by previous

researchers (Jin *et al.*, 2016). Further experiments are desirable such as knockdown of the folate receptor by RNAi to confirm receptor-mediated uptake. Alternatively, uptake could be characterized in more detail using confocal microscopy as there could be FRA internalisation mechanisms other than receptor-mediated endocytosis (Tsolou *et al.*, 2020).

5.11. Conclusion

The results that have been achieved in this chapter were propitious as there was a successful encapsulation of navitoclax inside the polymeric core, which was confirmed by measuring the physical characteristics of the formed nanoaggregates. Furthermore, there was an increment in the water solubility from negligible solubility to 60-fold higher and this could be improved by changing the feeding ratio and polymer concentration. The new formulation was highly stable when it was stored as freeze-dried cakes in the cold. Importantly encapsulation significantly improved the activity of navitoclax, both alone and in combination with carboplatin and this appeared to be dependent on binding to the folate receptor. This may improve the therapeutic index of navitoclax and facilitate its use in the treatment of ovarian cancer.

Chapter 6. Conclusion and future work

6.1. Conclusion

This work investigated the potential of nanoparticle formulations for the delivery of navitoclax to ovarian cancer. The goal was to increase the therapeutic window of navitoclax and potentially also improve its water solubility and its bioavailability, in addition trying to target navitoclax toward cancer cells

One of these important types of nanoplatforms with remarkable characteristics is the amphiphilic polymers, mainly comb-shaped polymers (Thompson *et al.*, 2008; Hoskins *et al.*, 2011). Poly(allylamine) (PAA) is a water-soluble, cationic, long-chain polymer (Alsuraifi *et al.*, 2018) and is one of the most widely used graft polymer backbones (Hoskins *et al.*, 2011). This PAA amphiphile has been grafted with several hydrophobic groups such as a cholesteryl moiety. This comb shaped polymer resulted in superior drug loading and has been applied with several hydrophobic drugs such as BNIPDaoct and showed improvement in the drug's water solubility (Hoskins *et al*., 2010). These features made this type of polymer ideal to improve the drawbacks with navitoclax. In the beginning, navitoclax was encapsulated with the PAA-ch_5, and a successful encapsulation in the polymeric core was achieved. Despite the poor loading efficiency, this improved the navitoclax solubility 100-fold. Herein, this was the first time navitoclax has been encapsulated in this type of polymers. Although increasing the drug: polymer ratio and the polymer concentration improved the encapsulation efficiency and water solubility substantially, the high price of drug prevented further optimization. The physical characteristics of the nanoaggregates showed an ideal size. Regarding the release of navitoclax from the polymeric core, it was low. However, this slow release could be advantageous in providing extended release of navitoclax inside the body and potentially avoiding high peak drug concentrations which might cause unwanted side

effects. The stability tests showed that the product could be stored for extended periods in a freeze-dried formulation, preferably at a cold temperature.

The goal of the research was to improve the therapeutic index of navitoclax, so the next step was to evaluate the efficacy of the formulation in cells. Until now, there has been limited research evaluating navitoclax nanoparticles in ovarian cancer (Chen *et al.*, 2016; Ding *et al.*, 2020). The effect of the encapsulated navitoclax was compared to that of free navitoclax. Its activity in combination with carboplatin was also tested to see if the synergy previously reported between free navitoclax and carboplatin could be reproduced (Stamelos *et al.*, 2013). Initial studies evaluated the toxicity of empty nanoparticles to ensure that the effect of the encapsulated navitoclax was due to the drug and not the polymer itself. Several time-consuming issues were encountered because the polymer interfered with SRB dye and other light absorbance assays. This was solved by using the more labour-intensive trypan blue assay. Using non-toxic concentrations of the polymer, the encapsulated navitoclax was evaluated and found to have twice the activity of free navitoclax at a comparable concentration. That promising result was supported by the observed increase in drug uptake which is most likely to be due to the effect of the polymer in inducing endocytosis (Zafar *et al.*, 2018). In drug combination assays, synergy was also observed with carboplatin. Altogether, these auspicious results could represent a new era in ovarian cancer treatment also represent a solution that could improve the navitoclax therapeutic index in general. However, the planned studies to measure the therapeutic index in animal studies could not be carried out because of the COVID19 pandemic. Ideally, these would have explored whether the encapsulated navitoclax had a reduced effect on platelets

compared to free navitoclax and also measured the anti-tumoural activity of the encapsulated navitoclax in combination with carboplatin.

To build on these promising results, active targeting of the nanoparticles was explored. Folic acid was chosen as an active targeting ligand because of its remarkable properties, in addition to its ability to bind FRA receptors which are highly expressed on ovarian cancer cells (Xing *et al.*, 2018). The folate labelled nanoparticles were anticipated to follow a “trojan horse method” and enter the cells through receptor mediated endocytosis mechanism (Blanco *et al.*, 2012; Jones *et al.*, 2017). Importantly, the results showed successful encapsulation, improvement in physical characteristics, and increment in water solubility by 60-fold. However, this was lower than that achieved with the PAA-ch$_5$. The folate labelled nanoparticles showed a better release profile than that achieved with PAA-ch$_5$. This new targeted polymer has not been used previously on any cancer cells and although it showed inherent toxicity, this was not substantially different from the untargeted polymer. Significantly, the encapsulated navitoclax in the folate targeted nanoparticles showed much higher toxicity compared to the non-targeted navitoclax nanoparticles and also higher than free navitoclax. This was further improved when it was combined with carboplatin where it showed a cellular toxicity close to 80% of the cancer cells under the conditions tested and, importantly, this was higher than achieved when free navitoclax was combined with carboplatin. Taken together, these data suggest encapsulation of navitoclax in nanoparticles has substantially improved its properties and further evaluation of the formulation in animal studies is warranted.

Although there are a limited number of drugs that have been incorporated with PAA-ch_5, these have mostly shown improvement in the solubility for most the drugs encapsulated in its core and some have shown improvement in cytotoxicity, it is worthwhile to compare the promising results that have been achieved here with those reported in the literature. The anticancer drug BNIPdaoct, which has been encapsulated in the same polymer and showed 30% drug loading and an improvement in water solubility from negligible concentration to be 0.3 mg/ml and this consistent of what happened with navitoclax where its solubility has also improved once encapsulated in the polymeric core. Significantly, encapsulation of navitoclax showed a two-fold increase in cytotoxicity on ovarian cancer cells *in vitro*, while BNIPdaoct failed to achieve significant difference with free form (Hoskins *et al*., 2010). In contrast, encapsulation of a thieno[2,3-b] pyridines derivative was examined on pancreatic adenocarcinoma cells (BxPC-3), and showed a slower drug release and higher *in vitro* cytotoxicity when compared with free form comparable to the results that have been achieved with navitoclax (Zafar *et al.*, 2018).

Navitoclax has also been encapsulated in other types of nanoparticles, including with doxorubicin in ultra pH-sensitive nanovesicles (Ding *et al.*, 2020). This led to improvement in drug uptake through the EPR effect and achieved higher cellular toxicity (Ding *et al.*, 2020). Moreover, co-encapsulation of navitoclax with other BH3 mimetics such as the Mcl-1 inhibitor S63845 in mesoporous silica nanoparticles (MSNs) that was actively targeted with a MUC1-targeting aptamer has been reported. These nanoparticles showed improvement in cellular toxicity and a decrease in thrombocytopenia (Vivo-Llorca *et al.*, 2020). In addition, Chen et al.(2016) fabricated navitoclax in nanoliposomes that was targeted with FH peptide and it showed also an

improvement in drug uptake and cellular toxicity (Chen *et al.*, 2016). Taken together, these data suggest a promising future for active targeting of BH3-mimetics in nanoparticles to treat cancer.

6.2. Future work

Although the results achieved here were very promising, further experiments are required to confirm the improved therapeutic index of the product. These were planned as part of this study but precluded by the COVID-19 pandemic which led to closure of key University facilities. Key experiments would have been to evaluate the activity of the nanoparticles *in vivo*, to see if they could have a synergistic anti-trumoural effect with carboplatin while reducing thrombocytopenia. In addition, adding paclitaxel to the combination of navitoclax and carboplatin could be tested as paclitaxel is considered a platelet sparing agent and increases the activity of the drug combination (Stamelos *et al*., 2013). Moreover, doing *in vivo* studies will be necessary to determine the pharmacokinetic and pharmacodynamic profiles of encapsulated navitoclax when it is encapsulated. This should be accompanied by investigation of platelets number in the blood circulation. Other *in vitro* experiments would also have been desirable. Using confocal microscopy will be very useful to give a full picture of the navitoclax nanoparticles drug uptake. Using other hydrophobic moieties with different molar ratios could be examined. Since there was a synergy between navitoclax and carboplatin, co-encapsulation of both drugs together could be explored, similar to that done with navitoclax and doxorubicin in ultra-pH sensitive nanovesicle (Ding *et al.*, 2020). Although we have investigated the role of receptor mediated endocytosis in navitoclax nanoparticles internalization using folic acid competition assay, this could be further investigated by demonstrating the effect of temperature on receptor mediated

endocytosis (Muralidharan *et al.*, 2016). Moreover, to confirm that the internalization happened through receptor mediated endocytosis or though other mechanism such as micropinocytosis or dynamin-dependent endocytosis which could be investigated by using two molecules to inhibit these mechanisms such as EIPA, a selective blocker of the Na+/H+ anti-port, which inhibits micropinocytosis or Dynasore which inhibits dynamin-dependent endocytosis (Tsolou *et al.*, 2020). Finally, use of siRNA to knockdown express of the folate receptor, and determine whether this affects uptake, deserves exploration.

References

1. Abbasi E, Aval SF, Akbarzadeh A, et al., 2014. Dendrimers : synthesis , applications , and properties. Nanoscale Research Letters, 9(1), p. 247. DOI: 10.1186/1556-276x-9-247.

2. Abdelwahed W, Degobert G, Stainmesse S, Fessi H, 2006. Freeze-drying of nanoparticles: formulation, process and storage considerations. Advanced Drug Delivery Reviews, 58(15), pp. 1688–1713. DOI: 10.1016/j.addr.2006.09.017.

3. Abed MN, Abdullah MI, Richardson A, 2016. Antagonism of Bcl-XL is necessary for synergy between carboplatin and BH3 mimetics in ovarian cancer cells. Journal of Ovarian Research, 9(1), pp. 1–9. doi: 10.1186/s13048-016-0234-y.

4. Ackler S, Mitten MJ, Chen J, Clarin J, Foster K, Jin S, Phillips DC, Schlessinger S, Wang B, Leverson JD, Boghaert ER, 2012. Navitoclax (ABT-263) and bendamustine ± rituximab induce enhanced killing of non-Hodgkin's lymphoma tumours in vivo. British Journal of Pharmacology, 167(4), pp. 881-891. doi: 10.1111/j.1476-5381.2012.02048.x.

5. Adams JM, 2012. Therapeutic potential of a peptide targeting BCL-2 cell guardians in cancer. Journal of Clinical Investigation, 122(6), pp. 1965–1967. doi: 10.1172/JCI64120.

6. Adams JM, Cory S, 2018. The BCL-2 arbiters of apoptosis and their growing role as cancer targets. Nature Publishing Group, 25(1), pp. 27–36. doi: 10.1038/cdd.2017.161.

7. Afreen S, Bohler S, Müller A, Demmerath EM, Weiss JM, Jutzi JS,

Schachtrup K, Kunze M, Erlacher M, 2020. BCL-XL expression is essential for human erythropoiesis and engraftment of hematopoietic stem cells. Cell Death and Disease, 11(1), p. 8. doi: 10.1038/s41419-019-2203-z.

8. Agrawal, Y. and Patel, V., 2011. Nanosuspension: An approach to enhance solubility of drugs. Journal of Advanced Pharmaceutical Technology & Research, 2(2), p. 81. doi: 10.4103/2231-4040.82950.

9. Al-naggar, R. A., Osman MT, Bobryshev YV., Yasmin S, Kadir A, 2013. Ovarian Cancer : Knowledge of Risk Factors and Symptoms among Working Malaysian Women, Middle-East Journal of Scientific Research, 14(4), pp. 549–553. doi: 10.5829/idosi.mejsr.2013.14.4.7365.

10. Alsuraifi A, Lin PKT, Curtis A, Lamprou DA, Hoskins C, 2018. A Novel PAA Derivative with Enhanced Drug Efficacy in Pancreatic Cancer Cell Lines. Pharmaceuticals; 11(4), p. 91. https://doi.org/10.3390/ph11040091.

11. Al Ameri J, Alsuraifi A, Curtis A, Hoskins C. 2020. Effect of Poly(allylamine) Molecular Weight on Drug Loading and Release Abilities of Nano-Aggregates for Potential in Cancer Nanomedicine', Journal of Pharmaceutical Sciences, 109(10), pp. 3125-3133. doi: 10.1016/j.xphs.2020.06.018.

12. American Cancer Society, 2016. Causes , Risk Factors , and Prevention What Are the Risk Factors for Ovarian Cancer ? Gynecologic surgery.

13. Amptoulach, S. and Tsavaris, N., 2011. Neurotoxicity Caused by the Treatment with Platinum Analogues, Chemotherapy Research and Practice, 2011, pp. 1–5. doi: 10.1155/2011/843019.

14. Anarjan, F.S., 2019. Active targeting drug delivery nanocarriers: Ligands. Nano-Structures & Nano-Objects, 19, p.100370. doi:

10.1016/j.nanoso.2019.100370.

15. Anees, M., Masood, MI, Ilyas M, Hussain T, Ammad M, 2016. NANOPARTICLES AS A NOVEL DRUG DELIVERY SYSTEM : A Review', Pakistan journal of pharmaceutical research, 2(2), pp. 160–167. DOI: 10.22200/pjpr.20162160-167.

16. Anilkumar, U. and Prehn, J. H. M., 2014. Anti-apoptotic BCL-2 family proteins in acute neural injury. Frontiers in Cellular Neuroscience, 8, p. 281. doi: 10.3389/fncel.2014.00281.

17. Anvekar RA, Asciolla JJ, Missert DJ, Chipuk JE, 2011. Born to be Alive : A Role for the BCL-2 Family in Melanoma Tumor Cell Born to be alive : a role for the BCL-2 family in melanoma tumor cell survival , apoptosis , and treatment. Frontiers in Oncology, 1(34), p. 34. doi: 10.3389/fonc.2011.00034.

18. Ashkenazi A, Fairbrother WJ, Leverson JD, Souers AJ., 2017. From basic apoptosis discoveries to advanced selective BCL-2 family inhibitors. Nature Publishing Group, 16(4), pp. 273-284. doi: 10.1038/nrd.2016.253.

19. Aslan B, Ozpolat B, Sood AK, Lopez-Berestein G., 2013. Nanotechnology in cancer therapy. journal of drug targeting, 21(10), pp. 904-13. doi: 10.3109/1061186X.2013.837469.

20. Attia MF, Anton N, Wallyn J, Omran Z, Vandamme TF., 2019. An overview of active and passive targeting strategies to improve the nanocarriers efficiency to tumour sites', Journal of Pharmacy and Pharmacology, 71(8), pp. 1185–1198. doi: 10.1111/jphp.13098.

21. Bankhead, C., Collins, C., Stokes-Lampard, H., Rose, P., Wilson, S., Clements, A., Mant, D., Kehoe, S. and Austoker, J., 2008. Identifying symptoms of ovarian cancer : a qualitative and quantitative study. BJOG: An International

Journal of Obstetrics & Gynaecology, 115, pp. 1008–1014. doi: 10.1111/j.1471-0528.2008.01772.x.

22. Barani M, Bilal M, Sabir F, Rahdar A, Kyzas GZ, 2020. Nanotechnology in ovarian cancer : Diagnosis and treatment', Life Sciences. Elsevier Inc., 266, p. 118914. doi: 10.1016/j.lfs.2020.118914.

23. Barnett CM, Lees MR, Curtis ADM, Lin PKT, Cheng WP & Hoskins C, 2013. Poly (allylamine) Magnetomicelles for Image Guided Drug Delivery, Pharmaceutical Nanotechnology, 1(3), pp. 224–238. https://doi.org/10.2174/22117385113019990002

24. Bartouskova M, Melichar B. and Mohelnikova-Duchonova B, 2015. Folate receptor: A potential target in ovarian cancer. Pteridines, 26(1), pp. 1–12. doi: 10.1515/pterid-2014-0013.

25. Basal E, Eghbali-Fatourechi GZ, Kalli KR, Hartmann LC, Goodman KM, et al., 2009. Functional folate receptor alpha is elevated in the blood of ovarian cancer patients. PLoS ONE, 4(7), pp. 1–7. doi: 10.1371/journal.pone.0006292.

26. Basourakos SP, Li L, Aparicio AM, Corn PG, Kim J, Thompson TC., 2016. Combination Platinum-based and DNA Damage Response-targeting Cancer Therapy: Evolution and Future Directions. Current Medicinal Chemistry, 24(15), pp. 1586–1606. doi: 10.2174/0929867323666161214114948.

27. Bauerschlag DO, Hilpert F, Meinhold-Heerlein I, Jonat W, Pfisterer J, 2007. First-line Chemotherapy in Patients with Advanced Ovarian Cancer. Oncology & Hematology Review (US), 1 (2), p. 71. doi: 10.17925/ohr.2007.00.2.71.

28. Bazak R, Houri M, El Achy S, Kamel S, Refaat T, 2016. Cancer active targeting by nanoparticles: a comprehensive review of literature Remon. J

Cancer Res Clin Oncol, 141(5), pp. 769–784. doi: 10.1007/s00432-014-1767-3.Cancer.

29. Behera, A. and Padhi, S., 2020. Passive and active targeting strategies for the delivery of the camptothecin anticancer drug: a review. Environmental Chemistry Letters. Springer International Publishing, 18(5), pp. 1557–1567. doi: 10.1007/s10311-020-01022-9.

30. Berek JS, Kehoe ST, Kumar L, Friedlander M., 2018. Cancer of the ovary , fallopian tube , and peritoneum. Int J Gynaecol Obstet., 143 Suppl 2, pp. 59–78. doi: 10.1002/ijgo.12614.

31. Bhatla, N. and Jones., A., 2018. The World Ovarian Cancer Coalition Atlas. World Ovarian Cancer Coalition, 2018, pp. 1–39. Available at: https://worldovariancancercoalition.org/wp-content/uploads/2018/10/THE-WORLD-OVARIAN-CANCER-COALITION-ATLAS-2018.pdf.

32. Bhattacharjee, S., 2016. DLS and zeta potential - What they are and what they are not?. Journal of Controlled Release, 235, pp. 337–351. doi: 10.1016/j.jconrel.2016.06.017.

33. Billard, C., 2013. BH3 mimetics: Status of the field and new developments. Molecular Cancer Therapeutics, 12(9), pp. 1691–1700. doi: 10.1158/1535-7163.MCT-13-0058.

34. Binju M, Amaya-Padilla MA, Wan G, Gunosewoyo H, Suryo Rahmanto Y, Yu Y., 2019. Therapeutic inducers of apoptosis in ovarian cancer. Cancers, 11(11), p. 1786. doi: 10.3390/cancers11111786.

35. BLANCO, M. D., TEIJÓN C, OLMO RM, TEIJÓN J. M, 2012. Targeted Nanoparticles for Cancer Therapy, in Recent Advances in Novel Drug Carrier Systems, pp. 604–609. doi: 10.5772/711.

36. Boiani M, Daniel C, Liu X, Hogarty MD, Marnett LJ., 2013. The Stress Protein BAG3 Stabilizes Mcl-1 Protein and Promotes Survival of Cancer Cells and Resistance to antagonist ABT-737. J Biol Chem, 288(10), PP. 6980-90. doi: 10.1074/jbc.M112.414177.

37. Bowtell DD, Böhm S, Ahmed AA, Aspuria P-J, Bast RC, Beral V, et al., 2015. Rethinking ovarian cancer II: reducing mortality from high-grade serous ovarian cancer. Nat Rev Cancer.1 5(11), PP. 668–79. doi: 10.1038/nrc4019.Rethinking.

38. Brett M. R, Jennifer B. P, Thomas A. S, Brett M. R, Jennifer B. P, Thomas A. S., 2017. Epidemiology of ovarian cancer: a review. Cancer Biology & Medicine, 14(1), pp. 9–32. doi: 10.20892/j.issn.2095-3941.2016.0084.

39. Brotin E, Meryet-Figuière M, Simonin K, Duval RE, Villedieu M, Leroy-Dudal J, et al., 2010. Bcl-xLand MCL-1 constitute pertinent targets in ovarian carcinoma and their concomitant inhibition is sufficient to induce apoptosis. International Journal of Cancer, 126(4), pp. 885–895. doi: 10.1002/ijc.24787.

40. Broxterman, H. J., Gotink, K. J. and Verheul, H. M. W., 2009. Understanding the causes of multidrug resistance in cancer: a comparison of doxorubicin and sunitinib. Drug Resistance Updates, 12(4–5), pp. 114–126. doi: 10.1016/j.drup.2009.07.001.

41. Bruno, P., Liu, Y., Park, G. et al., 2017. A subset of platinum-containing chemotherapeutic agents kill cells by inducing ribosome biogenesis stress rather than by engaging a DNA damage response. Nat Med., 23(4), pp. 461–471. doi: 10.1038/nm.4291.A.

42. Bykov VJN, Eriksson SE, Bianchi J, Wiman KG., 2017. Targeting mutant p53 for efficient cancer therapy. Nat Rev Cancer, 18(2), pp. 89–102. doi:

10.1038/nrc.2017.109.

43. Campbell, K. J. and Tait, S. W. G., 2018. Targeting BCL-2 regulated apoptosis in cancer. Open Biol, 8(5), P. 180002. doi: 10.1098/rsob.180002.

44. Cazzaniga ME, Mustacchi G, Pronzato P, De Matteis A, Di Costanzo F, Floriani I., 2007. Adjuvant treatment of early breast cancer: do the St Gallen recommendations influence clinical practice? Results from the NORA study. Annals of oncology : official journal of the European Society for Medical Oncology / ESMO, 18(12), pp. 1976–1980. doi: 10.1093/annonc/mdm365.

45. CEPHAM LIFE SCIENCES, 2019. SRB Cytotoxicity Assay. Available at: https://www.cephamls.com/srb-cytotoxicity-assay-kit-colorimetric/ (Accessed: 3 July 2020).

46. Cerella, C., Dicato, M. and Diederich, M., 2020. BH3 Mimetics in AML Therapy: Death and Beyond?', Trends in Pharmacological Sciences, 41(11), pp. 793–814. doi: 10.1016/j.tips.2020.09.004.

47. Cerqueira NM, Oliveira EF, Gesto DS, Santos-Martins D, Moreira C, Moorthy HN, Ramos MJ, Fernandes PA., 2016. Cholesterol Biosynthesis: A Mechanistic Overview. Biochemistry, 55(39), PP. 5483-5506. doi: 10.1021/acs.biochem.6b00342.

48. Certo M, Moore VDG, Nishino M, Wei G, Korsmeyer S, Armstrong SA, et al., 2006. Mitochondria primed by death signals determine cellular addiction to antiapoptotic BCL-2 family members. Cancer Cell, 9(5), pp. 351–365. doi: 10.1016/j.ccr.2006.03.027.

49. Chen B, Wang Z, Sun J, Song Q, et al., 2016. A tenascin C targeted nanoliposome with navitoclax for specifically eradicating of cancer-associated fibroblasts. Nanomedicine: Nanotechnology, Biology, and Medicine. Elsevier

B.V., 12(1), pp. 131–141. doi: 10.1016/j.nano.2015.10.001.

50. Chen VW, Ruiz B, Killeen JL, Coté TR, Wu XC, Correa CN., 2003. Pathology and classification of ovarian tumors. Cancer, 97(10 Suppl), pp. 2631–2642. doi: 10.1002/cncr.11345.

51. Cheung A, Bax HJ, Josephs DH, Ilieva KM, Pellizzari G, Opzoomer J, Bloomfield J, Fittall M, Grigoriadis A, Figini M, Canevari S, Spicer JF, Tutt AN, Karagiannis SN., 2016. Targeting folate receptor alpha for cancer treatment. Oncotarget, 7(32), PP. 52553-52574. doi: 10.18632/oncotarget.9651.

52. Chien J, Kuang R, Landen C, Shridhar V., 2013. Platinum-sensitive recurrence in ovarian cancer: The role of tumor microenvironment. Frontiers in Oncology, 3 (September), pp. 1–6. doi: 10.3389/fonc.2013.00251.

53. Chinen AB, Guan CM, Ferrer JR, Barnaby SN, Merkel TJ, Mirkin CA., 2015. Nanoparticle Probes for the Detection of Cancer Biomarkers , Cells , and Tissues by Fluorescence. Chem Rev., 115(19), PP. 10530-74.doi: 10.1021/acs.chemrev.5b00321.

54. Choi J-H, Wong AST, Huang H-F, Leung PCK., 2007. Gonadotropins and ovarian cancer. Endocrine Reviews, 28(4), pp. 440–461. doi: 10.1210/er.2006-0036.

55. Chong SJF, Marchi S, Petroni G, Kroemer G, Galluzzi L, Pervaiz S., 2020. Noncanonical Cell Fate Regulation by Bcl-2 Proteins. Trends in Cell Biology. Elsevier Ltd, 30(7), pp. 537-555. doi: 10.1016/j.tcb.2020.03.004.

56. Choo EF, Boggs J, Zhu C, Lubach JW, Catron ND, Jenkins G, Souers AJ, Voorman R., 2014. The Role of Lymphatic Transport on the Systemic Bioavailability of the Bcl-2 Protein Family Inhibitors Navitoclax (ABT-263) and ABT-199. Drug Metab Dispos., 42(2), pp. 207–212. doi:

10.1124/dmd.113.055053.

57. Christie, E. L. and Bowtell, D. D. L., 2017. Acquired chemotherapy resistance in ovarian cancer. Ann Oncol., 28(Supplement 8). PP. viii13-viii15. doi: 10.1093/annonc/mdx446.

58. Cimino, G. D., Pan, C. and Henderson, P. T., 2013. Personalized medicine for targeted and platinum-based chemotherapy of lung and bladder cancer. Bioanalysis, 5(3), pp. 369–391. doi: 10.4155/bio.12.325.

59. Clemons TD, Singh R, Sorolla A, Chaudhari N, Hubbard A, Iyer KS., 2018. Distinction between Active and Passive Targeting of Nanoparticles Dictate Their Overall Therapeutic Efficacy. Langmuir, 34(50), pp. 15343–15349. doi: 10.1021/acs.langmuir.8b02946.

60. Cohen K, Emmanuel R, Kisin-Finfer E, Shabat D, Peer D., 2014. Modulation of drug resistance in ovarian adenocarcinoma using chemotherapy entrapped in hyaluronan-grafted nanoparticle clusters. ACS Nano, 8(3), pp. 2183–2195. doi: 10.1021/nn500205b.

61. Cortez AJ, Tudrej P, Kujawa KA, Lisowska KM., 2018. Advances in ovarian cancer therapy. Cancer Chemotherapy and Pharmacology. Springer Berlin Heidelberg, 81(1), pp. 17–38. doi: 10.1007/s00280-017-3501-8.

62. Coskun, O., 2016. Separation techniques: Chromatography. Northern Clinics of Istanbul, 3(2), pp. 156–160. doi: 10.14744/nci.2016.32757.

63. Critical micelle concentration (CMC) and surfactant concentration | KRÜSS Scientific, no date. Available at: https://www.kruss-scientific.com/en/know-how/glossary/critical-micelle-concentration-cmc-and-surfactant-concentration (Accessed: 30 August 2020).

64. Cruet-Hennequart S, Glynn MT, Murillo LS, Coyne S, Carty MP., 2008.

Enhanced DNA-PK-mediated RPA2 hyperphosphorylation in DNA polymerase η-deficient human cells treated with cisplatin and oxaliplatin. DNA Repair, 7(4), pp. 582–596. doi: 10.1016/j.dnarep.2007.12.012.

65. Cuong, N. Van, Hsieh MF, Chen, YT, Liau, I., 2011. Doxorubicin-loaded nanosized micelles of a star-shaped poly(ε- caprolactone)-polyphosphoester block co-polymer for treatment of human breast cancer. Journal of Biomaterials Science, Polymer Edition, 22(11), pp. 1409–1426. doi: 10.1163/092050610X510533.

66. Czaplicki, S., 2013. Chromatography in bioactivity analysis of compounds. *Column chromatography*, pp.99-122. doi: 10.5772/55620.

67. Das, P. M. and Bast Jr, R. C., 2008. Early detection of ovarian cancer. Biomark Med., 2(3), pp. 291–303. doi: 10.2217/17520363.2.3.291.

68. Dasari, S. and Bernard Tchounwou, P., 2014. Cisplatin in cancer therapy: Molecular mechanisms of action. European Journal of Pharmacology, 740, pp. 364–378. doi: 10.1016/j.ejphar.2014.07.025.

69. Davids, M. S. and Letai, A., 2012. Targeting the B-cell lymphoma/leukemia 2 family in cancer. Journal of Clinical Oncology, 30(25), pp. 3127–3135. doi: 10.1200/JCO.2011.37.0981.

70. Delbridge, A. R. D. and Strasser, A., 2015. The BCL-2 protein family, BH3-mimetics and cancer therapy. Cell Death and Differentiation, 22(7), pp. 1071–1080. doi: 10.1038/cdd.2015.50.

71. Ding J, Zhang X, Chen C, Huang Y, Yu X, Li X., 2020. Ultra pH-sensitive polymeric nanovesicles co-deliver doxorubicin and navitoclax for synergetic therapy of endometrial carcinoma. Biomaterials Science. Royal Society of Chemistry, 8(8), pp. 2264–2273. doi: 10.1039/d0bm00112k.

72. Diniz PM, Carvalho JP, Baracat EC, Carvalho FM., 2011. Fallopian tube origin of supposed ovarian high-grade serous carcinomas. Clinics, 66(1), pp. 73–76. doi: 10.1590/S1807-59322011000100013.

73. Dinkelspiel HE, Tergas AI, Zimmerman LA, Burke WM, Hou JY, Chen L, Hillyer G, Neugut AI, Hershman DL, Wright JD, 2015. Use and duration of chemotherapy and its impact on survival in early-stage ovarian cancer. Gynecologic Oncology. Elsevier Inc., 137(2), pp. 203–209. doi: 10.1016/j.ygyno.2015.02.013.

74. Donati, A. and Castro, L. G. M., 2011. Cutaneous adverse reactions to chemotherapy with taxanes . The dermatologist ' s point of view. An Bras Dermatol., 86(4), pp. 755–758. English, Portuguese.doi: 10.1590/S0365-05962011000400020.

75. Dong, M., 2019. HPLC Applications in Food, Environmental, Chemical, and Life Sciences Analysis. HPLC and UHPLC for Practicing Scientists, pp. 335–369. doi: 10.1002/9781119313786.ch13.

76. Doubeni CA, Doubeni ARB, M. A., 2016. Diagnosis and Management of Ovarian Disorders. American Family Physician, 93(11), pp. 937–944. doi: 10.1016/B978-012053642-9/50043-0.

77. Du YZ, Wang L, Yuan H, Wei XH, Hu FQ, 2009. Preparation and characteristics of linoleic acid-grafted chitosan oligosaccharide micelles as a carrier for doxorubicin. Colloids and Surfaces B: Biointerfaces, 69(2), pp. 257–263. doi: 10.1016/j.colsurfb.2008.11.030.

78. Eckstein, N., 2011. Platinum resistance in breast and ovarian cancer cell lines. Journal of Experimental & Clinical Cancer Research, 30(1), p. 91. doi: 10.1186/1756-9966-30-91.

79. Engelberth, S. A., Hempel, N. and Bergkvist, M., 2014. Development of Nanoscale Approaches for Ovarian Cancer Therapeutics and Diagnostics. Critical reviews in oncogenesis, 19 (3-4), pp. 281–316. Available at: https://doi.org/10.1615/CritRevOncog.2014011455

80. Erickson, B. K., Conner, M. G. and Jr, C. N. L., 2013. The role of the fallopian tube in the origin of ovarian cancer. The American Journal of Obstetrics & Gynecology, 209(5), pp. 409–414. doi: 10.1016/j.ajog.2013.04.019.

81. Erlanson, D., Fesik, S., Hubbard, R. et al., 2016. Twenty years on : the impact of fragments on drug discovery', Nat Rev Drug Discov, 15(9), pp. 605–619. doi: 10.1038/nrd.2016.109.

82. Esim O, Gumustas M, Hascicek C, Ozkan SA, 2020. A novel stability-indicating analytical method development for simultaneous determination of carboplatin and decitabine from nanoparticles. Journal of Separation Science, 43 (17), pp. 3491-3498. doi: 10.1002/jssc.202000320.

83. Fathalla MF., 2013. Incessant ovulation and ovarian cancer – a hypothesis re-visited. Facts, views Vis ObGyn, 5(4), pp. 292–297. Available from: http://www.ncbi.nlm.nih.gov/pubmed/24753957%0Ahttp://www.pubmedcentral.nih.gov/articlerender.fcgi?artid=PMC3987381.

84. Fay, F. and Scott, C. J., 2011. Antibody-targeted nanoparticles for cancer therapy. Immunotherapy, 3(3), pp. 381–394. doi: 10.2217/imt.11.5.

85. Fernández, M., Javaid, F. and Chudasama, V., 2018. Advances in targeting the folate receptor in the treatment/imaging of cancers. Chemical Science, 9(4), pp. 790–810. doi: 10.1039/c7sc04004k.

86. Fonseca, A. C., Serra, A. C. and Coelho, J. F. J., 2015. Bioabsorbable

polymers in cancer therapy: Latest developments. EPMA Journal, 6(1), pp. 1–18. doi: 10.1186/s13167-015-0045-z.

87. Foster T, Brown TM, Chang J, Menssen HD, Blieden MB, Herzog TJ., 2009. A review of the current evidence for maintenance therapy in ovarian cancer. Gynecologic Oncology, 115(2), pp. 290–301. doi: 10.1016/j.ygyno.2009.07.026.

88. Fotopoulou C, Hall M, Cruickshank D, Gabra H, Ganesan R, Hughes C, Kehoe S, Ledermann J, Morrison J, Naik R, Rolland P, Sundar S., 2014. British Gynaecological Cancer Society (BGCS) Epithelial Ovarian / Fallopian Tube / Primary Peritoneal Cancer Guidelines : Recommendations for Practice. Eur J Obstet Gynecol Reprod Biol, 213, pp. 123-139. doi: 10.1016/j.ejogrb.2017.04.016.

89. Fukada I, Araki K, Kobayashi K, Kobayashi T, Horii R, Akiyama F, et al., 2016. Therapeutic effect of taxanes on metastatic breast cancer of various immunohistochemical subtypes. Oncology Letters, 12(1), pp. 663–669. doi: 10.3892/ol.2016.4627.

90. Gadducci A, Guarneri V, Peccatori FA, Ronzino G, Scandurra G, Zamagni C, Zola P, Salutari V., 2019. Current strategies for the targeted treatment of high-grade serous epithelial ovarian cancer and relevance of BRCA mutational status. Journal of Ovarian Research, 12(1), p. 9. doi: 10.1186/s13048-019-0484-6.

91. Gajjar K, Ogden G, Mujahid MI, Razvi K., 2012. Symptoms and Risk Factors of Ovarian Cancer: A Survey in Primary Care. ISRN Obstetrics and Gynecology, 2012, p. 754197. doi: 10.5402/2012/754197.

92. Galluzzi L, Senovilla L, Vitale I, Michels J, Martins I, Kepp O, et al., 2012.

Molecular mechanisms of cisplatin resistance. Oncogene, 31(15), pp. 1869–1883. doi: 10.1038/onc.2011.384.

93. Ganesan, A. and Barakat, K., 2017. Solubility : A speed – breaker on the drug discovery highway. MOJ Bioequiv Availab, 3(3), pp. 56–58. doi: 10.15406/mojbb.2017.03.00033.

94. Gao Y, Xie J, Chen H, Gu S, Zhao R, Shao J, Jia L., 2013. Nanotechnology-based intelligent drug design for cancer metastasis treatment. Biotechnology Advances, 32(4), pp. 761-777. doi: 10.1016/j.biotechadv.2013.10.013.

95. Garcia-Bennett, A., Nees, M. and Fadeel, B., 2011. In search of the Holy Grail: Folate-targeted nanoparticles for cancer therapy. Biochemical Pharmacology, 81(8), pp. 976–984. doi: 10.1016/j.bcp.2011.01.023.

96. Gerendash, B. S. and Creel, P. A., 2017. Practical management of adverse events associated with cabozantinib treatment in patients with renal-cell carcinoma. OncoTargets and Therapy, 10, pp. 5053–5064. doi: 10.2147/OTT.S145295.

97. Giornelli, G. H., 2016. Management of relapsed ovarian cancer : a review. SpringerPlus, 5(1), p.1197. doi: 10.1186/s40064-016-2660-0.

98. Gmeiner, W. H. and Ghosh, S., 2014. Nanotechnology for cancer treatment. Nanotechnology Reviews, 3(2), pp. 111–122. doi: 10.1515/ntrev-2013-0013.

99. GOFF, B., 2012. Symptoms Associated With Ovarian Cancer. Clinical Obstetrics and Gynecology, 55(1), pp. 36–42. doi: 10.1097/GRF.0b013e3182480523.

100. Goff, B. A., Mandel L.S., Melancon, C.H., Muntz, H.G., 2004. Frequency

of Symptoms of Ovarian Cancer in Women Presenting to Primary Care Clinics. JAMA, 291(22), pp. 2705–2712. Available from: http://jama.jamanetwork.com/article.aspx?doi=10.1001/jama.291.22.2705

101. Goff BA, Mandel LS, Drescher CW, Urban N, Gough S, Schurman KM, Patras J, Mahony BS, Andersen MR., 2006. Development of an Ovarian Cancer Symptom Index Possibilities for Earlier Detection. Cancer, 109(2), pp. 221-227. doi: 10.1002/cncr.22371.

102. Gómez-Hidalgo NR, Martinez-Cannon BA, Nick AM, Lu KH, Sood AK, Coleman RL, Ramirez PT., 2015. Predictors of optimal cytoreduction in patients with newly diagnosed advanced-stage epithelial ovarian cancer: Time to incorporate laparoscopic assessment into the standard of care. Gynecol Oncol, 137(3), pp. 553–558. doi: 10.1016/j.ygyno.2015.03.049.

103. González-Gualda E, Pàez-Ribes M, Lozano-Torres B, Macias D, Wilson JR 3rd, González-López C, Ou HL, Mirón-Barroso S, Zhang Z, Lérida-Viso A, Blandez JF, Bernardos A, Sancenón F, Rovira M, Fruk L, Martins CP, Serrano M, Doherty GJ, Martínez-Máñez R, Muñoz-Espín D., 2020. Galacto-conjugation of Navitoclax as an efficient strategy to increase senolytic specificity and reduce platelet toxicity. Aging Cell, 19(4), p. e13142. doi: 10.1111/acel.13142.

104. Goyal, L. D., Kaur, B. and Badyal, R. K., 2019. Malignant mixed germ cell tumors of the ovary: A series of rare cases. Journal of Reproduction and Infertility, 20(4), pp. 231–236.

105. Greenberg, E. F., Lavik, A. R. and Distelhorst, C. W., 2014. Bcl-2 regulation of the inositol 1,4,5-trisphosphate receptor and calcium signaling in normal and malignant lymphocytes: Potential new target for cancer treatment. Biochimica et Biophysica Acta - Molecular Cell Research, 1843(10), pp. 2205–

2210. doi: 10.1016/j.bbamcr.2014.03.008.

106. GU, F.X., KARNIK, R., WANG, A.Z., ALEXIS, F., LEVY-NISSENBAUM, E., HONG, S., LANGER, R.S. and FAROKHZAD, O.C., 2007. Targeted nanoparticles for cancer therapy. Nano Today, 2(3), pp. 14–21. doi: 10.1016/S1748-0132(07)70083-X.

107. Guarneri V, Piacentini F, Barbieri E, Conte PF., 2010. Achievements and unmet needs in the management of advanced ovarian cancer. Gynecologic Oncology, 117(2), pp. 152–158. doi: 10.1016/j.ygyno.2009.11.033.

108. Gubbels, J.A., Claussen, N., Kapur, A.K. et al., 2010. The detection, treatment, and biology of epithelial ovarian cancer, Journal of ovarian research, 3, p. 8. doi: doi: 10.1186/1757-2215-3-8.

109. Guerrero A, Guiho R, Herranz N, Uren A, Withers DJ, Martínez-Barbera JP, Tietze LF, Gil J., 2020. Galactose-modified duocarmycin prodrugs as senolytics. Aging Cell, 19(4), p. e13133. doi: 10.1111/acel.13133.

110. Gupta, S., Pathak, Y., Gupta, M.K. and Vyas, S.P., 2019. RETRACTED ARTICLE: Nanoscale drug delivery strategies for therapy of ovarian cancer: conventional vs targeted. Artificial cells, nanomedicine, and biotechnology, 47(1), pp.4066-4088. doi: 10.1080/21691401.2019.1677680.

111. Haddad, K., Le, T. and Acar, H., no date. Internalization of Folate Receptor Targeting Nanoparticles into Ovarian Cancer Cell Lines. Available at: https://2019.biomaterials.org/sites/default/files/abstracts/754.pdf

112. Hamilton, W. and Menon, U., 2010. EASILY MISSED? Ovarian cancer. BMJ, 340(7737), pp. 96–97. doi: 10.1136/bmj.b4650.

113. Hansen, E., Woods, R. J. and Read, A. F., 2017. How to Use a Chemotherapeutic Agent When Resistance to It Threatens the Patient. PLoS

Biol, 15(2), p. e2001110.. doi: 10.1371/journal.pbio.2001110.

114. Hartnett J, Thom B, Kline N., 2016. Caregiver Burden in End-Stage Ovarian Cancer. Clin J Oncol Nurs, 20(2), pp. 169–173. doi: 10.1188/16.CJON.169-173.

115. Hascicek, C. and Gun, O., 2017. Nano drug delivery systems for ovarian cancer therapy. Integrative Cancer Science and Therapeutics, 4(2), pp. 1–4. doi: 10.15761/ICST.1000235.

116. Hattori S, Kajiyama H, Fuji U, Furui Y, Ishibashi Y, Hattori Y, Takahashi N, Kikkawa F, Misawa T., 2016. Clinical characteristics of primary peritoneal carcinoma patients : a single-institution experience involving 8 patients. Nagoya J Med Sci, 78(4), pp. 407–414. doi: 10.18999/nagjms.78.4.407.

117. He Y, Zhang X, Chang J, Kim HN, Zhang P, Wang Y, Khan S, Liu X, Zhang X, Lv D, Song L, Li W, Thummuri D, Yuan Y, Wiegand JS, Ortiz YT, Budamagunta V, Elisseeff JH, Campisi J, Almeida M, Zheng G, Zhou D., 2020. Using proteolysis-targeting chimera technology to reduce navitoclax platelet toxicity and improve its senolytic activity', Nature Communications, 11(1), p. 1996. doi: 10.1038/s41467-020-15838-0.

118. Hekman MCH, Boerman OC, Bos DL, Massuger LFAG, Weil S, Grasso L, Rybinski KA, Oosterwijk E, Mulders PFA, Rijpkema M., 2017. Improved Intraoperative Detection of Ovarian Cancer by Folate Receptor Alpha Targeted Dual-Modality Imaging. Mol Pharm, 14(10), pp. 3457-3463. doi: 10.1021/acs.molpharmaceut.7b00464.

119. Henderson, J. T., Webber, E. M. and Sawaya, G. F. , 2018. Screening for Ovarian Cancer: An Updated Evidence Review for the U.S. Preventive Services Task Force [Internet]. Evidence Synthesis No. 157. Rockville (MD):

Agency for Healthcare Research and Quality (US).

120. Heurtault B, Saulnier P, Pech B, Proust JE, Benoit JP., 2003. Physico-chemical stability of colloidal lipid particles. Biomaterials, 24(23), pp. 4283–4300. doi: 10.1016/S0142-9612(03)00331-4.

121. Hirst, J., Crow, J. and Godwin, A., 2018. Ovarian Cancer Genetics: Subtypes and Risk Factors. Ovarian Cancer - From Pathogenesis to Treatment. IntechOpen. doi: 10.5772/intechopen.72705.

122. Hiss, D., 2012. Optimizing molecular-targeted therapies in ovarian cancer: The renewed surge of interest in ovarian cancer biomarkers and cell signaling pathways. Journal of Oncology, 2012, p. 737981. doi: 10.1155/2012/737981.

123. Horta, M. and Cunha, T. M., 2015. Sex cord-stromal tumors of the ovary: A comprehensive review and update for radiologists. Diagnostic and Interventional Radiology, 21(4), pp. 277–286. doi: 10.5152/dir.2015.34414.

124. Hoskins, C., Ouaissi, M., Lima, S. C., Cheng, W. P., Loureirio, I., Mas, E., et al., 2010. In vitro and in vivo anticancer activity of a novel nano-sized formulation based on self-assembling polymers against pancreatic cancer. Pharmaceutical Research, 27(12), pp. 2694–2703. doi: 10.1007/s11095-010-0268-6.

125. Hoskins, C, Kong Thoo Lin, P, Tetley, L & Cheng, WP, 2011. Novel fluorescent amphiphilic poly (allylamine) and their supramacromolecular self-assemblies in aqueous media. Polymers for Advanced Technologies, 23(3), pp. 710–719. doi: 10.1002/pat.1962.

126. Hoskins C, Lin PK, Tetley L, Cheng WP., 2011. The Use of Nano Polymeric Self-Assemblies Based on Novel Amphiphilic Polymers for Oral

Hydrophobic Drug Delivery. Pharm Res., 29(3), pp. 782–794. doi: 10.1007/s11095-011-0602-7.

127. Hoskins, C., 2020. Cancer Nanomedicine. Cancers, 12(8), p. 2127. doi: 10.3390/cancers12082127.

128. Hoskins, C., Thoo-Lin, P. K. and Cheng, W. P., 2012. A review on comb-shaped amphiphilic polymers for hydrophobic drug solubilization. Therapeutic Delivery, 3(1), pp. 59–79. DOI: 10.4155/tde.11.130.

129. Hoskins, W. J., 1993. Surgical staging and cytoreductive surgery of epithelial ovarian cancer. Cancer, 71(4 Suppl), pp. 1534–40. Available at: http://www.ncbi.nlm.nih.gov/pubmed/8431891.

130. Hulin-Curtis, S.L., Davies, J.A., Nestić, D. et al., 2020. Identification of folate receptor α (FRα) binding oligopeptides and their evaluation for targeted virotherapy 0applications. Cancer Gene Ther, 27, pp. 785–798. doi: 10.1038/s41417-019-0156-0.

131. Hussein, Y. H. A. and Youssry, M., 2018. Polymeric Micelles of Biodegradable Diblock Copolymers : Enhanced Encapsulation of Hydrophobic Drugs. Materials, 11(5), p. 688. doi: 10.3390/ma11050688.

132. Indran IR, Tufo G, Pervaiz S, Brenner C., 2011 . Recent advances in apoptosis, mitochondria and drug resistance in cancer cells. Biochimica et Biophysica Acta - Bioenergetics, 1807(6), pp. 735–745. doi: 10.1016/j.bbabio.2011.03.010.

133. Itani R, Al Faraj A., 2019. siRNA Conjugated Nanoparticles — A Next Generation Strategy to Treat Lung Cancer. Int J Mol Sci., 20(23), p. 6088. doi: 10.3390/ijms20236088.

134. Jain, H. V. and Meyer-Hermann, M., 2011. The molecular basis of

synergism between carboplatin and ABT-737 therapy targeting ovarian carcinomas. Cancer Research, 71(3), pp. 705–715. doi: 10.1158/0008-5472.CAN-10-3174.

135. Janbaz, K., Ashfaq, M., Qadir, M., Ahmad, B., 2013. Ovarian Cancer: Characteristics & Management. Advances in Cancer Research & Treatment, 2014 (2014). doi: 10.5171/2014.900592.

136. Jelovac, D. and Armstrong, D. K. D., 2011. Recent progress in the diagnosis and treatment of ovarian cancer. CA: a cancer journal for clinicians, 61(3), pp. 183–203. doi: 10.3322/caac.20113.

137. Jensen, M. M., Erichsen KD, Björkling F, Madsen J, Jensen PB, Sehested M, Højgaard L, Kjær A., 2013. Imaging of treatment response to the combination of carboplatin and paclitaxel in human ovarian cancer xenograft tumors in mice using FDG and FLT PET. PloS one, 8(12), p. e85126. doi: 10.1371/journal.pone.0085126.

138. Jessmon P, Boulanger T, Zhou W, Patwardhan P., 2017. Epidemiology and treatment patterns of epithelial ovarian cancer. Expert Review of Anticancer Therapy. Taylor & Francis, 17(5), pp. 427–437. doi: 10.1080/14737140.2017.1299575.

139. Jin H, Pi J, Yang F, Jiang J, Wang X, Bai H, Shao M, Huang L, Zhu H, Yang P, Li L, Li T, Cai J, Chen ZW., 2016. Folate-Chitosan Nanoparticles Loaded with Ursolic Acid Confer Anti-Breast Cancer Activities in vitro and in vivo. Scientific Reports. Nature Publishing Group, 6, p. 30782. doi: 10.1038/srep30782.

140. Johnstone, T. C., Park, G. Y. and Lippard, S. J., 2014. Understanding and improving platinum anticancer drugs - Phenanthriplatin. Anticancer

Research, 34(1), pp. 471–476. doi: 10.1016/j.micinf.2011.07.

141. Jones, P. M. and Drapkin, R.. 2013. Modeling high-grade serous carcinoma: How converging insights into pathogenesis and genetics are driving better experimental platforms. Frontiers in Oncology, 3, p. 217. doi: 10.3389/fonc.2013.00217.

142. Jones SK, Sarkar A, Feldmann DP, Hoffmann P, Merkel OM., 2017. Revisiting the Value of Competition Assays in Folate Receptor-Mediated Drug Delivery. Biomaterials, 138, pp. 35–45. doi: 10.1016/j.biomaterials.2017.05.034.Revisiting.

143. Juin P, Geneste O, Gautier F, Depil S, Campone M., 2013. Decoding and unlocking the BCL-2 dependency of cancer cells. Nature Reviews Cancer, 13(7), pp. 455–465. doi: 10.1038/nrc3538.

144. Kabanov, A. V, Batrakova, E. V and Yu, V., 2002. Pluronic block copolymers as novel polymer therapeutics for drug and gene delivery. journal of controlled release, 82(2-3), pp. 189-212. Available at: https://doi.org/10.1016/S0168-3659(02)00009-3

145. Kaefer A, Yang J, Noertersheuser P, Mensing S, Humerickhouse R, Awni W, Xiong H., 2014. Mechanism - based pharmacokinetic / pharmacodynamic meta - analysis of navitoclax (ABT - 263) induced thrombocytopenia. Cancer Chemother Pharmacol, 74(3), pp. 593–602. doi: 10.1007/s00280-014-2530-9.

146. Kafshdooz L, Kafshdooz T, Razban Z, Akbarzadeh A., 2016. The application of gold nanoparticles as a promising therapeutic approach in breast and ovarian cancer The application of gold nanoparticles as a promising therapeutic approach in breast and ovarian cancer. Artif Cells Nanomed Biotechnol, 44(5), pp. 1222-1227. doi: 10.3109/21691401.2015.1029625.

147. Kale, J., Osterlund, E. J. and Andrews, D. W., 2017. BCL-2 family proteins : changing partners in the dance towards death. Cell Death Differ, 25, pp. 65-80. doi: 10.1038/cdd.2017.186.

148. Kalli KR, Oberg AL, Keeney GL, Christianson TJ, Low PS, Knutson KL, Hartmann LC., 2008. Folate receptor alpha as a tumor target in epithelial ovarian cancer. Gynecol Oncol, 108(3), pp. 619–626. doi: 10.1016/j.ygyno.2007.11.020.

149. Kampan NC, Madondo MT, McNally OM, Quinn M, Plebanski M., 2015. Paclitaxel and Its Evolving Role in the Management of Ovarian Cancer. Biomed Res Int, 2015, p. 413076. doi: 10.1155/2015/413076.

150. Kazakevich, Y. V. and LoBrutto, R., 2007. Part I: HPLC Theory and Practice. in HPLC for Pharmaceutical Scientists, pp. 1–23.

151. Keefe, A. D., Pai, S., & Ellington, A., 2010. Aptamers as therapeutics. *Nature reviews Drug discovery*, *9*(7), pp. 537-550. https://doi.org/10.1038/nrd3141

152. Kelland, L., 2007. The resurgence of platinum-based cancer chemotherapy. Nature Reviews Cancer, 7(8), pp. 573–584. doi: 10.1038/nrc2167.

153. Kellogg EH, Hejab NMA, Howes S, Northcote P, Miller JH, Díaz JF, Downing KH, Nogales E., 2017. Insights into the Distinct Mechanisms of Action of Taxane and Non-Taxane Microtubule Stabilizers from Cryo-EM Structures', Journal of Molecular Biology, 429(5), pp. 633–646. doi: 10.1016/j.jmb.2017.01.001.

154. Khiewvan B, Torigian DA, Emamzadehfard S, Paydary K, Salavati A, Houshmand S, Werner TJ, Alavi A, 2017. An update on the role of PET/CT and

PET/MRI in ovarian cancer. European Journal of Nuclear Medicine and Molecular Imaging, 44(6), pp. 1079–1091. doi: 10.1007/s00259-017-3638-z.

155. Khoshnevisan, K. and Barkhi, M., 2015. Information about Zeta Potential. DOI: 10.13140/RG.2.1.4554.3844

156. Kim, H. S. and Song, Y. S., 2009. International Federation of Gynecology and Obstetrics (FIGO) staging system revised : what should be considered critically for gynecologic cancer ?. J gynecol oncol, 20(3), pp. 135–136. doi: 10.3802/jgo.2009.20.3.135.

157. Kim J, Shim MK, Yang S, Moon Y, Song S, Choi J, Kim J, Kim K., 2020. Combination of cancer-specific prodrug nanoparticle with Bcl-2 inhibitor to overcome acquired drug resistance. Journal of Controlled Release, 330, pp. 920–932. doi: 10.1016/j.jconrel.2020.10.065.

158. Kipps TJ, Eradat H, Grosicki S, Catalano J, Cosolo W, Dyagil IS, Yalamanchili S, Chai A, Sahasranaman S, Punnoose E, Hurst D, Pylypenko H., 2015. A phase 2 study of the BH3 mimetic BCL2 inhibitor navitoclax (ABT-263) with or without rituximab, in previously untreated B-cell chronic lymphocytic leukemia. Leukemia and Lymphoma, 56(10), pp. 2826–2833. doi: 10.3109/10428194.2015.1030638.

159. Kivioja JL, Thanasopoulou A, Kumar A, Kontro M, Yadav B, Majumder MM, Javarappa KK, Eldfors S, Schwaller J, Porkka K, Heckman CA., 2019. Dasatinib and navitoclax act synergistically to target NUP98-NSD1 +/FLT3-ITD+ acute myeloid leukemia. Leukemia, 33(6), pp. 1360–1372. doi: 10.1038/s41375-018-0327-2.

160. Konopleva M, Pollyea DA, Potluri J, Chyla B, Hogdal L, Busman T, McKeegan E, Salem AH, Zhu M, Ricker JL, Blum W, DiNardo CD, Kadia T,

Dunbar M, Kirby R, Falotico N, Leverson J, Humerickhouse R, Mabry M, Stone R, Kantarjian H, Letai A., 2017. Efficacy and Biological Correlates of Response in a Phase II Study of Venetoclax Monotherapy in Patients with Acute Myelogenous Leukemia. Cancer Discov, 6(10), pp. 1106–1117. doi: 10.1158/2159-8290.CD-16-0313.

161. Krystofiak, E. S., Matson, V.Z., Steeber, D.A., Oliver, J.A., 2012. Elimination of tumor cells using folate receptor targeting by antibody-conjugated, gold-coated magnetite nanoparticles in a murine breast cancer model. Journal of Nanomaterials, 2012, pp.1-9. doi: 10.1155/2012/431012.

162. Kurman, R. J., 2018. Origin and molecular pathogenesis of ovarian high-grade serous carcinoma. Annals of Oncology, 24, pp.16-21. doi: 10.1093/annonc/mdt463.

163. Kurosaki A, Hasegawa K, Kato T, Abe K, Hanaoka T, Miyara A, O'Shannessy DJ, Somers EB, Yasuda M, Sekino T, Fujiwara K., 2016. Serum folate receptor alpha as a biomarker for ovarian cancer: Implications for diagnosis, prognosis and predicting its local tumor expression. Int J Cancer, 138(8), pp. 1994–2002. doi: 10.1002/ijc.29937.

164. Van de Laar, R. Zusterzeel PL, Van Gorp T, Buist MR, van Driel WJ, Gaarenstroom KN, Arts HJ, van Huisseling JC, Hermans RH, Pijnenborg JM, Schutter EM, Pelikan HM, Vollebergh JH, Engelen MJ, Inthout J, Kruitwagen RF, Massuger LF., 2014. Cytoreductive surgery followed by chemotherapy versus chemotherapy alone for recurrent platinum-sensitive epithelial ovarian cancer (SOCceR trial): A multicenter randomised controlled study'. BMC cCancer, 14, p.22. doi: 10.1186/1471-2407-14-22.

165. Labidi-Galy SI, Papp E, Hallberg D, Niknafs N, Adleff V, Noe M,

Bhattacharya R, Novak M, Jones S, Phallen J, Hruban CA, Hirsch MS, Lin DI, Schwartz L, Maire CL, Tille JC, Bowden M, Ayhan A, Wood LD, Scharpf RB, Kurman R, Wang TL, Shih IM, Karchin R, Drapkin R, Velculescu VE., 2017. High grade serous ovarian carcinomas originate in the fallopian tube. Nature Communications, 8(1), p. 1093. doi: 10.1038/s41467-017-00962-1.

166. Law, J., Yu, V. C. and Baksh, S., 2012. Modulator of Apoptosis 1 : A Highly Regulated RASSF1A-Interacting BH3-Like Protein. Mol Biol Int, 2012, p. 536802. doi: 10.1155/2012/536802.

167. Lech, K., 2018. High Performance Liquid Chromatography (HPLC). The Encyclopedia of Archaeological Sciences, pp. 1–7. doi: 10.1002/9781119188230.saseas0303.

168. Ledermann JA, Luvero D, Shafer A, O'Connor D, Mangili G, Friedlander M, Pfisterer J, Mirza MR, Kim JW, Alexandre J, Oza A, Brown J., 2014. Gynecologic cancer intergroup (GCIG) Consensus review for mucinous ovarian carcinoma. International Journal of Gynecological Cancer, 24(9), pp. S14–S19. doi: 10.1097/IGC.0000000000000296.

169. Ledermann, J. A., Canevari, S. and Thigpen, T., 2015. Targeting the folate receptor: Diagnostic and therapeutic approaches to personalize cancer treatments. Annals of Oncology, 26(10), pp. 2034–2043. doi: 10.1093/annonc/mdv250.

170. Lessene, G., Czabotar, P., Sleebs, B. et al., 2013. Structure-guided design of a selective BCL-XL inhibitor. Nature Chemical Biology, 9, pp. 390-397. doi: 10.1038/nchembio.1246.

171. Lindqvist LM, Heinlein M, Huang DC, Vaux DL., 2014. Prosurvival Bcl-2 family members affect autophagy only indirectly , by inhibiting Bax and Bak.

Proc Natl Acad Sci U S A, 111(23), pp. 8512-8517. doi: 10.1073/pnas.1406425111.

172. Liu, Q. and Wang, H.G., 2012. Anti-cancer drug discovery and development: Bcl-2 family small molecule inhibitors. Communicative & integrative biology, 5(6), pp. 557–65. doi: 10.4161/cib.21554.

173. Liu Z, Ding Y, Ye N, Wild C, Chen H, Zhou J., 2016. Direct Activation of Bax Protein for Cancer Therapy. Med Res Rev, 36(2), pp. 313–341. doi: 10.1002/med.21379.

174. Lombardo, D., Kiselev, M.A., Magazù, S. and Calandra, P., 2015. Amphiphiles self-assembly: basic concepts and future perspectives of supramolecular approaches. Advances in Condensed Matter Physics, 2015. doi: 10.1155/2015/151683.

175. Lopez J, Tait SW., 2015. Mitochondrial apoptosis : killing cancer using the enemy within. British Journal of Cancer, 112(6), pp. 957–962. doi: 10.1038/bjc.2015.85.

176. Di Lorenzo G, Ricci G, Severini GM, Romano F, Biffi S., 2018. Imaging and therapy of ovarian cancer: clinical application of nanoparticles and future perspectives. Theranostics, 8(16), pp. 4279-4294. doi: 10.7150/thno.26345.

177. Low, J. J. H., Ilancheran, A. and Ng, J. S., 2012. Malignant ovarian germ-cell tumours. Best Practice and Research: Clinical Obstetrics and Gynaecology, 26(3), pp. 347–355. doi: 10.1016/j.bpobgyn.2012.01.002.

178. Lu Y, Cuellar-Partida G, Painter JN, Nyholt DR. et al., 2015. Shared genetics underlying epidemiological association between endometriosis and ovarian cancer. Hum Mol Genet, 24(20), pp. 5955-5964. doi: 10.1093/hmg/ddv306.

179. Luqmani, Y. A., 2005. Mechanisms of Drug Resistance in Cancer Chemotherapy. medical principles and practice, 14(suppl 1), pp. 35-48. doi: 10.1159/000086183.

180. Luvero, D., Milani, A. and Ledermann, J. A., 2014. Treatment options in recurrent ovarian cancer: Latest evidence and clinical potential. Therapeutic Advances in Medical Oncology, 6(5), pp. 229–239. doi: 10.1177/1758834014544121.

181. Maeda, H. and Matsumura, Y., 1986. A new concept for macromolecular therapeutics in cancer chemotherapy: mechanism of tumoritropic accumulation of proteins and the antitumor agent smancs. Cancer Research, 46(12 Pt 1), pp. 6387–6392. Available at: http://www.ncbi.nlm.nih.gov/pubmed/2946403%5Cnhttp://www.ncbi.nlm.nih.gov/sites/entrez.

182. Malviya R, Bansal V, Pal O and Sharma P, 2010. High Performance Liquid Chromatography: A Short Review. Journal of Global Pharma Technology, 2, PP. 22-26.

183. Mang J, Merkle K, Heller M, Schüler J, Tolstov Y, Li J, Hohenfellner M, Duensing S., 2017. Molecular complexity of taxane-induced cytotoxicity in prostate cancer cells. Urologic Oncology: Seminars and Original Investigations. Elsevier, 35(1), pp. 32.e9-32.e16. doi: 10.1016/j.urolonc.2016.07.017.

184. Mansoori B, Mohammadi A, Davudian S, Shirjang S, Baradaran B., 2017. The Different Mechanisms of Cancer Drug Resistance : A Brief Review. Advanced pharmaceutical bulletin, 7(3), pp. 339–348. doi: 10.15171/apb.2017.041.

185. Mantia-Smaldone, G., Edward, R. p and Vlad, A., 2011. Targeted

treatment of recurrent platinum-resistant ovarian cancer : current and emerging therapies. cancer management and research, 3, pp.25-38. doi: 10.2147/CMR.S8759.

186. Marchetti C, Palaia I, Giorgini M, De Medici C, Iadarola R, Vertechy L, Domenici L, Di Donato V, Tomao F, Muzii L, Benedetti Panici P., 2014. Targeted drug delivery via folate receptors in recurrent ovarian cancer: A review. OncoTargets and Therapy, 7, pp. 1223–1236. doi: 10.2147/ott.s40947.

187. Markman JL, Rekechenetskiy A, Holler E, Ljubimova JY., 2013. Nanomedicine therapeutic approaches to overcome cancer drug resistance. Adv Drug Deliv Rev, 65(13-14), pp. 1866–1879. doi: 10.1016/j.addr.2013.09.019.

188. Marquez, R. and Xu, L., 2012. Autophagy-apoptosis toggle switch by Bcl-2:Beclin 1. Am J Cancer Res, 2(2), pp. 214–221. Available at: https://www.ncbi.nlm.nih.gov/pmc/articles/PMC3304572/pdf/ajcr0002-0214.pdf.

189. Martín-Cameán María, Delgado-Sánchez Elsa, Piñera Antonio, Diestro Maria Dolores, De Santiago Javier, Zapardiel Ignacio, 2016. The role of surgery in advanced epithelial ovarian cancer. Ecancermedicalscience, 10. doi: 10.3332/ecancer.2016.666.

190. Mason, K.D., Carpinelli, M.R., Fletcher, J.I., Collinge, J.E., Hilton, A.A., Ellis, S., Kelly, P.N., Ekert, P.G., Metcalf, D., Roberts, A.W. and Huang, D.C., 2007. Programmed anuclear cell death delimits platelet life span. Cell, 128(6), pp.1173-1186. doi: 10.1016/j.cell.2007.01.037.

191. Masood, A., Azmi, A.S. and Mohammad, R.M., 2011. Small molecule inhibitors of bcl-2 family proteins for pancreatic cancer therapy. Cancers, 3(2),

pp.1527-1549. doi: 10.3390/cancers3021527.

192. McGrogan, B.T., Gilmartin, B., Carney, D.N. and McCann, A., 2008. Taxanes, microtubules and chemoresistant breast cancer. Biochimica et Biophysica Acta (BBA)-Reviews on Cancer, 1785(2), pp.96-132. doi: 10.1016/j.bbcan.2007.10.004.

193. McLemore, M.R., Miaskowski, C., Aouizerat, B.E., Chen, L.M. and Dodd, M.J., 2009. Epidemiologic and genetic factors associated with ovarian cancer. Cancer nursing, 32(4), p.281. doi: 10.1097/NCC.0b013e31819d30d6.

194. McWhinney, S.R., Goldberg, R.M. and McLeod, H.L., 2009. Platinum neurotoxicity pharmacogenetics. Molecular cancer therapeutics, 8(1), pp.10-16. doi: 10.1158/1535-7163.MCT-08-0840.

195. Meng, F., Sun, Y., Lee, R.J., Wang, G., Zheng, X., Zhang, H., Fu, Y., Yan, G., Wang, Y., Deng, W. and Parks, E., 2019. Folate receptor-targeted albumin nanoparticles based on microfluidic technology to deliver cabazitaxel. Cancers, 11(10), p.1571. doi: 10.3390/cancers11101571.

196. Merino, D., Kelly, G.L., Lessene, G., Wei, A.H., Roberts, A.W. and Strasser, A., 2018. BH3-mimetic drugs: blazing the trail for new cancer medicines. Cancer cell, 34(6), pp.879-891. doi: 10.1016/j.ccell.2018.11.004.

197. Microamaze, 2015. Bicinchoninic acid (BCA) assay for proteins. Available at: http://microamaze.blogspot.com/2015/10/bicinchoninic-acid-bca-assay-for.html (Accessed: 12 August 2020).

198. Mikuła-Pietrasik, J., Witucka, A., Pakuła, M., Uruski, P., Begier-Krasińska, B., Niklas, A., Tykarski, A. and Książek, K., 2018. Comprehensive review on how platinum-and taxane-based chemotherapy of ovarian cancer affects biology of normal cells. Cellular and Molecular Life Sciences, 76(4),

pp.681-697. doi: 10.1007/s00018-018-2954-1.

199. Mills K and Fuh K., 2017. Recent Advances in Understanding, Diagnosing, and Treating Ovarian Cancer. F1000Research, 6, p. 84. doi: 10.12688/f1000research.9977.1.

200. Ming, M., Ma, Z.L., Xu, Y.T., Sun, F.Y. and Cui, X.H., 2017. Carboplatin-based Nanomedicine to Enhance the Anticancer Effect in SK-NEP-1 Wilms'Tumor Cells. Iranian journal of pharmaceutical research: IJPR, 16(4), p.1305. Available at: https://pubmed.ncbi.nlm.nih.gov/29552042/

201. Minisini, A.M., Tosti, A., Sobrero, A.F., Mansutti, M., Piraccini, B.M., Sacco, C. and Puglisi, F., 2003. Taxane-induced nail changes: incidence, clinical presentationand outcome. Annals of oncology, 14(2), pp.333-337. doi: 10.1093/annonc/mdg050.

202. ModePalli, N. and VeNugoPal, S.B., 2016. Clinicopathological study of surface epithelial tumours of the ovary: An institutional study. Journal of clinical and diagnostic research: JCDR, 10(10), p.EC01. doi: 10.7860/JCDR/2016/21741.8716.

203. Mohamad Anuar, N.N., Nor Hisam, N.S., Liew, S.L. and Ugusman, A., 2020. Clinical review: navitoclax as a pro-apoptotic and anti-fibrotic agent. Frontiers in Pharmacology, 11, p.1817. doi: 10.3389/fphar.2020.564108.

204. Mohanty, C., 2017. Improvement of Cancer Therapy by Nanotechnology. Virology & Immunology Journal Improvement, 1(3), p.000116. Available at: https://www.medwinpublishers.com/VIJ/VIJ16000116.pdf

205. Momenimovahed, Z., Tiznobaik, A., Taheri, S. and Salehiniya, H., 2019. Ovarian cancer in the world: epidemiology and risk factors. International journal of women's health, 11, p.287. doi: 10.2147/IJWH.S197604

206. Moncsek, A., Al-Suraih, M.S., Trussoni, C.E., O'Hara, S.P., Splinter, P.L., Zuber, C., Patsenker, E., Valli, P.V., Fingas, C.D., Weber, A. and Zhu, Y., 2018. Targeting senescent cholangiocytes and activated fibroblasts with B-cell lymphoma-extra large inhibitors ameliorates fibrosis in multidrug resistance 2 gene knockout (Mdr2−/−) mice. Hepatology, 67(1), pp.247-259. doi: 10.1002/hep.29464.Targeting.

207. Ruiz-Cabello, F.J.M., Trefalt, G., Maroni, P. and Borkovec, M., 2014. Electric double-layer potentials and surface regulation properties measured by colloidal-probe atomic force microscopy. Physical Review E, 90(1), p.012301. doi: 10.1103/PhysRevE.90.012301.

208. Morris, P.G. and Fornier, M.N., 2008. Microtubule active agents: beyond the taxane frontier. Clinical cancer research, 14(22), pp.7167-7172. doi: 10.1158/1078-0432.CCR-08-0169.

209. Movassaghian, S., Merkel, O.M. and Torchilin, V.P., 2015. Applications of polymer micelles for imaging and drug delivery. Wiley Interdisciplinary Reviews: Nanomedicine and Nanobiotechnology, 7(5), pp.691-707. doi: 10.1002/wnan.1332.

210. Muralidharan, R., Babu, A., Amreddy, N., Basalingappa, K., Mehta, M., Chen, A., Zhao, Y.D., Kompella, U.B., Munshi, A. and Ramesh, R., 2016. Folate receptor-targeted nanoparticle delivery of HuR-RNAi suppresses lung cancer cell proliferation and migration. Journal of nanobiotechnology, 14(1), pp.1-17. doi: 10.1186/s12951-016-0201-1.

211. Nakajima, W., Sharma, K., Hicks, M.A., Le, N., Brown, R., Krystal, G.W. and Harada, H., 2016. Combination with vorinostat overcomes ABT-263 (navitoclax) resistance of small cell lung cancer. Cancer biology &

therapy, 17(1), pp.27-35. doi: 10.1080/15384047.2015.1108485.

212. Nakajima, W. and Tanaka, N., 2016. BH3 mimetics: their action and efficacy in cancer chemotherapy. Integrative Cancer Science and Therapeutics, 3(3), pp.437-441. doi: 10.15761/icst.1000184.

213. Nakamura, Y., Mochida, A., Choyke, P.L. and Kobayashi, H., 2016. Nanodrug delivery: is the enhanced permeability and retention effect sufficient for curing cancer?. Bioconjugate chemistry, 27(10), pp.2225-2238. doi: 10.1021/acs.bioconjchem.6b00437.

214. Navitoclax drugbank, 2018. Available at: https://www.drugbank.ca/drugs/DB12340 (Accessed: 2 November 2018).

215. Norton, N., Youssef, B., Hillman, D.W., Nassar, A., Geiger, X.J., Necela, B.M., Liu, H., Ruddy, K.J., Polley, M.Y.C., Ingle, J.N. and Couch, F.J., 2020. Folate receptor alpha expression associates with improved disease-free survival in triple negative breast cancer patients. NPJ breast cancer, 6(1), pp.1-9. doi: 10.1038/s41523-020-0147-1.

216. O'Shannessy, D.J., Somers, E.B., Wang, L.C., Wang, H. and Hsu, R., 2015. Expression of folate receptors alpha and beta in normal and cancerous gynecologic tissues: correlation of expression of the beta isoform with macrophage markers. Journal of ovarian research, 8(1), pp.1-9. doi: 10.1186/s13048-015-0156-0.

217. Ojima, I., Lichtenthal, B., Lee, S., Wang, C. and Wang, X., 2016. Taxane anticancer agents: a patent perspective. Expert opinion on therapeutic patents, 26(1), pp.1-20. doi: 10.1517/13543776.2016.1111872.

218. Oliver, K. E. and McGuire, W. P., 2014. Ovarian cancer and antiangiogenic therapy: caveat emptor. Journal of clinical oncology : official

journal of the American Society of Clinical Oncology, 32(30), pp. 3353–3356. doi: 10.1200/JCO.2014.57.4574.

219. Olson, S.H., Mignone, L., Nakraseive, C., Caputo, T.A., Barakat, R.R. and Harlap, S., 2001. Symptoms of ovarian cancer. Obstetrics & Gynecology, 98(2), pp.212-217. Available at: https://doi.org/10.1016/S0029-7844(01)01457-0

220. Ooya, T., Lee, J. and Park, K., 2003. Effects of ethylene glycol-based graft, star-shaped, and dendritic polymers on solubilization and controlled release of paclitaxel. Journal of Controlled Release, 93(2), pp. 121–127. doi: 10.1016/j.jconrel.2003.07.001.

221. Oshiro, C., Marsh, S., McLeod, H., Carrillo, M., Klein, T. and Altman, R., 2009. Taxane pathway. Pharmacogenetics and genomics, 19(12), pp. 979-983. doi: 10.1097/FPC.0b013e3283335277.

222. Ou, A., Louis, H., Oo, O., Bi, I., Pi, A., Philip, M, 2018. Utility of Nanomedicine for Cancer Treatment. Journal of Nanomedicine & Nanotechnology, 9(1), pp. 1–6. doi: 10.4172/2157-7439.1000481.

223. Oun, R., Moussa, Y.E. and Wheate, N.J., 2018. The side effects of platinum-based chemotherapy drugs: a review for chemists. Dalton transactions, 47(19), pp.6645-6653. doi: 10.1039/c8dt00838h.

224. Ovarian cancer statistics | Cancer Research UK, 2015. Available at: https://www.cancerresearchuk.org/health-professional/cancer-statistics/statistics-by-cancer-type/ovarian-cancer (Accessed: 23 September 2018).

225. Ozols, R.F., 2005. Treatment goals in ovarian cancer. *International Journal of Gynecologic Cancer*, *15*(Suppl 1), pp.3-11. Available at:

http://dx.doi.org/10.1136/ijgc-00009577-200505001-00002

226. Pan, J., Li, D., Xu, Y., Zhang, J., Wang, Y., Chen, M., Lin, S., Huang, L., Chung, E.J., Citrin, D.E. and Wang, Y., 2017. Inhibition of Bcl-2/xl with ABT-263 selectively kills senescent type II pneumocytes and reverses persistent pulmonary fibrosis induced by ionizing radiation in mice. International Journal of Radiation Oncology* Biology* Physics, 99(2), pp.353-361. doi: 10.1016/j.ijrobp.2017.02.216.

227. Patel, M.M. and Patel, B.M., 2017. Crossing the blood–brain barrier: recent advances in drug delivery to the brain. CNS drugs, 31(2), pp.109-133. doi: 10.1007/s40263-016-0405-9.

228. Patel, N.R., Piroyan, A., Ganta, S., Morse, A.B., Candiloro, K.M., Solon, A.L., Nack, A.H., Galati, C.A., Bora, C., Maglaty, M.A. and O'Brien, S.W., 2018. In Vitro and In Vivo evaluation of a novel folate-targeted theranostic nanoemulsion of docetaxel for imaging and improved anticancer activity against ovarian cancers. Cancer biology & therapy, 19(7), pp.554-564. doi: 10.1080/15384047.2017.1395118.

229. Peres, L.C., Risch, H., Terry, K.L., Webb, P.M., Goodman, M.T., Wu, A.H., Alberg, A.J., Bandera, E.V., Barnholtz-Sloan, J., Bondy, M.L. and Cote, M.L., 2018. Racial/ethnic differences in the epidemiology of ovarian cancer: a pooled analysis of 12 case-control studies. International journal of epidemiology, 47(2), pp.460-472. doi: 10.1093/IJE/DYX252.

230. Perini, G.F., Ribeiro, G.N., Neto, J.V.P., Campos, L.T. and Hamerschlak, N., 2018. BCL-2 as therapeutic target for hematological malignancies. Journal of hematology & oncology, 11(1), pp.1-15. doi: 10.1186/s13045-018-0608-2.

231. Pfeffer, C.M. and Singh, A.T., 2018. Apoptosis: a target for anticancer

therapy. International journal of molecular sciences, 19(2), p.448. doi: 10.3390/ijms19020448.

232. Piccart, M.J., Bertelsen, K., James, K., Cassidy, J., Mangioni, C., Simonsen, E., Stuart, G., Kaye, S., Vergote, I., Blom, R. and Grimshaw, R., 2000. Randomized intergroup trial of cisplatin–paclitaxel versus cisplatin–cyclophosphamide in women with advanced epithelial ovarian cancer: three-year results. Journal of the National Cancer Institute, 92(9), pp.699-708. doi: 10.1093/jnci/92.9.699.

233. Pinato, D.J., Graham, J., Gabra, H. and Sharma, R., 2013. Evolving concepts in the management of drug resistant ovarian cancer: dose dense chemotherapy and the reversal of clinical platinum resistance. Cancer treatment reviews, 39(2), pp.153-160. doi: 10.1016/j.ctrv.2012.04.004.

234. Pokhriyal, R., Hariprasad, R., Kumar, L. and Hariprasad, G., 2019. Chemotherapy resistance in advanced ovarian cancer patients. Biomarkers in cancer, 11, p.1179299X19860815. doi: 10.1177/1179299X19860815.

235. Poy, D., Ebrahimi Shahemabadi, H., Akbarzadeh, A., Moradi-Sardareh, H. and Ebrahimifar, M., 2018. Carboplatin liposomal nanoparticles: Preparation, characterization, and cytotoxicity effects on lung cancer in vitro environment. International Journal of Polymeric Materials and Polymeric Biomaterials, 67(6), pp.367-370. doi: 10.1080/00914037.2017.1332624.

236. Promega, 2020. Caspase-Glo® 3/7 Assay System. Available at: https://www.promega.co.uk/products/cell-health-assays/apoptosis-assays/caspase_glo-3_7-assay-systems/?catNum=G8090 (Accessed: 3 July 2020).

237. Pujade-Lauraine, E., Banerjee, S. and Pignata, S., 2019. Management

of platinum-resistant, relapsed epithelial ovarian cancer and new drug perspectives. Journal of Clinical Oncology, 37(27), pp.2437-2448. doi: 10.1200/JCO.19.00194.

238. Qiu, L.Y. and Bae, Y.H., 2006. Polymer architecture and drug delivery. Pharmaceutical research, 23(1), pp.1-30. doi: 10.1007/s11095-005-9046-2.

239. Qiu, L.Y. and Yan, M.Q., 2009. Constructing doxorubicin-loaded polymeric micelles through amphiphilic graft polyphosphazenes containing ethyl tryptophan and PEG segments. Acta biomaterialia, 5(6), pp.2132-2141. doi: 10.1016/j.actbio.2009.02.005.

240. Ramirez, I., Chon, H.S. and Apte, S.M., 2011. The role of surgery in the management of epithelial ovarian cancer. Cancer Control, 18(1), pp.22-30. doi: 10.1177/107327481101800104.

241. Rauh-Hain, J.A., Krivak, T.C., Del Carmen, M.G. and Olawaiye, A.B., 2011. Ovarian cancer screening and early detection in the general population. Reviews in obstetrics and gynecology, 4(1), p.15. doi: 10.3909/riog0143.

242. Riganti, C. and Contino, M., 2019. New Strategies to Overcome Resistance to Chemotherapy and Immune System in Cancer. International Journal of Molecular Sciences, 20(19), p. 4783. doi: 10.3390/ijms20194783.

243. Rodriguez, E.F., Monaco, S.E., Khalbuss, W., Austin, R.M. and Pantanowitz, L., 2013. Abdominopelvic washings: A comprehensive review. Cytojournal, 10. doi: 10.4103/1742-6413.111080.

244. Rooth, C., 2013. Ovarian cancer: risk factors, treatment and management. British journal of nursing, 22(Sup17), pp. S23-S30. doi:

10.12968/bjon.2013.22.Sup17.S23.

245. Rosen, D.G., Yang, G., Liu, G., Mercado-Uribe, I., Chang, B., Xiao, X.S., Zheng, J., Xue, F.X. and Liu, J., 2009. Ovarian cancer: pathology, biology, and disease models. Frontiers in bioscience: a journal and virtual library, 14, pp. 2089-2102. doi: 10.2741/3364.

246. Sadhukha, T. and Prabha, S., 2014. Encapsulation in nanoparticles improves anti-cancer efficacy of carboplatin. Aaps Pharmscitech, 15(4), pp.1029-1038. doi: 10.1208/s12249-014-0139-2.

247. Salager, J.L., 2002. Surfactants types and uses. FIRP booklet, 300.

248. Sarafraz, M. and Ahmadi, K., 2008. Paraclinical evaluation of side-effects of Taxanes on auditory system. Acta otorhinolaryngologica Italica, 28(5), pp. 239–242. Available at: http://www.pubmedcentral.nih.gov/articlerender.fcgi?artid=2689535&tool=pmcentrez&rendertype=abstract.

249. Schmid, D., Jarvis, G.E., Fay, F., Small, D.M., Greene, M.K., Majkut, J., Spence, S., McLaughlin, K.M., McCloskey, K.D., Johnston, P.G. and Kissenpfennig, A., 2014. Nanoencapsulation of ABT-737 and camptothecin enhances their clinical potential through synergistic antitumor effects and reduction of systemic toxicity. Cell death & disease, 5(10), pp.e1454-e1454. doi: 10.1038/cddis.2014.413.

250. Sebastian, R., 2017. Nanomedicine-the future of cancer treatment: A review. J. Cancer Prev. Curr. Res, 8(1), p.00265.doi: 10.15406/jcpcr.2017.08.00265.

251. Shi, J., Zhou, Y., Huang, H.C. and Mitchison, T.J., 2011. Navitoclax (ABT-263) accelerates apoptosis during drug-induced mitotic arrest by

antagonizing Bcl-xL. Cancer research, 71(13), pp.4518-4526. doi: 10.1158/0008-5472.CAN-10-4336.

252. Siddiqui, W.A., Ahad, A. and Ahsan, H., 2015. The mystery of BCL2 family: Bcl-2 proteins and apoptosis: an update. Archives of toxicology, 89(3), pp.289-317. doi: 10.1007/s00204-014-1448-7.

253. De Silva, E. and Kim, H., 2018. Drug-induced thrombocytopenia: Focus on platelet apoptosis. Chemico-biological interactions, 284, pp.1-11. doi: 10.1016/j.cbi.2018.01.015.

254. Smith, C.G., 2017. A resident's perspective of ovarian cancer. Diagnostics, 7(2), p.24. doi: 10.3390/diagnostics7020024.

255. Souers, A.J., Leverson, J.D., Boghaert, E.R., Ackler, S.L., Catron, N.D., Chen, J., Dayton, B.D., Ding, H., Enschede, S.H., Fairbrother, W.J. and Huang, D.C., 2013. ABT-199, a potent and selective BCL-2 inhibitor, achieves antitumor activity while sparing platelets. Nature medicine, 19(2), pp.202-208. doi: 10.1038/nm.3048.

256. De Sousa, G.F., Wlodarczyk, S.R. and Monteiro, G., 2014. Carboplatin: molecular mechanisms of action associated with chemoresistance. Brazilian Journal of Pharmaceutical Sciences, 50, pp.693-701. doi: 10.1590/S1984-82502014000400004.

257. De Souza, R., Zahedi, P., Badame, R.M., Allen, C. and Piquette-Miller, M., 2011. Chemotherapy dosing schedule influences drug resistance development in ovarian cancer. Molecular cancer therapeutics, 10(7), pp.1289-1299. doi: 10.1158/1535-7163.MCT-11-0058.

258. Stamelos, V.A., Robinson, E., Redman, C.W. and Richardson, A., 2013. Navitoclax augments the activity of carboplatin and paclitaxel combinations in

ovarian cancer cells. Gynecologic oncology, 128(2), pp.377-382. doi: 10.1016/j.ygyno.2012.11.019.

259. Stetefeld, J., McKenna, S.A. and Patel, T.R., 2016. Dynamic light scattering: a practical guide and applications in biomedical sciences. Biophysical reviews, 8(4), pp.409-427.doi: 10.1007/s12551-016-0218-6.

260. Stordal, B., Timms, K., Farrelly, A., Gallagher, D., Busschots, S., Renaud, M., Thery, J., Williams, D., Potter, J., Tran, T. and Korpanty, G., 2013. BRCA1/2 mutation analysis in 41 ovarian cell lines reveals only one functionally deleterious BRCA1 mutation. Molecular oncology, 7(3), pp.567-579. doi: 10.1016/j.molonc.2012.12.007.

261. Sundar, S., Neal, R.D. and Kehoe, S., 2015. Diagnosis of ovarian cancer. Bmj, 351, p. h4443. doi: 10.1136/bmj.h4443.

262. Sundaram, H., Vijayalakshmi, N. and Srilatha, K.P., 2009. High performance liquid chromatography and its role in identification of mycobacteriae: an overview. NTI Bulletin, 45(1-4).

263. Tahir, S.K., Smith, M.L., Hessler, P., Rapp, L.R., Idler, K.B., Park, C.H., Leverson, J.D. and Lam, L.T., 2017. Potential mechanisms of resistance to venetoclax and strategies to circumvent it. BMC cancer, 17(1), pp.1-10. doi: 10.1186/s12885-017-3383-5.

264. Tamura, N., Fujiwara, Y., Hashimoto, T., Shiraishi, H., Kitano, S., Shimizu, T., Kuwano, K., Yamamoto, N. and Motoi, N., 2020. Correlation between the expression of folate receptor alpha (FRα) and clinicopathological features in patients with lung adenocarcinoma. Lung Cancer, 145, pp.152-157. doi: 10.1016/j.lungcan.2020.05.002.

265. Tannan, N.B., Manzari, M.T., Herviou, L., Ferreira, M.D.S., Hagen, C., Kiguchi, H., Manova-Todorova, K., Seshan, V., de Stanchina, E., Heller, D.A. and Younes, A., 2021. Tumor-targeted nanoparticles improve the therapeutic index of BCL2 and MCL1 dual inhibition. Blood, 137(15), pp.2057-2069. Available at: https://doi.org/10.1182/blood.2020008017

266. Tapia, G. and Diaz-Padilla, I., 2013. Molecular mechanisms of platinum resistance in ovarian cancer. Ovarian Cancer-A clinical and translational update. DOI: 10.5772/55562.

267. Tarudji, A.W. and Kievit, F.M., 2020. Active targeting and transport. In Nanoparticles for Biomedical Applications (pp. 19-36). Elsevier. doi: 10.1016/B978-0-12-816662-8.00003-5.

268. Taylor, D.D. and Gercel-Taylor, C., 2008. MicroRNA signatures of tumor-derived exosomes as diagnostic biomarkers of ovarian cancer. Gynecologic oncology, 110(1), pp.13-21. doi: 10.1016/j.ygyno.2008.04.033.

269. Tessoulin, B., Papin, A., Gomez-Bougie, P., Bellanger, C., Amiot, M., Pellat-Deceunynck, C. and Chiron, D., 2019. BCL2-family dysregulation in B-cell malignancies: from gene expression regulation to a targeted therapy biomarker. Frontiers in oncology, 8, p.645. doi: 10.3389/fonc.2018.00645.

270. The American Cancer Society medical and editorial content team, 2018. What Is Ovarian Cancer ?. American cancer society, pp. 1–14.

271. Thompson, C.J., Ding, C., Qu, X., Yang, Z., Uchegbu, I.F., Tetley, L. and Cheng, W.P., 2008. The effect of polymer architecture on the nano self-assemblies based on novel comb-shaped amphiphilic poly (allylamine). Colloid and Polymer Science, 286(13), pp.1511-1526. doi: 10.1007/s00396-008-1925-8.

272. Timucin, A.C., Basaga, H. and Kutuk, O., 2018. Selective targeting of antiapoptotic BCL-2 proteins in cancer. Medicinal research reviews, 39(1), pp.146-175. doi: 10.1002/med.21516.

273. Tolcher, A.W., LoRusso, P., Arzt, J., Busman, T.A., Lian, G., Rudersdorf, N.S., Vanderwal, C.A., Kirschbrown, W., Holen, K.D. and Rosen, L.S., 2015. Safety, efficacy, and pharmacokinetics of navitoclax (ABT-263) in combination with erlotinib in patients with advanced solid tumors. Cancer chemotherapy and pharmacology, 76(5), pp.1025-1032. doi: 10.1007/s00280-015-2883-8.

274. Tone AA, Salvador S, Finlayson SJ, Tinker AV, Kwon JS, Lee CH, Cohen T, Ehlen T, Lee M, Carey MS, Heywood M, Pike J, Hoskins PJ, Stuart GC, Swenerton KD, Huntsman DG, Gilks CB, Miller DM, McAlpine JN, 2012. The role of the fallopian tube in ovarian cancer', Clinical Advances in Hematology and Oncology, 10(5), pp. 296–306. Available at: https://pubmed.ncbi.nlm.nih.gov/22706539/

275. Toss, A., De Matteis, E., Rossi, E., Casa, L.D., Iannone, A., Federico, M. and Cortesi, L., 2013. Ovarian cancer: can proteomics give new insights for therapy and diagnosis?. International journal of molecular sciences, 14(4), pp.8271-8290. doi: 10.3390/ijms14048271.

276. Touzeau, C., Dousset, C., Le Gouill, S., Sampath, D., Leverson, J.D., Souers, A.J., Maiga, S., Bene, M.C., Moreau, P., Pellat-Deceunynck, C. and Amiot, M., 2014. The Bcl-2 specific BH3 mimetic ABT-199: a promising targeted therapy for t (11; 14) multiple myeloma. Leukemia, 28(1), pp.210-212. doi: 10.1038/leu.2013.216.

277. Trang Le, N. T., Nguyen, C.K. and Nguyen, D.H., 2020. Carboplatin delivery system based on poly (ethylene glycol) methyl ether–cholesterol

modified soy lecithin liposomes. Advances in Natural Sciences: Nanoscience and Nanotechnology, 11(4), p.045016. doi: 10.1088/2043-6254/abcaf7.

278. Trimbos, B., Timmers, P., Pecorelli, S., Coens, C., Ven, K., Van der Burg, M. and Casado, A., 2010. Surgical staging and treatment of early ovarian cancer: long-term analysis from a randomized trial. Journal of the National Cancer Institute, 102(13), pp.982-987. doi: 10.1093/jnci/djq149.

279. Tsolou, A., Angelou, E., Didaskalou, S., Bikiaris, D., Avgoustakis, K., Agianian, B. and Koffa, M.D., 2020. Folate and Pegylated Aliphatic Polyester Nanoparticles for Targeted Anticancer Drug Delivery. International Journal of Nanomedicine, 15, p.4899. doi: 10.2147/IJN.S244712

280. Types & Stages - National Ovarian Cancer Coalition, 2020. Available at: http://ovarian.org/about-ovarian-cancer/what-is-ovarian-cancer/types-a-stages (Accessed: 3 May 2020).

281. Types of surgery | Ovarian cancer | Cancer Research UK, 2016. Available at: https://www.cancerresearchuk.org/about-cancer/ovarian-cancer/treatment/surgery/types-surgery (Accessed: 24 September 2018).

282. Vaillant, F., Merino, D., Lee, L., Breslin, K., Pal, B., Ritchie, M.E., Smyth, G.K., Christie, M., Phillipson, L.J., Burns, C.J. and Mann, G.B., 2013. Targeting BCL-2 with the BH3 mimetic ABT-199 in estrogen receptor-positive breast cancer. Cancer cell, 24(1), pp.120-129. doi: 10.1016/j.ccr.2013.06.002.

283. Villalobos-Ortiz, M., Ryan, J., Mashaka, T.N., Opferman, J.T. and Letai, A., 2019. BH3 profiling discriminates on-target small molecule BH3 mimetics from putative mimetics. Cell Death & Differentiation, 27(3), pp.999-1007. doi: 10.1038/s41418-019-0391-9.

284. Vinotha, T., Anitha, T., Ajit, S., Rachel, C. and Abraham, P., 2016. The

role of completion surgery in ovarian cancer. The Journal of Obstetrics and Gynecology of India, 66(1), pp.435-440. doi: 10.1007/s13224-015-0796-4.

285. Virgen-Ortíz, J.J., Dos Santos, J.C., Berenguer-Murcia, Á., Barbosa, O., Rodrigues, R.C. and Fernandez-Lafuente, R., 2017. Polyethylenimine: A very useful ionic polymer in the design of immobilized enzyme biocatalysts. Journal of Materials Chemistry B, 5(36), pp.7461-7490. doi: 10.1039/C7TB01639E.

286. Vivo-Llorca, G., Candela-Noguera, V., Alfonso, M., García-Fernández, A., Orzáez, M., Sancenón, F. and Martínez-Máñez, R., 2020. MUC1 aptamer-capped mesoporous silica nanoparticles for navitoclax resistance overcoming in triple-negative breast cancer. Chem.-A Eur. J, 26, pp.16318-16327. doi: 10.1002/chem.202001579.

287. Vogler, M., Hamali, H.A., Sun, X.M., Bampton, E.T., Dinsdale, D., Snowden, R.T., Dyer, M.J., Goodall, A.H. and Cohen, G.M., 2011. BCL2/BCL-XL inhibition induces apoptosis, disrupts cellular calcium homeostasis, and prevents platelet activation. Blood, The Journal of the American Society of Hematology, 117(26), pp.7145-7154. doi: 10.1182/blood-2011-03-344812.

288. Walaszczyk, A., Dookun, E., Redgrave, R., Tual-Chalot, S., Victorelli, S., Spyridopoulos, I., Owens, A., Arthur, H.M., Passos, J.F. and Richardson, G.D., 2019. Pharmacological clearance of senescent cells improves survival and recovery in aged mice following acute myocardial infarction. Aging Cell, 18(3), p.e12945. doi: 10.1111/acel.12945.

289. Wang, B., Du, H. and Zhang, J., 2011. Synthesis and characterisation of new types of side chain cholesteryl polymers. Steroids, 76(1-2), pp.204-209. doi: 10.1016/j.steroids.2010.10.011.

290. Wang, X., Yang, L., Chen, Z. and Shin, D.M., 2008. Application of

nanotechnology in cancer therapy and imaging. CA: a cancer journal for clinicians, 58(2), pp.97-110. doi: 10.3322/CA.2007.0003.

291. Weaver, B.A., 2014. How Taxol/paclitaxel kills cancer cells. Molecular biology of the cell, 25(18), pp.2677-2681. doi: 10.1091/mbc.E14-04-0916.

292. Westphal, D., Kluck, R.M. and Dewson, G., 2014. Building blocks of the apoptotic pore: how Bax and Bak are activated and oligomerize during apoptosis. Cell Death & Differentiation, 21(2), pp.196-205. doi: 10.1038/cdd.2013.139.

293. Witham, J., Valenti, M.R., Alexis, K., Vidot, S., Eccles, S.A., Kaye, S.B. and Richardson, A., 2007. The Bcl-2/Bcl-XL family inhibitor ABT-737 sensitizes ovarian cancer cells to carboplatin. Clinical cancer research, 13(23), pp.7191-7198. doi: 10.1158/1078-0432.CCR-07-0362.

294. Wong, M., Tan, N., Zha, J., Peale, F.V., Yue, P., Fairbrother, W.J. and Belmont, L.D., 2012. Navitoclax (ABT-263) reduces Bcl-xL–mediated chemoresistance in ovarian cancer models. Molecular cancer therapeutics, 11(4), pp.1026-1035. doi: 10.1158/1535-7163.MCT-11-0693.

295. Wu L, Liu Y, Huang R, Zhao H, Shu W., 2017. Rapid and Selective Determination of Folate Receptor α with Sensitive Resonance Rayleigh Scattering Signal. International Journal of Analytical Chemistry, 2017, p.1670812. DOI: 10.1155/2017/1670812.

296. Xing, L., Xu, Y., Sun, K., Wang, H., Zhang, F., Zhou, Z., Zhang, J., Zhang, F., Caliskan, B., Qiu, Z. and Wang, M., 2018. Identification of a peptide for folate receptor alpha by phage display and its tumor targeting activity in ovary cancer xenograft. Scientific reports, 8(1), pp.1-13. doi: 10.1038/s41598-018-26683-z.

297. Xiong, H., Pradhan, R.S., Nada, A., Krivoshik, A.P., Holen, K.D., Rhodes,

J.W., Gordon, G.B., Humerickhouse, R. and Awni, W.M., 2014. Studying Navitoclax, a targeted anticancer drug, in healthy volunteers–ethical considerations and risk/benefit assessments and management. Anticancer research, 34(7), pp.3739-3746. Available at: https://pubmed.ncbi.nlm.nih.gov/24982396/

298. Xu, J.P., Ji, J., Chen, W.D. and Shen, J.C., 2005. Novel biomimetic polymersomes as polymer therapeutics for drug delivery. Journal of controlled release, 107(3), pp.502-512. doi: 10.1016/j.jconrel.2005.06.013.

299. Yanagibashi, T., Gorai, I., Nakazawa, T., Miyagi, E., Hirahara, F., Kitamura, H. and Minaguchi, H., 1997. Complexity of expression of the intermediate filaments of six new human ovarian carcinoma cell lines: new expression of cytokeratin 20. British journal of cancer, 76(7), pp.829-835. doi: 10.1038/bjc.1997.471.

300. Yang, X., Chen, S., Chen, S. and Xu, H., 2019. Influencing factors on liquid crystalline properties of cholesterol side-chain liquid crystalline polymers without spacer: molecular weight and copolymerisation. Liquid Crystals, 46(12), pp.1827-1842. doi: 10.1080/02678292.2019.1606352.

301. Yin, H., Liao, L. and Fang, J., 2014. Enhanced permeability and retention (EPR) effect based tumor targeting: the concept, application and prospect. JSM Clin Oncol Res, 2(1), p.1010. doi: 10.1007/978-1-60761-609-2_3.

302. Yoo, J., Park, C., Yi, G., Lee, D. and Koo, H., 2019. Active targeting strategies using biological ligands for nanoparticle drug delivery systems. Cancers, 11(5), p.640. doi: 10.3390/cancers11050640.

303. Yusa, S. I., 2012. Self-assembly of cholesterol-containing water-soluble polymers, International Journal of Polymer Science, 2012. doi:

10.1155/2012/609767.

304. Zafar, A., Pilkington, L.I., Haverkate, N.A., Van Rensburg, M., Leung, E., Kumara, S., Denny, W.A., Barker, D., Alsuraifi, A., Hoskins, C. and Reynisson, J., 2018. Investigation into improving the aqueous solubility of the thieno [2, 3-b] pyridine anti-proliferative agents. Molecules, 23(1), p.145. doi: 10.3390/molecules23010145.

305. Zaidan, A., Ilhami, F., Fahmi, M.Z., Purwanto, B. and Kharisma, R.Z., 2017. Folate receptor mediated in vivo targeted delivery of human serum albumin coated manganese ferrite magnetic nanoparticles to cancer cells. In Journal of Physics: Conference Series, 853(1), p.012048. doi: 10.1088/1742-6596/853/1/012048.

306. Zeppernick, F. and Meinhold-Heerlein, I., 2014. The new FIGO staging system for ovarian, fallopian tube, and primary peritoneal cancer. Archives of gynecology and obstetrics, 290(5), pp.839-842. doi: 10.1007/s00404-014-3364-8.

307. Zervantonakis, I.K., Iavarone, C., Chen, H.Y., Selfors, L.M., Palakurthi, S., Liu, J.F., Drapkin, R., Matulonis, U., Leverson, J.D., Sampath, D. and Mills, G.B., 2017. Systems analysis of apoptotic priming in ovarian cancer identifies vulnerabilities and predictors of drug response. Nature communications, 8(1), pp.1-13. doi: 10.1038/s41467-017-00263-7.

308. Zhang, D., Yang, R., Wang, S. and Dong, Z., 2014. Paclitaxel: new uses for an old drug. Drug design, development and therapy, 8, pp.279-284. doi: 10.2147/DDDT.S56801.

309. Zhang, L., Lin, J. and Lin, S., 2007. Aggregate morphologies of amphiphilic graft copolymers in dilute solution studied by self-consistent field

theory. The Journal of Physical Chemistry B, 111(31), pp.9209-9217. Available at: https://doi.org/10.1021/jp068429l

310. Zheng, M., Gong, P., Zheng, C., Zhao, P., Luo, Z., Ma, Y. and Cai, L., 2015. Lipid-polymer nanoparticles for folate-receptor targeting delivery of doxorubicin. Journal of nanoscience and nanotechnology, 15(7), pp.4792-4798. doi: 10.1166/jnn.2015.9604.

311. Zheng, Y. and Wyman, I.W., 2016. Supramolecular nanostructures based on cyclodextrin and poly (ethylene oxide): Syntheses, structural characterizations and applications for drug delivery. Polymers, 8(5), p.198. doi: 10.3390/polym8050198.

312. Zhou, Y., Briand, V.A., Sharma, N., Ahn, S.K. and Kasi, R.M., 2009. Polymers comprising cholesterol: synthesis, self-assembly, and applications. Materials, 2(2), pp.636-660. doi: 10.3390/ma2020636.

313. Zhou, Y., Li, K., Li, F., Han, S., Wang, Y., Li, X. and Zhan, Y., 2019. Doxorubicin and ABT-199 coencapsulated nanocarriers for targeted delivery and synergistic treatment against hepatocellular carcinoma. Journal of Nanomaterials, 2019. Available at: https://doi.org/10.1155/2019/5274598

314. Zivanovic, O., Sima, C.S., Iasonos, A., Hoskins, W.J., Pingle, P.R., Leitao Jr, M.M., Sonoda, Y., Abu-Rustum, N.R., Barakat, R.R. and Chi, D.S., 2010. The effect of primary cytoreduction on outcomes of patients with FIGO stage IIIC ovarian cancer stratified by the initial tumor burden in the upper abdomen cephalad to the greater omentum. Gynecologic oncology, 116(3), pp.351-357. doi:10.1016/j.ygyno.2009.11.022.

Appendices

Appendix A: A table of IC50 comparing all the results obtained for all the conditions

Drug	IC_{50}	
	OV8	OVSAHO
Navitoclax	4.78 ± 0.31 µM	4.32 ± 0.44 µM
Carboplatin	7.59 ± 2.38 µM	13.02 ± 1.45 µM
PAA-Ch_5 (NP(E))	28.57 ± 0.37 µg/ml	38.36 ± 2.3 µg/ml
PAA-Ch_5-FA (NPF(E))	37.15± 1.53 µg/ml	71.87 ± 1.33 µg/ml

Appendix B: A table comparing between the passively targeted nanoparticles (chapter 3 and 4) and the actively targeted nanoparticles (chapter 5).

Type of effect	Type of nanoparticle targeting	
	Passively targeted nanoparticle	Actively targeted nanoparticle (with FA)
Loading of navitoclax using a polymer concentration of 1 mg/ml	0.0213 mg/ml	0.0123 mg/ml
Release (%)	Did not exceed 12% after 72 hours	Exceed 20% after 72 hours

Polymer toxicity	**On OVCAR-8**: 28.57 ± 0.37 µg/ml **On OVSAHO**: 38.36 ± 2.3 µg/ml	**On OVCAR-8**: 37.15± 1.53 µg/ml **On OVSAHO**: 71.87 ± 1.33 µg/ml
Encapsulated navitoclax toxicity	Showed two-times toxicity compared with free navitoclax at a final concentration of 2.5 µM	Showed more than three-times toxicity compared with free navitoclax at a final concentration of 1 µM
Navitoclax uptake	The encapsulated navitoclax showed two-times drug uptake compared with free navitoclax after 72 hours for both OVCAR-8 and OVSAHO.	The encapsulated navitoclax showed three-times drug uptake compared with free navitoclax after 72 hours for both OVCAR-8 and OVSAHO.
Combination with carboplatin	The encapsulated navitoclax showed a significant synergism when given concomitantly with carboplatin,	The encapsulated navitoclax showed a significant synergism when given concomitantly with carboplatin.